Department of Applied Chemistry

Characterisation of Aquatic Natural Organic Matter by Micro-Scale Sealed Vessel Pyrolysis

Lyndon J. Berwick

This thesis is presented for the Degree of
Doctor of Philosophy
of
Curtin University of Technology

December 2009

Declaration

To the best of my knowledge and belief this thesis contains no material previously published by any other person except where due acknowledgment has been made.

This thesis contains no material which has been accepted for the award of any other degree or diploma in any university.

Signature: …….

Date: ……...

Acknowledgments

Firstly I would like to express my gratitude to my principle supervisor, Dr. Paul Greenwood, for his advice, guidance and encouragement throughout the course of my PhD research. Paul's contribution to the preparation of this thesis, and the constructive and extremely thorough critique of the written work was invaluable. Secondly, I wish to thank Professor Jean-Philippe Croué (University of Poitiers, France) for providing most of the samples analysed in this study and for his consistently positive attitude, enthusiasm and constructive suggestions regarding my research.

Thanks to Dr. Ron Smernik (University of Adelaide, South Australia) for NMR analyses, Dr. Helen Talbot (University of Newcastle, UK) for LC-MS analyses, and Professor Colin Snape and Dr. Will Meredith (University of Nottingham, UK) for hydropyrolysis analyses. Thanks also to Mr. Geoff Chidlow and Mr. Kieran Pierce (Curtin University of Technology, Western Australia) for assistance with technical aspects of GC-MS analyses, and Dr. Daniel Dawson and Dr. Brad Allpike for constructive reviews of several chapters. Thanks also to Mr. Bob Gray (Brisbane Water) for providing a water sample from the North Pine Dam (Queensland).

I would also like to acknowledge Curtin University of Technology for provision of a Curtin University Post-Graduate Scholarship and the Cooperative Research Centre for Water Quality and Treatment (CRC-WQT) for additional financial support.

Very special thanks to my parents, Ian and Sandy, and my sister Gabrielle, who have always supported me in every aspect of my life. I credit much of this achievement to you. To Mum in particular, your unwavering encouragement, understanding and constant reassurance that it 'would all be worth it in the end' were invaluable. You are an inspiration to me and I hope I can exhibit in life the same courage, determination and compassion that you have shown. Thanks also to Charles for putting up with me during the many late nights preparing this thesis, and Sally for generously buying me a new computer when I really needed one.

To my great mates Darryn, Frankie and Mick, the friendship, laughter and companionship won't ever be forgotten. Thanks for your support and reassurance and the occasional reality checks on a Friday or Saturday night!

Finally but most importantly, to my beautiful girlfriend Sandy, I wish to thank you with all my heart. Your unconditional love and steadfast belief in me when at times I didn't believe in myself were truly appreciated. You have always supported me and I would not be where I am today without you by my side.

Publications arising from this thesis

Refereed journal articles

1. **Berwick, L.J**., Greenwood, P.F., Smernik, R., 2009. The use of MSSV pyrolysis to assist the molecular characterisation of aquatic natural organic matter. Water Research, *submitted*, November 2009.
2. **Berwick, L.J**., Greenwood, P.F., Meredith, W., Snape, C., Talbot, H.M., 2009. Comparion of microscale sealed vessel pyrolysis (MSSVpy) and hydropyrolysis (Hypy) for the characterisation of extant and sedimentary organic matter. Journal of Analytical and Applied Pyrolysis, *in press*.
3. **Berwick**, **L.J.**, Greenwood, P.F., Kagi, R.I., Croué, J-P., 2007. Thermal release of nitrogen-organics from natural organic matter (NOM) by micro-scale sealed vessel (MSSV) pyrolysis. Organic Geochemistry 38, 1073-1090.
4. Greenwood, P.F., Leenheer, J.A., McIntyre, C., **Berwick**, **L**.**J**., Franzmann, P., 2006. Bacterial biomarkers thermally released from dissolved organic matter. Organic Geochemistry 37, 597-609.

Conference presentations and proceedings

1. Greenwood, P.F., **Berwick, L**.**J**., Croué, J-P., 2009. Characterization of natural and effluent OM by controlled MSSV pyrolysis GCMS. AWWA Water Quality Technology Conference & Exposition (WQTC), 15-19th November, Seattle, Washington.
2. Lavaud, A., **Berwick**, **L**., Chabbi, A., Greenwood, P., Croué, J-P., 2008. Isolation and characterization of groundwater (Lysimetric plate collected water) NOM: Comparison with surface water NOM. IWA Natural Organic Matter Research: From Source to Tap, Bath, UK, 2-4th September 2008.
3. **Berwick**, **L**.**J**., Greenwood, P.F., Kagi, R.I., Croué, J-P., 2007. Compositional characterisation of aquatic NOM by micro-scale sealed vessel (MSSV) pyrolysis. 23rd International Meeting on Organic Geochemistry (IMOG), Torquay, UK, 9-14th September 2007.

4. **Berwick**, **L**.**J**., Greenwood, P.F., Meredith, W., Snape, C.E., 2007. Comparison of MSSV pyrolysis and hydropyrolysis to facilitate the thermal release of bound hydrocarbon biomarkers from immature organic matter. 234th ACS National Meeting, Boston, U.S., 19-23rd August 2007.
5. **Berwick**, **L**.**J**., Croué, J-P., Kagi, R.I., Greenwood, P.F., 2006. The utility of micro-scale sealed vessel (MSSV) pyrolysis for compositional characterisation of natural organic matter (NOM). Proceedings of 5th CRC WQT Post-Graduate Student Conference, Melbourne, Victoria, 10-13th July 2006, p 169-177.
6. Greenwood, P.F., Croué, J-P., **Berwick**, **L**.**J**., Boyd, L., Busetti, F., Grice, K., Harbou, H., 2006. Molecular and isotopic characterisation of the organic foulant of an RO membrane. Enviro 06 Conference and Exhibition, Sydney, Australia, 9-11th May 2006.
7. **Berwick**, **L**.**J**., Croué, J-P., Kagi, R.I., Greenwood, P.F., 2006. The thermal release of N-containing products from natural organic matter (NOM) by micro-scale sealed vessel (MSSV) pyrolysis. Proceedings of Combined Australian Organic Geochemists/Natural Organic Matter Users Conference, Perth, Western Australia, 12-15th February 2006, p 37-38.
8. Croué, J-P., Gallard, H., Ambonguilat, S., Greenwood, P., **Berwick**, **L**.**J**., Boyd, L., Grice, K., 2006. Characterisation of colloids isolated from surface waters. Proceedings of Combined Australian Organic Geochemists/Natural Organic Matter Users Conference, Perth, Western Australia, 12-15th February 2006, p 25-26.
9. **Berwick**, **L**.**J**., Greenwood, P., Kagi, R., 2005. The use of micro scale sealed vessel (MSSV) pyrolysis to thermally release biomarkers from natural organic matter. Proceedings of EMSI/North Central NOM Workshop, The Ohio State University, Columbus, Ohio, 15–17th June 2005, p 18.

List of abbreviations

AB	alkyl benzene
AMW	apparent molecular weight
AP	alkyl phenol
APCI	atmospheric pressure chemical ionisation
APh	alkyl phenanthrene
AF	alkyl furan
AN	alkyl naphthalene
BF	biofoulant
BHP	bacteriohopanepolyol
BSA	bovine serum albumin
C	carbon
COL	colloid
CPMAS	cross polarisation magic angle spinning
CSIA	compound specific isotope analysis
CSW	concentrated source water
DBP	disinfection byproduct
DM	dimethyl
DOC	dissolved organic carbon
DOM	dissolved organic matter
Ef-OM	effluent organic matter
ESI	electrospray ionisation
FAME	fatty acid methyl ester
FS	full scan
FTIR	Fourier transform infrared
FTICR	Fourier transform ion cyclotron resonance
GC	gas chromatography
GSL	Great Salt Lake
H	hydrogen
HAA	haloacetic acid
HAN	haloacetonitrile
HC	hydrocarbon

HP	Hewlett Packard
HP-SEC	high performance size exclusion chromatography
HPLC	high performance liquid chromatography
HPI	hydrophilic
HPO	hydrophobic
HS	humic substances
HyPy	hydropyrolysis
LC	liquid chromatography
MRM	multiple reaction monitoring
MS	mass spectrometry
MSD	mass selective detector
MSSV	micro-scale sealed vessel
MQ	Milli-Q water
MW	molecular weight
N	nitrogen
NHS	non-humic substances
NMR	nuclear magnetic resonance
NOM	natural organic matter
NP	North Pine
O	oxygen
OCD	organic carbon detection
PAH	polycyclic aromatic hydrocarbon
PS	polysaccharide
PSS	polystyrene sulfonate
Py	pyrolysis
RE	rotary evaporation
RO	reverse osmosis
S	sulfur
SEC	size exclusion chromatography
sedOM	sedimentary organic matter
SIR	selected ion recording
SMP	soluble microbial products
SOM	soil organic matter
SRFA	Suwannee River fulvic acid

SUVA	specific ultraviolet absorbance
TCU	total colour units
THM	trihalomethane
TIC	total ion chromatogram
TeM	tetramethyl
TM	trimethyl
TMAH	tetramethylammonium hydroxide
TOC	total organic carbon
TPI	transphilic
TSB	Tomago Sand Beds
UV	ultraviolet
WWTP	waste water treatment plant

Abstract

The analytical capacity of MSSV pyrolysis has been used to extend the structural characterisation of aquatic natural organic matter (NOM). NOM can contribute to various potable water issues and is present in high concentrations (> 5 mg L^{-1}) in many Australian source supplies. NOM can also impede the filtration performance of ultrafiltration or other membranes used in the increasingly popular practices of desalination and wastewater treatment. Characterisation studies that provide a detailed understanding of the origins, structural features and reactivity of NOM in source waters will help predict its impact on potable supplies and allow targeted treatment.

MSSV pyrolysis GC-MS analyses were conducted on XAD fractions of NOM from selected rivers, reservoirs, ground waters and biologically treated waste waters. The analytical sensitivity of the MSSV Py approach was demonstrated by the detection of high concentrations and complex distributions of pyrolysates. These included many additional products to those detected by corresponding flash pyrolysis GC-MS analysis, which is often limited by excessive degradation or poor chromatographic resolution of pyrolysates of high structural polarity. Nevertheless, flash pyrolysis did lead to several unique products from some samples, reflecting the complementary nature of the two methods.

Despite the high product concentrations detected by MSSV pyrolysis of NOM, primary structural fragments are prone to further alteration due to the confined nature and extended (e.g. 72 hr) application of the moderate thermal conditions (e.g. 300˚C). This approach has not been widely applied to the characterisation of recent or immature OM. Consequently, the mechanistic formation of many NOM pyrolysates is poorly understood, seriously limiting interpretation of their source and significance. As articulated in CHAPTER 1, these issues are specifically addressed by the present research, which aims to extend the application of MSSV pyrolysis to the characterisation of NOM and related environmental organic materials rich in intact biochemical inputs. To gain a better understanding of product formation pathways, several samples, including soil leachates, the organic foulant of ultra filtration membranes and a suite of standards representing potential biochemical

precursors of NOM were separately analysed by MSSV Py. The effect of thermal conditions on product distributions was also addressed by analysis of a small sub-set of the samples at several different temperatures (260 – 330˚C for 72 hours).

The capacity of MSSV Py to convert functionalised biochemical precursors into hydrocarbon products more amenable to GC resolution was initially demonstrated by the conversion of bacterial hopanepolyols of several surface and ground water NOM fractions, a bacterial isolate and biomass growth from an ultrafiltration membrane into corresponding hopane biomarkers as described in CHAPTER 2. The significance and integrity of the hopane distribution of the MSSV data was assessed by analyses of the same samples by flash pyrolysis and the advanced analytical techniques of hydropyrolysis (HyPy) GC-MS and liquid chromatography (LC)-MS with atmospheric pressure chemical ionisation. Flash pyrolysis showed no evidence of hopanes.

In comparison to the distributions of intact biohopanoids detected by LC-MS, the microbial hopane biomarker signatures detected by MSSV Py and HyPy were generally consistent, although HyPy did produce higher concentrations of ββ–diastereoisomers and higher MW fragments indicating a lower degree of structural alteration. Hopane products were detected in very low concentrations in the NOM samples, hence bacterial contribution may be more conveniently detected with biological methods (e.g., microbial arrays, bacterial counts). Nevertheless, MSSV pyrolysis represents a simple, low cost analytical method able to confirm the occurrence of diagnostic bacterial biomarkers in complex environmental settings, such as source waters and surrounding catchments, and may be a useful screening method prior to more involved characterisation possible with LC-MS. Moreover, this application represents an elegant demonstration of the capacity of MSSV pyrolysis to provide new information concerning functionalised biological precursors which have historically proved difficult to analyse by GC(MS).

Additional source diagnostic molecular features detected by MSSV Py of the membrane biofoulant included sterane biomarkers of eukaryote triterpenoids (i.e. steroids), *n*-alkanes of fatty acids and C_{16}-C_{19} phenylalkanes indicative of common

surfactants used to clean the membranes. The vastly improved molecular characterisation of the polar lipid constituents of membrane foulants, including the identification of industrial chemicals used in cleaning processes, suggests that this analytical capacity might also be applicable to monitoring the fate of organic constituents through the entire potable water system, from source through treatment and distribution to tap.

Unlike the established bacterial hopanoid source of hopane biomarkers, the origins of most of the major products from MSSV pyrolysis of the NOM samples are not clear. Subsequent chapters were separately dedicated to a detailed investigation of several of the major product classes.

CHAPTER 3 focused on the alkyl aromatic pyrolysates of NOM. The multitude of potential precursors of alkyl substituted benzenes and polycyclic aromatics (e.g. naphthalenes, phenanthrenes) significantly limits their diagnostic potential, nevertheless they represented a major proportion (20 – 50 % of total GC amenable pyrolysate signal) of the MSSV, and to a lesser degree, the flash pyrolysates of the HPO fractions of several NOM samples. The more highly substituted alkyl aromatics (and heteroatom products) of potentially greater source diagnostic value were better preserved by MSSV Py. Distinctive distributions of alkyl aromatics were detected by MSSV Py of the HPO fractions of several surface waters and a lysimetric plate collected ground water. All samples showed high alkyl benzene (AB) concentrations, whilst the ground water showed higher alkyl naphthalene (AN) concentrations than the surface waters. Correlation of several isopropyl substituted benzenes indicative of plant resin terpenoids in a bark sample, suggested these may be a significant source of the alkyl aromatics products of NOM. Furthermore, several higher plant derived polycyclic aromatic terpenoid biomarkers (e.g. cadalene, eudalene, retene and dehydroabietins) were also identified in the NOM fractions. Allochthonous and autochthonous sourced terpenoids have been proposed to be significant precursors of aquatic NOM; however diagnostic flash pyrolysis information about these types of contributors is typically limited.

HPO fractions of two waste waters also showed consistently high concentration of alkyl aromatics, reflecting the general recalcitrance of their precursors to biological

treatment. The distributions of these products differed from the natural surface and ground waters. Resistant aliphatic biomolecules derived from algal and bacterial biomass, susceptible to cyclisation and aromatization during MSSV Py, were tentatively assigned as the source of these distinctive pyrolysates.

MSSV pyrolysis proved particularly sensitive to detection of heteroatom containing products of the NOM samples, and O products (25 – 50 %) and S products (1 – 5 %) were the focus of CHAPTER 4. The alkyl ($\leq C_4$) phenols (APs) of the HPO fractions of the humic rich Gartempe and Uruguay rivers accounted for ca. 40 % of the total product signal. Similarly high concentrations of APs were detected by MSSV Py of a lignin standard, demonstrating the laboratory simulated thermal transformation of methoxy phenolic structures into alkyl phenols. The high concentrations of APs and low concentrations of methoxyphenol biomarkers of lignin typically detected in NOM (e.g. by flash pyrolysis, ^{13}C NMR) suggests that a similar structural change may also be diagenetically mediated. The detection of APs, therefore, may be a more sensitive indicator of lignin input than guiaicyl or syringyl based biomarkers. The polyphenol structural units of selected tannin standards did not survive MSSV Py treatment, so are not likely responsible for the AP MSSV pyrolysates of the NOM samples. The HPO fraction of the waste waters showed similarly high concentrations of APs and alkyl aromatics (as discussed in Chapter 3), suggesting these products are recalcitrant to biological treatment. The Naintré waste waters also contained additional higher MW $C_{4\text{-}10}$ alkyl substituted phenols not detectable by flash pyrolysis. Several of these products were indicative of industrial chemicals of potential health concern.

The TPI and COL fractions showed significant concentrations of alkyl furans which along with cyclic ketones were present in much lower abundance than APs in the HPO fractions. These products were attributed to carbohydrate sources following correlation with mono- and polysaccharide standards including glucose, cellulose and chitin. Trace or low relative abundances of these products in the biologically treated wastewaters reflects their vulnerability to mineralization. The HPO fractions of the NOM samples also showed low concentrations of alkyl benzofurans, similar distributions of which were detected in the SRFA standard, suggesting these are

more stable polysaccharide metabolites, but still prone to further biodegradation as evident by only trace concentrations detected in the waste waters.

Whilst MSSV provided increased access to several S-structural constituents of NOM, their relatively low concentrations and as yet undefined structural origins remain a challenge to source characterisation. Nevertheless, similar alkyl thiophene (AT) distributions were also generated from an S-containing amino acid standard. Notably higher concentrations of S-products in the waste waters may reflect additional anthropogenic sources (e.g. sewerage, industrial chemicals), which may also involve thermally catalysed reaction between H_2S and humic substances, analogous to the interaction of inorganic S and functionalised lipids during sedimentary diagenesis.

CHAPTER 5 was concerned with the notably high concentrations of N products (3 - 50 %) detected by MSSV Py GC-MS of the NOM samples. These products included a large range of alkyl- pyrroles, pyridines, pyrazines and pyridinamines, as well as amine substituted mono-aromatics and condensed N-heterocyclics. They were consistently detected over a broader range of MSSV Py conditions. Many of these products, particularly those with increased alkyl substitution were not detected by flash pyrolysis; leading to an historic underestimation of their contribution to NOM. Highest concentrations of N-products were detected in the COL fraction of NOM. Similarly high concentrations and distributions were also detected from the organic material prone to foul ultrafiltration membranes, confirming the colloid rich nature of this material. The distinctive low MW N-heterocyclic products of the COL fractions were correlated with the N-products of the amino sugar standard, and to a lesser extent the protein standards. The occurrence in high concentrations of low MW heterocyclics also provides potentially rare evidence for the environmental occurrence of Maillard reactions. The interaction of sugars and amino acids via Maillard processes may be an important contributor to humic substances, although there is much doubt about whether this process is supported by ambient or near surface temperatures. As these reactions are more favourable at high temperatures they may be artefacts of the MSSV Py process. However, MSSV Py of mixtures of carbohydrate and amino acid standards showed no evidence for the production of additional low MW heterocyclics. The waste waters showed relatively high

concentrations of alkyl carbazoles and β-carbolines, potentially derived from alkaloid precursors of plants, algae and bacteria, which have been implicated in toxic N-DBPs from potable water treatment.

To practically assess the analytical benefits of MSSV pyrolysis for NOM characterisation, it was used in combination with other established analytical methods to holistically characterise the NOM of the North Pine (NP) reservoir, a major source of the potable water supplies of Brisbane and SE Queensland. The NP water is of low colour and has moderate dissolved organic carbon (DOC; 5 mg L^{-1}) levels, but is impacted by algae which periodically occur in bloom proportions. The hydrophobic (HPO; 65 % initial DOC) and transphilic (TPI; 12 %) fractions from XAD resin separation of the DOC both showed high (>1) H/C values, low UV_{abs} characteristics and low aromatic-C measured by NMR, which are all indicative of a relatively low degree of aromaticity. However, MSSV Py of both fractions, in particular the HPO fraction, yielded prolific distributions of alkyl substituted aromatic hydrocarbon (i.e., benzenes, naphthalenes) and hydroaromatic (e.g. tetralins) products. These were attributed to aromatisation of aliphatic structural precursors, including terpenoids of algae and plants, which are usually difficult to detect by analytical pyrolysis. MSSV Py of both fractions also yielded high concentrations of alkyl phenols, which likely reflect contribution from non-methoxylated lignin units of catchment grasses, consistent with the vast forest cleared grassland regions of the NP catchment, but may also derive from algal biopolymers. None of the analytical methods used showed any significant evidence of dihydroxy or methoxy aromatic structures of wood lignin or tannin inputs.

MSSVpy of the TPI fraction showed very high abundances of N-products (e.g., alkyl pyrroles, pyridines, indoles) reflecting the structural significance of diagenetically altered proteins, most likely derived from algal biomass. In contrast, much fewer N-products were detected by flash Py. This demonstrates the analytical capacity of MSSV to access the significant N content of this fraction, which was quantitatively indicated by low C/N ratio, measured by elemental analysis, and high amide and amine signals by ^{13}C NMR and FTIR spectroscopy.

Whilst MSSV generated much higher product concentrations than flash Py or TMAH thermochemolysis, the latter methods did include unique product information demonstrating the complementary nature of different pyrolysis methods. Overall, this case study demonstrates the significant contribution MSSV Py has made to characterising the structure and sources of the Brisbane source water, clearly distinguishing it from humic black waters such as the Gartempe, Arroyo Sanchez and Suwannee Rivers studied in preceding chapters.

This PhD project represents the first detailed study of the potential of using MSSV Py to assist the organic speciation and molecular characterisation of biochemically rich NOM. Important additional pyrolysis information can be released with this analytical method which represents an obvious complement to conventional flash pyrolysis techniques where chromatographic resolution of polar biochemicals can be limited. The full realization of this approach, however, will need much further development as briefly alluded to in the closing comments of CHAPTER 7. It is hoped that the present project makes a significant early step in the realization of this potential.

Table of contents

List of tables

Chapter 2

Chapter 3

Chapter 4

Chapter 5

Chapter 6

List of figures

Chapter 1

Chapter 2

Chapter 3

Chapter 4

Chapter 5

Chapter 6

Chapter 1

Introduction

1.1 Aquatic natural organic matter

Natural organic matter (NOM) is ubiquitous in terrestrial (e.g. soils), aquatic (e.g. riverine, marine) and sedimentary (e.g. kerogens) environments and represents one of the largest active organic carbon reservoirs in the biosphere (Amon and Benner, 1996). NOM broadly refers to organic molecules originating from fresh and decomposing plant and animal biomass. Dissolved organic matter (DOM) is the water-soluble component of NOM present in freshwater aquifers and marine systems (Croué *et al*., 1999). It is operational defined as the quantity of organic matter that passes through a 0.45 μm membrane (Croué *et al*., 1999). DOM is often measured as dissolved organic carbon (DOC) using combustion based carbon analysers. Conversions between the two measurements are made by assuming that DOM is 45-55 % organic carbon by mass (McDonald *et al*., 2004). DOM can account for approximately 90 % of the NOM in natural waters (Amy, 1993). The remaining NOM consists of higher MW fractions including colloids, which are suspended solids associated with mineral phases that are operationally considered solutes (Aiken, 2002), and insoluble coarse and fine particulate organic matter (POM; Leenheer and Croué, 2003). NOM is typically more abundant in freshwater systems (e.g. 1-50 mg/L DOC in groundwaters, rivers, lakes and marshes; Thurman, 1985), than in marine environments (e.g. 1 mg/L DOC; Hedges and Oades, 1997) due to the more substantial input from terrigenous sources (Wershaw, 2004; Pancost and Boot, 2004). The present research is concerned with NOM of freshwaters, the most common source of drinking waters.

The chemical characteristics of aquatic NOM are dependent on many factors including source, hydrology, primary productivity, photolytic (Frimmel, 1994; 1998, Engelhaupt *et al*., 2002) and biological degradation (Kalbitz *et al*., 2003), transformation, sedimentation, sequestration and other biogeochemical conditions encountered during flow or reservoir storage. Consequently, the chemical nature of

NOM is extremely complex and heterogenous and can vary significantly with spatial and seasonal patterns.

NOM plays a significant role in the biogeochemical functioning of aquatic ecosystems. It is a major carbon and energy source for biota (Hunt *et al*., 2000; Aiken, 2002), and influences nutrient availability (Aiken, 2002), turbidity and pH buffering capacity (McDonald *et al*., 2004). NOM can serve as an electron donor in metal complexation reactions (Howe *et al*., 1997; Lu and Johnson, 1997; Lu *et al*., 1998; Frimmel, 1998; Haitzer *et al*., 2002), increasing the biological availability of metal ions. In addition, NOM affects the degradation and transport of hydrophobic organic contaminants (Carter and Suffet, 1982; Murphy *et al*., 1990) and aromatic hydrocarbons (e.g. crude oil pollution; Johnsen and Gribbestad, 1988) by sorption and sequestration.

1.1.1 Implications of NOM on potable water resources

The concentration and properties of dissolved NOM can directly impact many aspects of drinking water systems. Declining annual rainfall as a result of global warming in recent decades has severely affected the availability and quality of Australia's source waters, many of which now contain very high concentrations of NOM (e.g. > 20 mg L^{-1} DOC; Davidson, 1995; Fabri *et al*., 2008). High NOM levels in source waters can increase consumption of treatment chemicals, reduce the performance efficiency of treatment processes (e.g. filtration, coagulation, oxidation and adsorption), promote fouling of ultra- and nano-filtration membranes, increase microbial regrowth during water distribution (Franzmann *et al*., 2001), and reduce the aesthetic qualities of taste, colour and odour (Heitz *et al*., 2000; 2002; Franzmann *et al*., 2001).

In addition to operational and aesthetic considerations, NOM is also a precursor of potentially toxic by products formed on reaction with chemical disinfectants such as chlorine and monochloramine (e.g. Rook, 1974; 1976; 1977). Many classes of disinfection byproducts (DBPs) have been identified and several, including trihalomethanes (THMs), haloacetic acids (HAAs), haloketones, and haloacetonitriles (HANs), are regulated in Australian drinking water supplies. The current total THM limit in Australian drinking water is 250 µg L^{-1} (NHMRC and

NRMMC, 2004), however this value may be further reduced to align with the stricter United States guideline value of 80 μg L^{-1} (United States Environmental Protection Agency, 2001). Despite intensive research and analysis, there is still suspicion that a significant proportion of the DBPs produced by chlorination or chloramination treatments remain unknown. Drinking water guidelines continue to change and the list of regulated compounds extends as new DBPs of human health significance are identified.

The removal, reactivity and recalcitrance of aquatic NOM in drinking water sources is dependent on physicochemical properties such as molecular weight (MW), elemental composition, aromaticity, and functional group content (Cabaniss *et al*., 2000). Molecular characterisation techniques that can provide a detailed understanding of the structural chemistry of NOM are important for predicting its source and diagenetic formation pathways, as well as its behaviour and reactivity in source reservoirs and treatment plants. A better chemical definition of NOM may also provide insight into the precursory sources and formation of DBPs, and will help in the development of improved catchment management strategies and targeted treatment technologies.

1.1.2 Sources and composition of aquatic NOM

NOM consists of a complex mixture of selectively preserved, partially degraded and chemically transformed compounds derived from the breakdown of naturally occurring biochemicals present in plants, animals and microbes. The major biochemical classes of freshwater NOM precursors include polysaccharides (e.g. cellulose), amino sugars, amino acids, proteins, lignins, tannins, terpenoids, fatty acids, lipids and waxes (e.g. Thurman, 1985; Kaiser *et al*., 2003; Wershaw, 2004; Filley *et al*., 2006, Lee *et al*., 2006; Mao *et al*., 2007). These derive predominantly from allochthonous sources, such as leachate from surrounding soils, riparian vegetation and grasses, but also include autochthonous microbial and algal metabolites. Anthropogenic pollutants from domestic and industrial wastes, agricultural activities and storm water run-off (e.g. polycyclic aromatic hydrocarbons, pharmaceuticals, surfactants) and their degradation products may also contribute to DOC by incorporation into NOM macromolecules (Kruge *et al*., 1998; Kruge and Permanyer, 2004).

1.1.3 Humic and non-humic substances

NOM is commonly described in terms of two fractions termed humic (i.e. hydrophobic) and non-humic (i.e. hydrophilic) substances. Non-humic substances (NHSs) consist of unaltered biochemicals such as amino acids, proteins, carbohydrates, lipids and resins. Typically, labile organic biomolecules present in soils and aquatic systems, such as proteins and carbohydrates, are rapidly mineralised by microbial processing during early diagenesis (Hedges *et al*., 1985; Stout *et al*., 1988; Hatcher *et al*., 1989a; Huang *et al*., 1998; Knicker and Skjemstad, 2000; Westerhoff and Mash, 2002; Wershaw, 2004). However, more refractory molecules may be selectively preserved. Detailed studies of chemically resistant humic materials revealed the presence of biologically resistant aliphatic biopolymers derived from plant cuticles (Tegelaar *et al*., 1989b; Nierop, 1998) and algal cell walls (de Leeuw *et al*., 1991; Derenne *et al*. 1991). Proteins may also be preserved by physical encapsulation within humic macromolecules, which can provide resistance to chemical hydrolysis (Knicker and Hatcher, 1997; Zang *et al*., 2000). Primary biochemical structures typically represent only a minor proportion (ca. 20 %; Thurman, 1985) of DOC, however it is often very difficult to distinguish between the novel chemical structures formed by humification and partially degraded biomolecules (Wershaw *et al*., 2004). Kelleher and Simpson (2006) reported that most of the NMR signals in soil humic substances (HS) could be assigned to intact biopolymers and their degradation products.

Humic substances account for a much higher proportion of DOC, typically 50 – 75 % in freshwaters (Aiken, 1985) and up to 90 % in highly coloured waters (Croué *et al*., 1999). Humification involves a combination of complex microbially (e.g. enzymatic) and abiotically (e.g. photochemical, Maillard reaction) driven processes. These result in the degradation and alteration of natural biochemicals, as well as the formation of new products by random polymerisation of small reactive intermediates released during metabolic processing (e.g. Hedges, 1988; Malcolm, 1990; Hedges *et al*., 2000; Wershaw, 2004). Aquatic HS represent a complex mixture of aliphatic and aromatic structures possessing extensive alkyl and other functional group (e.g. carboxylic, hydroxyl, ester, ether, phenol, methoxyl, ketone, amide, N-heterocycle) substitution over a wide MW range (e.g. 100 - 100000 Dalton; Leenheer and Croué, 2003). HS are essentially highly altered or newly synthesised organic products (Lu *et*

al., 2000; Leenheer *et al*., 2003b), which often bear little structural relationship with the biochemicals from which they originate (Clapp and Hayes, 1999). These heterogeneous, macromolecular, polyfunctional molecules (Schulten and Gleixner, 1999) are highly refractory to biodegradation (McDonald *et al*., 2004). Various models have been proposed to describe the structure and diagenetic formation of humic substances and aquatic NOM. These include simple conceptual models, as well as more detailed structures based on computer modelling of molecular data from analytical techniques such as NMR spectroscopy, thermal and chemical degradation and electron microscopy (Schulten *et al*. 1991; Schulten and Leinweber, 1996; Schulten, 1999; Diallo *et al*., 2003; Leenheer, 2004; Wershaw, 2004; Cabaniss *et al*., 2005). A structural model of aquatic humic substances proposed by Schulten and Leinweber (1996) is shown in **Figure 1.1**.

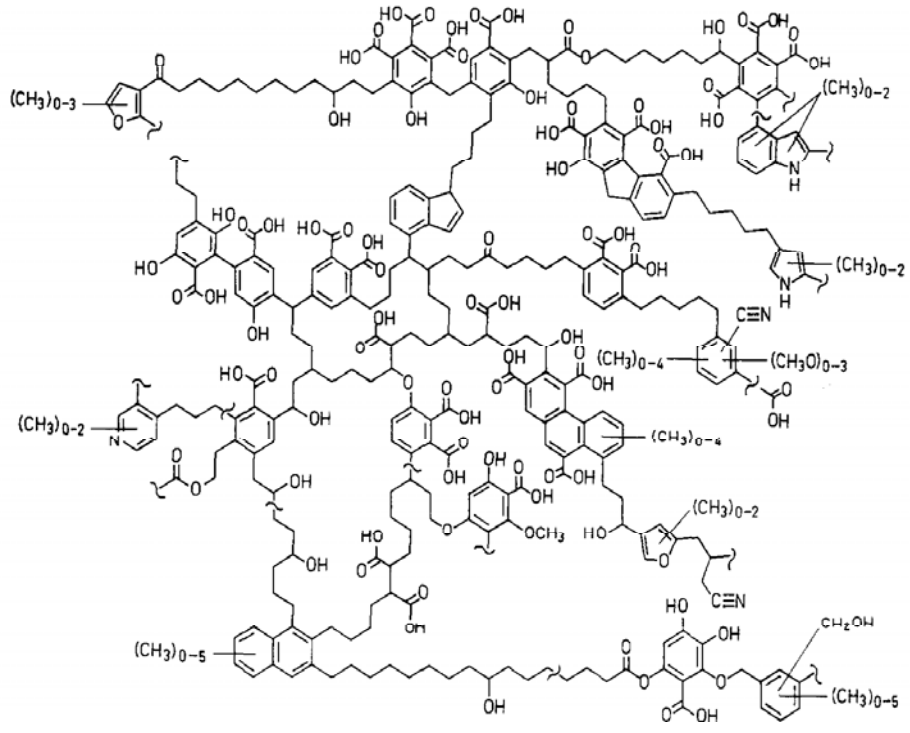

Figure 1.1 Humic acid structure proposed by Schulten and Leinweber (1996).

1.2 Isolation and characterisation of aquatic NOM

The inherent complexity, recalcitrance, and high biologically inherited chemical functionality of aquatic NOM pose significant challenges to analytical

characterisation. A variety of complementary analytical tools are typically required for robust and holistic characterisation (Abbt-Braun *et al*., 2004). Since a significant proportion of NOM remains poorly characterised or unexplored (Hedges *et al*., 2000), innovative new technologies able to provide additional insight into these globally significant materials are continually sought. Despite considerable progress over recent decades in the application of advanced spectroscopic techniques such as mass spectrometry (e.g. GC-MS, LC-ESI-MS, FT-ICR-MS; e.g. Schulten and Gleixner, 1999; McIntyre *et al*., 1997; Leenheer *et al*., 2001b; Kujawinski *et al*., 2002; 2004) and solid state nuclear magnetic resonance (NMR) spectroscopy (e.g. Knicker *et al*., 1996a; Leenheer *et al*., 2003a; 2003b; Kelleher and Simpson, 2006; Mao *et al*., 2007), detailed information about the molecular structure, source and diagenetic formation of aquatic NOM remains limited (Lu *et al*., 2000; González-Vila *et al*., 2001; Abbt-Braun *et al*., 2004; Nimmagadda *et al*., 2007a)

Few analytical techniques possess sufficient sensitivity to directly detect NOM in the typically low concentration in which it occurs in freshwater sources. A variety of methods have been successfully used to concentrate and/or isolate NOM from aquatic environments, each with their own advantages and limitations. The isolation protocol plays an important role in determining the properties of the sample (Abbt-Braun *et al*., 2004). Therefore the method employed should address the specific analytical requirements of the intended application. Membrane and sorption based techniques are most commonly used to isolate NOM (Croué *et al.*, 2000).

1.2.1. Membrane separation of NOM fractions

Membrane filtration using reverse osmosis, ultrafiltration or nanofiltration, followed by lyophilisation (freeze-drying) of the retentate, is an efficient protocol for extracting NOM from aquatic environments (Croué *et al*., 2000). Large volumes of water can be processed quickly. Furthermore it is not necessary to control as is often required for sorption based isolation methods. pH alteration has the potential to change the structural properties of NOM (Croué *et al*., 2000). DOC recovery using membrane techniques is typically high (e.g. > 85%), however several researchers have reported significant DOC losses due to organic fouling of the membrane (Amy and Cho, 1999; Cho *et al*., 1999). The major disadvantage of this isolation method is

the non-removal of salts, resulting in undesirably high concentrations of inorganic species, which can interfere with analytical characterisation.

1.2.2 Resin adsorption separation of NOM fractions

Removal of inorganic salts can be achieved with sorption based separation techniques. Presently, the most common sorption technique is the XAD resin procedure (Leenheer and Huffman 1976; Thurman and Malcolm, 1981; Leenheer, 1981; Leenheer and Noyes; 1984, Aiken, 1985; Croué *et al*., 2000). Elution of raw or pre-concentrated sample through serially positioned non-ionic macroporous sorbents composed of styrene divinylbenzene (e.g. XAD-4) and acrylic esters (XAD-8) separates NOM constituents into several fractions based on their polarity and acid-base properties.

Adsorption of DOC at acidic pH on XAD-8 resin separates the hydrophobic (HPO) and hydrophilic (HPI) moieties (Leenheer, 1981). These basic fractions provide an indication of the relative proportion of humic and non-humic substances. A transphilic (TPI) fraction can be further obtained from the XAD-8 eluent/HPI fraction by adsorption on XAD-4 resin. Typically, greater than 90 % (Croué *et al.*, 2000) of the HPO material sorbed on the XAD-8 resin can be recovered with base or organic solvents and ca. 80 % of the TPI fraction can be desorbed from the XAD-4 resin with base (Malcolm and MacCarthy, 1992, Croué *et al*., 1993). The HPO and TPI fractions can be further separated with additional resins to obtain acidic, basic and neutral fractions, however this requires considerable effort and may offer only low yields (Croué *et al.*, 2000).

The main advantage of the XAD sorption technique is the separation of NOM into more homogenous organic rich fractions (HPO, TPI), relatively free from inorganic species. However, the procedure is more laborious than membrane techniques (Leenheer, 1981, Croué *et al*., 2000) and usually no more than 75 % of the total NOM is recovered. The HPI fraction which passes through both resins under acid conditions is enriched in salts. Isolation of this material requires advanced procedures such as ion-exchange and precipitation or co-precipitation (Leenheer and Noyes, 1984; Croué *et al.*, 2000; Leenheer, 2004). However, colloidal OM present in the HPI fraction can be isolated by dialysis prior to XAD resin fractionation

(Leenheer *et al*., 2000), thereby increasing the total recovery of DOM. The HPI fraction typically consists of non-humic substances and low MW, polyelectrolytic organic acids (Leenheer *et al*., 1981).

1.3 Analytical characterisation of aquatic NOM

A multitude of analytical techniques have been used to assist the quantitative and qualitative characterisation of aquatic NOM in solution or isolated forms (Abbt-Braun *et al*., 2004). Spectrophotometry (UV/Vis, fluorescence spectroscopy) can effectively provide a basic characterisation of NOM in solution (Korshin *et al*., 1997; Weishaar *et al*., 2003; Hudson *et al*., 2007). The molecular weight profile of NOM in whole waters can be measured by high performance size exclusion chromatography (e.g. Chin *et al*., 1994; Allpike *et al*., 2005). Molecular structural elucidation requires the coupling of degradative (pyrolysis, oxidation, hydrolysis, chemical), chromatographic (GC, LC), and spectroscopic (FTIR, NMR, mass spectrometry) procedures. Several of the commonly employed NOM characterisation methods are described in more detail below.

1.3.1 Spectrophotometric analysis

Ultraviolet/visible (UV/vis) spectroscopy and fluorescence absorbance spectroscopy are both routinely used to characterise aqueous NOM. Absorbance of UV light, typically at $\lambda = 254$ nm, is attributed to aromatic chromophores present in NOM molecules, while absorbance at $\lambda = 400$ nm, possibly due to quinone like and conjugated ketonic C=O structures (Stevenson, 1982), is used as a measure of colour. Colour can be due to the presence of natural metallic ions (e.g. iron, manganese), humic substances and peat materials, plankton, weeds and industrial contamination (Wang *et al*., 1990; Clesceri *et al*., 1998).

Specific UV absorbance (SUVA) describes the ratio of UV_{254} absorbance to DOC concentration and provides an indication of the aromaticity of the sample (Weishaar *et al*., 2003). SUVA values (Leenheer and Croué, 2003) are often used for basic monitoring of the chemical nature of NOM in source waters, through treatment processes and during distribution. High SUVA waters are generally enriched in HPO NOM and humic substances (Croué *et al*., 1999). SUVA has also been correlated

with disinfection by product formation potential (Reckhow *et al*., 1990) and is often used as a surrogate indicator of disinfection byproduct precursors (Croué *et al*., 2000).

Fluorescence spectroscopy can also reveal certain chemical aspects of aquatic humic substances and has also helped study the interactions between HS and metals (Senesi, 1990; Wang *et al*., 1990). Although < 1 % of the aromatic moieties in NOM emit fluorophores (Lapen and Seitz, 1982), high resolution three dimensional fluorescence spectroscopy is an order of magnitude more sensitive than UV absorbance (Leenheer and Croué, 2003). The most efficient fluorophores in DOM correspond to humic and protein (e.g. tyrosine and tryptophan) aromatic structures (Coble, 1996; Hudson *et al*., 2007) and /or highly unsaturated aliphatic chains (Senesi, 1990).

1.3.2 High performance size exclusion chromatography

High performance size exclusion chromatography (HP-SEC) is used to determine the organic MW distribution of NOM (Chin *et al*., 1994). Ease of operation, simplicity of sample preparation and high sensitivity (i.e. minimal sample volumes) have led to its wide application in NOM characterisation studies. However, the complexity and heterogeneity of NOM limits chromatographic resolution and average MWs, rather than specific MWs are determined. Aquatic NOM typically elutes as a broad, monomodal distribution with subtle shoulders and small peaks (Chin *et al*., 1994). UV absorbance is the traditional method of detection. However many NOM structures such as proteins, sugars, amino sugars and aliphatic acids, have low UV-molecular-absorption. UV detection is therefore not quantitative for all organic carbon. The recent development of HP-SEC with dedicated DOC detectors has allowed quantitation of all organic constituents of NOM (Huber and Frimmel, 1994; Her *et al*., 2002; Allpike *et al*., 2005), irrespective of their functionality.

The monitoring of MW distribution dynamics by SEC can help assess the effectiveness of drinking water treatment processes. For example, low MW fractions are thought to be the most difficult to remove using conventional coagulation treatment (Chow *et al*., 1999; Aoustin *et al*., 2001; Drikas *et al*., 2003). They contribute disproportionately to bioavailable organic matter and the promotion of

biofilm formation in drinking water distribution systems (Volk *et al*., 2000, Hem and Efraimsen, 2001). Higher MW HPO fractions on the other hand, represent major DBP precursor sites (Leenheer and Croué, 2003).

1.3.3 Fourier transform infra red spectroscopy

Fourier transform infrared (FTIR) spectroscopy is commonly used for qualitative detection of organic functional groups. Various structural functionalities have been assigned to specific infra-red absorbance bands (Silverstein and Webster, 1997), however the complexity of NOM renders spectral interpretation difficult and since only the strongest bands can be identified the data is often not quantitatively representative (Croué *et al*., 1999). FTIR characterisation can be particularly useful for identifying the proteinaceous component of NOM, which is difficult to identify using ^{13}C-NMR. In addition, the relative abundances of hydrocarbons and carbohydrates moieties can be used as an indicator of the hydrophobic/hydrophilic nature of NOM (Croué *et al*., 2000).

1.3.4 ^{13}Carbon nuclear magnetic resonance spectroscopy

NMR spectroscopy is an extremely valuable tool for characterising the complex naturally occurring organic constituents of soil, sedimentary and aquatic environments and has significantly enhanced the understanding of the structure of aquatic NOM and humic substances. NMR is a non-destructive method providing qualitative and semi-quantitative organic structural information about molecular environments of hydrogen (^{1}H), carbon (^{13}C) and nitrogen (^{15}N) in solution or solid state (Wilson, 1987). ^{13}C-NMR chemical shifts have been assigned to various carbon structural features of NOM including methyl, methylene, aromatic, carbonyl, carboxyl, hydroxyl, amide and amine groups. Analysis of isolated aquatic NOM is more commonly performed by solid-state ^{13}C cross-polarisation magic angle spinning (^{13}C CP/MAS) NMR. The typically low solvent solubility of NOM and the differential solubility of various NOM components have limited the application of solution NMR (Smernik and Oades, 2000a; 2000b).

NMR studies of NOM are usually conducted in parallel with other complementary analytical techniques including FTIR spectroscopy or pyrolysis GC-MS for holistic characterisation. NMR, like FTIR, preserves the sample for further investigation.

However, NMR is not as sensitive as FTIR or pyrolysis GC-MS, which are both able to provide molecular speciation information on ca. 50 times less sample. Quantitative issues with solid-state ^{13}C CPMAS NMR spectra of complex organic materials also include long-spin lattice relaxation times, strong C-H and N-H dipolar interactions, chemical shift anisotropy, spectral alterations by paramagnetic materials and poor quantitation at high fields (Nanny *et al*., 1997; Smernik *et al*., 2000a; 2000b; Hatcher *et al*., 2001). All of these issues can complicate the quantitative interpretation of ^{13}C-NMR data. Literature on the application of ^{13}C-NMR for structural investigations of humic substances, aquatic NOM and other environmental organics is extensive and comprehensive reviews can be found in Kögel-Knabner (1997) and Cardoza *et al*. (2004).

Solid state ^{15}N-NMR has also been used to characterise the structural forms and diagenetic and thermal alteration of organic nitrogen in humic substances, predominantly in soil and algal derived OM (e.g. Knicker and Lüdemann, 1995; Knicker *et al*., 1995, 1996a, 1996b; Knicker and Hatcher, 1997, Knicker and Skjemstad, 2000; Knicker *et al*., 2002; Almendros *et al*., 2003; Templier *et al*., 2005b; Mao *et al*., 2007). Major peaks for amide, amine and heterocyclic nitrogen structures have been observed in the ^{15}N NMR spectra of soil and aquatic humic substances. However the spectra are often compromised by the low natural abundance of ^{15}N and are not as well resolved as that of ^{13}C-NMR (Knicker and Lüdemann, 1995).

1.3.5 Liquid chromatography mass spectrometry

High performance liquid chromatography (HPLC) coupled with soft ionisation techniques (e.g. electrospray ionisation (ESI) or atmospheric pressure chemical ionisation; APCI) and high resolution (e.g. time of flight) or multi dimensional mass spectrometry (e.g. ion trap, triple quadrupole, Fourier transform ion cyclotron resonance) have significantly progressed the molecular level characterization of complex macrobiomolecules. The powerful utility of these techniques for the trace detection of polar biochemicals (e.g. Talbot *et al*., 2001; 2003a; 2003b) and xenobiotics such as pharmaceuticals, personal care products (e.g. Gros *et al*., 2006; Göbel *et al*., 2004; Pojana *et al*. 2004; Busetti *et al*., 2008) and other priority pollutants (e.g. Gimeno *et al*., 2002; Grosse and Letzel, 2007) in recent sedimentary,

aquatic and aerosol environments has been demonstrated. ESI is particularly well suited to the analysis of polar compounds, whereas APCI is very effective in the analysis of medium-polarity and low-polarity substances.

There is also growing interest in LC-MS characterisation of humic substances (e.g. McIntyre *et al*., 1997; 2002; Fievre *et al*., 1997; Kujawinski *et al*., 2002; 2004; Hatcher *et al*., 2001; Leenheer *et al*., 2001b; Kim *et al*., 2003). ESI-MS has been the main direct MS approach for obtaining molecular information from humic substances (Hatcher *et al*., 2001). This method allows direct mass measurement whilst minimising fragmentation, and has been used to provide detailed molecular level mass data for polycarboxylic acids from aquatic fulvic acids (e.g. McIntyre *et al*., 1997; 2002). It is also useful for determining exact formula weights from which elemental formulas and possible structures can be elucidated (Leenheer *et al*., 2001b; Kujawinski *et al*., 2002). However, the extremely complex and heterogenous nature of NOM again presents a major challenge to molecular level characterisation by this approach. Low chromatographic, and in some cases MS resolution can complicate mass spectral interpretations. In fact, even if humic substances can be ionized readily by ESI or APCI techniques, the subsequent MS spectra are extremely complex because of the presence of peaks virtually at every *m/z* value. In addition, the possible production of multiply charged ions and sodium or potassium adducts, and the dependence on various parameters such as cone voltage and LC mobile phase, can further complicate MW determinations by ESI-MS (McIntyre *et al*., 2002). The application of ESI-MS to NOM characterisation is still at a developmental stage and further research will be required to realise the full analytical potential of this technique.

1.3.6 Gas chromatography mass spectrometry

Gas chromatography mass spectrometry (GC-MS) coupled with a variety of sample introduction devices including vapourised injection of liquid samples, analytical pyrolysis, and solid phase micro-extraction (SPME), is routinely used to identify and quantify many individual organic constituents present in modern and palaeoenvironments (e.g. Philp, 1985; Philp and Gilbert, 1987; Peters and Moldowan, 1993). The largely macromolecular nature of aquatic NOM is recalcitrant to direct GC-MS analysis of solvent extracts but can be thermally or

chemically degraded into smaller fragments compatible with the MW/size limitations of this gaseous phase procedure. A wide variety of chemical reagents have proved useful for oxidative (e.g. Ertel *et al*., 1984; Quénéa *et al*., 2005b), reductive (e.g. Eglite *et al*., 2003; Nimmagadda *et al*., 2007a) and hydrolytic (Parsons, 1989) cleavage of macromolecular bonds. Oxidative treatment of aquatic NOM with alkaline cupric oxide (CuO) has helped characterise lignin structures in complex organic mixtures (Ertel *et al*., 1984; Ertel and Hedges; 1984, Lehtonen *et al*., 2004). Chemical degradation is typically performed off-line and often requires additional preparation such as separation of polarity fractions by stationary phase column chromatography and/or chemical derivatisation prior to GC analysis. However, chemical or enzymatic degradation methods are often laborious and typically afford only low product yields due to limited access of the substrate to active sites in the macromolecule, or analyte loss during the extensive work-up procedures required (Farrimond *et al*., 2003). Nevertheless, these preparative approaches can support higher chromatographic resolution of individual products, which is important for advanced levels of molecular characterisation or other complementary analytical methods such as compound specific isotope analysis (CSIA), where baseline chromatographic resolution is required.

1.3.7. Analytical pyrolysis GC-MS

Analytical pyrolysis (Py) coupled with GC-MS is frequently used to assist the molecular characterisation of aquatic NOM and other complex bio- and geomacromolecules from terrestrial (e.g. Saiz-Jimenez and de Leeuw, 1984a; 1986b, Schulten, 1999), aquatic (e.g. Bruchet, 1985, Gadel and Bruchet, 1987; Bruchet *et al*., 1990, Abbt-Braun *et al*., 1989, Schulten and Gleixner, 1999, González-Vila *et al*., 2001, Templier *et al*., 2005a) and sedimentary systems (e.g. Larter and Senftle, 1985, Sinninghe Damsté *et al*., 1992a; Hartgers *et al*., 1992; Peulve *et al*., 1996, Garcette-Lepecq *et al*., 2000). Thermal energy is used to dissociate NOM into fragments amenable to GC analysis. It generally acts in a relatively non-selective manner compared to the specific molecular interactions targeted by chemical reagents, often resulting in complex product distributions. A range of different pyrolysis approaches have been used to characterise aquatic NOM. Pyrolysis typically involves a dedicated thermal control device integrated to the GC injector that is carefully controlled to give reasonably reproducible results. The approach is

simple, rapid and sensitive, requires only small sample quantities (nanogram to sub mg range; Saiz-Jimenez, 1994), and does not involve complicated and time-consuming extraction, fractionation and derivatisation procedures (Saiz-Jimenez, 1994).

Fast pyrolysis techniques such as flash or *Curie*-point pyrolysis are most commonly used. High amounts of thermal energy are applied in an inert environment to ballistically heat the sample to high temperatures (> 500˚C). High MW OM dissociates into a wide range of lower MW fragments, which can be detected by GC-MS and provide insight into the composition and source of the parent macromolecules. Fast pyrolysis is generally performed 'on-line' in open-system configurations, facilitating rapid and direct transfer of the pyrolysis products (pyrolysates) from the heated zone of the pyrolysis chamber to the GC column. Rapid pyrolysate transfer and the use of inert carrier gases (e.g. helium) reduce the impact of secondary reactions which can alter the structure of pyrolysates (del Rio *et al*., 1996). Off-line analysis with purpose built apparatus is also possible if further preparative treatments are required prior to analysis. The combination of off-line pyrolysis and stationary phase column chromatography can provide less complex polarity based fractions of the pyrolysates.

Numerous flash pyrolysis products of aquatic NOM and humic substances have been correlated with a wide range of biomolecular precursors, including amino acids, proteins, carbohydrates, amino sugars, lignin and tannin (e.g. Saiz-Jimenez and de Leeuw, 1986 b; Bruchet, 1985, Gadel and Bruchet, 1987; Bruchet *et al*., 1990; Page *et al*., 2002). The pyrolysis of lignin for example, produces a characteristic distribution of hydroxy- and methoxy- aromatic products, which are unique indicators of vascular plant matter (Hedges and Mann, 1979a; Saiz-Jimenez and de Leeuw, 1984b; 1986a; Opsahl and Benner, 1997). Carbohydrates typically yield furans and furaldehydes (Pouwels *et al*., 1987; 1989; Pastorova *et al*., 1994), proteins generate low MW nitrogen compounds such as pyridines and pyrroles (Bruchet, 1985; Saiz-Jimenez and de Leeuw, 1986b; Chiavari and Galletti, 1992), and amino sugars yield acetamide derivatives (Bruchet, 1985; Stankiewicz *et al*., 1996; Christy *et al*., 1999). The peak areas of pyrolysis products can thus be used to estimate the relative proportions of the major biopolymers present in NOM (Bruchet *et al*., 1990).

Whilst fast pyrolysis can provide detailed structural information on complex aquatic macromolecules, the recalcitrance and high structural polarity of these materials represents a significant analytical challenge (Saiz-Jimenez, 1994, del Rio *et al*., 1996; Hedges *et al*., 2000). GC-MS identification of polar pyrolysis fragments is limited because of their low thermal volatility, and generally poor chromatographic behaviour (Dignac *et al*., 2006) as a result of intermolecular hydrogen bonds that inhibit separation (Leenheer and Noyes, 1989). In addition, certain moieties of NOM macromolecules (e.g. black carbon; Hedges *et al*., 2000) are thermally intractable even at excessive pyrolysis temperatures. A large proportion of semi- or non-volatile compounds may condense within the sample tube or inlet system reducing the proportion of pyrolysis products transferred from the pyrolysis unit to the GC column (Saiz-Jimenez, 1994). Nevertheless, for mature samples such as kerogen, which have lost much of the chemical functionality of primary precursors via sedimentary thermal maturation, the hydrocarbon products of fast pyrolysis appear to provide compositional information representative of gross structure and not about atypical, readily volatised moieties (Larter and Senftle, 1985).

Conversely, thermally susceptible chemical bonds and functionalities may be extensively degraded or modified during pyrolytic heating, resulting in the loss of structural information. For example, whilst FTIR and ^{13}C NMR spectroscopic studies have identified that aliphatic and aromatic carboxylic groups are major components of humic substances and aquatic DOM (e.g. Leenheer *et al*., 1995; Leenheer *et al*., 2003b), decarboxylation results in very minor yields of these products by fast pyrolysis (Saiz-Jimenez, 1993; Saiz-Jimenez, 1994; del Rio *et al*., 1996). Furthermore, flash pyrolysis of fatty acids in the presence of clay minerals and/or sulphur can produce alkyl benzenes, indenes and naphthalenes via cyclisation and aromatisation reactions (Saiz-Jimenez, 1994; 1995; Faure *et al*., 2006a; 2006b). Structural alterations due to secondary processes can limit the diagnostic value and significance of the pyrolysis products detected. As such, the GC resolvable products of flash pyrolysis may represent only a quantitatively small fraction of the parent material (Saiz-Jimenez, 1994), only partially reflect the precursory structures of NOM, and contribute to misinterpretations and biased conclusions.

1.3.8 Thermochemolysis GC-MS

Thermochemolysis is an adjunct pyrolysis technique performed in the presence of tetramethylammonium hydroxide (TMAH; Challinor, 1989; Challinor, 1991). It has been applied to the characterisation of a very wide range of natural biopolymers including the lignin component of fresh and biodegraded wood (e.g. Challinor, 1995; 2001; Martin *et al*., 1995a; Hatcher and Minard, 1996; McKinney and Hatcher, 1996; Filley *et al*., 1999; Filley *et al*., 2000), polyphenolics from plant tannins (e.g. Galletti *et al*., 1995; Filley *et al*., 2006; Nierop and Filley, 2007), carbohydrates (Fabbri and Helleur, 1999), aliphatic polymers such as cutin and suberin (González-Vila *et al*., 1996; del Rio and Hatcher, 1998), higher plant resins (Anderson and Winans, 1991), peptides and amino acids (Zang *et al*., 2001; Gallois *et al*., 2007). Thermochemolysis has also been particularly successful for structural characterisation of complex NOM in aquatic systems (del Rio *et al*., 1998; Lehtonen *et al*., 2000a; 2000b; González-Vila *et al*., 2001; Frazier *et al*., 2003) as well as soils (Hatcher and Clifford, 1994; Martin *et al*., 1994; 1995b; Chefetz *et al*., 2002; Ikeya *et al*., 2004), recent sediments (Mansuy *et al*., 2001; Simpson *et al*., 2005), kerogens and coals (Kralert *et al*., 1995).

Thermochemolysis overcomes some of the limitations of traditional analytical pyrolysis, allowing the separation and detection of many additional pyrolysates of structural and source significance. It promotes the highly selective cleavage of ester and ether linkages in macromolecules via saponification/transesterifcation reactions (de Leeuw and Baas, 1993; Martin *et al*., 1994). Subsequent methylation of the pyrolysates yields methylated ester or ether derivatives of many polar constituents of NOM including fatty acids, aromatic and phenolic carboxylic acids and alcohols. Methylation of acidic functional groups reduces the formation of intermolecular hydrogen bonds that typically inhibit separation of polar compounds by GC (Leenheer and Noyes, 1989) and minimises secondary reactions (e.g. decarboxylation, aromatisation) and alterations of primary pyrolysates (Martin *et al*., 1994). Off-line thermochemolysis performed in sealed glass tubes at relatively moderate pyrolysis temperatures (e.g. 250-300˚C; McKinney *et al*., 1995) has also been developed. This allows removal of TMAH byproducts and quantitation of pyrolysate yields using internal standards. Application of these additional preparative procedures can improve chromatographic separation and minimise the

deterioration of injection systems and column stationary phases by attack from aggressive reagents or byproducts (Joll *et al*., 2004).

One of the main limitations of the TMAH thermochemolysis procedure, however, is the inability to distinguish between pre-existing methoxyl groups and those produced by methyl derivatization of hydroxy groups. This is a significant drawback for the characterisation of microbially degraded lignin (Filley *et al*., 2000; 2006). Filley *et al.* (1999; 2000; 2006) recently demonstrated the use of ^{13}C labelling of TMAH, allowing distinction between lignin, demethylated lignin, hydrolysable tannin, and other phenolic acid constituents of soil organic matter (SOM). Partial decarboxylation of susceptible carboxylic groups is also possible (Joll *et al*., 2003), whilst oxidation of hydroxy functional groups can yield secondary carboxylic acid products (Hatcher and Minard, 1995), both of which can lead to incorrect interpretation of precursory structures. It is also important to note that TMAH thermochemolysis is not capable of analysing highly humified structures (del Rio *et al*., 1994; Lehtonen *et al*., 2000a) or condensed tannins where acidic decomposition is required (Hernes and Hedges, 2000).

1.4 Present research

The focus of this PhD study is to assess and develop the analytical capability of micro-scale sealed vessel (MSSV) pyrolysis as an alternative thermal degradation approach for the molecular characterisation of aquatic NOM. MSSV pyrolysis involves closed system heating of OM using much lower temperatures over longer time periods than conventional open-system fast pyrolysis. The closed system and relatively moderate thermal conditions of this approach may facilitate the analysis of a variety of constituents that are traditionally recalcitrant to characterisation using conventional analytical pyrolysis approaches. This should provide additional molecular information useful for evaluating the origins and structural features of NOM in source waters.

1.4.1 MSSV pyrolysis GC-MS

Micro-scale sealed vessel (MSSV) pyrolysis is performed on small amounts (0.1 – 5 mg) of sample in 10 μL closed tubes, typically at temperatures of 250-350˚C for

periods of several hours or days. Unlike the open system configuration of fast pyrolysis, the pyrolysates are confined within the sealed MSSV tube. Online GC-MS analysis of the volatile gaseous and higher MW (C_1-C_{35}) hydrocarbon products is performed by cracking the tube in a purpose built injector port (Horsfield *et al*., 1989). **Figure 1.2** shows the MSSV Py instrument configuration. Dead volume is removed by packing the tubes with pre-annealed glass beads allowing high partial pressures up to 10 bar to be maintained (Horsfield and Dueppenbecker, 1991). This supports thermally promoted hydrogenation reactions critical to the conversion of immature sedimentary macromolecules into liquid hydrocarbons (Monthioux *et al*., 1985, Landais *et al*., 1993). MSSV pyrolysis has proved very useful for laboratory simulation of the kinetic formation of petroleum, natural gas and other hydrocarbons in diagenetic and catagenetic sedimentary processes such as humification, peatification and coalification (Horsfield *et al*., 1989; 1992; Horsfield, 1990; Horsfield and Dueppenbecker, 1991; van Aarssen *et al*., 1991).

Hydrous pyrolysis is a related closed pyrolysis method that is performed in the presence of excess water (Lewan *et al*., 1979). It is also very useful for simulating fossil fuel generation from source OM (Lewan, 1985; Lewan, 1993; Lewan, 1997; Barth, 1999; Behar *et al*., 2003), and for releasing hydrocarbon biomarkers weakly bound by sulfur or oxygen linkages to the kerogen moiety of immature, sulfur-rich organic sediments (Koopmans *et al*., 1995, 1996, 1997, 1998). Another closely related method is confined gold tube pyrolysis, which is performed in pressurised gold vessels (Monthioux *et al*., 1985; Landais and Monthioux, 1988; Mansuy *et al*., 1995; Michels *et al*., 2000). The benefit of this approach is that the inert nature of gold limits secondary reactions.

MSSV pyrolysis has been widely used for kinetic studies of liquid petroleum HC formation from sedimentary source rocks, kerogens and coals (Horsfield *et al*., 1989; Horsfield, 1990; Horsfield and Dueppenbecker, 1991; Schenk and Horsfield, 1993; Diekmann *et al*., 1998; 2000). It has also been used to release hydrocarbon biomarkers from very early oil charges trapped and preserved within asphaltene fractions of heavily biodegraded or altered oils (Ruble *et al*., 2000a 2000b), as well as the characterisation of suspended organics from urban dust (Hall *et al*., 1999). The

maturation behaviour and oil generating potential of certain biopolymers have also been addressed by MSSV Py (Tegelaar *et al*., 1989a; van Aarssen *et al*., 1991).

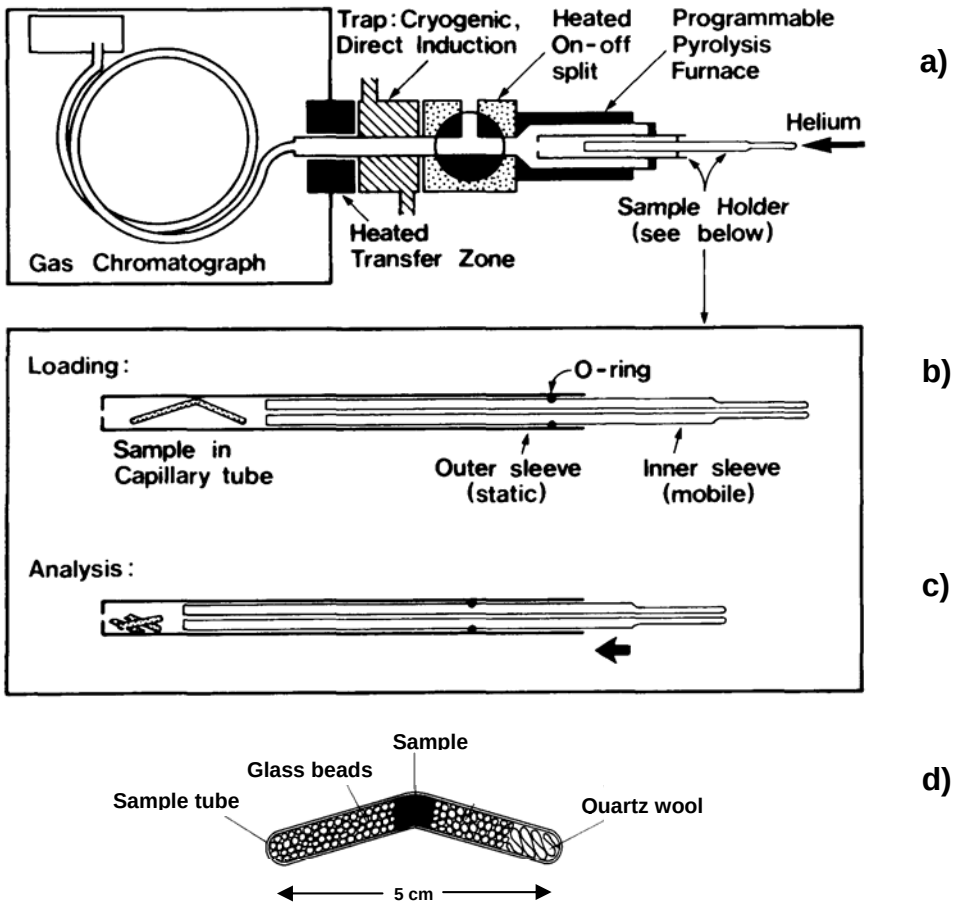

Figure 1.2 MSSV pyrolysis instrument configuration taken from Horsfield *et al*., (1991). **a)** Injector system coupled to GC inlet, **b)** Position of sample tube and inner sleeve (plunger) prior to analysis, **c)** Analysis of volatile products generated by off-line MSSV heating is performed by cracking the sample tube with the plunger, **d)** MSSV capillary tube containing sample and glass beads.

MSSV pyrolysis offers broader potential for the molecular characterisation of the complex, immature OM of more recent aquatic and terrestrial (e.g. soil OM) environments. The application of MSSV as a more general characterisation tool has received relatively little attention. In contrast to the widespread fragmentation associated with fast pyrolysis methods, the lower thermal energies of MSSV Py may provide control over fragmentation processes, facilitating the softer pyrolytic release of hydrocarbon products. Application of progressively higher thermal energy can be

used to sequentially target NOM moieties on the basis of their thermodynamic susceptibility. Hydrogen transfer reactions (Mansuy *et al*., 1995, Landais *et al*., 1993), which can partially reduce the chemical functionality of immature polar organics, may also be supported by the thermal conditions of MSSV Py. MSSV can potentially facilitate the thermal defunctionalisation of a wide variety of biochemical constituents of aquatic NOM, yielding hydrocarbon products that are more amenable to GC-MS analysis. This may effectively enable characterisation of an increased proportion of the material, including structural constituents which have historically proved recalcitrant to conventional fast pyrolysis analysis.

1.4.2 Catalytic hydro-pyrolysis GC-MS

Catalytic hydropyrolysis (HyPy) is another emerging pyrolysis technique with similar attributes to MSSV pyrolysis. HyPy involves open-system, temperature-programmed pyrolysis (300-550˚C) in the presence of a dispersed sulphided molybdenum catalyst under high hydrogen pressure (> 10 Mpa). The pyrolysis products are collected off-line in a cold-trap, allowing polarity based fractions to be separated by column chromatography prior to GC-MS analysis. HyPy can promote cleavage and reductive removal of heteroatomic bonds, including ether, sulfide, carboxyl, hydroxyl, thiols, and simple thiophenic groups (Love *et al*., 2005). It has been shown to generate very high yields of liquid hydrocarbon products (typically > 85 wt. %) from Type I-III kerogens (Snape *et al*., 1989; 1994).

The open-system configuration, rapid removal of products from the heated zone of the reactor and use of moderate heating rates (e.g. 10˚C/min), has been shown to preserve much of the structural, isomeric and isotopic integrity of the hydrocarbon precursors (Love *et al*., 1995, 1997, 2005; Sephton *et al*., 2005). Catalytic HyPy has proven effective for accessing vital biomarker profiles in circumstances where information from free hydrocarbons is limited. Geochemical applications include the generation of biomarker profiles from asphaltene fractions of heavily biodegraded crude oils to reconstruct oil charge history (Russell *et al*., 2004). In recent years catalytic HyPy has been increasingly applied to the characterisation of immature organic macromolecules, such as the organic nitrogen and bacterial biohopanepolyol constituents of immature lacustrine sediments (Bishop *et al*., 1998, Bennett *et al*., 2004) and extant algal and bacterial biomass (Bennett *et al*., 2004; Love *et al*.,

2005), as well as functionalised model compounds such as steroids and fatty acids (Sephton *et al*., 2005; Meredith *et al*., 2006). In the present project, the innovative HyPy technique is directly compared with MSSV pyrolysis by separate analysis of several extant biological materials in Chapter 2.

1.5 Scope and objectives of the present research project

The aim of this PhD research project is to assess, develop and optimise the analytical capacity of MSSV pyrolysis to extend the structural characterisation of aquatic NOM. Comprehensive MSSV analyses of a suite of aquatic NOM samples from several diverse freshwater environments, including those rich in specific organic precursors (e.g. lignin, protein, amino sugar, terpenoid) have been conducted. XAD resin and colloid fractions of NOM from pristine source reservoirs, black water rivers, groundwater aquifers, soluble soil leachates, post treated wastewater effluents and biological foulants of high pressure ultra filtration membranes have been separately studied. All NOM fractions were isolated by dialysis (colloids) and/or XAD resin adsorption (HPO/TPI), ensuring analytical consistency and direct comparability of the data.

The MSSV pyrolysate distributions were rigorously evaluated and scrutinised for evidence of additional or complementary molecular information to that provided by other pyrolytic (e.g. flash pyrolysis, thermochemolysis, hydropyrolysis), chromatographic (e.g. LC-MS), and advanced spectroscopic (e.g. ^{13}C-NMR) characterisation of the samples. This provided a robust assessment of the integrity, utility and value adding capacity of the MSSV technique. A major focus was to assess the ability of MSSV pyrolysis to discern differences in the chemical nature, structural features and biomolecular sources of NOM from different aquatic environments. The extended analytical capability provided by MSSV pyrolysis may help rectify some of the large knowledge gaps with respect to the composition, origins and early diagenetic processes of recent and extent NOM.

Confined thermal treatment of NOM can result in a variety of complex chemical reactions and the mechanistic formation of most MSSV pyrolysates is not particularly well understood. This presents a significant challenge to the realization

of the full characterisation potential of this approach. A better understanding of structural precursors of MSSV products was sought by corresponding analysis of a variety of selected model compounds of simple sugars, amino acids, fatty acids, peptides, porphyrins, lignin and tannin monomers and representative materials including polysaccharide, amino sugar, protein, lignin, wood, bark and cultured bacteria. This systematic analytical approach will help establish product-source relationships and facilitate a more robust interpretation of the data, including recognition of both selectively preserved biochemical structures, and products arising from secondary thermal processes.

The effect of temperature on MSSV pyrolysate distributions needs to be considered. The thermal properties of the organic constituents of NOM can influence both the nature and yield of the pyrolysates detected, with the generation of products proceeding at different rates according to variations in the thermal properties and stabilities of their structural precursors. MSSV experiments over a range of different thermal conditions were performed on selected samples and standard precursors to investigate the thermal profiles of several major MSSV product classes. This should help elucidate mechanistic formation pathways and provide insight into the optimal thermal conditions for targeting different biomolecular constituents of NOM.

Chapter 2

Thermal release of hopane biomarkers from bacterial terpenoids by MSSV pyrolysis of aquatic NOM

Some of the work in this chapter has been published as:

Berwick, L.J., Greenwood, P.F., Meredith, W., Snape, C., Talbot, H.M., 2009. Comparion of microscale sealed vessel pyrolysis (MSSVpy) and hydropyrolysis (Hypy) for the characterisation of extant and sedimentary organic matter. Journal of Analytical and Applied Pyrolysis, *in press*.

Greenwood, P.F., Leenheer, J.A., McIntyre, C., Berwick, L., Franzmann, P., 2006. Bacterial biomarkers thermally released from dissolved organic matter. Organic Geochemistry 37, 597-609.

2.1 Introduction

Biomarkers are organic compounds possessing unique and identifiable structures whose biological distribution is limited to specific plants or organisms (Lu *et al*., 2000). The basic structural skeleton of a biomarker preserves an unambiguous link to its biological origin, despite the possibility of some structural alteration due to diagenetic or other processes. Biomarkers are commonly used molecular tools for assessing the source inputs, degree of degradation and thermal maturity of sedimentary OM (sedOM), and for reconstructing palaeoenvironmental conditions that prevailed in the water column during sediment deposition (e.g. Philp, 1985; Philp and Gilbert, 1987, Peters and Moldowan, 1993, Ertel *et al*., 1993, van Aarssen *et al*., 2000, Pancost and Boot, 2004; Peters *et al*., 2005). Lu *et al*. (2000) suggested that there are a broad range of unique biomarkers in aquatic humic substances; however, high chemical functionality and macromolecular binding may limit their analysis by fast pyrolysis and conventional extraction methods.

Hopanes are a group of saturated triterpane biomarkers derived from amphiphilic polyhydroxy hopanoids (bacteriohopanepolyols; BHPs) present in the lipid cell membrane of many bacterial species (Ourisson *et al*., 1982). The ubiquity of microbes and the relative stability of the hydrocarbon skeleton of hopanes have resulted in their extensive use as maturity and source indicators in organic geochemical studies of crude oils and ancient sedimentary rocks (e.g. Philp and Gilbert, 1987; Bennett and Abbot, 1999; Farrimond *et al*., 2002).

Hopanes in sedOM are formed over geological timeframes through natural thermal maturation processes (diagenesis/catagenesis), which reduce the polyhydroxy functionality of the biohopanoid precursors. Free hopane products in the bitumen fraction are amenable to solvent extraction while those bound within the kerogen fraction may be thermally released by flash pyrolysis. However, the polar side chain moiety of hopanoid precursors, which can inhibit their direct GC-MS detection, is largely maintained in immature materials of recent environmental OM. As such, there has been little evidence of hopane occurrence in flash pyrolysis studies of aquatic NOM (Leenheer *et al*., 2003a), although high concentrations of hopene/hopane products have been detected in the direct flash pyrolysis GC-MS analysis of bacterial biomass (Sugden *et al*., 2005). The general absence of hopanes in pyrolytic studies of NOM isolates is likely attributed to their modest concentrations in these materials, compared with hopanoid-producing bacterial cultures.

Our initial investigation here is focused on the thermal reduction of hydroxylated biohopanoids into saturated hopane biomarkers. This well-defined maturation process serves as an appropriate natural model to demonstrate the controlled thermal alteration of biological precursors into GC amenable hydrocarbons by MSSV pyrolysis. The MSSV approach is less expensive and labour intensive than chemical degradation or derivatisation methods (e.g. *methylation* of side-chain hydroxyl groups), which have been used previously to render more of the BHP content of fossilized OM amenable to GC detection (Mycke *et al*., 1987, Richnow *et al*., 1992, Abbott *et al*., 2001). Although chemical reagents offer highly selective covalent bond cleavage and better preservation of structural and stereochemical features, they are relatively time-consuming and the yields are typically lower than that obtained

by pyrolysis, particularly for highly macromolecular matrices recalcitrant to reagent access such as kerogen and NOM (Farrimond *et al*., 2003).

To robustly interpret the source and mechanistic formation of the hopanes detected by MSSV pyrolysis it is necessary to understand the effect of different pyrolysis parameters on their composition, particularly in relation to isomerisation and carbon number distributions. In this study, a cultured sample of a hopanoid-containing bacterium (Frateuria *aurantia*), an organic biofoulant isolated from a high-pressure membrane filtration system, and two aquatic NOM samples isolated from bacterially impacted waters (Great Salt Lake, Utah, United States; Tomago Sand Beds groundwater, NSW, Australia) were analysed by MSSV pyrolysis GC-MS over the temperature range 260 – 340˚C/72hrs. Flash pyrolysis analyses of the same samples were undertaken for comparative purposes.

Previous elemental, pyrolytic (flash pyrolysis, thermochemolysis) and spectroscopic (FTIR, ^{13}C-NMR) analyses of the bio-foulant indicated a strong microbial signature with a protein and carbohydrate rich composition (Croué *et al*., 2003b). Likewise, evidence of bacterial and higher plant terpenoid precursors of the Tomago Sand Beds (TSB) NOM was recently inferred using NMR, stable carbon isotope ratios and electrospray ionisation MS (Leenheer *et al*., 2003a, McIntyre *et al*., 2005). However, whilst bacterial contribution is expected in any aquatic system, none of these analytical methods provided definitive biomarker evidence of bacterial input to the macromolecular structure of the NOM studied.

A key factor in determining source specific structural information is the ability of the analytical technique employed to preserve the main structural and stereochemical features of the precursor material. To assess the significance and integrity of the hopane signature obtained by MSSV Py, the hopanoid-rich bacterium and biofoulant were additionally analysed using the advanced methods of LC-MS and hydropyrolysis (HyPy) GC-MS. Both of these techniques have demonstrated considerable utility for characterising the polar constituents of extant biomass and recent sedimentary OM, and have been shown to provide an accurate representation of the hopanoid composition of bacterial sources.

Like MSSV pyrolysis, catalytic HyPy promotes the reductive release of hydrocarbon biomarkers from functionalised and macromolecularly bound precursors (Love *et al*., 2005). Love *et al*. (1995) demonstrated the ability of this technique to maximise the yields of covalently bound biomarkers in pyrolysates, without adversely affecting their structure and stereochemistry. The hopane distributions detected from bacterial cultures (Love *et al*., 2005), recent sediments (Bishop *et al*., 1998, Farrimond *et al*., 2003) and kerogens of different thermal maturity (Love *et al*., 1995, Murray *et al*., 1998) have been shown to be dominated by extended hopanes up to C_{35} with the biologically inherited but thermodynamically unstable 17β(H), 21β(H) configuration.

Recent developments in the application of LC-MS have facilitated the direct detection of intact BHPs from bacterial species and recent sedimentary environments (Talbot *et al*., 2001; 2003 a,b; Talbot and Farrimond, 2007). A range of BHP structures differing subtly in the nature and positioning of the functional groups on their alkyl side chains have been exhibited by different taxonomic classes of bacteria (Talbot and Farrimond, 2007). These biomarkers can be used to fingerprint hopanoid-producing bacterial populations, and monitor microbial processes (Talbot and Farrimond, 2007) in geological as well as modern aquatic and terrestrial environments. Compositional data measured by LC-MS will be used to scrutinise the integrity of the hopane distributions formed by MSSV Py and HyPy.

2.2 Experimental

2.2.1 Samples

2.2.1.1 *Frateuria aurantia*

An acetic-acid bacterium ***Frateuria aurantia*** DSM 6220^T (DSM = German National Culture Collection, Braunschweig, Germany) known to contain hopanoids (Joyeux *et al*., 2004) was grown at 30˚C for 24 hours in yeast-peptone-mannitol medium that consisted of yeast extract, 5.0 g; peptone, 3.0 g; mannitol, 25.0 g, in 1 litre distilled water, sterilized at 121˚C for 15 min. After growth, the cell density was 4.0±0.6 x 10^9 cells mL^{-1}. Cells were harvested from 1850 mL of medium by centrifugation at 10 000 g, washed in distilled water, recollected by centrifugation and the resultant pellet was freeze dried, to produce a dry weight of 0.7503 g. The pellet contained 9.86 x 10^9 cells $(mg\ dry\ wt)^{-1}$.

2.2.1.2 Membrane biofoulant

Membrane sheets were obtained from spiral-wound modules taken at different stages of the train of a high-pressure membrane filtration unit of a drinking water treatment plant. The ***biofoulant*** (BF) material was physically removed from the membrane, sonicated in MQ water and centrifuged to separate the soluble and insoluble fractions (Croué *et al*., 2003b). The insoluble fraction is discussed in this Chapter.

2.2.1.3 Aquatic NOM

Polarity-based fractions of lake and ground water NOM were the hydrophobic acid (HPO-A) fraction of Tomago Sand Beds (Australia) and the hydrophobic neutral fraction (HPO-N) of Great Salt Lake (US). Brief descriptions of the geographical locations and environmental settings of the water samples and the isolation procedures used to obtain the organic fractions are given below.

Great Salt Lake (GSL) Utah, USA, is highly saline and dominated by primary phytoplanktonic production and secondary bacterial production although terrigenous inputs, from coniferous and deciduous plants from the Wasatch Mountains to the east, occur during the spring snowmelt (Domalgalski *et al*., 1989). Water was sampled on April 1, 2002 at the lake surface in the south arm of the GSL at latitude N40˚53'56", longitude W112˚20'56" (Leenheer *et al*., 2004). Sampling occurred prior to the annual green algae bloom that is responsible for the majority of annual biomass productivity (Stephens and Gillespie, 1976). 38 litres of water, filtered through an alum porosity glass fibre filter, was passed through a 1 L bed-volume XAD-8 column. Following passage of the sample, the column was rinsed with 4 L of 0.01 M hydrochloric acid (HCl) and desorbed with 800 mL of 75% acetonitrile/25% water, which was evaporated and freeze-dried to isolate the HPO-N fraction.

Tomago Sand Beds (TSB) are located 200 km north of Sydney, Australia and are a dune system of reworked Pleistocene marine sands that have developed podsol soil profiles since stabilisation (12,000 BP). The groundwater is used as a source of potable water for nearby populations. Dry sclerophyll forests dominate the overlying vegetation at the site with low areas containing swamps. The vegetation is rich in terpenoid resins and pine plantations are within 1 km of the sampling site (Prosser and Roseby, 1995). Groundwater was sampled on March 18, 2002 from a control

piezometer located at UTM 56H 372940 1371020 (Leenheer *et al*., 2003a). NOM was isolated by adsorption onto XAD-7 resin using a modified method of Thurman and Malcolm (1981), which is detailed in McIntyre *et al*. (1997). This yielded a hydrophobic acid fraction determined to be 98% fulvic acid, which was analysed without further fractionation. The isolated HPO-A fraction had an elemental composition of 52.3% C, 4.1% H and 41.5% O. A full characterisation of this sample is given in McIntyre *et al*. (2005).

2.2.1.4 AGSO standard oil 2

AGSO Standard Oil 2 was used as an instrument calibration and chromatogram peak reference standard. This sample comprises a branched and cyclic hydrocarbon fraction derived from a mixture of five crude oils that collectively contain the full suite of terpenoid (e.g. hopane) and sterane biomarkers typically found in Australian crude oils (Sandison and Edwards, 2003).

2.2.2 Molecular analysis

2.2.2.1 MSSV pyrolysis GC-MS

Small amounts of sample (~ 0.1-1.0 mg) were loaded into the middle of 5 cm long x 5 mm i.d. glass tubes. Glass beads were added above and below the sample to fill the void volume and the ends of the tubes were flame sealed, taking care to avoid direct heating of the sample. The sealed vessels were then heated isothermally in an oven for a period of 72 hrs. The *Frateuria aurantia* bacterium, TSB fraction and biofoulant were separately heated at several temperatures within the range 240-340˚C. Limited quantities of GSL NOM precluded its analysis at different temperatures so a single analysis was performed at 300˚C, which was the optimal temperature for hopane generation from the TSB NOM fraction (see R&D section below).

The sealed vessel was inserted into the MSSV injector port installed on the top of a GC oven and subjected to a two stage analytical procedure (Horsfield *et al*., 1992). Two separate analyses referred to henceforth as analysis ***I*** and analysis ***II***, were run for selected samples in the following manner.

I. The first procedure involved cracking the tube with the plunger whilst keeping the injector port isothermal at 300˚C. Under these conditions the

MSSV pyrolysates generated by the off-line heating were released and transferred by the helium carrier gas to the GC column. The products were initially trapped at the beginning of the column in liquid nitrogen for 1 minute. The GC-MS analysis was started on removal of the liquid nitrogen trap.

II. The second procedure involved heating the residue from analysis ***I*** in the injector port from 300˚C to 540˚C at a rate of 40˚C min^{-1} to induce fast pyrolysis of the residue. A liquid nitrogen trap at the beginning of the GC column was used throughout the heating process to trap the released volatiles. The GC-MS analysis was started on removal of the liquid nitrogen trap.

Fresh aliquots of unheated samples were also subjected to the first analytical procedure (***I***) to help distinguish MSSV pyrolysates from volatile products of the fresh sample at the 300˚C temperature of the MSSV injector port. The GSL fraction was not analysed in this manner due to very limited sample quantities.
GC-MS analysis was performed with a Hewlett Packard (HP) 5890 Series II GC interfaced to an Autospec (UltimaQ) double focusing mass spectrometer. A 25 m x 0.32 mm x 0.52 μm film DB5 capillary column was used with helium carrier gas at a constant pressure of 55 kPa. The bacterial extract was typically run with a 100 mL min^{-1} split flow and the NOM fractions and bio-foulant with a 20 mL min^{-1} split flow. One of two GC oven temperature programmes was used.

1. An initial temperature of 40˚C, 2 minutes isothermal, then programmed at 4˚C min^{-1} to 300˚C with 20 minutes isothermal – typically used when investigating the full range of products.
2. An initial temperature of 40˚C, 2 minutes isothermal, then increased at 10˚C min^{-1} to 240˚C then 4˚C min^{-1} to 300˚C and held isothermal for 20 minutes – typically used when specifically monitoring the high molecular weight (MW) hopane products.

Full scan (FS), selected ion recording (SIR) and multiple (metastable) reaction monitoring (MRM) data were separately acquired for the bacterial extract and NOM fractions. FS analyses were performed over the range *m/z* 50 – 550 at ~3 scans s^{-1}. Ions analysed by SIR in magnet stepping mode were *m/z* 123.1, 172.1, 177.1, 183.1, 191.1, 205.2, 217.2, 218.2 and 231.2. MRM analyses of spontaneous field free

region (FFR1) transitions of the molecular ions of the C_{27}-C_{31} hopanes (*m/z* 370, 384, 398, 412 and 426) to their diagnostic *m/z* 191 fragment ion were conducted using the linked B/E scan approach. Other generally standard mass spectral conditions were typically applied: e.g., electron energy = 70 eV; filament current = 200 μA, source temperature = 250˚C; accelerating potential = 8 kV, electron multiplier = 200 V for FS and SIR analyses and 350 V for MRM analyses; mass resolution = 1000 for FS and 500 for SIR and MRM.

2.2.2.2 Flash pyrolysis GC-MS

Flash pyrolysis of 0.5-1 mg sample was performed at ca. 600˚C (heating rate ca. 20˚C/ms) for 20 seconds using a Chemical Data Systems analytical Pyroprobe 5250 with the pyrolysis chamber maintained at 300˚C. Pyrolysates were analysed using an HP 6890 gas chromatograph coupled with an HP 5973 mass selective detector (MSD). A 30 m x 0.25 mm i.d. ZB5-MS column with 1 μm phase (J&W Scientific) was used with helium as the carrier gas (93 kPa) in split mode (split ratio 20:1 - 50:1). The GC oven temperature was initially held at –20˚C for 1 min, increased at 4˚C/min to a final temperature of 320˚C and held isothermal for 20 min. Full scan mass spectra were acquired between *m/z* 20-620 at ca. 4 scans sec^{-1}. The mass spectrometer operated in electron impact mode at 70 eV with a transfer line temperature of 320˚C and a source temperature of 230˚C. Tentative peak identification was based on retention time, mass spectral comparison with library spectra (Wiley 275 and NIST 05 databases) and literature data.

2.2.2.3 Liquid chromatography-mass spectrometry

Following the procedure outlined in Talbot and Farrimond (2007) the freeze-dried samples of F. *aurantia* (50 mg) and BF (57 mg) were ground to a fine powder and extracted with dichloromethane/methanol (180 mL, 2:1 v/v). The extract was evaporated under a stream of N_2 and an aliquot was acetylated (acetic anhydride-pyridine, 4 mL; 1:1 v/v; 50˚C, 1 h). The reagents were removed by rotary evaporation and the derivatised sample dried under a stream of N_2, and then dissolved in ca. 1 mL methanol/2-propanol (60/40 v/v) prior to LC-MS analysis. Reverse-phase HPLC analysis was carried out as described by Talbot *et al*. (2003 a,b) using a Surveyor HPLC system (Thermofinnigan, Hemel Hempstead, UK) fitted with a Genesis (Jones Chromatography, Hengoed, UK) C_{18} 4 μm column (150 mm x

4.6 mm i.d.) and a 4 μm pre-column (10 mm x 4.6 mm) of the same material. Separation was performed at ambient temperature with a flow rate of 0.2 mL min^{-1} and the following gradient profile: 90% A and 10% B (0-3 min); 59% A, 1% B and 40% C (at 25 min), then isocratic to 60 min (where A = methanol, B = water and C = 2-propanol; all HPLC grade, from Fisher [Loughborough, UK]).

LC-MS was performed using a ThermoFinnigan LCQ ion trap mass spectrometer equipped with an atmospheric pressure chemical ionization (APCI) source operated in positive ion mode. LC-MS parameters included a capillary temperature of 155˚C, APCI vaporizer temperature of 400˚C, corona discharge current of 8 μA, sheath gas flow of 40 and auxiliary gas of 10 (arbitrary units). The instrument was tuned as described by Talbot *et al*., 2003a. LC-MS analysis was carried out in data-dependent mode with three scan events: SCAN 1. Full mass spectrum (400-1300 *Da*); SCAN 2. Data dependent MS^2 spectrum of the most intense ion from SCAN 1; SCAN 3. Data dependent MS^3 spectrum of the most intense ion from SCAN 2. Detection was performed at an isolation width of *m/z* 3.0 and fragmentation with normalized collisional dissociation energy of 35%. Structures were assigned by comparison with authentic standards and published spectra (Talbot *et al*., 2003 a,b) or by comparison of APCI MS^2 and MS^3 spectra with those of known compounds.

2.2.2.4 Catalytic hydropyrolysis GC-MS

2.2.2.4.1 Catalytic hydropyrolysis

The apparatus and procedure for fixed bed hydropyrolysis has been described in detail elsewhere (Love *et al*., 1995; Meredith *et al*., 2006). Prior to hydropyrolysis, the samples were mixed with a dispersed sulphided molybdenum catalyst [$(NH_4)_2MoO_2S_2$, 10 mg, dissolved in a minimum of 20% methanol in water], dried gently and then transferred into the pyrolysis reactor. The catalyst-loaded samples (38 mg F. *aurantia*, 30 mg BF) were then heated in a stainless steel reactor tube from ambient temperature to 250˚C at 300˚C min^{-1}, then to 500˚C at 8˚C min^{-1}. A constant hydrogen flow of 5 L min^{-1}, measured at ambient temperature and pressure, ensured that the volatile products were quickly removed from the reactor vessel. The products were collected in a silica gel-filled trap cooled with dry ice as described in Meredith *et al*. (2004).

2.2.2.4.2 Fractionation of hydropyrolysates using liquid chromatography

Silica gel 60 (0.063 – 0.200 mm, Merck) used for column chromatography was activated at 120˚C for more than 8 hours, and pre-rinsed with solvent prior to use. The hydropyrolysate (adsorbed on silica gel) was introduced to the top of a large column (20 cm x 0.9 cm i.d.) of activated silica gel. The aliphatic hydrocarbon (saturate) fraction was eluted with purified *n*-pentane (35 mL), the aromatic fraction with a solution of purified dichloromethane in *n*-pentane (30%, 40 mL) and the polar fraction with equal parts dichloromethane and methanol (40 mL). The extracts were then concentrated to small volume (ca. < 1mL) prior to GC-MS analysis by evaporation of the solvent on a sand bath at 60˚C.

2.2.2.4.3 GC-MS analysis of hydropyrolysis fractions

GC-MS analysis of the aliphatic hydrocarbon fractions was performed using a Hewlett-Packard 6890 GC interfaced to a Hewlett-Packard 5973 mass selective detector (electron energy 70eV, source temperature 230˚C, electron multiplier 1800 V, transfer line 310˚C). Data acquisition was performed in full scan (*m/z* 50-550 at ~ 2 scan s^{-1}) or selected ion mode (26 ions, 20 ms dwell time). The sample (1 μL) was injected by an HP 6890 autosampler fitted to the vaporizing injector, which was operated in pulsed splitless mode (207 kPa, 0.5 min) using helium as carrier gas (constant flow, 1 mL min-1). GC separation was performed on a 60 m x 0.25 mm i.d. x 0.25 μm Phenomenex ZB-5 fused silica capillary column. The GC oven temperature was programmed from 40˚C (1 min) to 310˚C (30 min) at a rate of 3˚C min^{-1}.

2.3 Results and Discussion

2.3.1 MSSV pyrolysate distributions of aquatic NOM and membrane biofoulant

2.3.1.1 Tomago Sand Beds and Great Salt Lake NOM

The GC-MS total ion chromatograms (TIC) generated by off-line MSSV thermal treatment (300˚C/72hr, analysis ***I***), and subsequent fast pyrolysis of the residue (300 – 540˚C @ 20˚C/min, analysis ***II***), for the Great Salt Lake (GSL) and Tomago Sand Beds (TSB) NOM samples are shown in **Figure 2.1**. MSSV pyrolysis yielded large and complex distributions of GC amenable products and exhibited excellent reproducibility for repeat analyses. The TICs obtained from three replicate 300˚C/72hr analyses (***I***) of SRFA are provided in Appendix 1. Quantitatively, the MSSV data (***I***) showed generally higher product abundances compared to the residue pyrolysates (***II***). This was more pronounced for the GSL data (**Fig. 2.1 a-b**).

Qualitatively similar product distributions were detected from the TSB and GSL NOM fractions. The major products identified on the basis of mass spectral interpretation were alkyl substituted aromatics including benzenes, phenols, naphthalenes and phenanthrenes. Hopane biomarkers were generally minor pyrolysates. However, unlike the well defined hopanoid precursor, hopane product relationship, source assignment of many pyrolysates can be challenging due to the largely undefined MSSV thermal behaviour of their precursors and potential derivation from multiple sources. A preliminary assessment of the potential origins of some of the prominent aromatic products is given here, however more detailed investigations of the thermal formation and structural precursors of several major MSSV product classes is provided in Chapters 3, 4 and 5.

Alkyl phenols (AP) were major pyrolysates of both NOM fractions. These products are also commonly detected by flash pyrolysis of aquatic and terrestrial NOM (e.g. van Heemst *et al*., 1999). APs are most often attributed to polyphenolic lignin and tannin constituents of plant tissues. Previous flash pyrolysis and thermochemolysis GC-MS analyses of TSB NOM also yielded low concentrations of lignin derived products (McIntyre *et al*., 2005). The aromatic substitution patterns of the phenolic constituents of lignin and tannin are different (Leenheer and Rostad, 2004) and this may be reflected in the isomeric distribution of AP MSSV products, provided the isomeric integrity is preserved during thermal treatment (see Chapter 4).

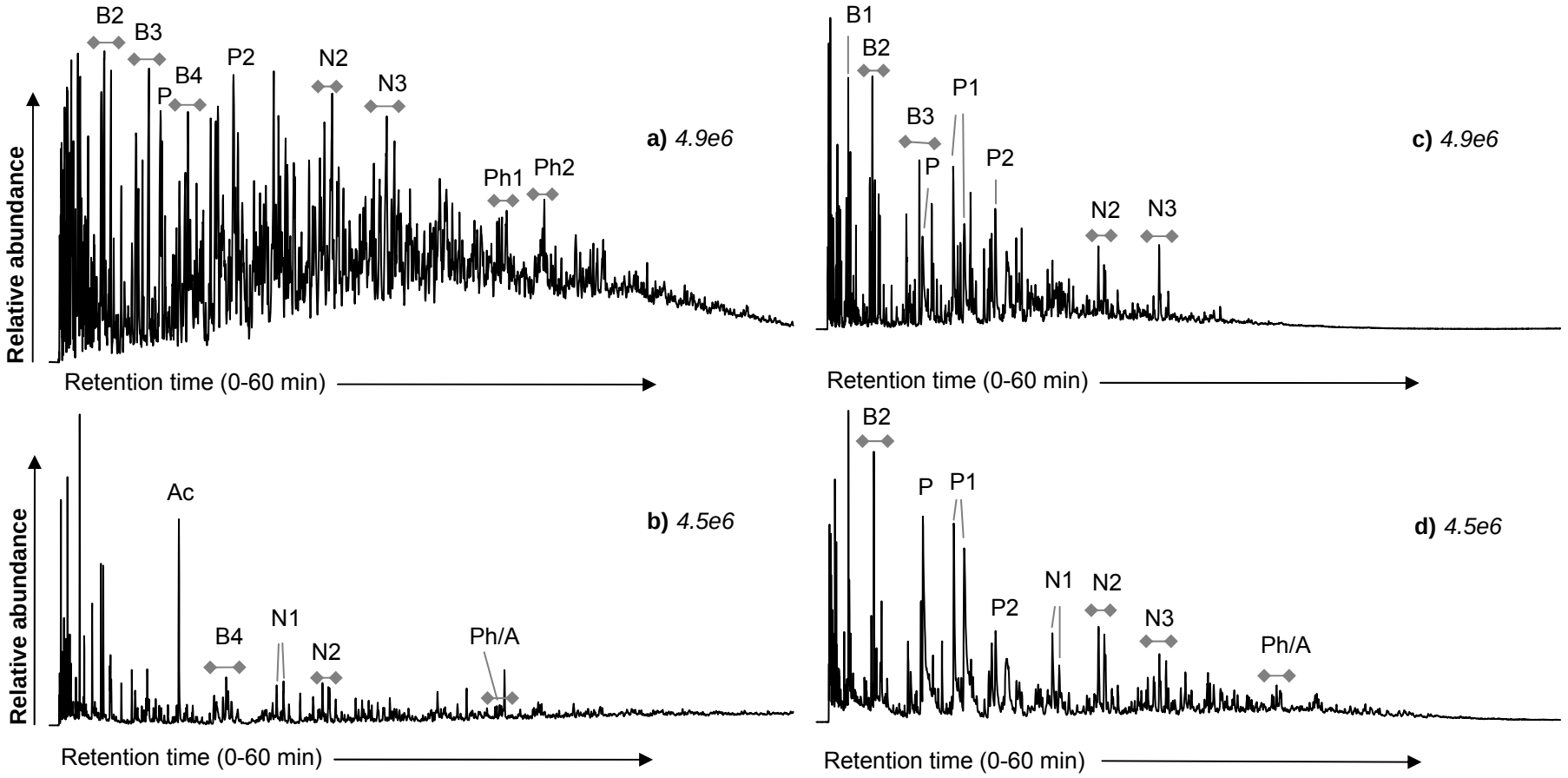

Figure 2.1 Total ion chromatograms from 300˚C/72 hr MSSV pyrolysis GC-MS analysis of Great Salt Lake (GSL) and Tomago Sand Beds (TSB) DOM. **a)** analysis ***I*** of GSL; **b)** analysis ***II*** of GSL; **c)** analysis ***I*** of TSB and **d)** analysis ***II*** of TSB. B=benzene; P=phenol; N=naphthalene; Ac=acetophenone; Ph=phenanthrene; A=anthracene; B2 etc. = C_2-benzene (e.g. ethylbenzene, dimethylbenzene). Relative abundances of a-d indicated in italics.

Alkyl naphthalenes (AN) were also identified in high abudnance from the TSB and GSL fractions. These products possibly derive from land plant terpenoids present in plant resins, bark and leaf tissues, which are recognized as a major source of aromatic hydrocarbons in thermally mature sediments, coals and crude oils (Smith *et al*., 1995; Watson *et al*., 2005). The TSB site, for example, is dominated by plant species rich in terpenoid resins (Prosser and Roseby, 1995). Several recent spectroscopic studies (FTIR, ^{13}C-NMR; Leenheer *et al*., 2003a, Leenheer and Rostad, 2004; Leenheer *et al*., 2004) have identified the significant precursor contribution of terpenoids in certain aquatic fulvic acids, including TSB, despite an absence of diagnostic products from flash pyrolysis and thermochemolysis. MSSV pyrolysis of TSB yielded low concentrations of the plant terpenoid biomarkers retene and cadalene, which were identified by their diagnostic fragment ions (*m/z* 219 and *m/z* 183 respectively; Greenwood *et al*., 2006). Sesquiterpenoid precursors (e.g. cadinane, cadinol) of cadalene are ubiquitous in higher plants (van Aarssen *et al*., 1991), while retene is a characteristic thermal maturation product of abietane diterpenoids present in conifer resins (Simoneit, 1985). The MSSV formation and terpenoid origins of several aromatic product classes are discussed in detail in Chapter 3.

2.3.1.2 Biofoulant

The TIC from MSSV pyrolysis analysis ***I*** (300˚C/72hr) of the membrane biofoulant (BF) is shown in **Figure 2.2a**. The BF yielded a very different product distribution to the aquatic NOM, dominated by $C_{10} - C_{31}$ *n*-alkanes and low MW alkyl substituted nitrogen and oxygen heterocycles, including furans, pyrroles, pyridines and indoles. Hopane biomarkers were detected in higher relative abundance than in the TSB and GSL fractions, reflecting the more significant contribution from extant microbial biomass.

A fresh aliquot (i.e. unheated) of the BF was also analysed (**Fig. 2.2b**) to distinguish MSSV pyrolysates from the volatile products of the fresh sample at the MSSV injector port temperature of 300˚C. The fresh sample was weighed and sealed inside an MSSV capillary tube but was not subjected to the off-line heating. Several volatile products were detected from the fresh material, however the higher abundances and many additional products observed in MSSV analysis ***I*** can be attributed to the off-line thermal treatment. It has previously been reported that

approximately 10% of Type I or II kerogen/OM is volatilized with the MSSV conditions of 300˚C/72hr (Horsfield and Dueppenbecker, 1991), however this value may be significantly higher for immature thermally labile biomass such as the BF. Unfortunately, the on-line nature of MSSV pyrolysis does not lend itself to simple quantitative determination of pyrolysate yields.

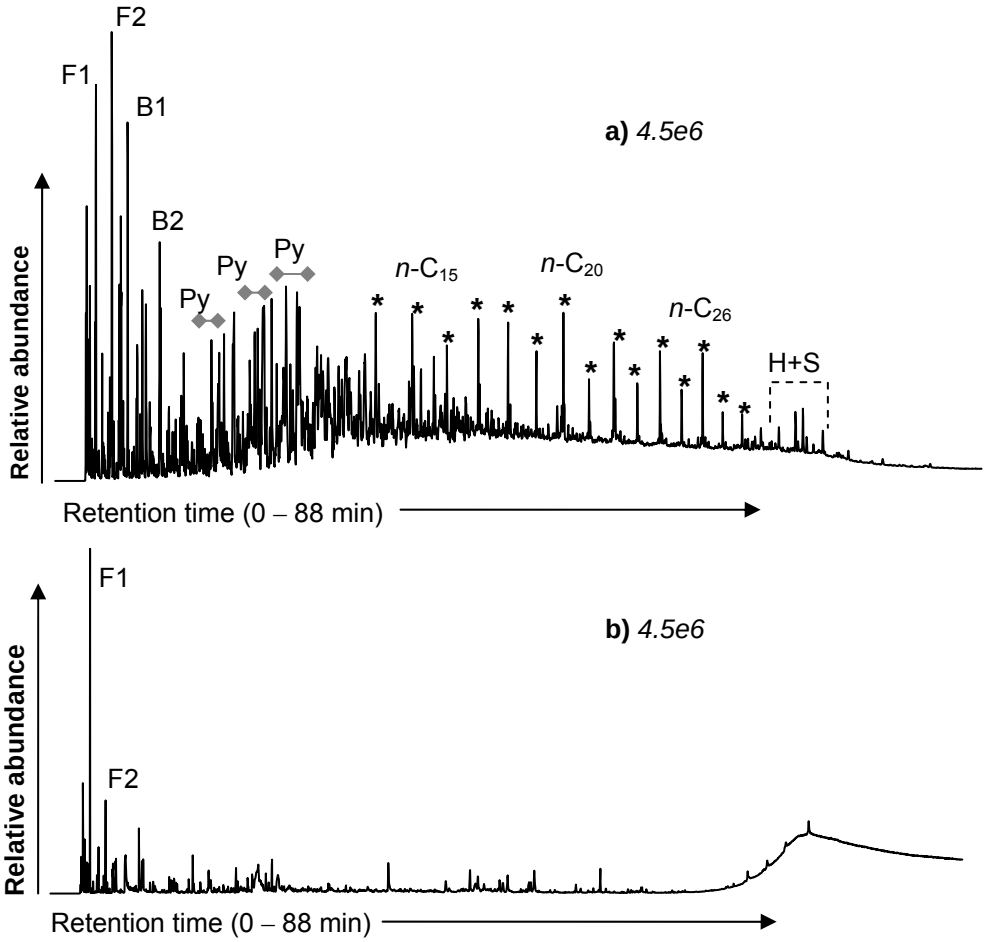

Figure 2.2 TICs from MSSV pyrolysis GC-MS analysis ***I*** of the bio-foulant sample; **a)** 300˚C/72 h, and **b)** fresh non-matured sample (300˚C injector temperature). F=furan, B=benzene, Py=pyrrole, H=hopanes, S=steranes, ***** = *n*-alkanes. Numbers refer to carbon number of alkyl substituents. Relative abundances of a-b are indicated in italics.

In addition to the hopanes, which are discussed in more detail in section 2.3.3.2, several other source diagnostic products were detected from the BF. For example, C_{27} and C_{29} sterenes and steranes, highlighted in the *m/z* 215 + 217 summed ion chromatogram of **Figure 2.3a**, derive from functionalised triterpenoids present in eukaryote cell membranes, mainly algae and higher plants (Mackenzie *et al*., 1982).

The steroid and sterol precursors of several steranes identified in sedimentary environments and oil asphaltenes have been well defined (Mackenzie *et al*., 1982).

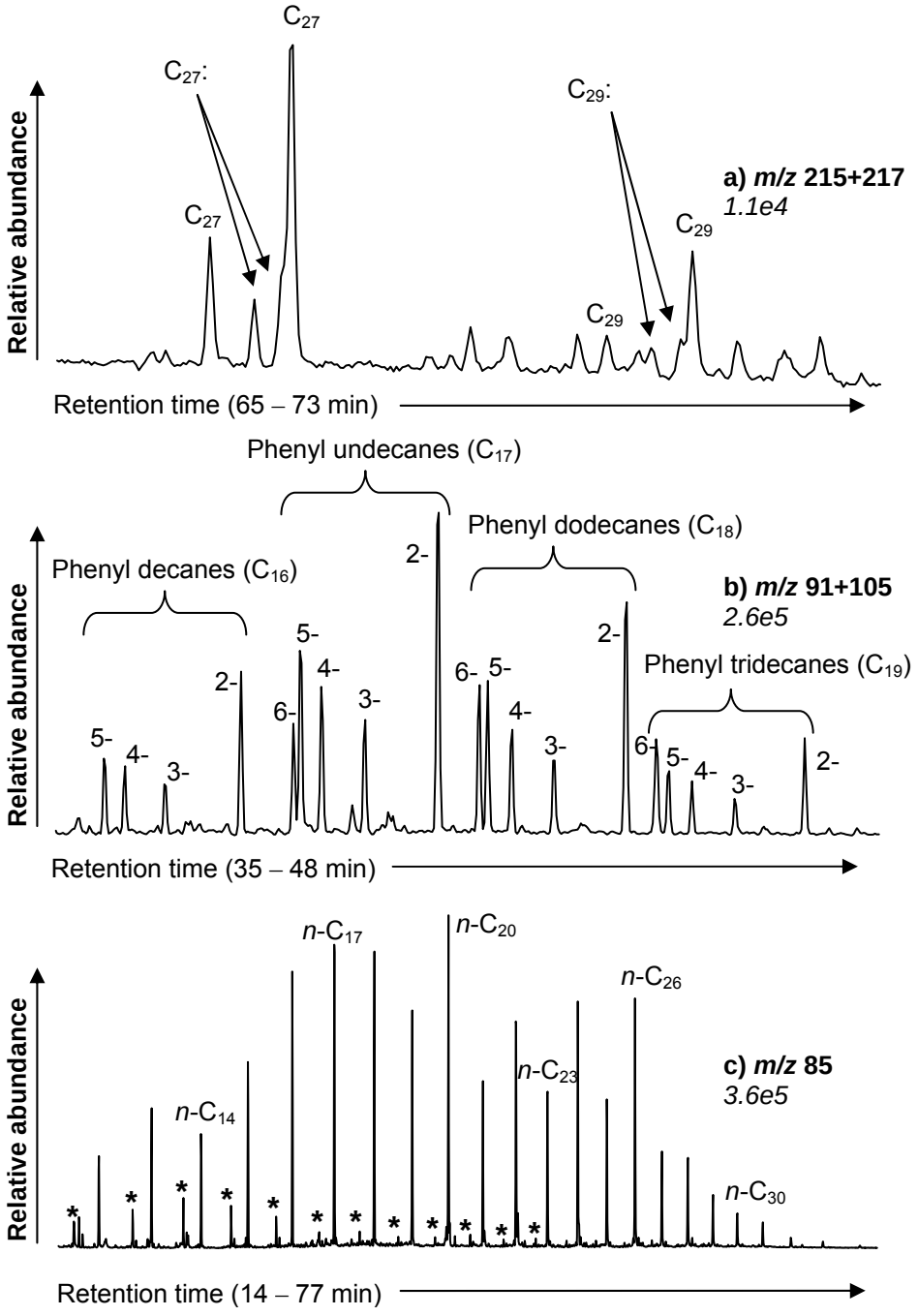

Figure 2.3 Selected ion chromatograms from MSSV pyrolysis GC-MS analysis ***I*** (300˚C/72 hr) of the biofoulant showing the distribution of **a)** C_{27} and C_{29} steranes and sterenes (:) **b)** C_{16}-C_{19} phenylalkanes (numbers indicate position of the phenyl substitution on the alkyl chain), and **c)** *n*-alkanes. ***** = monomethyl alkanes. Relative abundances of a-c are indicated in italics.

An interesting feature of the MSSV pyrolysate of the BF was the detection of a prominent series of $C_{16} – C_{19}$ phenylalkanes, highlighted in the *m/z* 91 + 105 summed ion chromatogram of **Figure 2.3b**. These compounds are environmental markers for common detergents produced from linear alkylbenzenesulfonates and are often found in wastewater effluents (Eganhouse *et al*., 1983, Takada and Ishiwatari, 1987). The incorporation of these compounds into the macromolecular structure of the biofoulant probably occurs during membrane cleaning processes. Isomers with the phenyl substitution towards the interior of the chain, such as the 5- and 6-phenylalkanes, are more resistant to biodegradation than the 2- and 3-phenyl isomers (Takada and Ishiwatari, 1990). The prominence of the 2-phenylalkanes thus indicates that the detergent residues in the BF are only partially biodegraded. Kruge and Permanyer (2004) previously reported similar long chain phenylalkanes in flash pyrolysates of contaminated marine sediments. However, these products were not detected by flash pyrolysis of the BF, which can be attributed to the polarity of the sulfonate group or excessive thermal degradation of the alkyl side chains. MSSV Py facilitates the analysis of these amphiphilic compounds by reductive removal of the sulfonate group, whilst preserving the parent hydrocarbon structure.

Similarly, controlled MSSV reduction of the fatty acid moiety of the BF yielded a distinctive distribution of C_9-C_{30} *n*-alkanes and C_{10}-C_{19} mono-methyl alkanes, which are well resolved by the *m/z* 85 selected ion chromatogram shown in **Figure 2.3c**. The $< C_{16}$ *n*-alkanes reflect an odd–over-even carbon preference, which reverses to an even over-odd-carbon preference above *n*-C_{19}. Corresponding flash pyrolysis revealed only trace levels of *n*-alkanes and the precursor fatty acids, although previous thermochemolysis analysis (Croué *et al*., 2003b) revealed a distinctive fatty acid methyl ester (FAME) distribution reflecting a smooth Gaussian profile from *n*-C_{22} to *n*-C_{36} (*n*-C_{30} maximum) with no notable carbon number preferences. The distinctive carbon trends evident in the *n*-alkane distribution of the MSSV data is indicative of a biosynthetic source, possibly including long chain fatty acid precursors loosely bound by ester/ether linkages within microbial or algal precursors (Grice *et al*., 2003). Similarly, mono-methylated alkane series are common among bacterial lipids (Koster *et al*. 1999), reflecting the significant microbial element of the foulant structure.

The remainder of this chapter is focused on the MSSV detection of hopane biomarkers. Functionalised bacteriohopanepolyols constitute a minor part of the lipid cell membrane and the total cell biomass of certain bacterial species; hence their concentrations in aquatic NOM are likely to be relatively low. This is consistent with the low abundance of hopanes detected from the TSB and GSL pyrolysates. Despite accounting for less than 1% of the total hydrocarbon signal, the thermal formation of hopanes represents an elegant model with which to monitor the controlled transformation of functionalised NOM precursors. The structural alterations of biohopanoids during geothermal maturation are very well defined (e.g. Mackenzie *et al*., 1980; Rohmer *et al*., 1992), allowing the integrity of the hopane data obtained by MSSV Py to be robustly evaluated.

2.3.2 LC-MS identification of intact bacteriohopanepolyols

LC-MS was used to assess the bacteriohopanepolyol (BHP) structural constituents of F. *aurantia* and the biofoulant. Compositional data measured by LC-MS will be used to evaluate the integrity of the hopane signatures generated from these BHP precursors by MSSV pyrolysis. The aquatic NOM fractions (TSB, GSL) were not analysed by this technique due to insufficient sample quantities.

The relative abundances of the major bacteriohopanepolyols (as their acetylated derivatives) detected by LC-MS analysis of F. *aurantia* and the biofoulant are shown in the mass chromatograms of **Figure 2.4** and **2.5**. Corresponding structural assignments of the parent BHPs are given in **Figure 2.6**. The major BHPs from F. *aurantia* were bacteriohopanepentol cyclitol ether (**9**) and bacteriohopanetetrol cyclitol ether (**7**) as well as bacteriohopanetetrol (**1**) and minor quantities of bacteriohopanetetrol glucosamine (**8**). Each of these BHPs possesses a basic C_{35} hydrocarbon skeleton, although *F. aurantia* is also known to biosynthesise C_{30} hopanoids including the monounsaturated diploptene, hop-17(21)-ene and fern-7-ene (Joyeux *et al*., 2004), which lack alkyl side-chain hydroxylation.

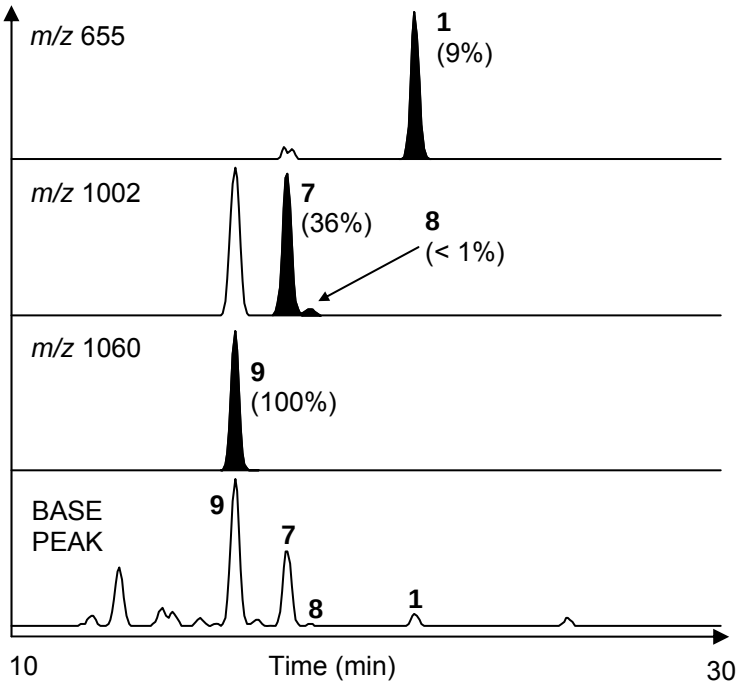

Figure 2.4 Mass chromatograms of acetylated BHPs obtained by LC-APCI-MS of Frateuria *aurantia.* The abundance relative to the most intense component is shown in parentheses.

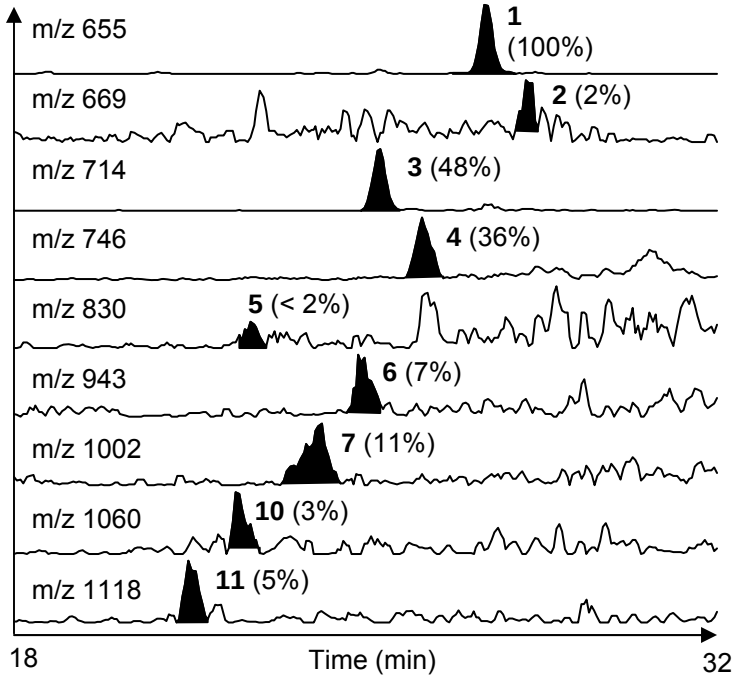

Figure 2.5 Mass chromatograms of acetylated BHPs obtained by LC-APCI-MS of the biofoulant. The abundance relative to the most intense component is shown in parentheses.

The diverse bacterial community of the biofoulant reflects a more complex hopanoid profile (**Fig. 2.5**) with at least 7 known BHPs detected, together with two tentatively identified novel compounds. The C_{35} hopanoids bacteriohopanetetrol (**1**) and bacteriohopanetetrol cyclitol ether (**7**), also detected in F. *aurantia*, as well as peak **3** (35-aminobacteriohopanetriol) may derive from a variety of possible source organisms (Talbot and Farrimond, 2007). More source diagnostic information may be inferred from the detection of 35-aminobacteriohopanepentol (**5**), which is only found in Type I methane oxidising bacteria (Talbot *et al*., 2001) and adenosylhopane (**4**) a suspected indicator of soil microbes (Talbot and Farrimond, 2007; Cooke *et al*., 2008). Compound **6** (tentatively named bacteriohopanetetrol pseudopentose; Talbot *et al*., 2008) has also only previously been reported in one species of cyanobacteria, although additional sources of these particular markers may also exist. Two additional novel compounds, bacteriohopanepentol glucosamine (**10**; Coolen *et al*., 2008) and bacteriohopanehexol glucosamine (**11**), were tentatively identified in the BF, both of which have no known source at present.

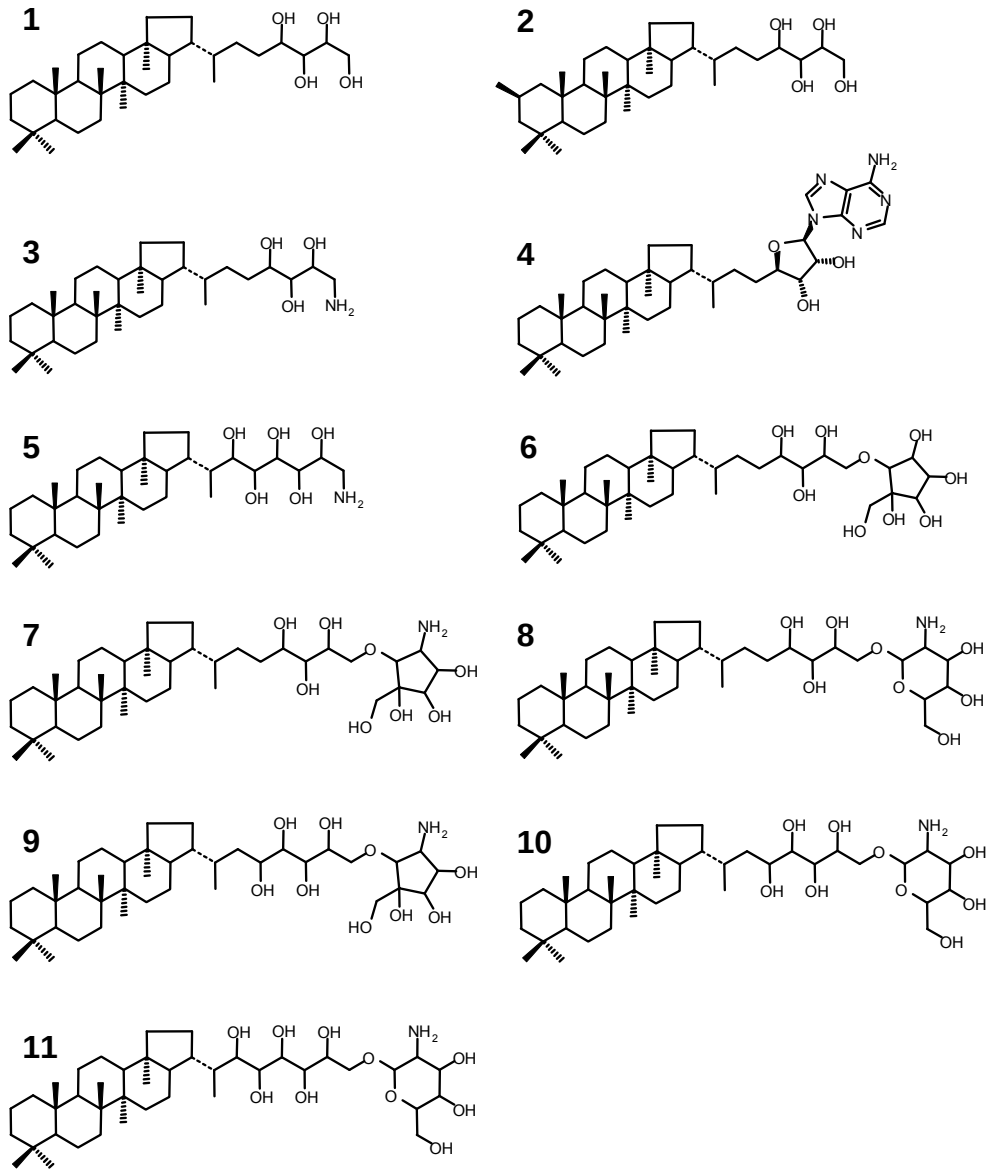

Figure 2.6 Parent BHPs identified by LC-APCI-MS analysis of F. *aurantia* and membrane biofoulant.

2.3.3 Detection of hopane biomarkers by MSSV pyrolysis GC-MS

The isomeric identities of the major hopane products detected by both MSSV pyrolysis and catalytic hydropyrolysis from the bacterial culture, biofoulant and NOM fractions are listed in **Table 2.1.** These were assigned based on GC-MS correlation with AGSO Standard Oil 2 and separate selected ion recording (SIR) of *m/z* 191 and multiple (metastable) reaction monitoring (MRM) analyses. SIR and MRM analyses offer greater sensitivity over full scan acquisition with MRM also providing an additional dimension of selectivity.

Table 2.1 Hopane and hopene compounds identified in MSSV pyrolysis and hydropyrolysis analyses of Frateuria *aurantia,* bio-foulant and aquatic NOM fractions. Ions comprising a 4-point mass spectrum (i.e. the 4 most abundant ions) are also shown.

Peak No.	Abbrev.	MW	Compound	4pt. Mass Spectrum
1	T_s	370	18α(H)-22, 29, 30-trisnorhopane	370, 355, 191, 149
2	C_{27}H:	368	Monounsaturated C_{27} hopene	368, 231, 191, 147
3	T_m	370	17α (H)-22, 29, 30-trisnorhopane	370, 355, 191, 149
4	27β	370	17β (H)-22, 29, 30-trisnorhopane	370, 355, 191, 149
5	C_{29}H:	396	Monounsaturated C_{29} hopene	396, 379, 191, 121
6	C_{29}H	398	17α, 21β-30-norhopane	398, 383, 191, 177
7	C_{29}H:	396	Monounsaturated C_{29} hopene	396, 367, 231, 191
8	C_{30}H:	410	Monounsaturated C_{30} hopene	410, 367, 231, 191
9	C_{29}βα	398	17β, 21α-30-normoretane	398, 383, 191, 177
10	C_{30}H	412	17α, 21β-hopane	412, 397, 191, 95
11	C_{29}ββ	398	17β, 21β-30-norhopane	398, 383, 191, 177
12	C_{30}βα	412	17β, 21α -moretane	412, 397, 369, 191
13	C_{30}H:	410	Monounsaturated C_{30} hopene	410, 367, 231, 191
14	C_{31}H(S)	426	17α, 21β-30-homohopane (22S)	426, 411, 205, 191
15	C_{31}H(R)	426	17α, 21β-30-homohopane (22R)	426, 411, 205, 191
16	C_{30}ββ	412	17β, 21β-hopane	412, 397, 369, 191
17	C_{31}βα(R)	426	C_{31} 17β, 21α-hopane (22R)	426, 411, 205, 191
18	C_{32}H(S)	440	C_{32} 17α, 21β-hopane (22S)	440, 425, 219, 191
19	C_{32}H(R)	440	C_{32} 17α, 21β-hopane (22R)	440, 425, 219, 191
20	C_{32}βα(R)	440	C_{32} 17β, 21α-hopane (22R)	440, 425, 219, 191
21	C_{31}ββ	426	17β, 21β-30-homohopane	426, 369, 205, 191
22	C_{33}H(S)	454	C_{33} 17α, 21β-hopane (22S)	454, 439, 233, 191
23	C_{33}H(R)	454	C_{33} 17α, 21β-hopane (22R)	454, 439, 233, 191
24	C_{33}βα(R)	454	C_{33} 17β, 21α-hopane (22R)	454, 439, 233, 191
25	C_{32}ββ	440	C_{32} 17β, 21β-hopane	440, 369, 219, 191
26	C_{34}H(S)	468	C_{34} 17α, 21β-hopane (22S)	468, 453, 247, 191
27	C_{34}H(R)	468	C_{34} 17α, 21β-hopane (22R)	468, 453, 247, 191
28	C_{33}ββ	454	C_{33} 17β, 21β-hopane	454, 369, 233, 191
29	C_{35}H(S)	482	C_{35} 17α, 21β-hopane (22S)	482, 467, 261, 191
30	C_{35}H(R)	482	C_{35} 17α, 21β-hopane (22R)	482, 467, 261, 191
31	C_{35}βα(R)	482	C_{35} 17β, 21α-hopane (22R)	482, 467, 261, 191
32	C_{34}ββ	468	C_{34} 17β, 21β-hopane	468, 369, 247, 191
33	C_{35}:H	480	Monounsaturated C_{35} hopene	480, 369, 259, 191
34	C_{35}:H	480	Monounsaturated C_{35} hopene	480, 367, 259, 191
35	C_{35}ββ	482	C_{35} 17β, 21β-hopane	482, 369, 261, 191
36	C_{35}:H	480	Monounsaturated C_{35} hopene	480, 367, 259, 191

2.3.3.1 Hopanes from *Frateuria aurantia*

Freeze-dried cells of the bacterium Frateuria *aurantia* were analysed at several different MSSV pyrolysis temperatures over the range 260 – 340˚C (72hrs). As expected, the full scan GC-MS analysis ***I*** (300˚C/72hr) of the hopanoid-rich bacteria detected hopanes in much higher abundance than the aquatic NOM fractions and BF. The *m/z* 191 selected ion chromatogram in **Figure 2.7a** shows the hopane profile of F. *aurantia*. Separate SIR and MRM analyses (**Fig. 2.8a-f**) were conducted to aid specific identification of the compounds.

C_{27} – C_{33} hopanes were detected with the major isomers being the C_{29} and C_{30} 17β, 21α hopanes (9 and 12) and the C_{27} and C_{29}–C_{33} (22R)-17β, 21β hopane series (4, 11, 16, 21, 25 and 28). The prominent 22R-ββ stereochemical isomers are inherited from the precursor BHPs biosynthesised by F. *aurantia*, however, some isomeric rearrangement is evident from the abundance of βα and αβ stereoisomers. The relatively low proportion of hopane products >C_{33} also indicates that thermal degradation of the alkyl side chain has occurred. Several C_{27} and C_{29}-C_{30} monounsaturated hopanes (2, 7, 8, and 13) were also detected by MSSV pyrolysis, although their exact isomeric configuration was not confirmed. Joyeux *et al*. (2004) previously identified trace quantities of mono-unsaturated triterpenes based on the C_{30} carbon skeleton (e.g. diploptene, hop-17(21)-ene and fern-7-ene) by derivatisation and GC-MS of extracted F. *aurantia* cells.

No hopane products were detected from the analysis of a fresh aliquot of F. *aurantia* as shown by the *m/z* 191 selected ion chromatogram in **Figure 2.7b**. This can be attributed to macromolecular binding and high structural polarity of the precursor hopanoids, which significantly inhibits their direct GC analysis. Flash pyrolysis (**Fig. 2.7c**) of the bacterium detected low concentrations of several C_{27} and C_{29}-C_{31} hopane and hopene products (2, 4, 7, 9, 11, 16 and 21), which likely derive predominantly from the hydroxyl free unsaturated triterpenes (diploptene, hop-17(21)-ene and fern-7-ene) present in F. *aurantia*. The much higher abundances and additional hopane products identified by MSSV Py can be attributed to the more efficient thermal reduction of hydroxylated BHP precursors, rendering a greater proportion of the BHP content amenable to GC analysis.

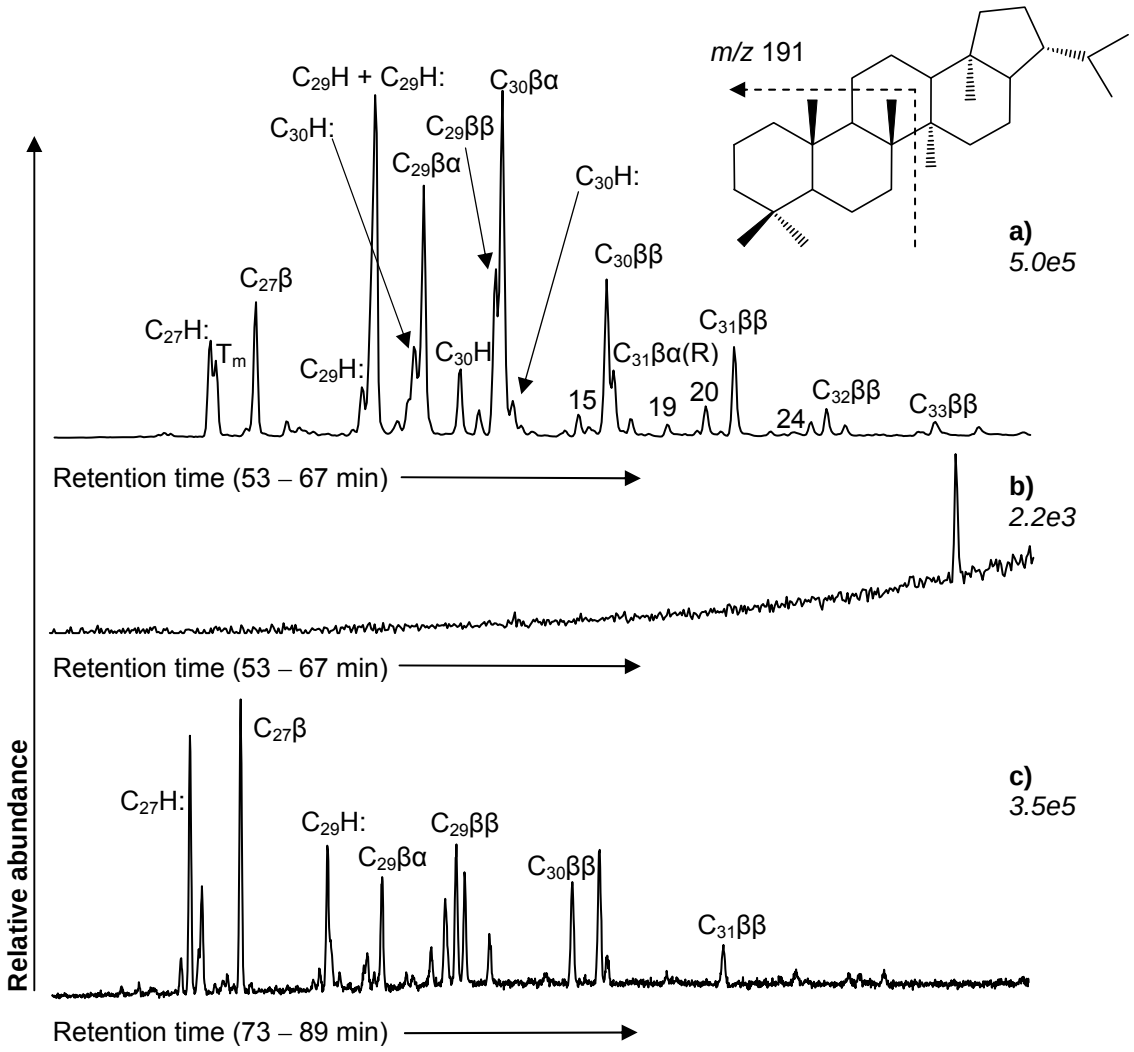

Figure 2.7 Partial *m/z* 191 chromatogram from **a)** 300˚C/72 h MSSV pyrolysis GC-MS (scan mode); **b)** fresh unheated sample (300˚C injector temperature); and **c)** flash pyrolysis (550˚C/20 seconds) GC-MS of Frateuria *aurantia*. The insert shows the structure of the $C_{30}17\alpha$, 21β hopane, with indication of the AB ring fragment responsible for the prominent *m/z* 191 ion. Relative abundances of a-c are indicated in italics. Hopane assignments are listed in Table 2.1.

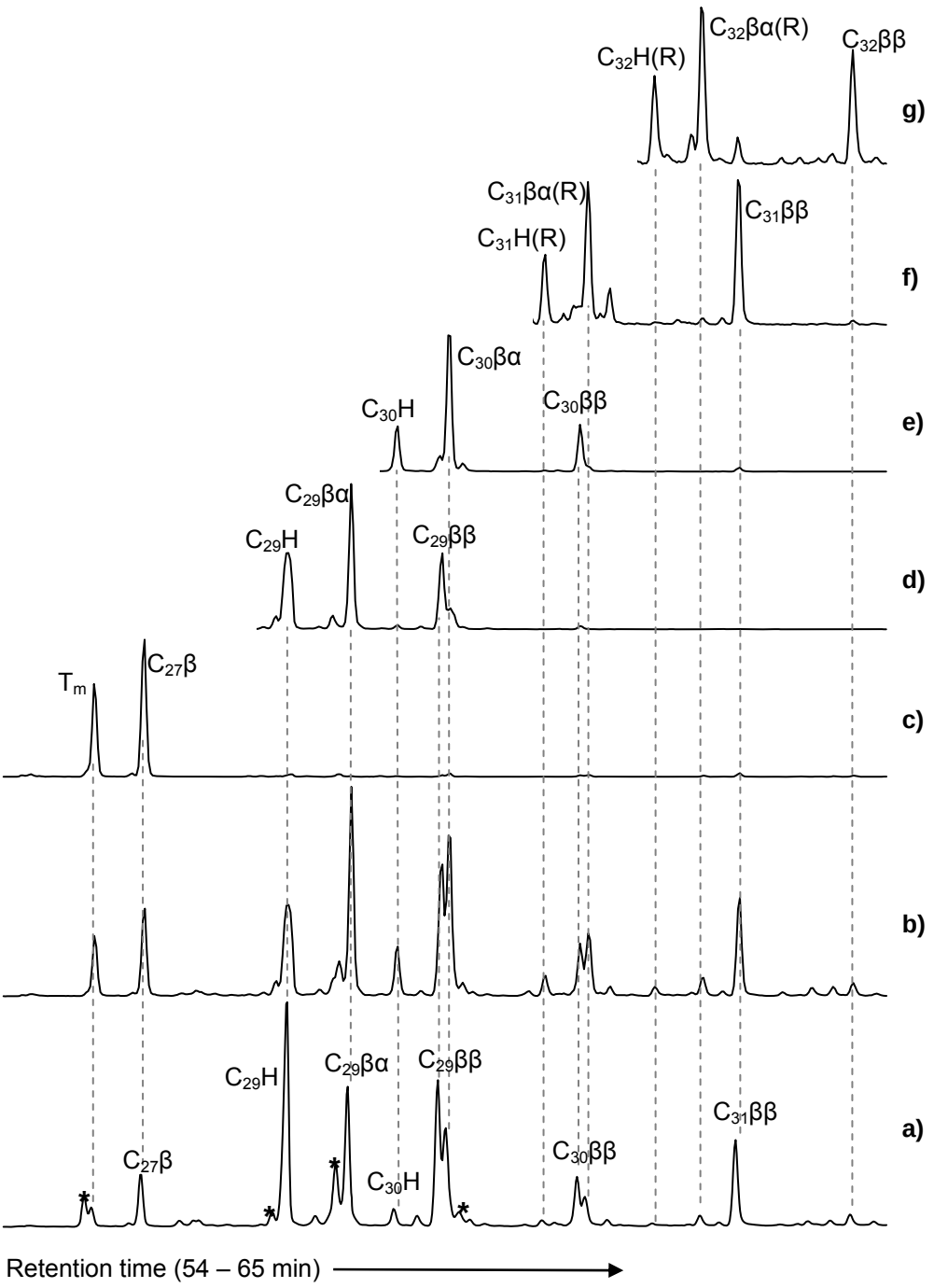

Figure 2.8 Hopane distributions from the 300˚C/72 h MSSV pyrolysis GC-MS analysis ***I*** of F. *aurantia*: **a)** Partial *m/z* 191 chromatogram from SIR analysis (***** = hopenes); and partial chromatograms from MRM analysis showing; **b)**∑ (M to *m/z* 191) where M = parent ion of C_{27} & C_{29}– C_{32} hopanes; **c)** *m/z* 370 – 191; **d)** *m/z* 398 – 191; **e)** *m/z* 412 – 191; **f)** *m/z* 426 – 191 and **g)** *m/z* 440 – 191. Hopane assignments are listed in Table 2.1.

The *m/z* 191 selected ion chromatograms highlighting the hopane distribution of *F. aurantia* at separate MSSV temperatures of **(a)** 260, **(b)** 300 and **(c)** 340˚C/72hr are shown in **Figure 2.9**. At 260˚C the distribution is dominated by monounsaturated C_{27}, C_{29} and C_{30} hopenes (2, 7 and 8) and the C_{27} and C_{29}-C_{32} 17β, 21β hopanes (4, 11, 16, 21 and 25). At 300˚C there is an increase in the overall abundance of hopane products and a notable increase in the relative abundance of the C_{29}-C_{32} βα and αβ isomers (6, 9, 10, 12, 17 and 20). At 340˚C significant changes in the distribution are evident, most notably a loss of the C_{29}-C_{32} ββ products and a significant reduction in the abundance of unsaturated products as a result of hydrogenation of the double bonds. Conversely, an increase in the relative abundance of the αβ and βα isomers (14, 15, 17, 19, 20 and 24) was evident at the higher pyrolysis temperature.

The changes observed in the hopane distribution with more severe thermal conditions are largely consistent with geothermally controlled isomeric transitions of hopanes. Mackenzie *et al*. (1980) demonstrated the conversion of ββ isomers to the more thermodynamically stable αβ series in sedimentary OM of increasing thermal maturity. Separate artificial maturation studies using hydrous pyrolysis conducted at various temperatures from 220˚C - 330˚C also showed a general decrease of ββ isomers with increasing temperature (Koopmans *et al*., 1996). However, the MSSV data needs to be considered with some caution since the molecular maturity indicators from natural and artificial heating are not always identical and can vary with different sample matrices. For example, Sugden and Abbott (2002) showed that the closed system pyrolysis temperature of 330˚C for just 8 hours was sufficient to induce epimerisation of ββ isomers into βα and αβ forms from thermally immature oil shales.

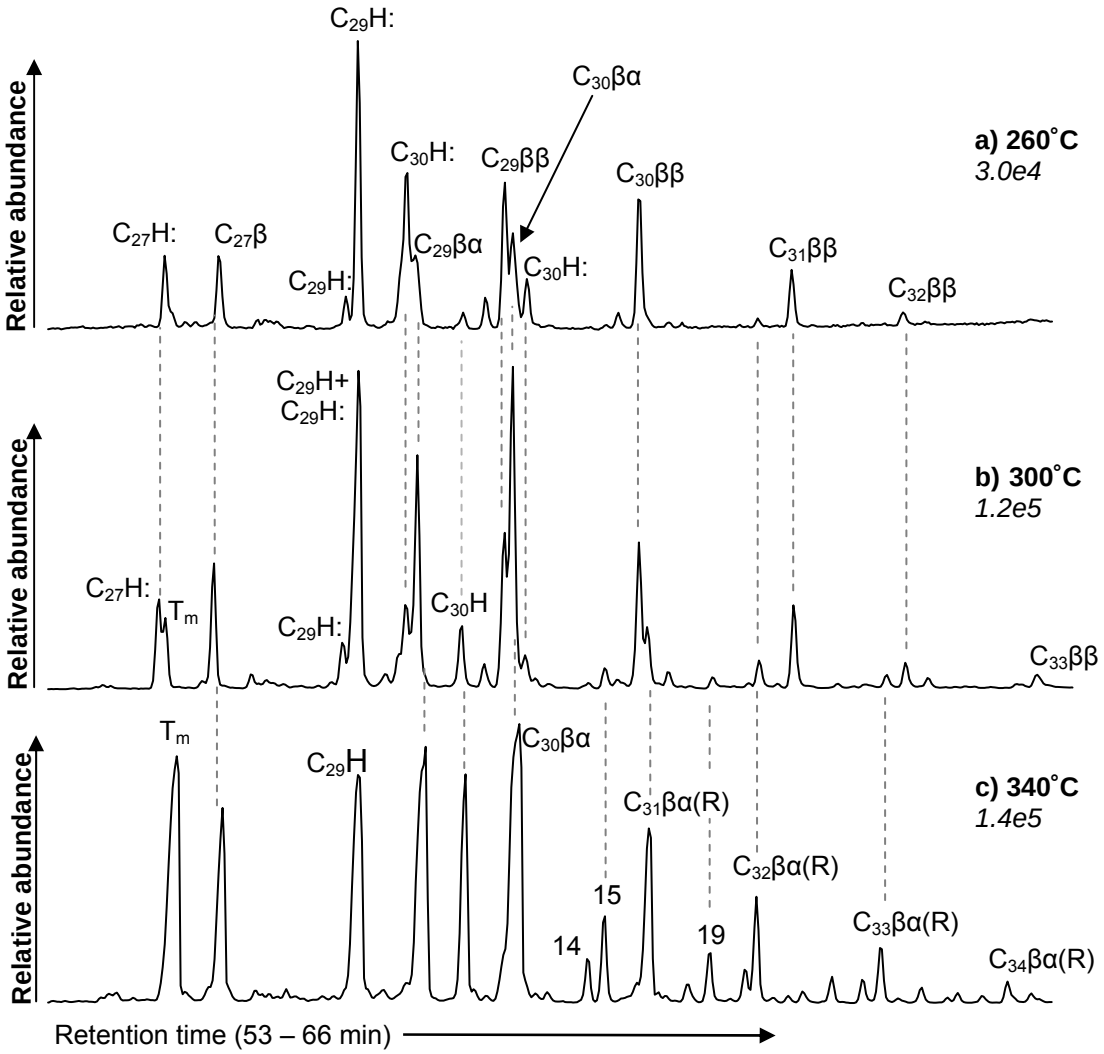

Figure 2.9 Partial *m/z* 191 chromatogram from MSSV pyrolysis GC-MS (scan mode) of Frateuria *aurantia* with MSSV pyrolysis conditions of **a)** 260˚C/72 h; **b)** 300˚C/72 h; and **c)** 340˚C/72 h. Relative abundances of a-c are indicated in italics. Hopane assignments are listed in Table 2.1.

2.3.3.2 Hopanes from biofoulant

The *m/z* 191 selected ion chromatograms of **Figure 2.10** show the C_{27} – C_{32} hopanoid distribution detected by MSSV pyrolysis of the bio-foulant over the temperature range 260 - 340°C/72hr. The consistently high hopane signal reflects the substantial input of microbial biomass to the foulant. The 300ºC/72hr distribution (**Fig. 2.10c**) was similar to that observed for *F. aurantia* under the same MSSV pyrolysis conditions. The most prominent isomers are the C_{29} norhopanes (αβ, ββ, βα; 6, 9 and 11), C_{30} αβ hopane (10), C_{30} and C_{31} βα hopanes (12, 17) and several C_{29} – C_{30} monounsaturated hopanes (7, 8 and 13). As observed for the bacterium,

hopanoid products were not detected in the volatile components of the fresh (i.e. unheated) bio-foulant. Flash pyrolysis (data not shown) also failed to detect hopanes which rules out the likelihood that those observed following the off-line MSSV thermal treatment were due to contamination from fossil fuels (Rowland and Maxwell, 1984).

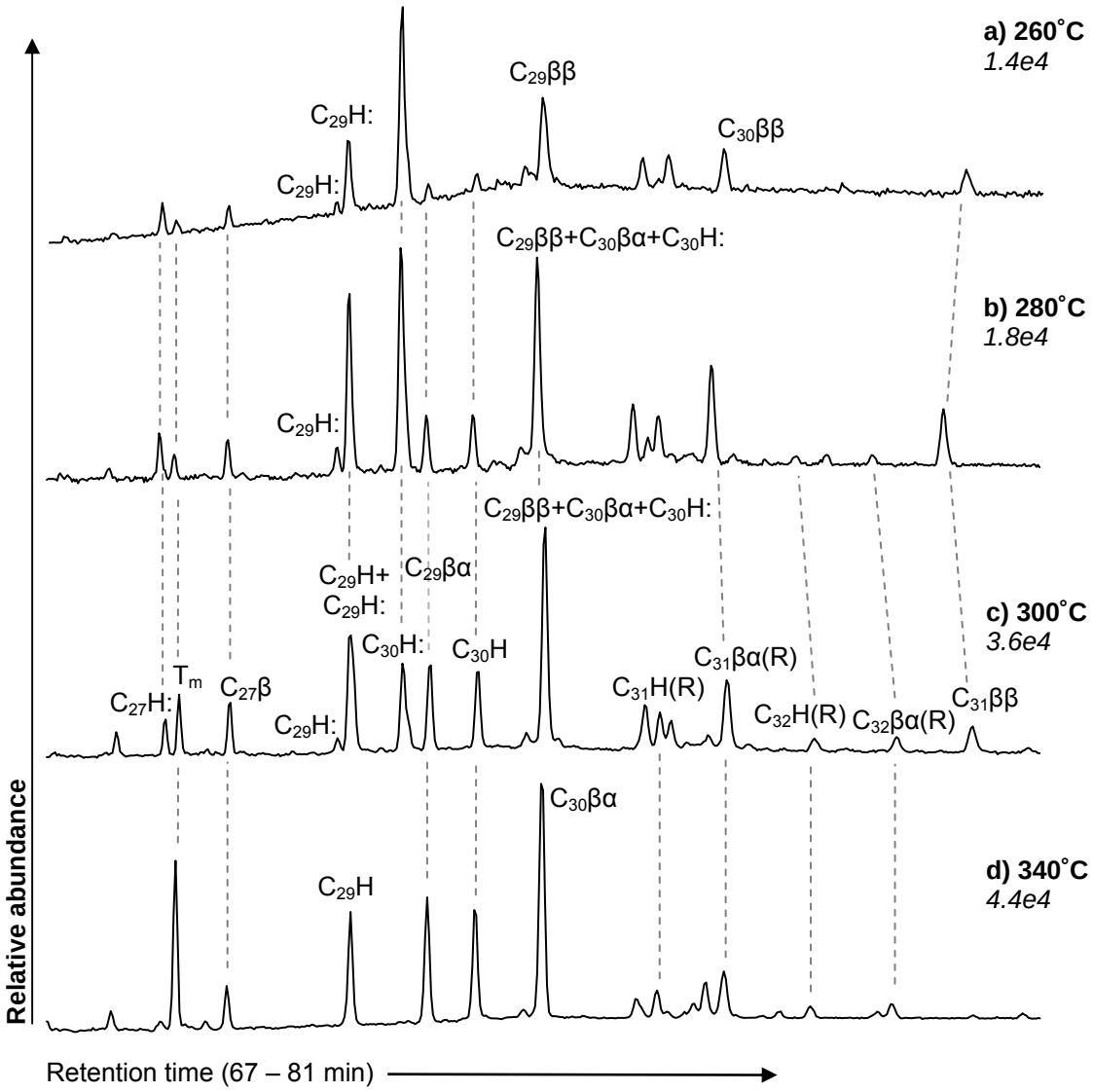

Figure 2.10 Partial *m/z* 191 chromatogram from MSSV pyrolysis GC-MS (scan mode) of biofoulant with MSSV pyrolysis conditions of **a)** 260˚C/72h ; **b)** 280˚C/72 h; **c)** 300˚C/72 h; and **d)** 340˚C/72 h. Relative abundances of a-d are indicated in italics. Hopane assignments are listed in Table 2.1.

The thermal profile of the hopanoid distributions from the bio-foulant was similar to the bacterial culture. At 260˚C/72h relatively few hopanes were detected. Low temperatures may partially inhibit the GC detection of hopanoid products due to insufficient reduction of the polyhydroxy side chain or only partial thermal release from the macromolecular network of the foulant. From 280-300˚C/72h the distribution is relatively stable apart from a decrease in the relative abundance of the hopenes (2, 7 and 8) at the higher temperature. By 340˚C, isomeric rearrangements include a reduction in ββ forms and loss of all unsaturated products. Thermal cracking reactions are also more pronounced at the higher temperature, with a reduction in abundance of the $>C_{31}$ products.

2.3.3.3 Hopanes from Tomago Sand Bed and Great Salt Lake NOM

The full scan GC-MS data of TSB and GSL NOM revealed much lower concentrations of hopane biomarkers compared to the bacterial culture and bio-foulant. As such, these products were subsequently targeted by selected ion recording (SIR) and multiple (metastable) reaction monitoring (MRM) experiments. The SIR (*m/z* 191) profiles of TSB NOM for MSSV analysis ***I*** at pyrolysis temperatures over the range 280 - 310˚C (at a constant 72h) are shown in **Figure 2.11**.

Compared to the bacterial culture and bio-foulant, hopanes were observed over the narrower temperature window of 290-310˚C, with highest abundances at 300˚C/72hrs. This is likely due to the much lower concentrations of BHP precursors in aquatic NOM but may also reflect synergistic effects imposed by the heterogenous sample matrix, which may inhibit the thermal release and reduction of hopanoid products or contribute to thermal degradation. These influences may be subtle and less apparent for samples containing high hopanoid concentrations, accounting for the wider temperature range at which hopanes were detected from F. *aurantia* and the BF. An offline temperature of 300˚C was previously identified to provide greater yields of hopanes than higher temperatures from the asphaltene fraction of biodegraded oils over a 72-hour period (Ruble *et al*., 2000a; 2000b). Pyrolysis of the MSSV residues (analysis ***II***) of both TSB and GSL (300˚C/72hrs) showed similar hopane distributions (data not shown), but of lower abundance by a factor of 3-10 compared to the MSSV analysis ***I*** pyrolysates (Greenwood *et al*., 2006). This is

attributed to the pyrolytic release and reduction of additional macromolecularly bound hopanoid structures. As observed for the BF, hopanes were absent in analysis ***I*** and ***II*** of the fresh (i.e. unheated) TSB sample. Flash pyrolysis GC-MS analyses of the fresh GSL and TSB NOM samples similarly revealed no hopane products, indicating that an oil contamination origin was unlikely.

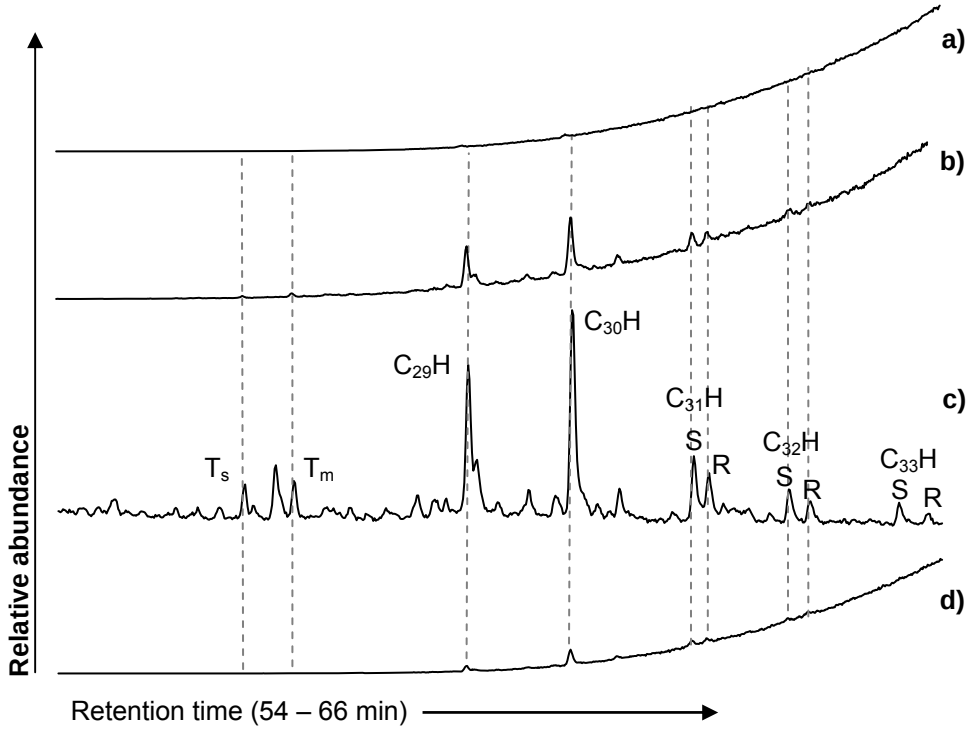

Figure 2.11 Partial *m/z* 191 chromatogram from MSSV pyrolysis GC-MS (SIR mode) of Tomago Sand Beds (TSB) NOM with MSSV pyrolysis conditions of **a)** 280˚C/72 h; **b)** 290˚C/72 h; **c)** 300˚C/72 h and **d)** 310˚C/72 h. Hopane assignments are listed in Table 2.1.

Partial SIR (*m/z* 191) and MRM (M → *m/z* 191) chromatograms of the C_{27}-C_{31} hopanes from analysis ***I*** of 300˚C/72hrs MSSV treated GSL and TSB samples are shown in **Figure 2.12**. MRM products (**Fig. 2.12c-f**) were assigned by retention time correlation with the hopanes detected in AGSO Standard Oil 2. The major products from both samples were the C_{29} and C_{30} αβ hopanes (6, 10), with decreasing proportions of the higher MW (> C_{31}) hopanes. The most notable difference in the hopane distribution was the occurrence of several hopenes (*) of significant abundance in the GSL data, although the low full scan mass spectra signals prevented isomeric assignment. The detection of these compounds in GSL but not TSB may be due to subtle maturity differences between the two samples.

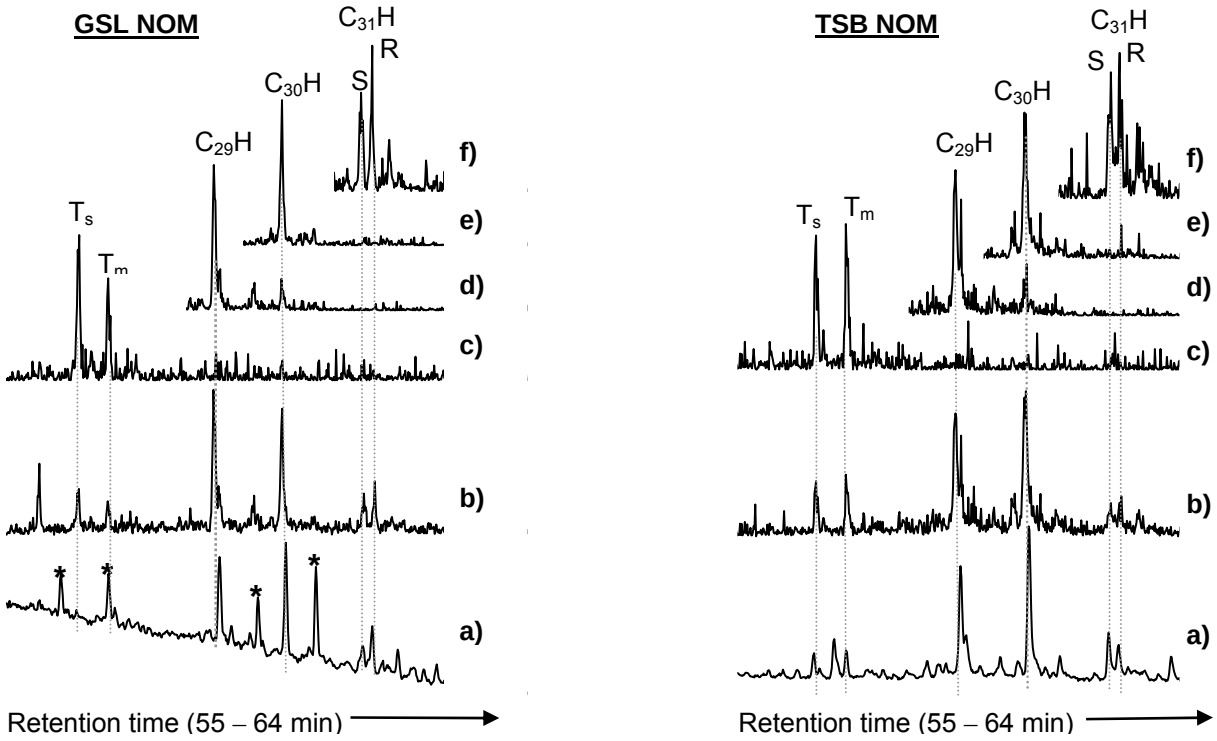

Figure 2.12 Hopane distributions from the 300˚C/72 h MSSV pyrolysis GC-MS analysis ***I*** of Great Salt Lake (GSL) NOM and Tomago Sand Beds (TSB) NOM: **a)** Partial *m/z* 191 chromatogram from SIR analysis (***** = hopenes); Partial chromatograms from MRM analysis showing; **b)** ∑ (M to *m/z* 191) where M = parent ion of C_{27} & C_{29}– C_{31} hopanes; **c)** *m/z* 370 – 191; **d)** *m/z* 398 – 191; **e)** *m/z* 412 – 191; and **f)** *m/z* 426 – 191. Hopane assignments are listed in Table 2.1.

Relatively high concentrations of terpenes may occur in OM of low thermal maturity, as seen for both the F. *aurantia* and BF data, but the absence of terpenes from TSB, even at lower MSSV temperatures (e.g. 290˚C) suggests specific differences in the hopanoid precursors present in the two samples.

The less thermally stable ββ and βα hopane isomers were not detected in either the TSB or GSL NOM fractions, despite being major components of the hopane distributions of the extant bacterium and BF. In addition, much lower proportions of higher MW (> C_{31}) hopanes were detected from the NOM samples. This may indicate that the BHP precursors of aquatic NOM are more susceptible to alkyl chain degradation and isomeric rearrangements during thermal treatment than those present in extant biological material. Although significant reduction or complete loss of ββ isomers at higher pyrolysis temperature (e.g. 340˚C/72 hours) was observed for the bacterium and bio-foulant (**Fig. 2.9 and 2.10**), the absence of these biologically inherited products in the TSB and GSL data even under the milder pyrolysis conditions of 280-300˚C/72hr suggests more extensive epimerisation to the stable αβ forms. Alternatively, isomeric transitions may have occurred prior to the off-line MSSV thermal treatment during early diagenetic transformation of BHPs in the water column, however this is considered unlikely.

The MSSV pyrolysis GC-MS detection of hopanes provides unequivocal evidence of the presence of hopanoid structural units in the TSB and the GSL NOM, confirming previous studies in which bacterial terpenoid contribution in these waters had been inferred (Leenheer *et al*., 2003a; 2004). Whilst hopane biomarkers provide qualitative evidence of BHP precursors, their occurrence does not allow an informative quantitative assessment of microbial contribution to NOM. The bacterial levels in GSL are known to be relatively high (Leenheer *et al*., 2004), however the degree of bacterial input into GSL or TSB NOM cannot be distinguished on the basis of these data alone. A better indication of the level of bacterial input might be provided by the use of GC-MS standards and a relative quantification on the basis of total hopane yields.

2.3.4 Complementary detection of hopane biomarkers by catalytic hydropyrolysis GC-MS

The complementary technique of catalytic hydropyrolysis (HyPy) was applied to the cultured bacteria and biofoulant samples to help assess the significance and integrity of the molecular data obtained by MSSV Py. The hopane distributions identified by HyPy GC-MS of F. *aurantia* and the bio-foulant are shown in **Figure 2.13**, and were similar to hopane distributions identified in previous HyPy studies of bacterial cultures (Bishop *et al*., 1998; Love *et al*., 2005). For both samples, the C_{35}-17β, 21β (22R) homohopane (35) was the major product. This hydrocarbon structure is directly inherited from the C_{35} BHP structural moieties of F. *aurantia* and the BF identified by LC-MS, which demonstrates the preservation of structural and stereochemical integrity by the relatively 'soft' pyrolytic release of BHP structural units.

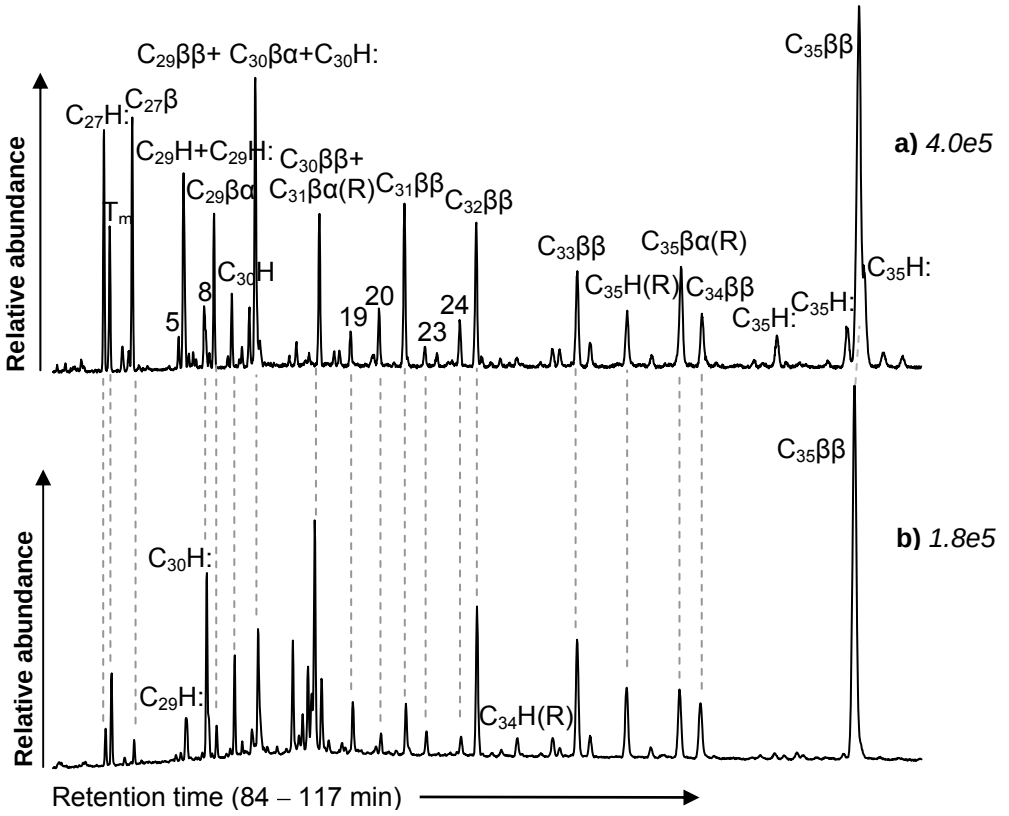

Figure 2.13 Partial *m/z* 191 chromatogram showing the distributions of hopanes detected by hydropyrolysis GC-MS of **a)** Frateuria *aurantia* (full scan); and **b)** biofoulant (selected ion recording of *m/z* 191). Relative abundances of a-b are indicated in italics. Hopane assignments are listed in Table 2.1.

The presence of C_{29}-C_{34} hopanes and βα and αβ isomers in the HyPy GC-MS data of both samples reflects the occurrence of some thermal cracking and molecular rearrangement, however the biological ββ(22R) configuration was still the dominant isomer of the lower MW hopane products (11, 16, 21, 25, 28, 32).
Similar distributions of C_{27}-C_{31} hopanes were observed by both HyPy and MSSV Py (300˚C/72hr) of F. *aurantia* and the BF, including the presence of several monounsaturated C_{27}-C_{30} hopenes. However, generally higher proportions of the higher MW hopanes and ββ stereochemical isomers were detected by HyPy. In comparison, the extended heating times and confined nature of MSSV Py led to more extensive cracking of the alkyl side-chain (lower concentrations of $>C_{31}$ hopanes), and more pronounced isomeric rearrangement (higher proportions of more thermodynamically stable βα and αβ isomers) of the weakened C-C covalent bonds adjacent to hydroxyl groups in the hopanoid extended side-chain (Rohmer *et al*., 1984). Nevertheless the different biohopanoid content of F. *aurantia* and the bio-foulant samples is reflected by different hopane product distributions. Although not as effective as hydropyrolysis at preserving the biological configuration of the hopane precursors, the MSSV analysis still provides valuable diagnostic information and might be considered an appropriate screening method to establish the presence of certain bacteria prior to more complex characterisation methods such as gene specific biological assays or LC-MS. The micro-scale quantities (i.e. < 1 mg) of sample required for MSSV pyrolysis (*Cf* > 30 mg for HyPy) represents an important advantage over HyPy where sample quantities are low, such is typical of NOM analyses where isolation of large samples is very time-consuming and labour intensive.

2.3.5 Correlation of other pyrolysates detected by MSSV Py and HyPy

The distribution of some of the other prominent product classes detected from the BF by MSSV and catalytic HyPy were also compared. The selected ion chromatogram (*m/z* 85) in **Figure 2.14c** shows the *n*-alkane profile obtained by hydropyrolysis of the biofoulant. The distribution is qualitatively similar to the *n*-alkane distribution of the MSSV data (**Fig. 2.14a**), however HyPy yielded higher concentrations of high MW *n*-alkanes and a more pronounced even over odd carbon preference across the entire carbon number range (C_{12} – C_{34}). This is again attributed to the relatively soft

thermal release of structural fragments using HyPy. On the other hand MSSV Py and HyPy of the BF yielded almost identical distributions of the C_{27} and C_{29} sterane biomarkers (**Figure 2.14b,d**), suggesting that steroid structural precursors exhibit similar thermal behaviour by both pyrolysis protocols.

2.4 Conclusions

Hopane products diagnostic of bacterial triterpenoids were detected in relatively high abundance by MSSV pyrolysis GC-MS analysis of Frateuria aurantia (cultured bacteria) and the biofoulant (BF) recovered from a membrane filtration system. Lower hopane concentrations were also detected in aquatic NOM fractions of Great Salt Lake (GSL) and Tomago Sand Beds (TSB). Hopanes were not detected in analysis ***I*** of a fresh (i.e. unheated) aliquot of these samples, or in the corresponding flash pyrolysis analyses. Their detection following MSSV thermal treatment is attributed to the controlled thermal release and reduction of the poly-hydroxy side chain moiety of bacteriohopanepolyols (BHP), yielding saturated hopane products which are more amenable to GC-MS detection than their functionalised precursors.

The MSSV pyrolysates of the NOM fractions and biofoulant also included several other source diagnostic molecular features such as sterane biomarkers of eukaryote triterpenoids (i.e. steroids), aromatic biomarkers of higher plant terpenoids, even carbon preferred *n*-alkanes of fatty acids, and C_{16}-C_{19} phenylalkanes characteristic of common detergents, demonstrating the utility of MSSV for the relatively 'soft' thermal release and reduction of a wide variety of polar organic constituents of NOM. Flash pyrolysis, which can be limited by excessive degradation or poor chromatographic resolution of pyrolysates of high structural polarity, showed no evidence (e.g. hopanes and steranes of aquatic NOM and BF) or much lower concentrations (e.g. hopanes of the bacterial culture, *n*-alkanes of the BF) of these molecular markers. MSSV pyrolysis can complement the characterisation afforded by traditional flash pyrolysis, providing additional molecular information useful for establishing the structures and source inputs of NOM of aquatic environments.

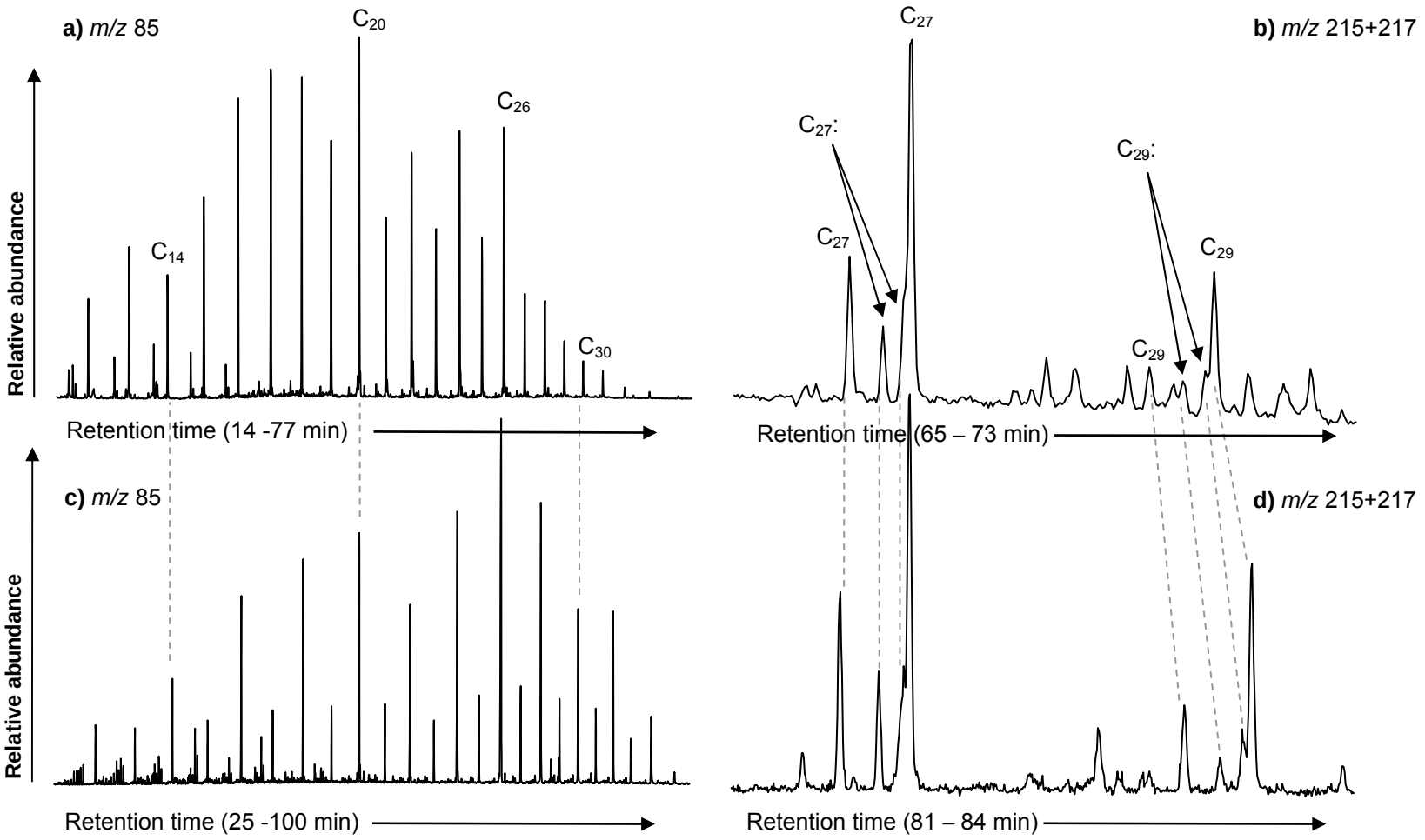

Figure 2.14 Selected ion chromatograms showing the distribution of *n*-alkanes (*m/z* 85) and steranes (*m/z* 215 + 217) from MSSV Py GC-MS **(a, b)** and HyPy GC-MS of the bio-foulant **(c, d)**. (C_{27} and C_{29} = steranes; C_{27}: and C_{29}: = sterenes).

Complementary characterisation of the biomass samples by catalytic hydropyrolysis (HyPy) revealed comparable qualitative features to MSSV Py. The microbial signature of the hopane biomarkers was altered less by the former technique (i.e. higher concentration of ββ diastereoisomers and higher MW fragments), attributed to the softer nature of HyPy bond cleavage. However, neither HyPy nor MSSV Py provides the same level of intact BHP speciation afforded by LC-MS. Nevertheless, the respective hopane distributions still reflect the different biohopanoid content of F. *aurantia* and the biofoulant. MSSV pyrolysis may therefore represent an appropriate screening method to establish the presence of bacterially-derived terpenoids prior to more complex characterisation methods such as LC-MS or gene specific biological assays. The micro-scale quantity (i.e. < 1 mg) of sample required for MSSV pyrolysis (*cf* > 30 mg for HyPy) is an important advantage for the characterisation of aquatic organic materials that are difficult to isolate in large quantities (e.g. NOM, biofoulants). Further studies of the MSSV approach are warranted to investigate the release and origins of other major product classes and to establish optimal thermal conditions for targeting different biomacromolecular constituents of NOM.

Chapter 3

Thermal release of aromatic hydrocarbons by MSSV pyrolysis: Insight into terpenoid structural precursors of aquatic NOM

Some of the work in this chapter has been published as:

Lavaud, A., Berwick, L., Chabbi, A., Greenwood, P., Croué, J-P., 2008. Isolation and characterization of groundwater (Lysimetric plate collected water) NOM: Comparison with surface water NOM. *Proceedings* of 4th IWA Specialist Conference: Natural Organic Matter Research Conference: From Source to Tap, Bath, UK, June 2-4 2008.

3.1 Introduction

The high pyrolysate yields afforded by MSSV pyrolysis contributes to very complex distributions of products, the majority of which lack the well defined precursory origins of the classical hopane and sterane biomarkers (Chapter 2), which are typically detected in low relative abundance. A detailed evaluation of the entire pyrolysate distribution will contribute to a more holistic characterisation of NOM structural features. At present however, specific source assignment of many MSSV products is challenging due to potential derivation from multiple structural precursors, and the largely undefined closed-system pyrolysis behaviour of thermally immature biomacromolecules of modern environments. This chapter focuses on the potential structural precursors and mechanistic formation of low molecular weight (MW) alkyl substituted aromatic hydrocarbons. Alkyl benzenes, naphthalenes and phenanthrenes represented some of the major products of the HPO fractions of the NOM isolated from the Great Salt Lake and Tomago Sand Bed samples (Chapter 2.3.1).

Aromatic hydrocarbons (HCs) are often reported from fast pyrolysis analyses of aquatic NOM (e.g. Saiz-Jimenez, 1993, Schulten and Gleixner, 1999, van Heemst *et*

al., 2000, González-Vila *et al*., 2001, Templier *et al*., 2005a). However, they are common pyrolysates of many different types of biomacromolecules, including higher plant materials (Saiz-Jimenez, 1993), phenylalanine-containing proteins (Chiavari and Galletti, 1992; Wang *et al*., 2004) and algae (van Heemst *et al*., 2000) and are rarely assigned to specific structural precursors or given source significance (Lu *et al*., 2000; Chefetz *et al*., 2002; Guo *et al*., 2003, White *et al*., 2003; Page *et al*., 2003). Furthermore, aromatic hydrocarbons have also been identified as secondary rearrangement products of the thermal degradation of cellulose (Pastorova *et al*., 1994) or via decarboxylation and aromatisation of fatty acids (Saiz-Jimenez, 1994, Page *et al*., 2002, Faure *et al*., 2006a; 2006b). This uncertainty limits the source diagnostic value of alkyl aromatic hydrocarbon pyrolysates.

Aromatic hydrocarbons are major constituents of sedimentary OM. High concentrations of many different aromatic compounds have been detected in solvent extracts of sediments (van Aarssen *et al*., 2000; Watson *et al*., 2005; Hautevelle *et al*., 2006a) and crude oils (Alexander *et al*., 1983; 1985; van Aarssen *et al*., 1990; 1992; Bastow *et al*., 1999) and in flash pyrolysates of humic substances present in kerogen (Hartgers *et al*. 1994a; Hoefs *et al*., 1995; Garcette-Lepecq *et al*., 2000) and coals (e.g. Hayatsu *et al*., 1990; Sinninghe Damste *et al*., 1992b; Hartgers *et al*., 1992; 1994b; Lu *et al*., 2000). Biosynthesised terpenoids of plants, algae and bacteria are common precursors of many of the mono- and polycyclic aromatic hydrocarbons (PAHs) present in geological environments (Hayatsu *et al*., 1990; Hartgers *et al*., 1994a; 1994b; Pancost and Boot, 2004; Hautevelle *et al*., 2006a). Bacterial terpenoids include the high MW bacteriohopanepolyols (triterpenoids), which give rise to the fully saturated hopane products as discussed Chapter 2. Higher plant terpenoids are abundant constituents of resins, bark and leaf tissues and include terpene hydrocarbons like pinene (monoterpenoid), resin acids such as abietic acid (diterpenoids), and essential oils like menthol (monoterpenoid) and farnesol (sesquiterpenoid).

Numerous diagenetic pathways have been proposed for the sedimentary formation of aromatic HCs from natural terpenoids (Smith *et al*., 1995). These processes may lead to structural alteration; however many aromatic products often maintain sufficient structural integrity to allow assignment of their biomolecular source. This source

dependence is often used as a diagnostic tool for terrestrial organic matter supply (van Aarssen *et al*., 1992; van Aarssen *et al*., 2000; Pancost and Boot, 2004; Hautevelle *et al*., 2006a; 2006b), palaeoenvironmental reconstuction (Hautevelle *et al*., 2006a) and oil-source rock correlation (Alexander *et al*., 1992). The formation of many aromatic HCs is also maturity dependent and the relative proportions of specific compounds have thus been used to establish geochemical maturity levels (Alexander *et al*., 1985; Strachan *et al*., 1988; Alexander *et al*., 1992).

Recent ^{13}C-NMR spectroscopy, electrospray ionization mass spectrometry (ESI-MS) and chemical reduction studies have shown that terpenoids derived from allochthonous (e.g. land plants) and autochthonous (e.g. microbial) sources can be major potential precursors of humic fractions of ground and surface water NOM (Leenheer *et al*., 2003a; 2004; Leenheer and Rostad, 2004; Leenheer, 2004; McIntyre *et al*., 2005; Nimmagadda *et al*., 2007). ^{13}C-NMR spectra of NOM isolates derived from terpenoids were generally characterised by high contents of aliphatic and aromatic polycyclic structures, extensively substituted with carboxylic and branched alkyl groups (Leenheer *et al*., 2003a; Leenheer, 2004; Leenheer and Rostad, 2004; McIntyre *et al*., 2005).

Minor elements of terrestrial vegetation such as terpenoid resin acids (e.g. abietic acid), which are highly soluble, stable, or resistant to degradation during transport through the catchment, may be concentrated in aquatic NOM at levels greater than typically found in plant biomass (Page *et al*., 2002). Terpenoids have been shown to be resistant to aerobic degradation processes (McDonald *et al*., 2004) and can readily infiltrate potable groundwater sources with little removal by soil/aquifer treatment (Leenheer *et al*., 2003a; Leenheer, 2004). In the context of potable water treatment, terpenoid derived NOM is difficult to remove by coagulation/flocculation treatment but produces relatively low DBP concentrations upon chlorination (Hwang *et al*., 2001; Leenheer, 2004).

Flash pyrolysis typically provides very limited molecular information about terpenoid precursors of recent OM (Leenheer and Rostad, 2004; McIntyre *et al*., 2005). This may be attributed to 1) excessive thermal degradation of terpenoid derived structures, which dissipates source specificity, or 2) high structural polarity

resulting from functional group substitution, which can hinder chromatographic resolution and detection of terpenoid pyrolysates. MSSV pyrolysis of immature NOM may facilitate the analysis of terpenoid constituents via reduction and aromatisation, in an analogous manner to the formation of aromatic HCs from terpenoids during natural sedimentary maturation.

In the present study, the aromatic HC distributions from the MSSV pyrolysis GC-MS analysis of several NOM samples, including humic surface waters, soluble soil leachates (i.e. ground waters) and post-treated wastewater effluents, were scrutinised in search of molecular features characteristic of these particular aquatic environments. Representative standards and plant elements were also separately analysed to help establish more definitive biomacromolecular origins, with particular attention on the identification of alkyl aromatics diagnostic of higher plant and other natural terpenoids.

3.2 Experimental

3.2.1 Samples

Polarity-based hydrophobic (HPO), transphilic (TPI) and colloid (COL) fractions of NOM isolated from Arroyo Sanchez (Uruguay) and Gartempe (France) Rivers, Poitiers groundwater (France), and St. Julien and Naintré waste water (WW) effluents (both France) were analysed. A brief description of the geographical location and the environmental setting of these waters and the isolation procedures used to obtain their organic fractions are given below. Model compounds (e.g. amino acids, fatty acids, syringic acid), standards (e.g. lignin, cellulose, protein, chitin) and specific plant elements (e.g. wood and bark) were also analysed to investigate the MSSV behaviour of potential precursors of aromatic hydrocarbon products.

3.2.1.1 Surface water NOM

The Arroyo Sanchez River is located in Rio Negro, a rural area to the northwest of Montevideo, Uruguay. This unprotected catchment receives significant input from terrigenous plant and soil leachate, resulting in highly coloured water with a DOC concentration of 9.2 mg L^{-1} (SUVA 4.23 m^{-1} L mg C^{-1}). The Gartempe River,

located in Vienne, France, contains a DOC concentration of 6.5 mg L^{-1} (SUVA = 4.4 m^{-1} L mg C^{-1}). Both of these source waters are considered humic waters.

Isolation of solid NOM fractions from these waters was conducted using the XAD-8/XAD-4 resin extraction protocol developed by Croué *et al*. (1999), at the Laboratoires Chimie de l'Eau et de l'Environment (LCEE), École Supérieure d'Ingénieurs de Poitiers (ESIP), University of Poitiers, France. In brief, the raw water was successively passed through a 10 µm Polygard CR filter, a 0.45 µm milligard cartridge filter and a sodium exchanger unit. The samples were then acidified to pH 2 and pumped through two superimposed XAD-8 and XAD-4 resins to yield HPO and TPI fractions, as termed by Croué *et al*. (1999). The NOM adsorbed onto the resins was recovered with a 75% water/25% acetonitrile mixture and lyophilized. The DOC distribution of these samples was 38 % HPO, 25 % TPI and 37 % hydrophilic (HPI) for the Arroyo Sanchez River and 66 % HPO, 19 % TPI and 15 % HPI for Gartempe River.

3.2.1.2 Ground water NOM

The Observatory for Environmental Research (ORE; Lusignan-Vienne) is located near Poitiers, France. The site is divided in several plots equipped with lysimetric plates which can recover water passing through the soil to a depth of 105 cm. The plates were positioned with an inclination of 5 degrees for natural drainage. Samples were collected continuously over 24 hours and then combined after 6 months. All samples were stored in a cold room at 4°C. Lysimetric plate samples collected during the first semester of 2007 were mixed together to provide a sufficient volume of water (40 litres, DOC = 1.2 mg L^{-1}, SUVA = 1.2 m^{-1} L mg C^{-1}) from which DOM fractions were isolated using the same XAD-8/XAD-4 resin extraction protocol used to isolate the surface water NOM fractions. The DOC distribution of the groundwater was 49 % HPO, 14 % TPI, and 37 % HPI. Only the HPO fraction was analysed here.

3.2.1.3 Waste water effluent OM

Secondary effluents were collected from French waste water treatment facilities in the cities of Saint Julien l'Ars (DOC = 5.9 mg L^{-1}) and Naintré (DOC = 14.4 mg L^{-1}). The process train of both these activated sludge plants consists of primary treatment,

aerobic basins, and secondary clarification, after which the effluent is discharged into a canal. St. Julien WWTP additionally employs anoxic basins and a longer contact time for biological treatment than Naintré WWTP. Part of the settled sludge from the secondary clarifiers is re-circulated to the anoxic/aerobic basins whilst the excess sludge is drained and stored in a sludge tank before further utilization in agricultural practices.

Isolation of the effluent OM (Ef-OM) was conducted at the Laboratoires Chimie de l'Eau et de l'Environment (LCEE), École Supérieure d'Ingénieurs de Poitiers (ESIP), University of Poitiers, France (Jarusutthirak, 2002) using a procedure adapted from Leenheer *et al*. (2000). In brief, 100 L of the wastewater effluent was collected and sequentially filtered through pre-rinsed 10 μm and 1 μm cartridge filters (Millipore) to remove particulate material. The filtered sample was then reduced to ca.1-L using a rotary evaporator and acidified to pH 1. Membrane dialysis (3500 *Da*) was used to separate the colloidal fraction. During this step, salts and lower MW Ef-OM were removed by dialysis against 0.1 M hydrochloric acid (HCl). Silica was removed by dialysis against 0.2 M hydrofluoric acid (HF), and excess HF was removed by dialysis against distilled water (Leenheer *et al*., 2000). The contents of the dialysis bag were freeze-dried to yield the colloid fraction. The lower MW Ef-OM separated from the colloids was then pumped through two superimposed XAD-8 and XAD-4 resins to yield HPO and TPI acid fractions, respectively. The HPO, TPI and colloid fractions accounted for 25 %, 19 % and 27 % of the DOC of St. Julien Ef-OM and 30 %, 18 % and 24% of Naintré Ef-OM, respectively.

3.2.1.4 Suwannee River fulvic acid

Suwannee River fulvic acid (SRFA) was purchased from the International Humic Substances Society (IHSS). At its headwaters in the Okefenokee Swamp (Georgia, USA), the blackwater Suwannee River has DOC concentrations ranging from 25-75 mg L^{-1} and pH values of less than 4.0. The Okefenokee Swamp contains extensive peat deposits and decomposing coniferous vegetation (Malcolm *et al*., 1989), which is believed to provide most of the DOC to the river. Water was sampled (8104 L) at this outlet in 1983 (Leenheer and Noyes, 1984). The NOM was processed onsite into HPO and hydrophilic (HPI) fractions by filtration and preferential adsorption on XAD-8 resin. The adsorbed HPO fraction was subsequently eluted by alkaline

extraction with aqueous NaOH, followed by precipitation of humic acid at low pH and a desalting step employing cation exchange to obtain the fulvic acid (Leenheer and Noyes, 1984). The fulvic acid fraction (SRFA) constituted 66 % of the DOC concentration, which was 38.4 mg L^{-1} at the time of sampling.

3.2.1.5 Plant elements

Fresh samples of wood and bark were collected from two higher plant species, *Wandoo eucalyptus* (angiosperm, hardwood) and *Pinus radiata* (gymnosperm, softwood), in bushland near the Mundaring Weir Dam in Perth, Western Australia (Miles, 2005). The samples were ground to a fine powder prior to analysis.

3.2.1.6 Representative standards

Cellulose (polysaccharide), lignin, bovine serum albumin (BSA, protein), chitin (amino sugar), syringic acid (lignin monomer), phenylalanine (amino acid) and stearic acid (fatty acid) were commercially sourced from Sigma-Aldrich.

3.2.2 Molecular analysis

3.2.2.1 MSSV pyrolysis GC-MS

MSSV pyrolysis of < 0.1 - 1 mg sample was performed according to the procedure described in section 2.2.2.1 of the previous chapter. All data correspond to MSSV analysis ***I*** at an off-line pyrolysis temperature of 300˚C for 72 hr, with the MSSV injector at a constant 300˚C. The lignin standard and Uruguay HPO fraction were studied at several additional temperatures over the range 260 – 340˚C. Fresh (i.e. unmatured) aliquots of selected samples were also analysed to distinguish MSSV pyrolysates from volatile products of the fresh material at the 300˚C of the MSSV injector port.

GC-MS analysis of the volatile MSSV pyrolysates was typically performed with a Hewlett-Packard (HP) 6890 GC coupled to a 5973 mass selective detector (MSD). Pyrolysates were separated using a 30 m x 0.32 mm i.d. x 0.25 μm DB5-MS capillary column (J&W Scientific). Helium carrier gas was used at 34 kPa head pressure with a split of between 20 – 50 mL $minute^{-1}$. The GC oven was held for 1 min at an initial temperature of -20˚C (using liquid CO_2 cryogenic control), then increased at 8˚C min^{-1} to 40˚C, then 4˚C min^{-1} to 310˚C and held isothermal for 20

minutes. Full scan analyses were performed over the range *m/z* 50 – 550 at ca. 4 scans s^{-1}. The mass spectrometer operated in positive ion electron impact mode at 70 eV with a transfer line temperature of 310˚C and a source temperature of 250˚C. Tentative peak identifications were based on GC elution times and order, mass spectral comparisons with library spectra (Wiley 275 and NIST 05 databases) and published data (Hartgers *et al*., 1992, 1994a; 1994b; Sinninghe-Damsté *et al*., 1992b).

3.2.2.2 Flash pyrolysis GC-MS

Flash pyrolysis of 0.5–1 mg sample was performed in pre-annealed quartz tubes at 550˚C for 20 seconds using a Chemical Data Systems 160 Pyroprobe with the pyrolysis chamber held at 250˚C. A HP 5890 Series II gas chromatograph coupled to a 5971 MSD was used for GC-MS analysis. The products were cryo-focused for 1.5 minutes at the start of the GC column using liquid nitrogen prior to starting the GC-MS analysis. Analyses were performed with a split of 20 ml min^{-1} using a 30 m x 0.25 mm i.d. x 1 μm phase ZB5-MS capillary column (Phenomenex), with helium carrier gas at 55 kPa. The GC oven was initially held for 2 minutes at 40˚C, increased at 4˚C min^{-1} to a final temperature of 310˚C, held isothermal for 20 min. Full scan mass spectra were acquired between *m/z* 50 –550 at ca. 4 scans sec^{-1}. The mass spectrometer operated in positive ion electron impact mode at 70 eV with a transfer line temperature of 310˚C and a source temperature of 230˚C. Tentative peak identification was based on retention time, mass spectral comparison with library spectra (Wiley 275, NIST 05) and literature data.

3.2.2.3 TMAH thermochemolysis GC-MS

U-HPO NOM (1 mg) was transferred into a pre-annealed quartz tube sealed at one end. Tetramethylammonium hydroxide (TMAH; Sigma-Aldrich) was added as a methanolic solution (5 μL, 25% w/w) and the open end plugged with pre-cleaned glass wool. Pyrolysis was performed at 650˚C for 20 seconds using a Chemical Data Systems 160 Pyroprobe, with the pyrolysis chamber held at 150˚C. GC-MS parameters were the same as for flash pyrolysis, but also included a 3-minute solvent delay to allow elution of methanol solvent and excess TMAH reagent.

3.3 Results and Discussion

3.3.1 Alkyl aromatic product distributions detected by MSSV and flash pyrolysis of aquatic NOM

High concentrations of alkyl aromatic products were detected by MSSV pyrolysis GC-MS analysis of the hydrophobic NOM fractions. The major aromatic HC products included homologous series of alkyl ($\leq C_6$) benzenes, alkyl ($\leq C_5$) phenols and alkyl ($\leq C_5$) naphthalenes, as well as lower concentrations of alkyl (C_1-C_4) phenanthrenes, alkyl (C_1-C_3) indenes and hydrogenated aromatics such as indanes and hydronaphthalenes (tetralins). Isomeric assignments of the major alkyl benzene, naphthalene and phenanthrene pyrolysates are provided in **Table 3.1**. Alkyl phenols (APs) were consistently detected in high abundance in all the NOM fractions analysed. Detailed evaluation of these products is provided in Chapter 4.

The total ion chromatograms (TIC) obtained by 300˚C/72hr MSSV pyrolysis GC-MS and flash pyrolysis (550˚C/20 seconds) GC-MS of the HPO fraction of NOM from the Arroyo Sanchez River (Uruguay; U-HPO) are given in **Figure 3.1a-b**. MSSV Py generated significantly higher overall concentrations of GC-MS detectable pyrolysates than flash pyrolysis. Prominent peaks for benzene, phenol and their C_1-C_2 alkylated derivatives were detected by flash Py, however, the higher substituted benzenes and phenols and the polycyclic aromatics were either absent, or present in very low abundance compared to MSSV Py. Several methoxy aromatic pyrolysates diagnostic of lignin structures detected by flash pyrolysis of U-HPO were not evident, or were detected in low abundance from the MSSV data. These products are addressed in further detail in Chapter 4.

Fresh (i.e. unmatured) aliquots of U-HPO (**Fig. 3.1c**), as well as SRFA (data not shown), were analysed to distinguish thermally labile aromatic components of the fresh material at the 300˚C temperature of the MSSV injector port. Phenol, guaiacol (2-methoxy phenol), dimethoxy phenol and methyl (C_1-C_2) furans were identified amongst the small number of thermally desorbed products of the fresh samples, reflecting the presence of free or loosely bound lignocellulose structures. Toluene and alkyl (C_2-C_3) benzenes, which may also derive from thermally labile aromatic ring structures were detected in very low abundance, however the lack of other alkyl

aromatic hydrocarbons rules out the likelihood of a petroleum or crude oil contamination.

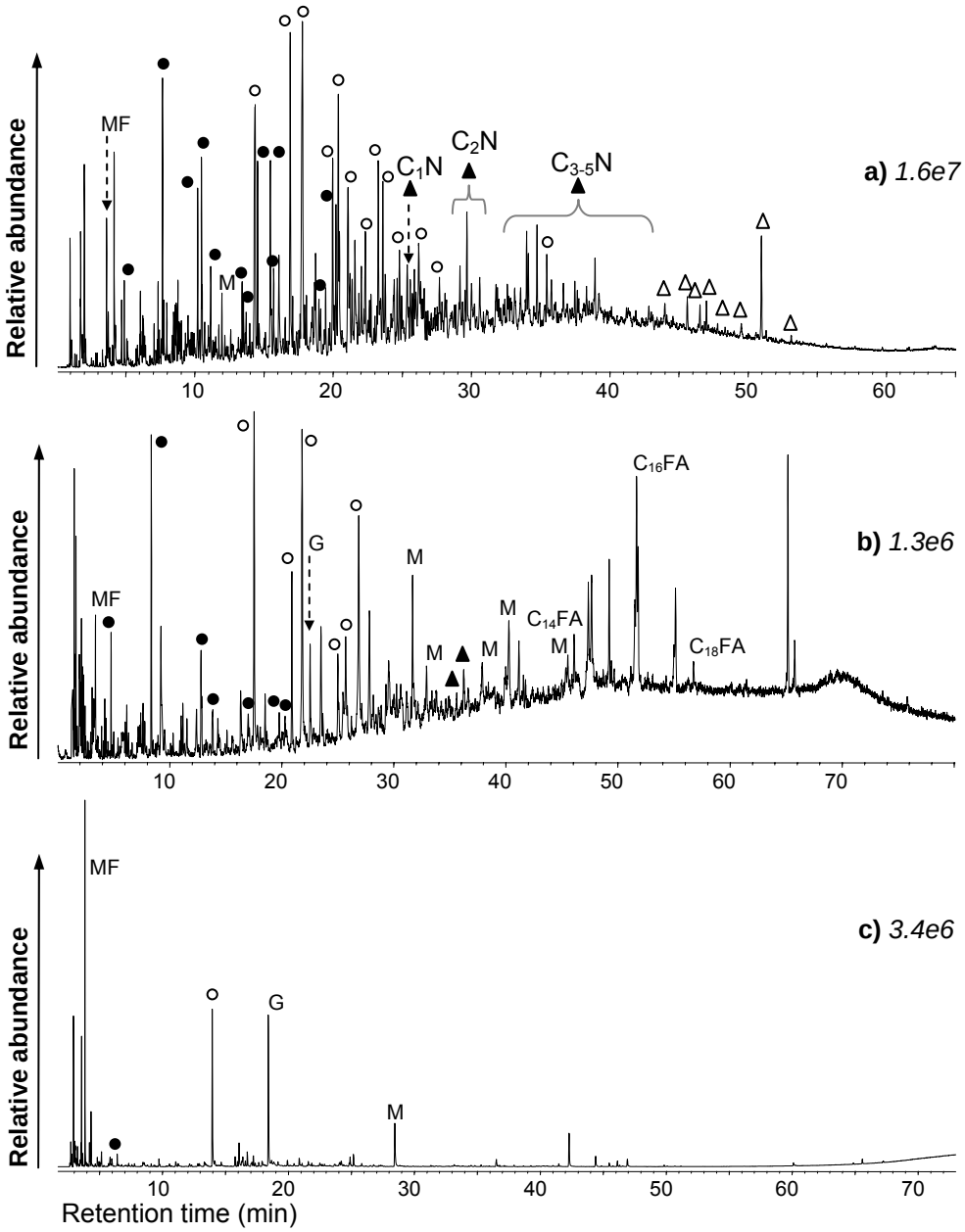

Figure 3.1 TICs from GC-MS analysis of U-HPO following **a)** 300˚C/72hr MSSV pyrolysis; **b)** 550˚C/20sec flash pyrolysis; and **c)** fresh non-matured analysis (300˚C injector temperature). Relative abundances of a-c are indicated in italics. ● = alkyl benzenes, ○ = alkyl phenols, ▲/$C_{1\text{-}5}$N = alkyl naphthalenes, Δ = alkyl phenanthrenes, MF = methyl furan, G = guaiacol, M = methoxy aromatics, FA = fatty acids.

Table 3.1 Aromatic hydrocarbon products identified by MSSV pyrolysis GC-MS analyses of aquatic NOM fractions and representative plant elements, model compounds and standard materials. A 4-point mass spectrum comprising the 4 most abundant ions is also shown to provide an indication of assignment integrity. Base peaks are indicated in bold. Abbreviations correspond to products identified within the text and in Figures 3.4-3.13.

Compound Identification	MW	Abbreviation	4 pt. mass spectrum
Alkyl Benzenes			
Toluene	92	T	92, **91**, 65, 51
Ethylbenzene	106	E	106, **91**, 65, 51
m-xylene (1,3-dimethylbenzene)	106	13	106, 105, **91**, 77
p-xylene (1,4-dimethylbenzene)	106	14	106, 105, **91**, 77
o-xylene (1,2 dimethylbenzene)	106	12	106, 105, **91**, 77
Isopropylbenzene (cumene)	120	iP	120, **105**, 77, 79
n-propylbenzene	120	*n*-propyl	120, **91**, 92, 65
1-methyl-3-ethylbenzene	120	1M-3E	120, **105**, 91, 77
1-methyl-4-ethylbenzene	120	1M-4E	120, **105**, 91, 77
1,3,5-trimethylbenzene	120	135	120, 119, **105**, 77
1-methyl-2-ethylbenzene	120	1M-2E	120, **105**, 91, 77
1,2,4-trimethylbenzene	120	124	120, 119, **105**, 77
sec-butylbenzene	134	*sec*-butyl	134, **105**, 91, 77
1,2,3-trimethylbenzene	120	123	120, 119, **105**, 77
1-methyl-3-isopropylbenzene (*m*-cymene)	134	*m*-cymene	134, **119**, 117, 91
1-methyl-4-isopropylbenzene (*p*-cymene)	134	*p*-cymene	134, **119**, 117, 91
1,3-diethylbenzene	134	13-DEB	134, **119, 105**, 91
1,4-diethylbenzene	134	14-DEB	134, **119, 105**, 91
n-butylbenzene	134	*n*-butyl	134, 105, 92, **91**
Dimethylethylbenzenes (unspecified isomers)	134	DMEB	134, **119**, 91, 77
sec-pentylbenzene	148	*sec*-pentyl	148, **105**, 91, 77
n-pentylbenzene	148	*n*-pentyl	148, 105, 92, **91**
1,2,4,5-tetramethylbenzene	134	1245	134, **119**, 91, 77
1,2,3,5-tetramethylbenzene	134	1235	134, **119**, 91, 77
1,2,3,4-tetramethylbenzene	134	1234	134, **119**, 91, 77
sec-hexylbenzene	162	*sec*-hexyl	162, **105**, 91, 77
n-hexylbenzene	162	*n*-hexyl	162, 105, 92, **91**
C_5 benzenes (unspecified isomers)	148	○	148, **133**, 105, 91
Ethylisopropylbenzenes (unspecified isomers)	148	EiPB	148, **133**, 105, 91
Dimethylisopropylbenzene	148	DMiPB	148, **133**, 105, 91
Pentamethylbenzene	148	PMB	148, **133**, 105, 91
Alkyl Naphthalenes			
1-methylnaphthalene	142	1-MN	**142**, 141, 115, 71
2-methylnaphthalene	142	2-MN	**142**, 141, 115, 71
1-ethylnaphthalene	156	1-EN	156, **141**, 128, 115

2-ethylnaphthalene	156	2-EN	156, **141**, 128, 115
3,6-dimethylnaphthalene	156	36-DMN	**156**, 141, 128, 115
2,7-dimethylnaphthalene	156	27-DMN	**156**, 141, 128, 115
1,3-dimethylnaphthalene	156	13-DMN	**156**, 141, 128, 115
1,7-dimethylnaphthalene	156	17-DMN	**156**, 141, 128, 115
1,6-dimethylnaphthalene	156	16-DMN	**156**, 141, 128, 115
1,4-dimethylnaphthalene	156	14-DMN	**156**, 141, 128, 115
2,3-dimethylnaphthalene	156	23-DMN	**156**, 141, 128, 115
1,5-dimethylnaphthalene	156	15-DMN	**156**, 141, 128, 115
1,2-dimethylnaphthalene	156	12-DMN	**156**, 141, 128, 115
1-propylnaphthalene	170	1-PN	170, **141**, 128, 115
Ethyl methyl or isopropylnaphthalenes	170	⧈	170, **155**, 128, 115
Trimethylnaphthalenes (unspecified isomers)	170	■	**170**, 155, 128, 115
1,3,6-trimethylnaphthalene	170	136-TMN	**170**, 155, 128, 115
1,4,6-trimethylnaphthalene	170	146-TMN	**170**, 155, 128, 115
1,3,5-trimethylnaphthalene	170	135-TMN	**170**, 155, 128, 115
1,2,7-trimethylnaphthalene	170	127-TMN	**170**, 155, 128, 115
1,6,7-trimethylnaphthalene	170	167-TMN	**170**, 155, 128, 115
1,2,6-trimethylnaphthalene	170	126-TMN	**170**, 155, 128, 115
1,2,5-trimethylnaphthalene	170	125-TMN	**170**, 155, 128, 115
1,2,3-trimethylnaphthalene	170	123-TMN	**170**, 155, 128, 115
1-butylnaphthalene	184	1-BN	184, **155**, 128, 115
Methylpropylnaphthalenes	184	MPN	184, **155**, 128, 115
Methylisopropylnaphthalene (eudalene)	184	MiPN	184, **168**, 154, 141
C_4 naphthalenes (unspecified isomers)	184	▫	184, 169, 153, 141
1,6-dimethyl-4-isopropylnaphthalene	198	Cadalene (C)	198, **183**, 168, 153
C_5 naphthalenes (unspecified isomers)	198	C_5N	198, 183, 168, 153
Alkyl Phenanthrenes and Derivatives			
3-Methylphenanthrene	192	3-MP	**192**, 191, 189, 165
2-Methylphenanthrene	192	2-MP	**192**, 191, 189, 165
9-Methylphenanthrene	192	9-MP	**192**, 191, 189, 165
1-Methylphenanthrene	192	1-MP	**192**, 191, 189, 165
Dimethylphenanthrenes	206	DMP	**206**, 205, 191, 189
1,7-dimethylphenanthrene	206	17-DMP	**206**, 205, 191, 189
Trimethylphenanthrenes (unspecified isomers)	220	TMP	**220**, 205, 189, 101
18-norabieta-8,11,13-triene	256	DHA	256, **241**, 185, 159
19-norabieta-8,11,13-triene	256	DHA	256, **241**, 185, 159
1,2,3,4-tetrahydroretene	238	THR	238, **223**, 181, 165
1-methyl-7-isopropylphenanthrene	234	Retene (R)	234, **219**, 204, 189
C_4 phenanthrenes	234	C_4P	**234**, 219, 204, 189
Methyl retene	248	MeR	248, **233**, 218, 203

3.3.2 Alkyl aromatic product distributions of surface, ground and waste waters

Variation in the relative abundances of the major alkyl aromatic products detected by MSSV Py was evident between the HPO fractions from different source environments. **Figure 3.2** shows the TICs from the MSSV pyrolysis GC-MS (300˚C/72hr) of the HPO fractions of Gartempe River (G-HPO), the lysimetric plate collected groundwater (L-HPO) and the Saint Julien (S-HPO) and Naintré (N-HPO) wastewater effluents. The relative abundances of the major aromatic product groups are quantitatively shown in **Figure 3.3**. Peak areas were calculated by integrating up to 200 of the most abundant peaks from those that were greater than 0.5% of the base peak. The peak areas from these ≤ 200 peaks were then summed to yield the total integrated peak area. Individual peak areas were expressed as percentages of the total integrated pyrolysate area. The abundances of the major product groups relative to the total peak area (i.e. ≤ 200 peaks) were calculated by summing the individual percentages for all peaks within a given product class.

3.3.2.1 Surface water NOM

Similar aromatic product distributions were observed by MSSV Py of the U-HPO (**Fig. 3.1 a**), G-HPO (**Fig. 3.2 a**) and SRFA (Appendix 2) surface water fractions, all of which are highly humic black waters. Alkyl phenols were the most abundant pyrolysates and are likely derived from phenolic lignin precursors (see Chapter 4). Flash pyrolysis (**Fig. 3.1b**) and thermochemolysis (data not shown) analyses of U-HPO and G-HPO (Templier *et al*., 2005a) confirmed the presence of lignin derived methoxyphenol products. Alkyl benzenes (ABs) were also detected in similar abundance from both surface waters; however U-HPO yielded a significantly higher proportion of alkyl naphthalenes (ANs) and alkyl phenanthrenes (APhs). ABs were also detected in similar abundance from the Uruguay TPI fraction, however APs, ANs and APhs were present in much lower concentrations, with the latter two product classes detected at only trace levels.

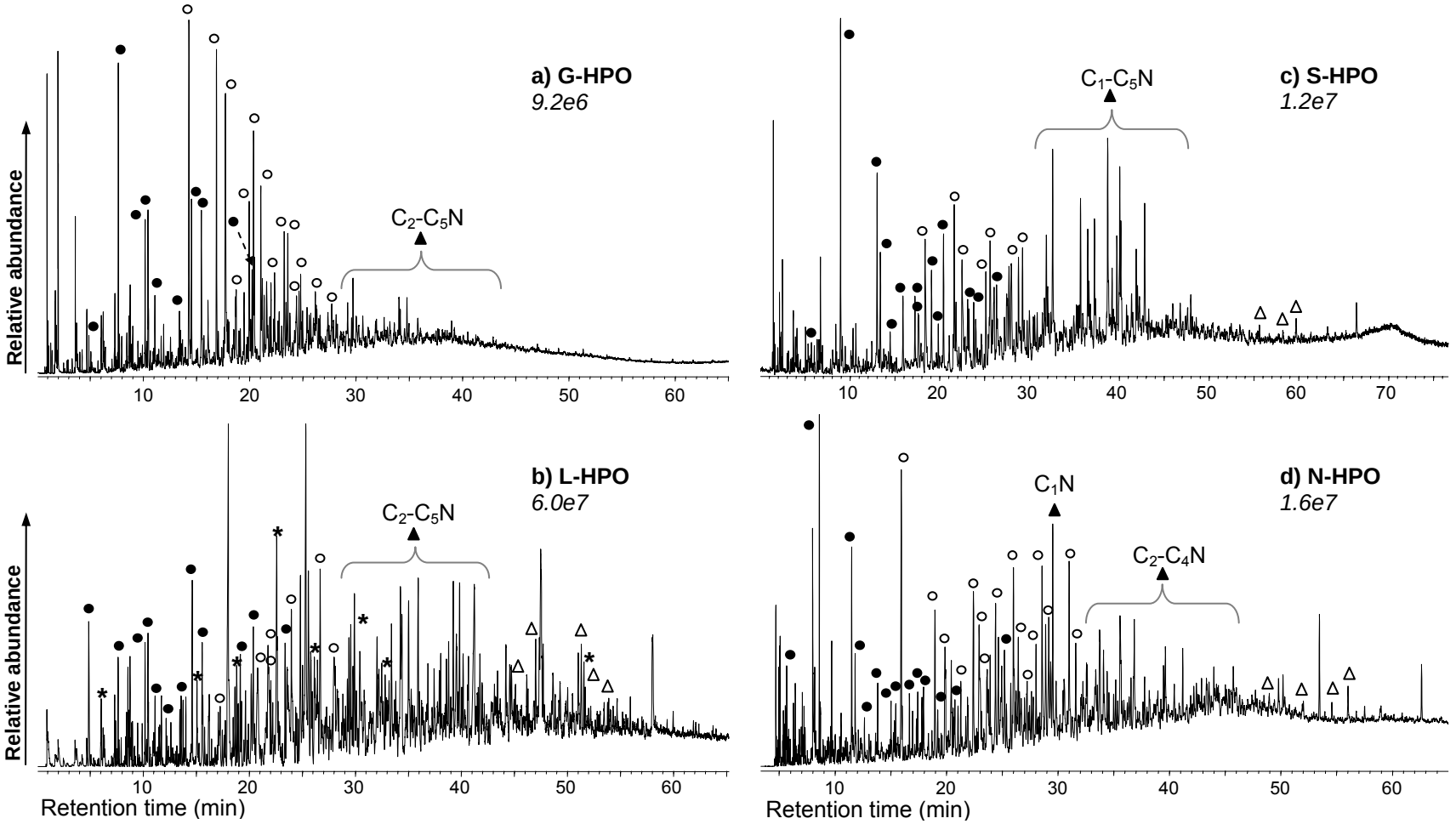

Figure 3.2 TICs from 300˚C/72hr MSSV pyrolysis GC-MS analysis of **a)** G-HPO, **b)** L-HPO, **c)** S-HPO and **d)** N-HPO. Relative abundances of a-d indicated in italics. ● = alkyl benzenes, ○ = alkyl phenols, ▲/$C_{1\text{-}5}$N = alkyl naphthalenes, △ = alkyl phenanthrenes, * = *n*-alkanes.

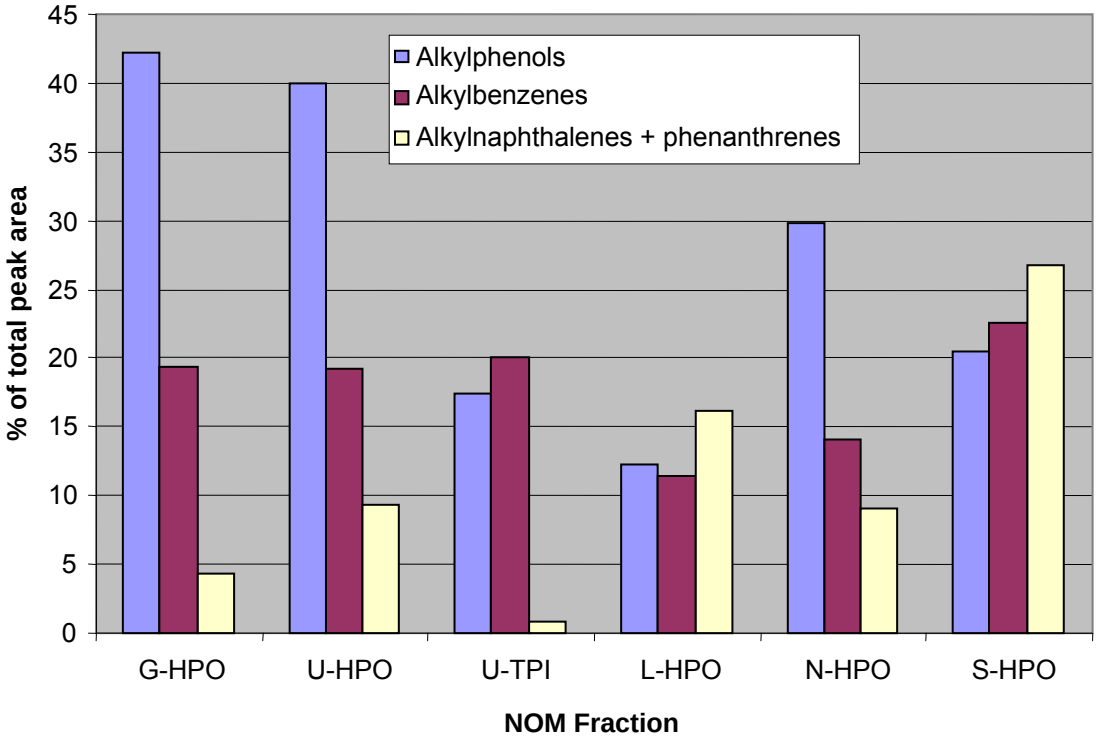

Figure 3.3 Relative abundances of alkyl phenol, alkyl benzene and combined alkyl naphthalene and phenanthrene product classes detected by 300˚C/72hr MSSV pyrolysis GC-MS of several NOM fractions.

3.3.2.2 Ground water NOM

The lysimetric plate groundwater NOM (L-HPO; **Fig. 3.2 b**) showed a very different distribution of alkyl aromatics to the humic surface waters, characterised by higher concentrations of ANs and much lower proportions of APs. The lower proportion of phenolic products of L-HPO (*cf*. G-HPO) was separately confirmed by corresponding flash pyrolysis (Lavaud *et al*., 2008). Likewise, diagnostic markers of lignin metabolites were detected at only trace levels by thermochemolysis analysis of L-HPO. McIntyre *et al*. (2005) previously showed that TMAH thermochemolysis products of degraded lignin components in ground water fulvic acids accounted for less than 1% of the total product yield. The removal of humic substances through the first soil horizon, due to preferential adsorption or biodegradation by soil microbiota, probably accounts for the different character of the ground and surface water NOM (Lavaud *et al*., 2008). Previous characterisation using size exclusion chromatography with ultraviolet (UV) and DOC detection demonstrated that the L-HPO fraction was depleted in humic like materials (Lavaud *et al*., 2008).

Similarly, solid state ^{13}C-NMR spectroscopy revealed that carboxyl, phenolic and aromatic carbon bands were proportionally less abundant for L-HPO than the humic waters (e.g. Gartempe R.), whilst the aliphatic C-C and C-H bands were proportionally enriched (Lavaud *et al*., 2008). The ^{13}C-NMR spectra and FTIR spectra of the L-HPO and G-HPO fractions were similar to previously characterised HPO-neutral and HPO-acid fractions of Anaheim Lake, respectively (Leenheer, 2004). Leenheer (2004) and Leenheer and Wershaw (2005) suggested that the HPO-acid fraction corresponded to fulvic acid like structures (high carboxyl and aromatic C contents) whilst the HPO-neutral fraction was rich in terpenoid precursors. Thus the L-HPO groundwater fraction may be considered to contain substantial input from terpenoid derived OM. Terpenoids have been shown to be resistant to aerobic degradation processes (McDonald *et al*., 2004) and can readily infiltrate ground waters with little removal by soil/aquifer treatment (Leenheer *et al*., 2003a). Detailed investigation of the MSSV pyrolysates, and in particular the high concentrations of alkyl naphthalenes from this sample may provide important insight into terpenoid structural precursors of aquatic NOM.

3.3.2.3 Waste water effluent OM

The HPO fractions of Saint Julien and Naintré Ef-OM (**Fig 3.2 c-d**) also showed high concentrations of aromatic products. Parallels in the composition of the wastewaters with surface water humic and fulvic acids have been previously observed from flash pyrolysis, elemental analysis, infra-red spectroscopy and size exclusion chromatography data (Jarusutthirak, 2002). Waste water effluents comprise highly refractory, non-biodegradable OM, which persists in potable water supplies following most potable water treatment strategies (Dignac *et al*., 2000; Drewes *et al*., 2003), as well as microbial metabolites that are retained in discharge effluents of biologically treated wastewater (Jarusutthirak, 2002). Namour and Müller (1998) found that the HPO fraction of Ef-OM was the most recalcitrant fraction to biological treatment and corresponded to humic substances.

Several differences were evident in the relative abundances of the aromatic pyrolysate distribution detected by MSSV Py of the two Ef-OM fractions. The N-HPO sample showed APs > ABs > ANs/APhs, closely resembling the product distributions of the surface waters. In contrast the reverse trend of ANs > ABs > APs

was observed for S-HPO. The longer biological treatment times used at the St. Julien WWTP may account for these quantitative differences. This suggests that the precursors of ANs, which were the most abundant products of S-HPO, are more resistant to degradation than the precursors of alkyl phenols.

3.3.3 Alkyl benzenes

3.3.3.1 Alkyl benzene distributions of aquatic NOM fractions

a) Surface and ground waters

Minimal variation was evident in the AB distributions of the HPO fractions of the ground and surface waters. The ABs ($\leq C_5$) detected by MSSV Py of U-HPO, U-TPI and L-HPO are highlighted in the summed ion chromatograms of **Figure 3.4**. Many AB isomers have very similar mass spectra and require additional GC retention time correlation with authentic standards for unequivocal identification (Hartgers *et al*., 1992). Therefore several of the isomeric assignments given in Figure 3.4-3.6 and Table 3.1 are tentative only.

High relative concentrations of toluene and C_2 benzenes (ethylbenzene, *o*-, *m*- and *p*-xylene) were detected in all three NOM fractions. These low molecular weight (MW) ABs are also common flash pyrolysates of aquatic NOM (e.g. Saiz-Jimenez, 1993; Schulten and Gleixner, 1999; van Heemst *et al*., 2000; González-Vila *et al*., 2001; Lu *et al*., 2001; Guo *et al*., 2003; Templier *et al*., 2005a). Since they can derive from several biomolecular sources they offer very limited source diagnostic value. The greater structural specificity of more highly substituted benzenes may provide more valuable precursory information. MSSV Py consistently detected higher concentrations of C_3-C_5 ABs than flash pyrolysis, which generally showed decreasing abundance with increasing alkyl substitution.

Several C_3 and C_4 alkyl benzenes, including 1,2,3- and 1,2,4-trimethylbenzene (TMB), 1,2,3,4-tetramethylbenzene (TeMB) and *p*-cymene (1-methyl-4-isopropylbenzene) were detected in high abundance from both the ground (L-HPO; **Fig. 3.4a**) and surface water (U-HPO; **Fig. 3.4b**) hydrophobic fractions. The major difference between these samples was the detection of higher concentrations of several additional ABs from L-HPO, including isopropyl benzene, 1,3,5-TMB, 1,2,4,5-TeMB, 1,2,3,5-TeMB, and several dimethylethylbenzenes (DMEB) and C_5

isomers. The major AB products of the U-TPI fraction (**Fig 3.4c**) were ethyl substituted isomers including ethylbenzene, 1M-3EB, 1M-4EB, 13-DEB and 14-DEB. This contrasted with the HPO fractions in which the polymethylated benzenes were detected in higher concentrations. This suggests that different AB precursors can be separated on the basis of polarity by the XAD procedure.

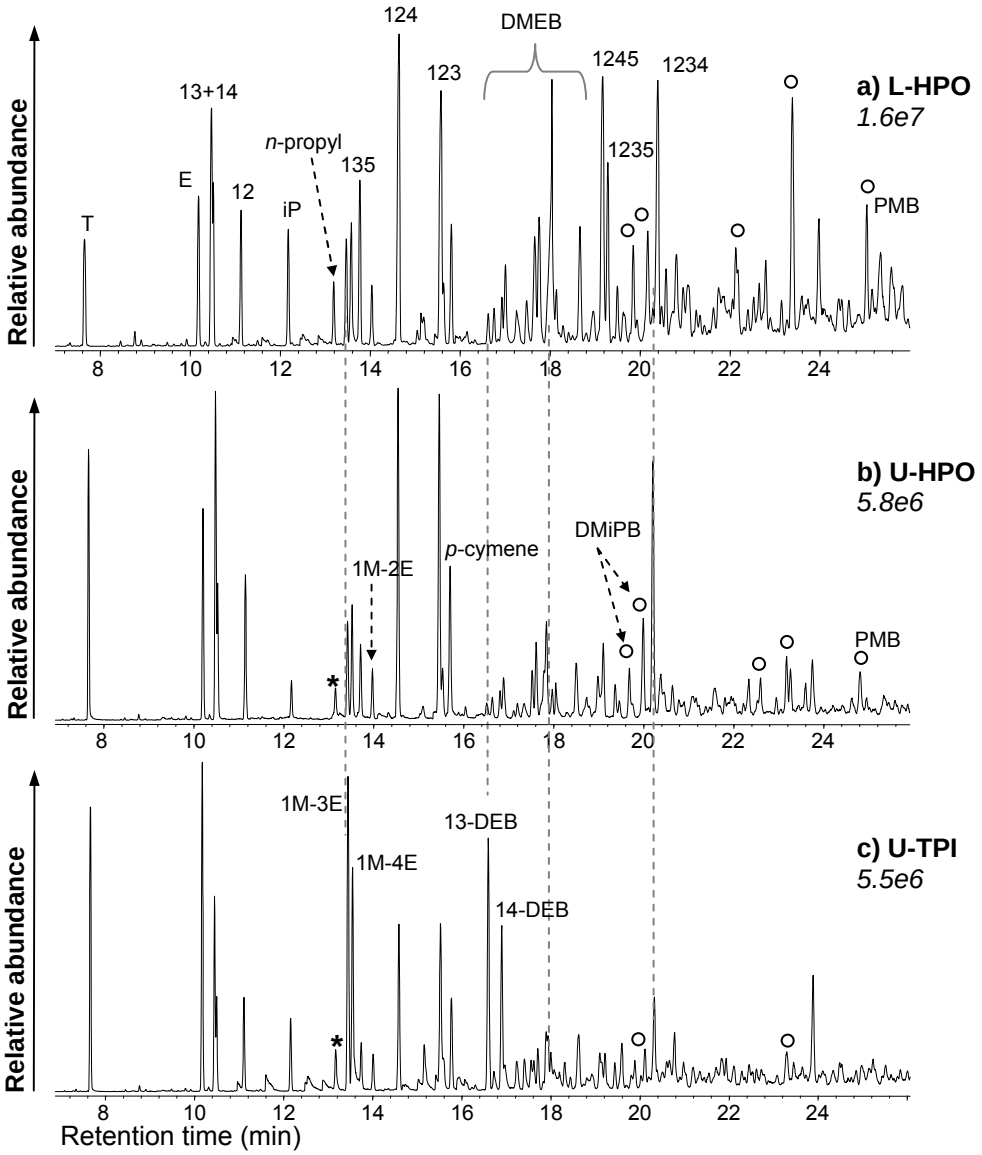

Figure 3.4 Summed *m/z* 91+105+106+119+120+133+134+148 chromatograms showing the alkyl (C_1-C_5) benzene distributions from the 300˚C/72hr MSSV pyrolysis GC-MS analysis of **a)** L-HPO, **b)** U-HPO and **c)** U-TPI fractions. Peak assignments correspond to products listed in Table 3.1. Relative abundances of a-c are indicated in italics.

b) Waste water effluents

The AB distributions detected from the HPO fractions of the two waste waters are shown in **Figure 3.5**. 1,2,4-TMB, 1,2,3-TMB and *p*-cymene were detected in similarly high concentrations to the surface and ground waters. However, the presence of C_3-C_6 *n*-alkyl benzenes and *sec*-alkyl benzenes distinguished the AB profiles of the waste water effluents. With the exception of *n*-propyl and isopropyl benzene, these products were not detected from the surface and ground water fractions. They may be indicative of specific waste water inputs, such as industrial or domestic chemicals or metabolites of unique microbial or algal communities. The generally lower concentration of ABs detected by flash pyrolysis, including absence of *n*-alkyl ($\geq C_4$) and *sec*-alkyl benzene products from the waste waters (Jarusutthirak, 2002), did not reflect any obvious variation between the samples.

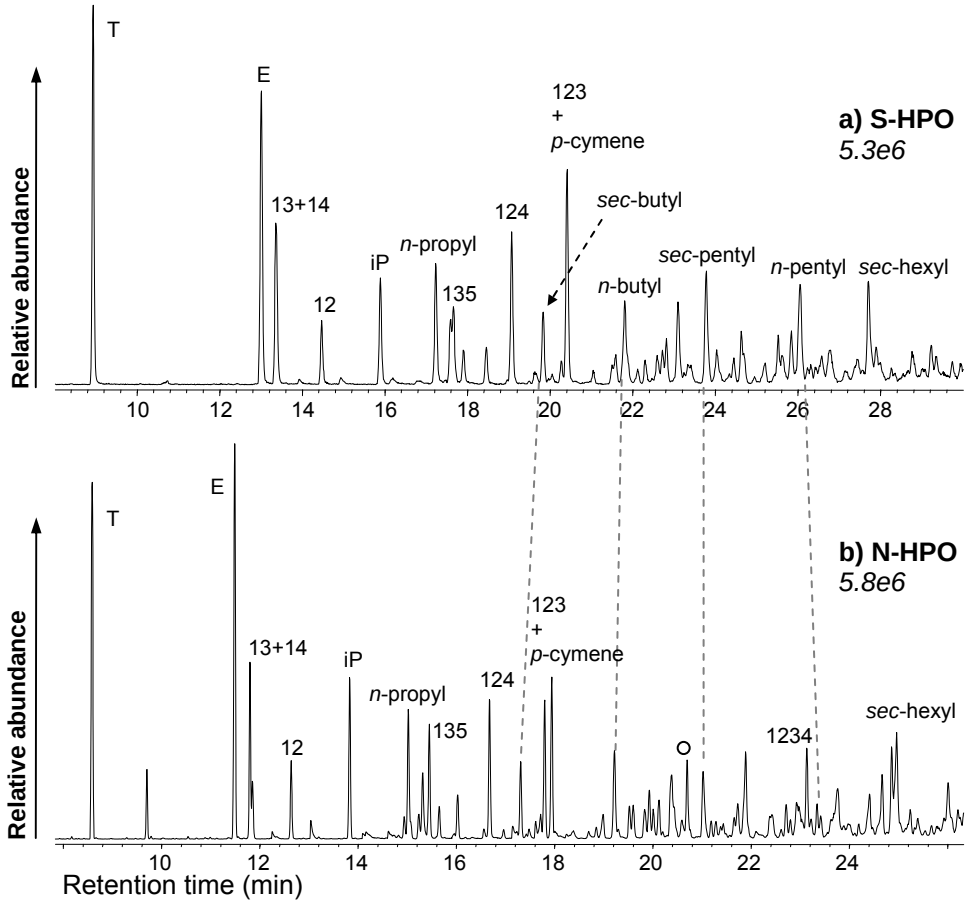

Figure 3.5 Summed *m/z* 91+105+106+119+120+133+134+148 chromatograms showing the alkyl (C_1-C_5) benzene distributions from the 300˚C/72hr MSSV pyrolysis GC-MS analysis of **a)** S-HPO and **b)** N-HPO. Peak assignments correspond to products identified in Table 3.1. Relative abundances of a-b are indicated in italics.

3.3.3.2 Alkyl benzene distributions of representative standards

Very few ABs have obvious natural biomolecular origins (Bastow, 1998). They have been proposed as primary structural units of humic substances (Schulten, 1993; 1996a; 1996b), but can also arise from the secondary thermal alteration of other NOM constituents. MSSV pyrolysis of model compounds and representative materials can provide information on potential AB precursors, thereby establishing the primary versus secondary nature of these pyrolysates with greater reliability.

Toluene and the C_2 benzenes were prominent products in the MSSV pyrolysates (300˚C/72hr) of all the standards, except stearic acid. This fatty acid yielded no aromatic products. The general prevalence of the low MW ABs significantly limits their diagnostic value. Low relative abundances of the C_1-C_2 ABs, and also isopropyl benzene, were detected from the amino sugar (chitin) and lignin monomer (syringic acid; Appendix 3). The albumin protein (BSA; **Fig. 3.6d**) and aromatic amino acid phenylalanine (Appendix 3) yielded high concentrations of toluene, ethylbenzene and *n*-propylbenzene, which are also common flash pyrolysates of these materials (Chiavari and Galetti, 1992). These products were the only major aromatic HCs detected from the colloid fractions of the waste waters (Appendix 2), consistent with the typically high proteinaceous and low humic content of colloidal OM (Rostad *et al*., 1997; Leenheer *et al*., 2001a).

a) Alkyl benzenes from lignin and cellulose

MSSV pyrolysis (300˚C/72hr) of cellulose (**Fig. 3.6 a**), lignin (**Fig. 3.6 b**) and extant wood samples of *Pinus radiata* and *Wandoo eucalyptus* yielded mostly oxygenated products such as alkyl furans, alkyl phenols and alkylmethoxy aromatics, but also included low concentrations of alkyl ($\geq C_3$) benzenes (Appendix 3). The AB products of cellulose cannot be ascribed to indigenous structural moieties but are instead produced by thermal degradation and rearrangement during off-line MSSV treatment. The dominant AB product of lignin and the wood samples was toluene, which is likely produced by depolymerisation and thermal cleavage of the methoxy and hydroxy aromatic ring substituents of lignin structural units. Lower concentrations of 1-M-3-EB, 1,2,4-TMB, 1,2,3-TMB and *p*-cymene were also detected.

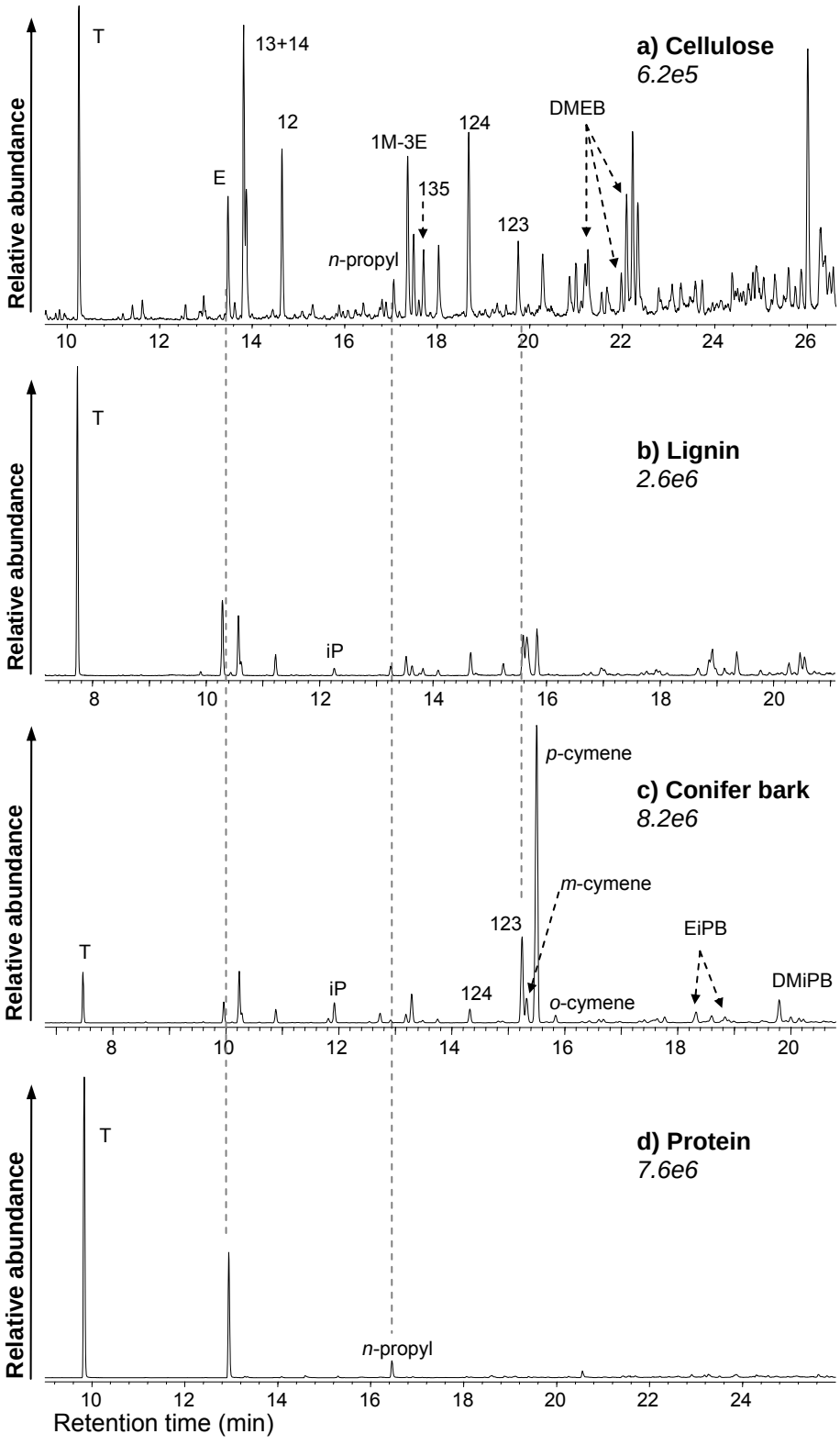

Figure 3.6 Summed *m/z* 91+105+106+119+120+133+ 134+148 chromatograms showing the alkyl (C_1-C_5) benzene distributions from the 300˚C/72hr MSSV pyrolysis GC-MS analysis of **a)** cellulose, **b)** lignin, **c)** *Pinus radiata* bark and **d)** BSA protein. Peak assignments correspond to the products listed in Table 3.1. Relative abundances of a-d are indicated in italics.

The thermal formation of aromatic hydrocarbons from methoxy phenol lignin structures following extended maturation processes (e.g. coalification) has been demonstrated both in natural environments (Hayatsu *et al*., 1986, Stout *et al*., 1988, Hatcher, 1988, Bates and Hatcher, 1989, Hatcher *et al*., 1989b) and by analogous closed system pyrolysis experiments of extant and fossilized wood (Behar and Hatcher, 1995) and immature coals (Mansuy *et al*., 1995; Michels *et al*., 2000). Bracewell *et al*. (1980) also demonstrated that the abundance of ABs in flash pyrolysates of relatively immature soil OM correlated with an increasing degree of humification, in parallel with the degradation of lignin-derived structures. However, humification of lignin structural moieties during hydrological transportation and water column residence would not be expected to account for the significantly higher abundances of alkyl benzenes in the NOM fractions compared with fresh lignocellulose biomass. Furthermore, although flash pyrolysis and thermochemolysis of the humic surface waters (i.e. U-HPO and G-HPO) yielded several diagnostic lignin markers, these products were detected in very low abundance from the flash pyrolysates of the ground (i.e. L-HPO; Lavaud *et al*., 2008) and waste waters fractions (Jarusutthirak, 2002). The MSSV data of all these fractions yielded abundant alkyl benzenes, indicating an alternative origin to lignin.

b) Alkyl benzenes from terpenoids

MSSV pyrolysis of the *Pinus radiata* bark produced relatively high concentrations of C_3-C_5 ABs (**Fig. 3.6c**). The major products included isopropyl benzene, 1,2,3-TMB, *p*-cymene, ethylisopropylbenzene (EiPB), methyl(methylpropyl)benzene and dimethylisopropylbenzene (DMiPB), several of which were also prominent in the MSSV data of the NOM fractions. Correlation with the *Pinus radiata* bark sample suggests these NOM products may derive from terpenoid constituents of plant resins.

Naturally occurring terpenoids occur in an extremely wide variety of structural configurations making it difficult to unequivocally identify specific terpenoid precursors of individual AB pyrolysates. Nevertheless, several possible terpenoid sources may be inferred for some of the dominant C_3-C_5 AB products presently detected by MSSV Py. For example, *p*-cymene is a naturally occurring aromatic monoterpenoid found in essential oils of many higher plants and was detected in high concentration from all the NOM fractions. This compound may therefore

represent a primary terpenoid product of higher plants. The sedimentary occurrence of *p*-cymene has also been attributed to diagenetic aromatisation and reduction of several structurally related higher plant (Radke, 1987; van Aarssen *et al*., 1990) and fungal terpenoids (Hartgers *et al*., 1994b), including unsaturated (e.g. limonene), functionalised (e.g. terpineol, menthol) and polymeric (e.g. polycadinene) compounds. The thermal release of mono- and sesquiterpenoids precursors of *p*-cymene may proceed without significant structural alteration (Peters *et al*., 2005). A number of C_5 benzenes present in the U-HPO, L-HPO and pine bark pyrolysates were also tentatively identified as alkylated derivatives of *p*-cymene (i.e. ethyl- and dimethylisopropylbenzenes).

Both 1,2,3,4- and 1,2,3,5-TeMBs, major MSSV pyrolysates of all HPO fractions, have been previously considered primary kerogen fragments on the basis of flash pyrolysis studies (Hartgers *et al*., 1994b). Their formation has been attributed to cleavage of macromolecularly-bound diaromatic carotenoids such as isorenieratene (Hartgers *et al*., 1994a; 1994b; 1994c; Pedentchouk *et al*., 2004). Carotenoids are tetraterpenoid organic pigments found widely in plants and other photosynthetic organisms like algae and some types of fungi and bacteria. 1,2,3,4-TeMB, in addition to 1,3- and 1,4-DMB and 1,2,3- and 1,2,4-TMB, have also been attributed to bound non-aromatic carotenoid precursors such as ββ-carotene present in the cell membranes of microalgae. These ABs were thought to form during diagenesis by cyclisation, aromatisation and possibly loss of methyl groups (Hartgers *et al*., 1994b; Koopmans *et al*., 1997; Brown *et al*., 2000; Pedentchouk *et al*., 2004).

c) Other non-terpenoid sources of alkyl benzenes

Monosubstituted C_3-C_6 *n*-alkylbenzenes (e.g. propyl-, butyl-, pentyl-, hexylbenzene) were abundant pyrolysates of the waste water fractions only. In flash pyrolysis studies of sedimentary OM (Derenne *et al*., 1991; Hartgers *et al*., 1994a; 1994b; Han and Kruge, 1999) and algal biomass (Hoefs *et al*. 1995), these products were thought to be formed by cyclisation and aromatisation of selectively preserved aliphatic biopolymers derived from algal cell walls (Douglas *et al*., 1991; Sinninghe Damsté *et al*., 1991; 1993). Hence, the high concentrations of *n*-alkyl benzenes of the HPO Ef-OM fractions may be attributed to aliphatic algal precursors. Algal contribution in

riverine and ground water NOM, on the other hand, is typically very low compared to input from terrigenous higher plant sources.

3.3.4 Alkyl naphthalenes

3.3.4.1 Alkyl naphthalene distributions of aquatic NOM fractions

a) Surface and ground waters

The distribution patterns of the alkyl (C_1-C_5) naphthalenes (ANs) detected by MSSV pyrolysis of the hydrophobic fractions of the Uruguay surface water (U-HPO) and the ground water (L-HPO) are shown in the summed ion chromatograms of **Figure 3.7**. The high concentrations and broad isomeric distribution of ANs from the L-HPO data suggests that many of these products originate from terpenoid derived structural moieties rich in this ground water. Polymethylated naphthalenes dominated the distribution but several higher MW alkyl isopropyl naphthalenes (e.g. eudalene, cadalene) were also prominent. Like ABs, isomeric ANs have very similar mass spectra and require additional retention time distinction, and often correlation with authentic standards, for unequivocal identification. Hence, several of the isomeric assignments given in Figures 3.7-3.9 and Table 3.1 are tentative only.

U-HPO was also characterised by high relative abundances of polymethylated naphthalenes. 1,6-dimethyl naphthalene (DMN), 1,2,5- and 1,2,7-trimethylnaphthalene (TMN) and 1,2,3,4-tetramethylnaphthalene (TeMN) were the major C_2-C_4 isomers. Cadalene was the major C_5 product; but was detected in much lower abundance relative to the C_1-C_4 polymethyl naphthalenes. The G-HPO and U-TPI fractions showed a similar distribution of ANs, but of lower relative abundance by factors of approximately two and ten, respectively (Fig. 3.3). This may reflect lower contribution from terpenoid OM.

b) Waste water effluents

The C_1-C_5 AN distributions detected by MSSV pyrolysis (300˚C/72hr) of the waste water HPO fractions are shown in the summed ion chromatograms of **Figure 3.8**. ANs were the most abundant group of pyrolysates from S-HPO, indicating that their precursory structures are recalcitrant to biological degradation. The AN distributions of the wastewater effluents, like the AB profiles, were very different to the surface and ground waters.

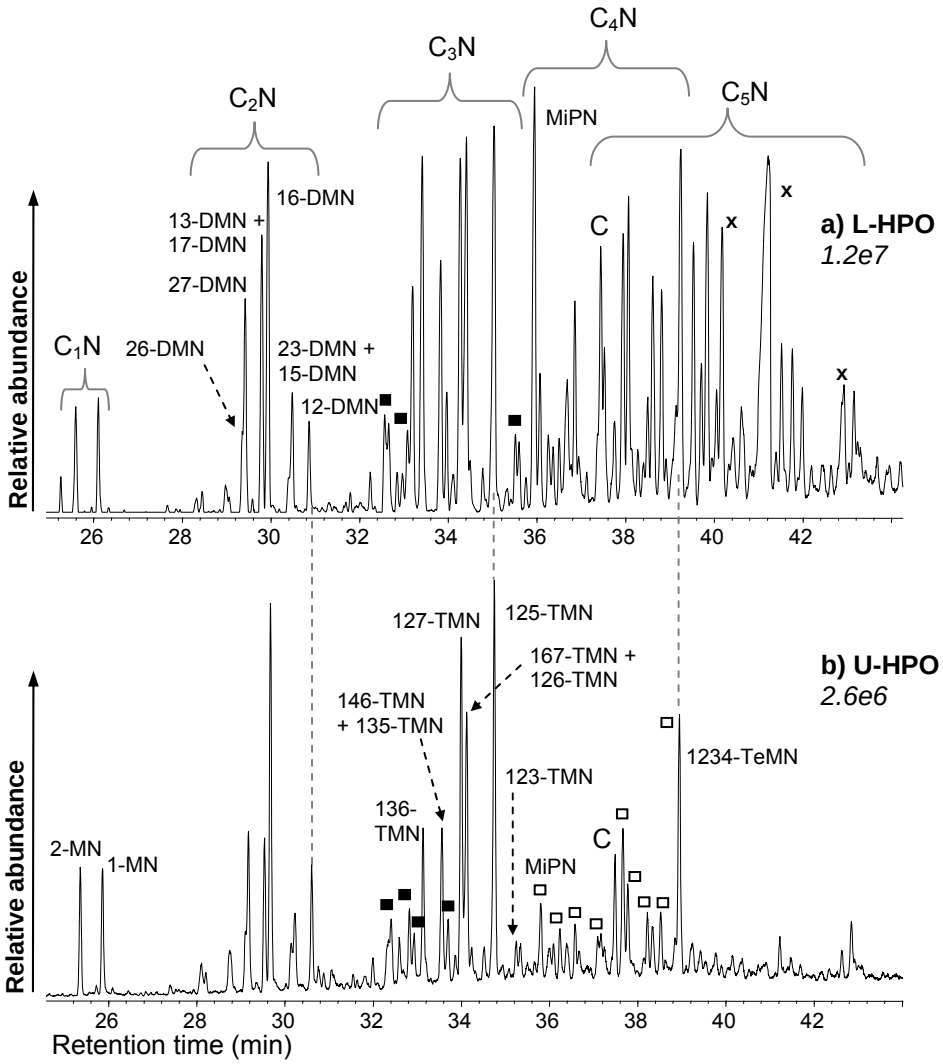

Figure 3.7 Summed *m/z* 141+142+155+156+169+170+183+184+198 chromatograms showing the alkyl (C_1-C_5) naphthalene distributions detected from the 300˚C/72hr MSSV pyrolysis GC-MS analysis of **a)** L-HPO (groundwater) and **b)** U-HPO (river water). Peak assignments correspond to products listed in Table 3.1. Relative abundances of a-b are indicated in italics. **x** = non-AN pyrolysates.

The major products of the waste waters included *n*-alkyl- (C_1-C_4), methylethyl- and methylpropylnaphthalenes. These products were detected in higher relative concentrations than the polymethylated products, which were the major ANs of the surface and ground water fractions. The prominence of *n*-alkylnaphthalenes mirrors the high concentrations of *n*-alkyl benzenes detected from the waste waters. These differences were not detected by flash pyrolysis, which consistently showed low AN concentrations, in which the parent and mono-methyl compounds were dominant.

MSSV Py may facilitate the softer thermal release of the precursory constituents of these products from the macromolecular network, allowing better preservation of their alkyl substitution patterns.

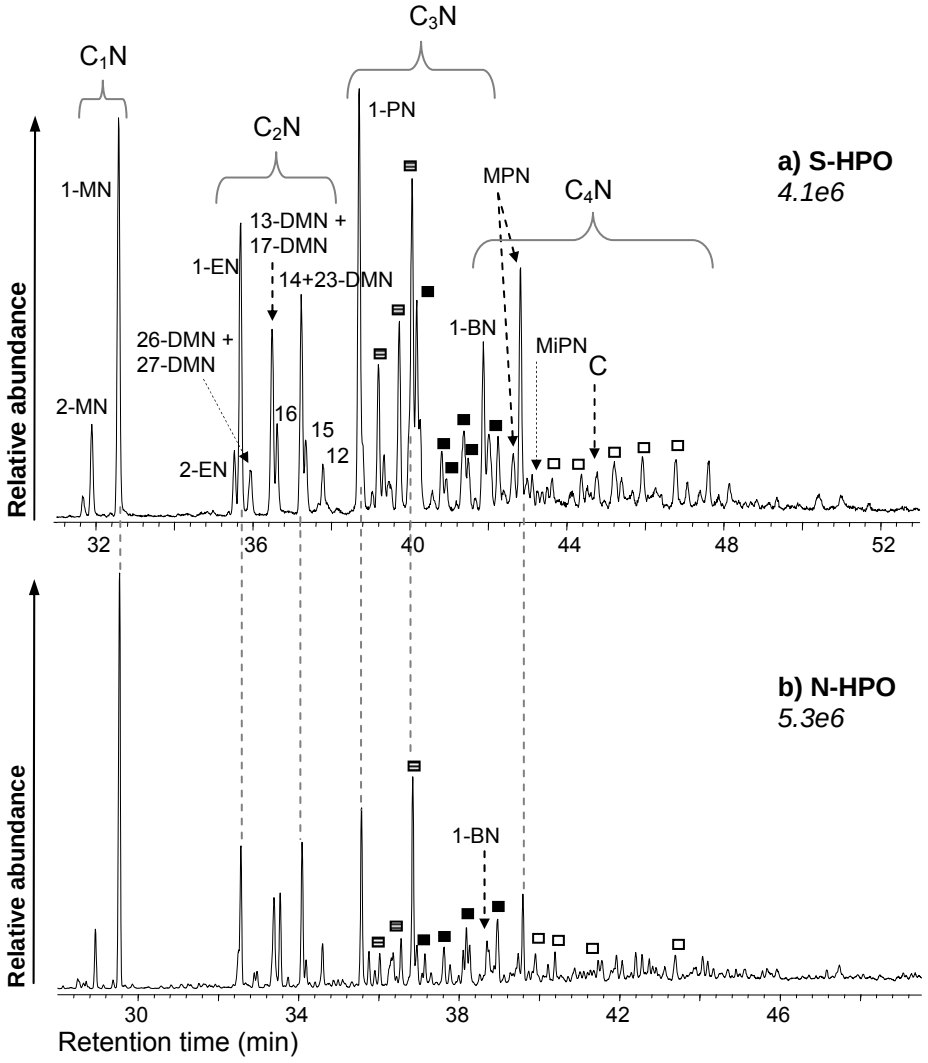

Figure 3.8 Selected *m/z* 141+142+155+156+169+170+183+184+198 chromatograms showing the alkyl (C_1-C_5) naphthalene distributions detected by the 300˚C/72hr MSSV pyrolysis GC-MS analysis of **a)** S-HPO and **b)** N-HPO. Peak assignments correspond to products listed in Table 3.1. Relative abundances of a-b are indicated in italics.

3.3.4.2 Alkyl naphthalene distributions of representative standards

Of the representative materials analysed by MSSV pyrolysis, only the *Pinus radiata* and *Wandoo eucalyptus* bark samples afforded high concentrations of ANs. ANs were either not detected or were very minor pyrolysates of the other standard

materials. Mono- and condensed aromatics are often considered to be secondary products of functionalised aliphatic biopolymers. Flash pyrolysis of fatty acids in the presence of clay minerals and/or sulphur, for example, produced alkyl benzenes, indenes and naphthalenes via decarboxylation and secondary cyclisation and aromatisation reactions (Saiz-Jimenez, 1994; 1995, Faure *et al*., 2006a; 2006b). The closed system conditions of MSSV may invoke similar secondary reactions; however MSSV analysis of stearic acid, an *n*-C_{18} alkanoic acid, gave no evidence for the formation of aromatic byproducts (data not shown). Aromatisation processes associated with flash pyrolysis may not be promoted to the same extent by the milder thermal conditions of the MSSV experiment. Several fatty acids (as methyl esters) were detected by thermochemolysis of U-HPO and L-HPO (Lavaud *et al*., 2008) but they are unlikely precursors of the aromatic hydrocarbons detected by MSSV Py.

A lignin origin for the ANs detected from the NOM fractions is also unlikely. MSSV pyrolysis (300˚C/72hr) of lignin showed very low concentrations of ANs. Artificial maturation studies of immature coals (Mansuy *et al*., 1995) and fossil woods (Behar and Hatcher, 1995), analogous to the MSSV pyrolysis procedure, have demonstrated that severe thermal heating, thought to represent extended maturation processes in natural systems, is necessary to generate aromatic HCs from methoxyphenol moieties of lignin (Hatcher, 1988). MSSV analysis of the lignin standard at 340˚C/72hr (Appendix 4) yielded higher abundances of naphthalenes (and benzenes) compared to the 300˚C experiment, however these pyrolysates were still minor compared to phenolics. The low abundance of ANs from lignin, even under more severe thermal treatment, does not account for the high concentrations observed in the aquatic NOM pyrolysates.

Higher plant terpenoids present in resins, bark and leaf tissues are often preserved as source specific AN biomarkers in sediments, coals and crude oils (Hayatsu *et al*., 1990, Smith *et al*., 1995; Watson *et al*., 2005). The C_1-C_5 AN distributions of the MSSV pyrolysed conifer and eucalyptus bark samples are shown in **Figure 3.9**. The pine bark was characterised by high concentrations of 1,6-DMN, 1,2,5-TMN, eudalene (methylisopropylnaphthalene; MiPN), cadalene and an isomer of TeMN. The major products of the *Wandoo* bark were TeMN, 1,6,7-TMN and 1,2,6-TMN. All of the major ANs identified in the bark pyrolysates were also detected in high

abundance in the surface and ground waters (Fig 3.7), providing evidence that these aquatic NOM pyrolysates originate from higher plant terpenoids.

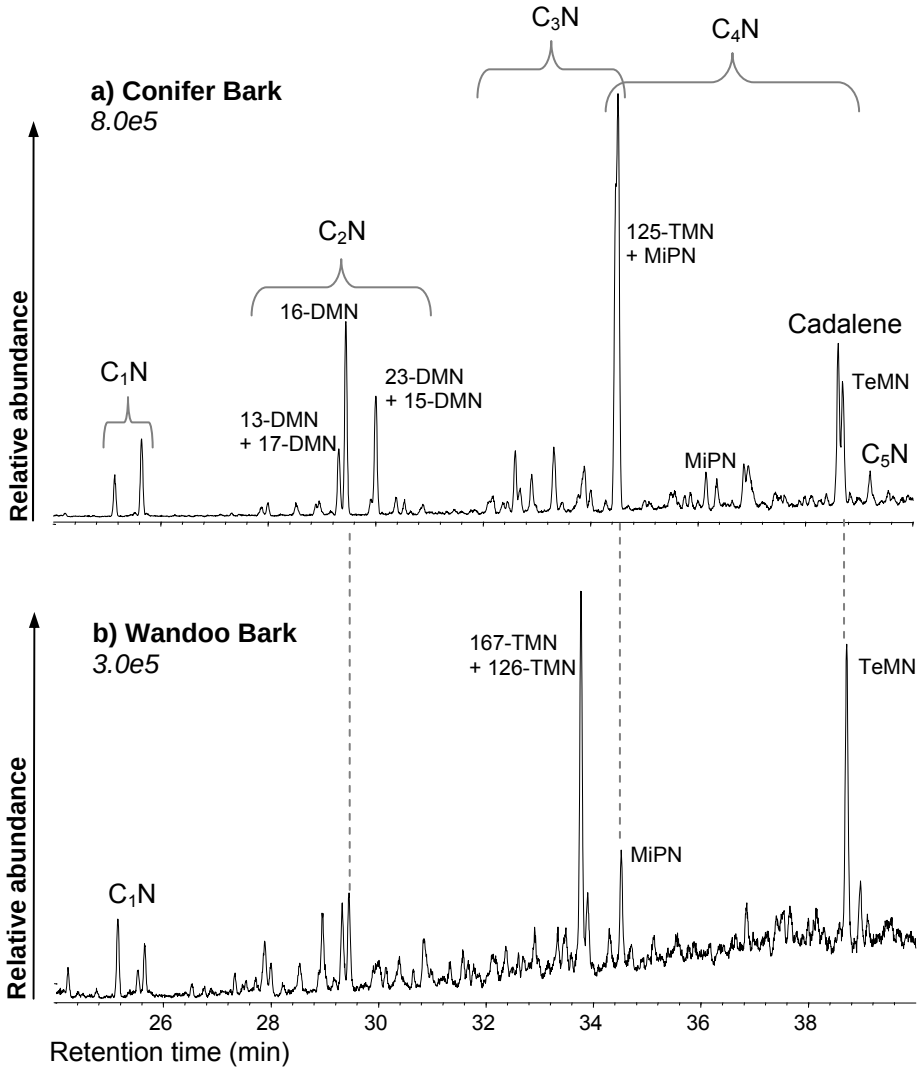

Figure 3.9 Summed *m/z* 141+142+155+156+169+170+183+184+198 chromatograms showing the alkyl (C_1-C_5) naphthalene distributions detected from the 300˚C/72hr MSSV pyrolysis GC-MS analysis of **a)** *Pinus radiata* and **b)** *Wandoo eucalyptus* bark. Peak assignments correspond to products listed in Table 3.1. Relative abundances of a-b are indicated in italics.

3.3.4.3 Higher plant terpenoid precursors of alkyl naphthalenes

Naturally occurring terpenoids comprise an extremely wide variety of aliphatic alicyclic, unsaturated, aromatic, and polymeric structures, often possessing functional group substituents. The biodegraded or otherwise diagenetically altered

products of terpenoids in aquatic ecosystems are not well established. Many higher plant terpenoids are cyclic and unsaturated and tend to undergo aromatisation during natural or artificial maturation (van Aarssen *et al*., 2000). Aromatisation of alicyclic terpenoids during MSSV thermal treatment may contribute to the high concentrations of aromatic HCs detected in several of the NOM samples (e.g. L-HPO and U-HPO). This thermal formation pathway would be consistent with the higher aliphatic and lower aromatic content of L-HPO identified by ^{13}C-NMR spectroscopy (Chapter 3.3.2.2). Whilst thermally promoted reactions during closed system pyrolysis may result in structural alteration, specific biomolecular sources can be inferred for some major AN products.

The higher plant biomarkers eudalene (MiPN) and cadalene were (tentatively) identified in the ground and surface water fractions (Fig 3.7). They are diagenetically formed in sediments from naturally occurring sesquiterpenoids possessing eudesmane and cadinene HC skeletons, which are ubiquitously present in many higher plant species (Simoneit, 1985). Cadalene may also derive from polycadinene, a component of dammar resin synthesized by some angiosperms such as Dipterocarpaceae (van Aarssen *et al*., 1994).

Other ANs previously detected in extracts and flash pyrolysates of oil, coal and sediments have also been attributed to further alteration of polycadinene (Hatcher and Clifford, 1997). Artificial maturation of fossilized and extant dammar resins by closed system isothermal pyrolysis demonstrated that cadinenes preferentially lose the isopropyl group with increasing maturity, corresponding to a higher relative abundance of 1,6-DMN compared to cadalene (van Aarssen *et al*., 1991). 1,6-DMN was the major C_2 naphthalene identified from the ground and surface water fractions. An increase in the relative abundance of this product was also observed by MSSV thermal treatment of U-HPO over the temperature range 260 - 340˚C (72hr), as shown in **Figure 3.10**. It is likely derived via aromatisation of sesquiterpenoids possessing the cadinene skeleton to form cadalene, followed by loss of the isopropyl group. The lower relative concentration of cadalene is consistent with its transformation to 1,6-DMN.

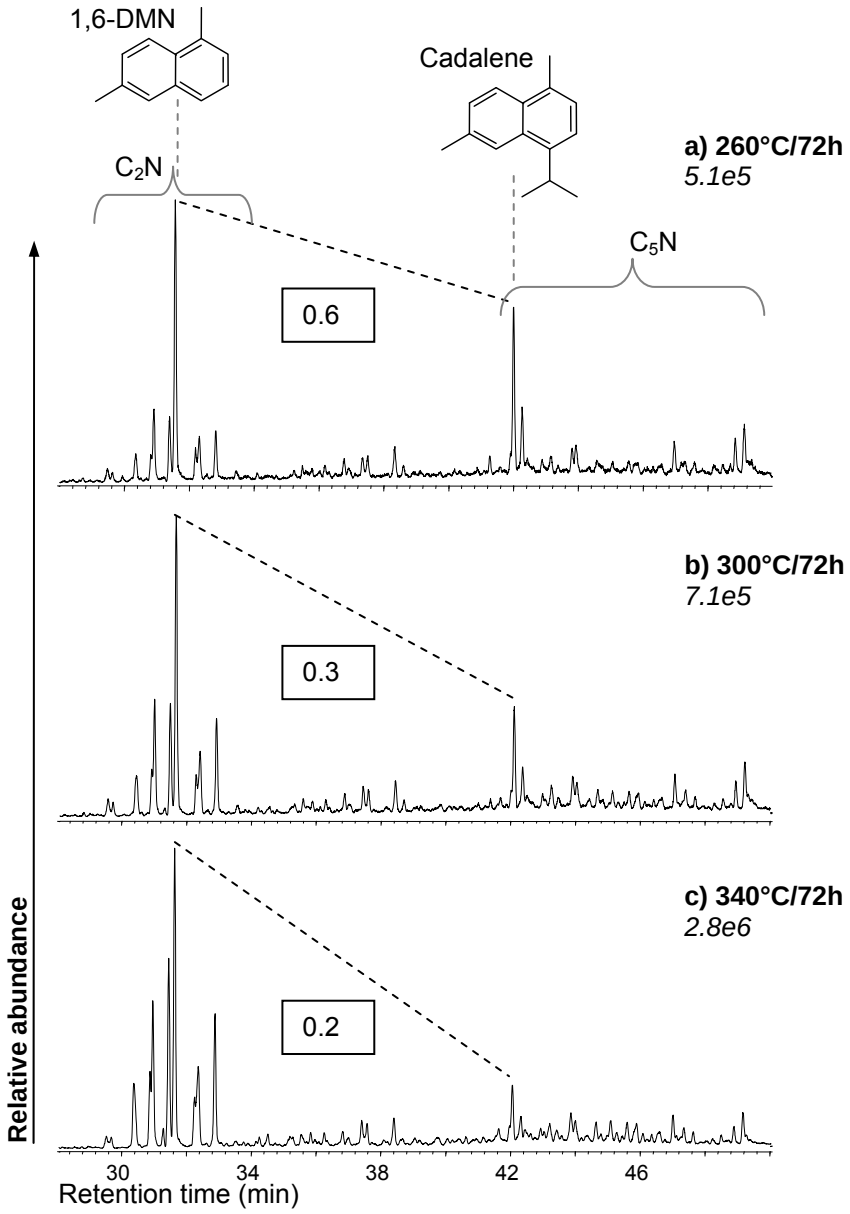

Figure 3.10 Summed *m/z* 141+156+183+198 chromatograms showing the relative abundances of 1,6-dimethylnaphthalene and cadalene detected from U-HPO at MSSV pyrolysis temperatures of **a)** 260˚C, **b)** 300˚C and **c)** 340˚C/72h. The 1,6-DMN/cadalene ratio calculated from the integrated peak areas are indicated in the boxed values. Relative abundances of a-c are indicated in italics.

Several other prominent ANs identified from the NOM fractions (Fig 3.7) may be attributed to higher plant terpenoids. 1,2,5-TMN, which was the most abundant C_3 isomer of the U-HPO, L-HPO and conifer bark samples, can derive from bicyclic diterpenoids (e.g. agathic acid) and resins common in conifers, or the compound onocerane, which has been found in vascular plants including ferns, horsetails and

lycopods (Pearson and Obaje, 1999; Watson *et al*., 2005). 1,2,5-TMN and 1,2,7-TMN, also prominent in the NOM pyrolysates, are diagenetic products of oleanane type pentacyclic triterpenoids (e.g. β-amyrin), which are specific to flowering plants (Strachan *et al*., 1988, Watson *et al*., 2005). In addition, 1,2,6-TMN can be formed by isomerization of the 1,2,5-TMN isomer (Strachan *et al*., 1988). TeMNs may derive from oxygenated triterpenoids such as arborene and fernene or from bicyclanes (Bastow, 1998).

3.3.4.4 Other non-terpenoid sources of alkyl naphthalenes

The major ANs of the St. Julien and Naintré HPO waste water fractions (Fig. 3.8), including ethyl, ethylmethyl, *n*-propyl, propylmethyl and *n*-butylnaphthalenes, were not detected from the natural waters and barks suggesting an alternative biochemical source. Audino *et al*. (1996) attributed the ubiquitous occurrence of ethylmethylnaphthalenes in crude oils to a microbial origin. Han and Kruge (1999) suggested an algal origin for *n*-alkylnaphthalenes due to their relative enrichment in flash pyrolysates of *Botryococcus* related alginites. *n*-Alkylnaphthalenes were thought to derive from the same straight chain aliphatic precursors as *n*-ABs, also enriched in the waste waters (section 3.3.4.2), via additional cyclisation and aromatisation steps (Hartgers *et al*., 1994b; Han and Kruge, 1999). In addition, 2,3- and 1,4-DMN have also been strongly correlated with algal derived OM (Han and Kruge, 1999) and were found to be the most abundant DMN isomers of both the N-HPO and S-HPO fractions. The AN data suggest the incorporation of algal and bacterial biomass into HPO fractions of the influent waste water stream, and subsequently the effluent OM.

3.3.5 Alkyl phenanthrenes

3.3.5.1 Alkyl phenanthrene distributions of aquatic NOM fractions

Alkyl phenanthrenes (APhs) were detected in significant abundance only from the MSSV pyrolysis of the Uruguayan surface water and the ground water. The C_1-C_3 APh distributions of these fractions are shown in **Figure 3.11**. Alkyl phenanthrenes are not common flash pyrolysates of aquatic NOM, but along with mono-aromatics and other condensed PAHs, may be molecular sub-units of humic substances (Schulten and Gleixner, 1999). 1-methylphenanthrene (1-MP) and 1,7-dimethylphenanthrene (1,7-DMP) were prominent in both samples. Sedimentary

occurrence of these compounds has been attributed to aromatisation of tricyclic diterpenoid constituents of conifer resins (Alexander *et al*., 1992; Smith *et al*., 1995). Several additional phenanthrene biomarkers diagnostic of diterpenoids were also detected in these samples and are discussed in the flowing section (3.3.5.2).

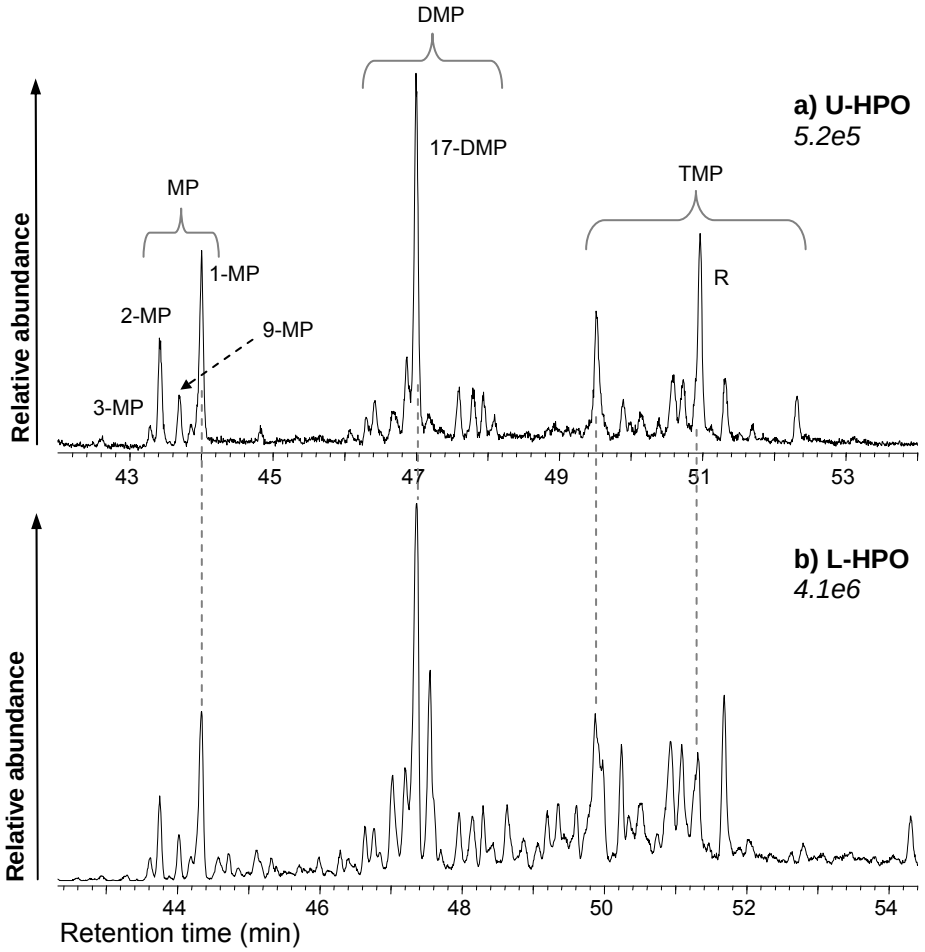

Figure 3.11 Summed *m/z* 192+206+220 chromatograms showing the distribution of C_1-C_3 alkyl phenanthrenes from the 300˚C/72hr MSSV pyrolysis GC-MS analysis of **a)** U-HPO and **b)** L-HPO. Peak assignments correspond to products listed in Table 3.1. Relative abundances of a-b are indicated in italics.

PAHs can also arise from inert aromatic NOM moieties (e.g. black carbon) generated by biomass or fossil fuel burning. Recent research (Almendros *et al*., 1998; Chefetz *et al*., 2002; Koch and Dittmar, 2006) has shown that part of the aromaticity of aquatic, soil and sedimentary humic substances can originate from stable thermogenic carbon derived from forest fires. Parent and alkylated phenanthrenes, fluoranthenes, pyrenes and other PAHs detected in extracts and flash pyrolysates of recent sediments have also been attributed to anthropogenic pollutants such as

petroleum or combusted fossil fuels (Blumer and Youngblood, 1975; Saiz-Jimenez, 1994; Deshmukh *et al*., 2001; Kruge and Permanyer, 2004; Simpson *et al*., 2005). PAH contaminants have been shown to bind rapidly to aquatic humic substances (Schlautman and Morgan, 1993).

Phenanthrene products were not identified amongst the thermal desorption products (MSSV injector 300˚C) or flash pyrolysates of the fresh NOM samples (**Fig. 3.1b-c**), suggesting their occurrence following MSSV pyrolysis is not due to readily labile free or surface adsorbed hydrocarbon constituents derived from forest fires or petroleum/oil contamination. Furthermore, if combusted biomass or fuels were significant contributors to the NOM samples a variety of other combustion derived PAHs (e.g. flourenes, chrysenes, pyrenes), dominated by the parent and mono-alkyl substituted hydrocarbons, would be expected (Watson *et al*., 2005).

3.3.5.2 Higher plant terpenoid precursors of alkyl phenanthrenes

Several branched and partially hydrogenated APhs were identified from the MSSV pyrolysis (300˚C/72hr) of the U-HPO fraction, as shown in the summed ion chromatograms of **Figure 3.12**. Retene (1-methyl-7-isopropyl phenanthrene) was most prominent and was detected in similar abundance to the major polymethyl naphthalene products. Retene, as well as cadalene, was common to the full suite of NOM fractions analysed in this study but the U-HPO fraction yielded this product in highest abundance. Retene is a generic biomarker of conifer input, derived predominantly from aromatisation of tricyclic diterpenoids possessing an abietane or phyllocladane hydrocarbon skeleton (Bastow *et al*., 2001). In sedimentary OM, retene is most commonly attributed to abietanoic acids present in pine resins (Wakeham, 1980). It is also a known diagenetic product of other diterpenoids such as phenolic and ketophenolic abietanes, which occur in non-*Pinaceae* conifer families. Several other biomarkers of abietic acid, including 18- and 19-norabieta-8,11,13-triene (dehydroabietins; DHAs), 1,2,3,4-tetrahydroretene (THR) and methyl retene (MeR), were also detected in the U-HPO fraction. The occurrence of these diterpenoid pyrolysates confirms the presence of pine resin acids and demonstrates the diagnostic information that established biomarkers can provide regarding the source of aquatic NOM. These products were not detected by corresponding flash pyrolysis. Likewise, thermochemolysis analysis of U-HPO detected only trace

amounts of methylated dehydroabietic acid (data not shown), although an isomeric phenanthrene carboxylic acid likely related to retene was tentatively identified from the thermochemolysate of L-HPO.

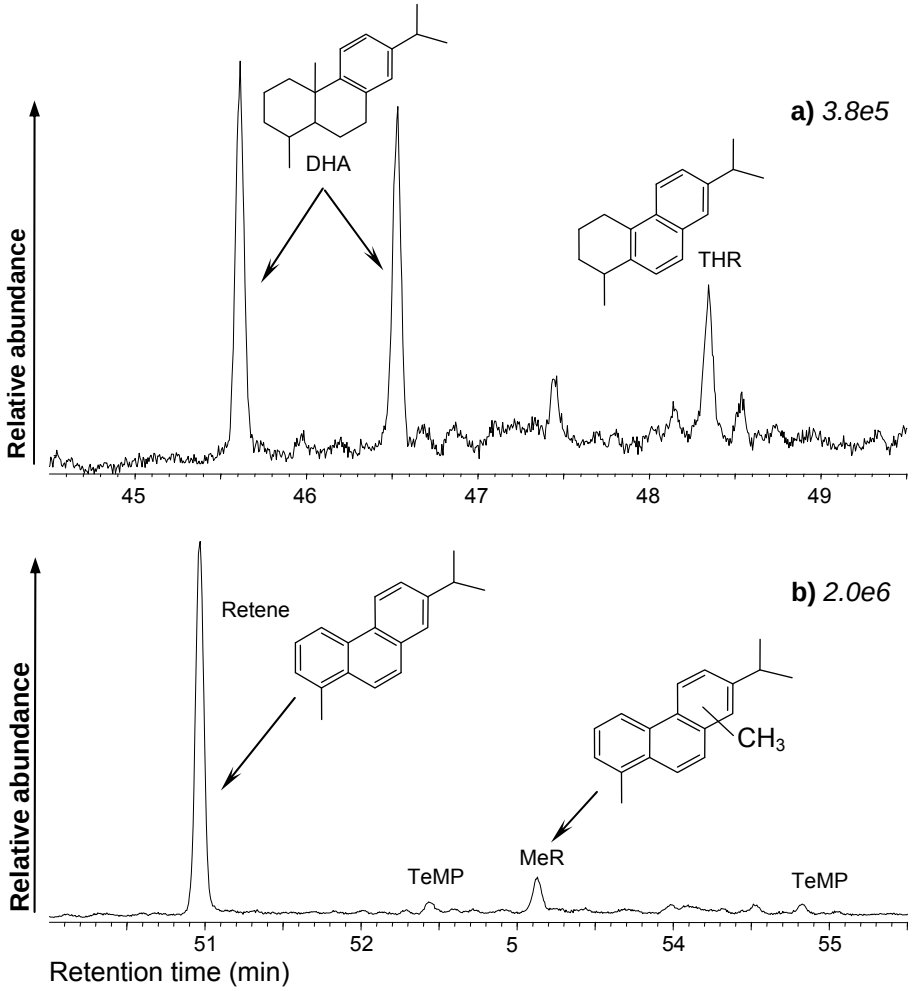

Figure 3.12 Summed *m/z* 223+238+241+256 **(a)** and *m/z* 219+234+233+248 **(b)** chromatograms showing the distribution of diterpenoid biomarkers from the 300˚C/72hr MSSV pyrolysis GC-MS analysis of U-HPO NOM. Peak assignments correspond to products listed in Table 3.1. Relative abundances of a-b are indicated in italics.

The diagenetic transformation of abietic acid to partially and fully aromatised terpenoid HCs has been well established from sedimentary studies (Hayatsu *et al*., 1990; Bastow *et al*., 2001; Hautevelle *et al*., 2006a; 2006b). MSSV pyrolysis of the *Pinus radiata* bark (**Fig. 3.13**) yielded a very similar distribution of alkylated phenanthrenes and diterpenoid biomarkers to those detected from U-HPO. The much higher concentrations of retene over the partially hydrogenated intermediate products

(i.e. DHAs, THR) suggests that full aromatisation of abietic acid is promoted by the MSSV conditions. Previous GC-MS analyses of the extractable fraction of conifer pyrolysates from large-scale confined gold tube pyrolysis (analogous to the MSSV procedure) showed a very similar distribution of aromatic biomarkers (Hautevelle *et al*., 2006b) as observed in this study. MSSV pyrolysis has the unique advantages of analysis of small sample quantities and on-line detection, allowing analysis of gaseous and low MW hydrocarbon products.

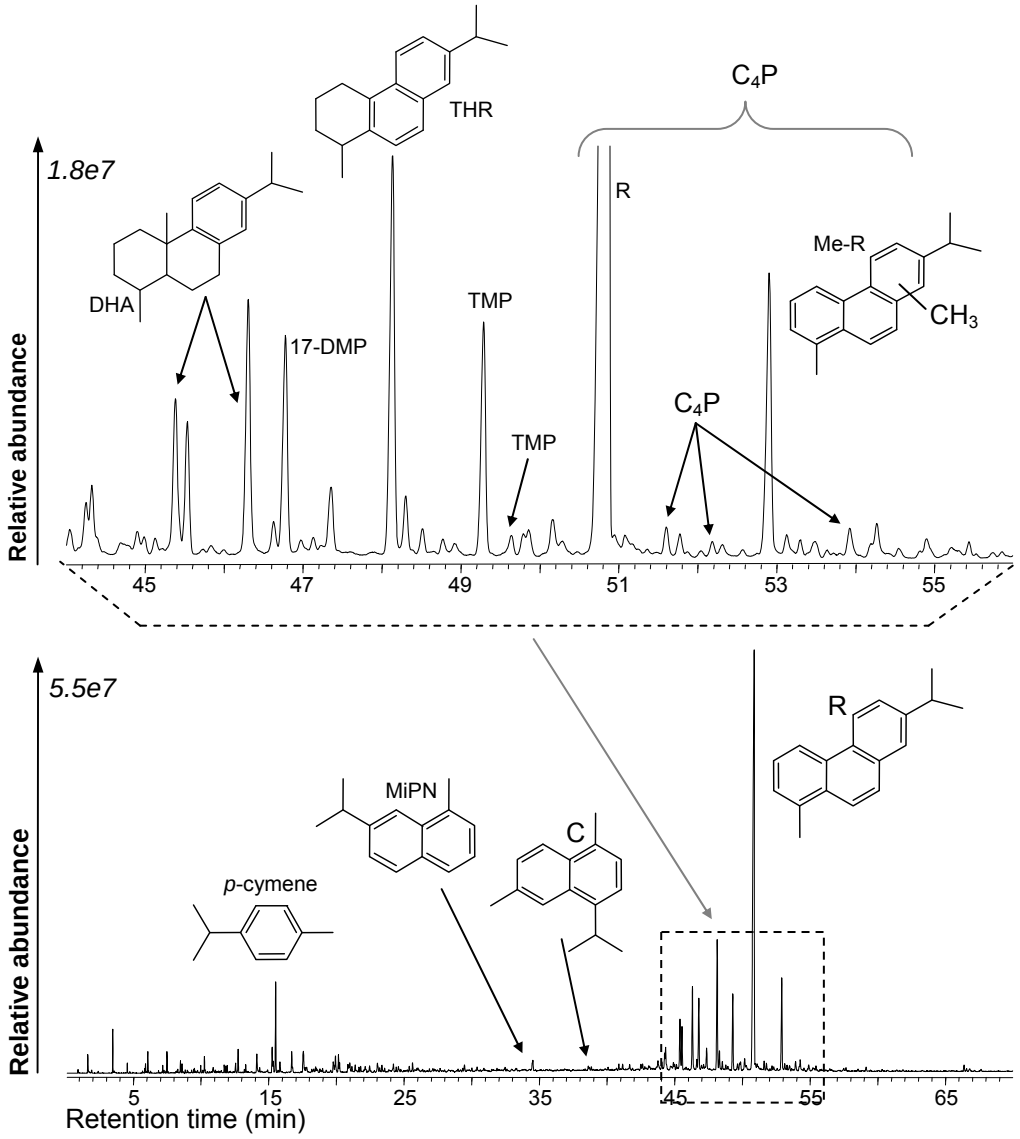

Figure 3.13 TIC obtained by 300˚C/72hr MSSV pyrolysis GC-MS analysis of *Pinus radiata* bark. The expanded region highlights the major diterpenoid biomarkers identified. Peak assignments correspond to products listed in Table 3.1. Relative abundances are indicated in italics.

MSSV pyrolysis of the conifer bark revealed much higher concentrations of retene and other alkyl phenanthrene products than alkyl naphthalenes. ANs such as cadalene and eudalene are typically associated with sesquiterpenoids of both angiosperms and gymnosperms. However, gymnosperm resins are known to contain significantly higher concentrations of abietane class diterpenoids (van Aarssen *et al*., 2000). In sedimentary OM the retene to cadalene ratio has been shown to reflect the relative contribution of angiosperm and gymnosperm vegetation, and has proved a very useful parameter for palaeoenvironmental reconstructions (van Aarssen *et al*., 2000; Hautevelle *et al*., 2006a). The higher relative abundance of retene identified from the U-HPO fraction is therefore indicative of more significant input from gymnosperms terpenoids. Conversely the much lower abundance of retene from the L-HPO fraction, relative to cadalene and other AN products, may indicate more significant contribution from angiosperm terpenoids.

3.3.6 Other aromatic hydrocarbons

A variety of other aromatic and hydroaromatic products, including alkyl (C_1-C_4) indenes, dihydroindenes and tetrahydronaphthalenes (tetralins), were also detected in high concentration by MSSV pyrolysis of the HPO NOM fractions (data not shown). Almendros *et al*. (2001) identified several alkyl-substituted indenes and tetralins in flash pyrolysates of gymnosperm fossils and coals. Confined gold tube pyrolysis of coal indicated that plant resins yielded a range of hydronaphthalene products (Michels *et al*., 2000), which are very efficient hydrogen donors and contribute significantly to the generation of petroleum hydrocarbons from coal (Hayatsu *et al*., 1990; Michels *et al*., 2000). Hydroaromatics probably represent an intermediate stage in the aromatisation of alicyclic terpenoid structural moieties (Wakeham, 1980; Simoneit *et al*., 1986; Hayatsu *et al*., 1987).

3.4 Conclusions

Alkyl aromatic hydrocarbons, including benzenes, naphthalenes and phenanthrenes, were major MSSV pyrolysis products of the HPO NOM fractions studied. The high concentrations of these products in the pyrolysates of several different aquatic environments, such as riverine surface waters, ground water, and secondary waste water effluents, facilitated a detailed investigation of their structural precursors.

Comparison of the aromatic product distributions of the NOM samples with several standard materials helped establish more definitive biomacromolecular origins.

Alkyl naphthalenes and phenanthrenes were strongly correlated with terpenoid constituents of higher plants. All of the of the major AN and APh products of the NOM fractions were detected in high abundance from the extant bark samples, but not from the other standards analysed, providing strong evidence for a terpenoid origin. Several aromatic higher plant terpenoid biomarkers of the bark samples were also detected in relatively high concentrations from the ground and surface water NOM fractions. These included cadalene and eudalene, diagnostic of sesquiterpenoids such as cadinene and cadinol, and retene, tetrahydroretene and dehydroabietin, diagnostic of tricyclic diterpenoids such as abietic acid. Flash pyrolysis consistently yielded much lower concentrations of ANs and APhs, with the distribution typically dominated by the parent and mono-methyl analogues. None of the terpenoid biomarkers were detected by flash pyrolysis. The MSSV detection of these products can be attributed to thermal defunctionalisation and aromatisation of their alicyclic precursors. This maturation pathway has been well established from studies of natural geochemical sequences.

The biodegraded or otherwise diagenetically altered products of terpenoids in aquatic ecosystems are not well established, making source assignment challenging. Nevertheless, several additional AN and APh products prominent in the ground and surface waters were also tentatively assigned to the thermal alteration higher plant terpenoids. Variation in the AN and APh distributions revealed distinctions in the terpenoid contribution between the two surface waters and the ground water. The ground water HPO fraction was dominated by ANs, which are typically attributed to angiosperm terpenoids. In contrast, the higher relative concentrations of phenanthrene biomarkers from the Uruguay surface black water indicate more significant input from diterpenoids present in pine resins. The other black water studied (Gartempe) showed much lower concentrations of AN and APh products, attributed to relatively minor terpenoid input.

Alkyl benzenes were generally detected in very similar concentrations from all the HPO fractions studied. Source assignment of these pyrolysates is difficult due to their common occurrence in the pyrolysates of several of the standard materials. Low MW alkyl benzenes ($\leq C_2$) were ubiquitous pyrolysates and offer little diagnostic information. However, several of prominent higher MW benzenes were tentatively correlated with terpenoid precursors from terrestrial higher plant sources (e.g. cymene; MIPB, EI) or aquatic micro-organisms (e.g. 1,2,3,4-TeMB).

The high concentration of aromatic pyrolysates from the HPO fractions of the St. Julien and Naintré secondary waste water effluents suggests their precursors are resistant to biodegradation. Many of the prominent aromatic products of the surface and ground waters, including retene, cadalene, and polymethylated benzenes and naphthalenes, were also common to the waste waters. However the separate occurrence of high concentrations of *n*-alkyl- and *sec*-alkylbenzenes (C_3-C_6) and *n*-alkyl- ($\leq C_4$), methylethyl- and methylpropylnaphthalenes clearly distinguished the AB and AN profiles of the waste waters. These specific isomeric products were either not detected or were present in minor concentrations in the natural waters. The origins of these products were tentatively attributed to the incorporation of resistant aliphatic biomolecules derived from algal and bacterial biomass into HPO fractions of the effluent OM.

The different aromatic pyrolysate signatures detected from the natural and effluent samples by MSSV Py were not evident from the flash pyrolysis data, which consistently showed much lower concentrations of the higher MW ABs ($\geq C_3$) and ANs ($\geq C_2$). MSSV Py is a promising tool for distinguishing the different structural characteristics and precursor origins of aquatic NOM. However, further investigation is required to expand the diagnostic capacity of the aromatic MSSV pyrolysates of NOM. This will allow more definitive interpretation of their structural significance, and improve the overall molecular characterisation potential of the MSSV pyrolysis approach.

Chapter 4

Distribution and structural origins of oxygen- and sulfur-containing MSSV pyrolysates of aquatic NOM

4.1 Introduction

This chapter focuses on the oxygen (O-) and sulfur (S-) containing products from the MSSV pyrolysis GC-MS analysis of aquatic NOM. Advanced structural elucidation of NOM and humic substances with such techniques as ^{13}C-NMR and FT-IR have identified them to contain a broad range of O-functional constituents. These include carboxylic acid, phenol, methoxyl, alcohol, ketone, aldehyde, ester, ether, O-heterocyclic and quinone (e.g. Leenheer *et al*., 1987; Leenheer *et al*., 1995; Diallo *et al*., 2003; Cardoza *et al*., 2004). Carboxylic and phenolic groups of humic substances are able to complex and reduce metal ions, increasing their solubility and biological availability (Howe *et al*., 1997; Lu and Johnson, 1997). Organic-S typically represents less than 1% of aquatic NOM (Abbt-Braun *et al*., 2004). However, definition of the S-speciation of such samples is important for understanding the biogeochemical cycling of S. Organic sulfides and mercapto groups, with lone electron pairs, are also known to form stable complexes with metals (Abbt Braun *et al*., 2004).

Many characteristic O-products from the thermal degradation of recent aquatic NOM have been attributed (often tentatively) to structural moieties derived from specific biopolymeric precursors. The pyrolysis of lignin for example, typically shows a characteristic distribution of hydroxy- and methoxy- aromatic products, which are unique indicators of vascular plant matter (Hedges and Mann, 1979a; Opsahl and Benner, 1997). However, alteration of the biochemical precursors of aquatic humic substances by microbial degradation or other diagenetic processes may significantly hinder the detection of traditional source diagnostic biomarkers

(Hedges *et al*., 1985). Unlike oxygenated NOM moieties, the structural precursors of S-compounds, such as S-containing amino acids (e.g. cystine) are not well documented, probably due to the low concentrations in which they have been detected in NOM using pyrolysis and other methods. The intrinsic polarity of S and O groups can limit the GC resolution of structurally intact S and O-pyrolysates from flash pyrolysis (Templier *et al*., 2005a). They can also undergo complex thermal reactions such as decarboxylation, rearrangement and condensation; which can lead to loss of structural information and underestimation of their structural contribution to NOM (del Rio *et al*., 1996; Saiz-Jimenez, 1994).

The emergence of TMAH thermochemolysis, in which acid and hydroxyl functionalities are methylated to reduce their polarity, has partially addressed this limitation. It has proved effective at detecting certain O-structures, including lignin phenols and fatty acids (e.g. Challinor, 1995; Martin *et al*., 1995a; Hatcher and Minard, 1996; McKinney and Hatcher, 1996; Filley *et al*., 1999; Filley *et al*., 2000; del Rio *et al*., 1998; Frazier *et al*., 2003).

The soft fragmentation provided by pyrolysis methods such as MSSV, hydrous pyrolysis and hydropyrolysis may also assist the O- and S-structural elucidation of NOM. These techniques have been shown to support the release and reduction of heteroatomic groups, including ether, carboxyl, hydroxyl, sulfide, thiols and simple thiophenic groups (e.g. Koopmans *et al*., 1995; 1996; 1997; Love *et al*., 1995; 1997; 2005; Putschew *et al*., 1998) from sedimentary macromolecules. The MSSV formation of saturated hopanes, steranes and aromatic hydrocarbons from O-containing structural precursors (i.e. bacteriohopanepolyols, sterols and resin acids, respectively) was demonstrated in Chapters 2 and 3. Natural humification and geological maturation of organic matter leads to gradual loss of oxygen and hydrocarbons are usually the major pyrolysates of sedimentary materials such as kerogens and coals. However, a significant portion of the O- and S-functionality of biochemical precursors may be retained in recent or immature sediments. Several O- and S-products, including alkyl furans, alkyl phenols, methoxy aromatics, cyclic ketones and alkyl thiophenes were prominent products from the MSSV pyrolysis GC-MS analysis of NOM.

Here, the O- and S-product distributions from the MSSV Py of NOM fractions isolated from several surface and two waste water effluents are evaluated. The pyrolysis of HPO and COL fractions will provide information about lignin/humic substances and polysaccharides, respectively. The NOM pyrolysates are compared to corresponding data from several selected standards reflecting potential O- and S-organic precursors of aquatic NOM. The identification of common pyrolysates from these standards may help establish the MSSV formation pathways of O- and S-pyrolysates of NOM. Flash pyrolysis GC-MS analyses of the same NOM fractions were also conducted to provide traditional O- and S-pyrolysate distributions of the samples.

4.2 Experimental

4.2.1 NOM Samples

The O- and S-pyrolysate distributions of several surface water and waste water NOM fractions were scrutinised for environmental or source characteristics. Further details of the HPO, TPI and COL fractions of the NOM samples follow.

4.2.1.1 Surface water NOM

The collection, fractionation and isolation of the HPO and TPI fractions of the NOM from the Gartempe (Vienne, France) and Arroyo Sanchez (Rio Negro, Uruguay) rivers and also the fulvic acid standard of the Suwannee River (Georgia, U.S.) were detailed in Chapter 3.2.1. As a complement to these humic sources, the COL fraction of the eutrophic Brittany Reservoir (Brittany, France) was additionally analysed. The Brittany reservoir experiences periodic algal blooms, and is dominated by autochthonously derived NOM (Lee *et al*., 2006). The COL fraction (49.5 % of DOC) of this NOM source was isolated by 3.5 *kDa* membrane dialysis (Lee *et al*., 2006); following the same procedure (Leenheer *et al*., 2000) described for the wastewater effluent fractions in Chapter 3.2.1.3.

4.2.1.2 Waste water effluent OM

Isolation of the COL and XAD resin fractions of Saint Julien (Saint Julien l'Ars, France) and Naintré (Naintré, France) secondary waste water effluent organic matter (Ef-OM) was described in Chapter 3.2.1.3.

4.2.2 Standards

4.2.2.1 Plant elements

Fresh samples of wood and bark were collected from two higher plant species, *Wandoo eucalyptus* (angiosperm/hardwood) and *Pinus radiata* (gymnosperm/ softwood), in bushland near the Mundaring Weir Dam in Perth, Western Australia (Miles, 2005). The samples were ground to a fine powder prior to analysis.

4.2.2.2 Model compounds and biochemical precursors

Lignin, syringic acid (lignin monomer), quercetin (tannin), ellagic acid (tannin), D-glucose (monosaccharide), cellulose (polysaccharide), N-acetyl-D-glucosamine (amino sugar monomer), chitin (amino sugar polymer), tyrosine (amino acid) and bovine serum albumin (BSA, protein) were commercially sourced from Sigma-Aldrich. All chemicals were used without further purification.

4.2.3 Molecular analysis

4.2.3.1 MSSV pyrolysis GC-MS

MSSV pyrolysis of 0.1-1 mg sample was performed following the same procedure as described in Chapter 2.2.2.1. All reported data correspond to MSSV analysis ***I***. The lignin and quercetin standards were also studied at several additional temperatures over the range 260 – 340˚C. GC-MS analysis of the volatile MSSV pyrolysates was typically performed with a Hewlett-Packard (HP) 6890 GC coupled to a 5973 mass selective detector (MSD). Pyrolysates were separated using a 30 m x 0.32 mm i.d. x 0.25 μm DB5-MS capillary column (J&W Scientific). Helium carrier gas was used at 34 kPa head pressure with a split of between 20 – 50 mL min^{-1}. The GC oven was cryogenically held for 1 min at an initial temperature of -20˚C using liquid CO_2, then increased at 8˚C min^{-1} to 40˚C, then 4˚C min^{-1} to a final 310˚C and held isothermal for 20 minutes. Full scan analyses were performed over the range *m/z* 50 – 550 at ca. 4 scans s^{-1}. The mass spectrometer was operated in positive ion electron impact mode at 70 eV with a transfer line temperature of 310˚C and a source temperature of 250˚C. Peak identifications (many tentative) were based on GC elution times and order, mass spectral comparisons with library spectra (Wiley 275 and NIST 05 databases) and published data (van Heemst *et al*., 1996; Iopollo *et al*., 1992; Iopollo-Armanos *et al*., 1995; Bastow *et al*., 2005)

4.2.3.2 Flash pyrolysis and thermochemolysis GC-MS

Flash pyrolysis and tetramethylammonium hydroxide (TMAH) thermochemolysis GC-MS analyses were performed following the procedures described in Chapter 3.2.2.2 and 3.2.2.3, respectively.

4.3 Results and Discussion

4.3.1 Oxygen- and sulfur-containing product distributions of aquatic NOM

MSSV Py GC-MS of the NOM fractions showed a large range of O- and S-pyrolysates. Total ion chromatograms (TIC) from the analysis of the HPO fractions of the Gartempe (G-HPO) and Arroyo Sanchez (U-HPO) rivers and the Naintré (N-HPO) and St. Julien (S-HPO) waste waters, together with the COL fraction of the Brittany reservoir (B-COL) and the Suwannee River fulvic acid (SRFA) are shown in **Figure 4.1.** The major O- products included alkyl ($\leq C_4$) and acetyl furans, alkyl ($\leq C_2$) benzofurans, alkyl ($\leq C_6$) phenols and low MW cyclic (e.g. alkyl cyclopentenones and cyclopentanones) and aliphatic (e.g. 2-butanone, 2-pentanone) ketones. The prominent S-products included alkyl ($\leq C_4$) thiophenes, alkyl ($\leq C_1$) thioanisoles and low MW alkyl sulfides and thiols. S-products were detected in much lower abundance than the O-products, reflecting the typically low concentration of organic S in NOM (Lu *et al*., 2001). Consequently, they were given less attention in this study than the more abundant O-products.

The major O- and S-products detected by MSSV pyrolysis of the surface water and waste water samples are listed in **Table 4.1**. The relative abundance of the alkyl furans, phenols, ketones and S-products are semi-quantitatively compared in **Figure 4.2**. These values were calculated as described in Chapter 3.3.2 (pg 71). Many qualitative differences were evident between the surface and waste waters. The concentrations of O-products in the HPO, TPI and COL fractions of the surface waters and the waste waters varied between 25 – 50 % and 18-35 % of the total pyrolysate signal based on integrated peak areas, respectively. Their distributions also reflected many qualitative differences.

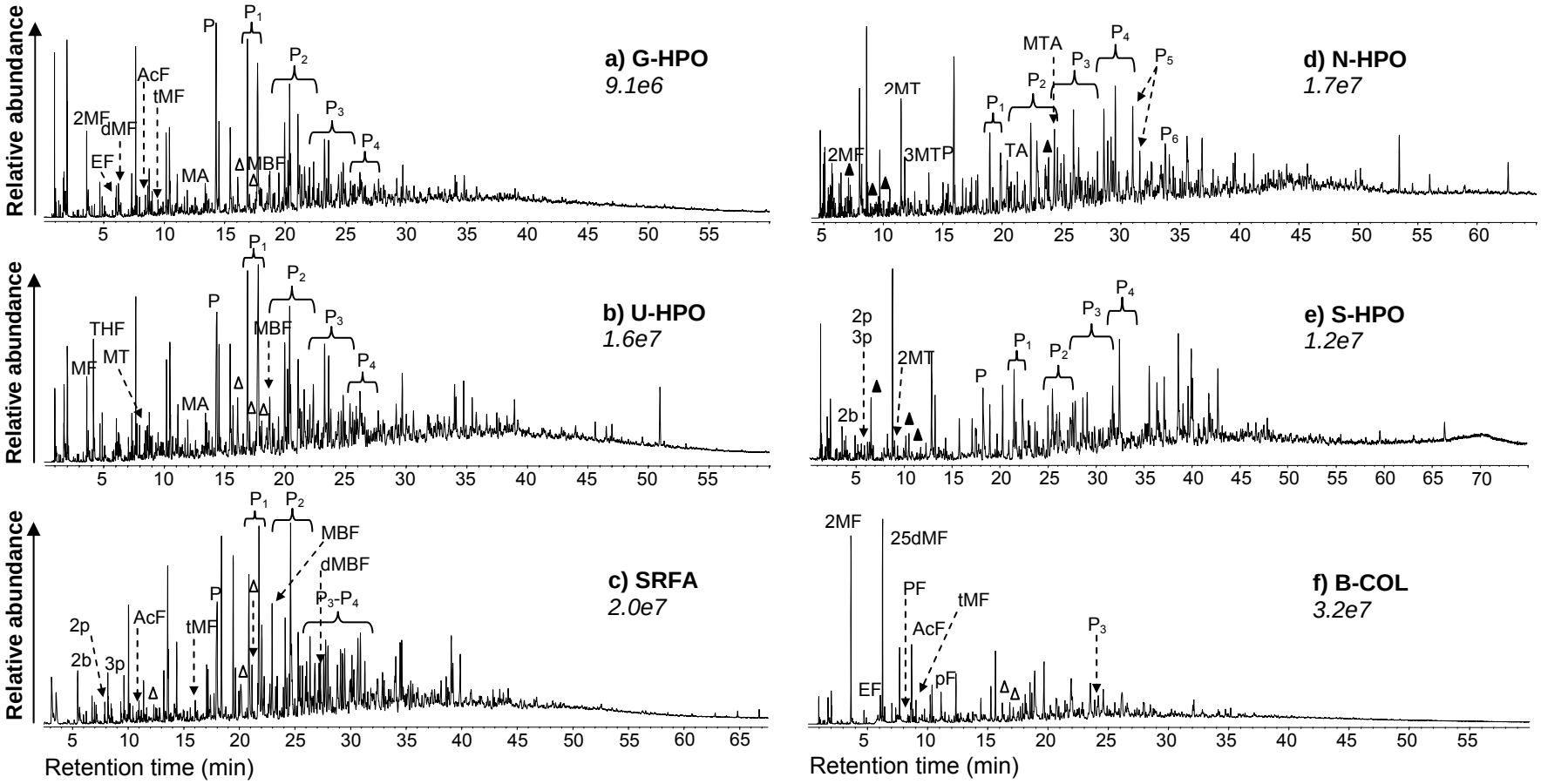

Figure 4.1 TICs from 300˚C/72hr MSSV pyrolysis GC-MS analysis of **a)** Gartempe River HPO, **b)** Uruguay HPO, **c)** Suwannee River fulvicacid, **d)** Naintré HPO **e)** St. Julien HPO and **f)** Brittany colloids. Relative abundances of a-f are indicated in italics. P_x = alkyl phenols, ∆ = alkyl cyclopentenones. Other peak assignments correspond to products listed in Table 4.1.

Table 4.1 Major O- and S-containing products identified by MSSV pyrolysis GC-MS of surface and waste water NOM fractions. A 4-point mass spectrum is included; bold = molecular ion, underline = base peak. The relative abundance of each product is indicated as a proportion of the total pyrolysate area; * = < 0.5%, ** = 0.5-1%, *** = 1-2%, **** = > 2%, t = trace, - = not detected.

Compound Identification	4 pt. mass spectrum	Peak Label	**Surface waters**						**Waste waters**		
			U-HPO	G-HPO	SRFA	U-TPI	G-TPI	B-COL	S-HPO	N-HPO	S-COL
Furans											
furan	**68**, 40, 39, 38	F	*	*	*	**	**	**	*	*	-
2-methylfuran	**82**, 81, 53, 39	2MF	**	**	t	****	****	****	-	*	***
3-methylfuran	**82**, 81, 53, 39	3MF	*	*	-	*	*	*	-	t	*
tetrahydrofuran	**72**, 71, 42, 41	THF	***	-	-	*	-	-	-	-	-
2-ethylfuran	**96**, 81, 67, 53	EF	*	*	-	*	**	*	-	*	*
2,5-dimethylfuran	**96**, 95, 81, 53	25dMF	*	*	t	***	***	****	-	*	***
2,4-dimethylfuran	**96**, 95, 81, 53	24dMF	*	*	t	**	**	*	-	-	-
2-propylfuran	**110**, 81, 53, 39	PF	-	-	-	*	*	*	-	-	t
2-acetylfuran	**110**, 95, 67, 41	AcF	**	**	*	**	***	****	*	*	*
trimethylfuran	**110**, 109, 95, 67	tMF	*	*	*	**	**	**	-	*	-
2-propionylfuran	**124**, 96, 95, 39	pF	-	-	-	*	*	***	-	-	*
tetramethylfuran	**124**, 123, 109, 82	teMF	*	*	*	*	*	-	-	-	-
2-methylbenzofuran	**132**, 131, 103, 77	MBF	**	**	**	*	***	**	*	t	-
dimethylbenzofuran	**146**, 145, 131, 115	dMBF	*	*	**	*	*	-	-	-	-
dimethylbenzofuran	**146**, 145, 131, 115	dMBF	*	*	*	-	*	-	t	-	-
dimethylbenzofuran	**146**, 145, 131, 115	dMBF	*	**	**	*	**	*	t	-	-
dimethylbenzofuran	**146**, 145, 131, 115	dMBF	*	**	**	-	**	-	*	*	-
2,2'-methylenebis-(5-methyl)-furan	**176**, 161, 133, 105		-	-	-	-		*	-	-	-
Proportion of pyrolysate area (%)			***5.2***	***5.3***	***5.3***	***7.9***	***12.5***	***17.5***	***< 1.0***	***1.6***	***4.7***
Phenols											
phenol	**94**, 66, 65, 55	P	****	****	****	**	***	*	***	***	**
2-methylphenol	**108**, 107, 79, 77	2MP	****	****	****	**	****	*	****	***	****
3- and 4-methylphenol	**108**, 107, 79, 77	3MP, 4MP	****	****	****	**	***	*	***	***	***
2,6-dimethylphenol	**122**, 121, 107, 91	26	***	**	**	**	**	-	***	**	t
2-ethylphenol	**122**, 107, 77, 79	2EP	***	****	***	**	****	-	***	****	***

2,4-dimethylphenol	**122**, 121, 107, 77	24	****	****	***	***	***	**	***	***	***
2,5-dimethylphenol	**122**, 121, 107, 77	25	***	**	**	*	**	-	**	**	**
4-ethylphenol	**122**, 108, 107, 77	4EP	****	****	***	**	***	-	*	***	**
3-ethylphenol	**122**, 108, 107, 77	3EP	*	**	*	*	*	-	*	*	*
3,5-dimethylphenol	**122**, 121, 107, 77	35	**	***	**	*	*	-	*	t	*
2,3-dimethylphenol	**122**, 121, 107, 77	23	**	**	**	*	*	-	*	t	*
isopropylphenol	**136**, 121, 103, 77	iPP	**	**	*	*	**	-	**	**	**
3,4-dimethylphenol	**122**, 121, 107, 77	34	**	***	**	**	***	*	*	t	*
2,4,6-trimethylphenol	**136**, 135, 121, 91	246	***	***	**	*	**	*	***	**	***
2-propylphenol	**136**, 107, 79, 77	2PP	*	**	*	*	*	-	*	**	**
C_3 phenol	**136**, 121, 91, 77	P_31	***	***	***	***	***	-	***	***	***
C_3 phenol	**136**, 121, 91, 77	P_32	*	**	***	*	*	-	*	*	-
C_3 phenol	**136**, 121, 91, 77	P_33	***	***	***	**	**	***	***	***	***
C_3 phenol	**136**, 121, 91, 77	P_34	*	**	*	*	*	-	*	-	t
4-propylphenol	**136**, 107, 79, 77	4PP	*	*	*	t	t	-	*	*	t
C_3 phenol	**136**, 135, 121, 91	P_35	**	**	**	**	**	-	**	**	*
C_3 phenol	**136**, 135, 121, 91	P_36	***	**	**	**	***	-	-	*	-
C_3 phenols (unspecified isomers)	**136**	●									
diethylphenol	**150**, 135, 121, 91	P_41	*	*	t	*	*	t	***	**	***
4-methyl-2-isopropylphenol (thymol)	**150**, 135, 115, 91	P_42	t	*	t	t	t	-	****	****	**
C_3 phenol	**136**, 135, 121, 91	P_37	*	*	*	t	**	-	-	-	-
2-methyl-4-isopropylphenol (carvacrol)	**150**, 135, 115, 91	P_43	**	**	**	**	*	t	**	****	**
trimethylphenol	**136**, 135, 121, 91	P_38	*	*	*	t	t	-	-	-	-
sec-butylphenol	**150**, 121, 91, 77	P_44	t	-	t	*	*	-	*	***	*
C_4 phenol	**150**, 121, 91, 77	P_45	*	t	-	-	-	-	*	**	*
C_4 phenol	**150**, 135, 121, 91	P_46	*	*	*	*	*	-	t	t	-
tetramethylphenol	**150**, 135, 105, 91	teMP	**	**	*	*	*	-	-	-	-
tetramethylphenol	**150**, 135, 107, 91	teMP	**	**	*	**	*	-	-	-	-
C_4 phenols (unspecified isomers)	**150**	○									
tert-butylmethylphenol	**164**, 149, 121, 107	P_51	-	-	-	-	-	-	**	***	**
tert-pentylphenol	**164**, 135, 121, 91	P_52	-	-	-	-	-	-	**	***	*
C_5 phenols (unspecified isomers)	**164**	◍	-	-	-	-	-	-	*	***	t

C_6 phenols (unspecified isomers)	**178**	○	-	-	-	-	-	-	t	*	-
C_7 phenols (unspecified isomers)	**192**	●								*	
4-*tert*-octylphenol	**206**, 136, 135, 107	*t*-OP	**	*	-	*	t	-	-	*	-
4-*tert*-octyl-2-methyl-phenol	**220**, 150, 149, 121	M-*t*-OP	-	-	-	-	-	-	-	*	-
4-*tert*-octyl-dimethylphenol	**234**, 163, 149, 135	dM-*t*-OP	-	-	-	-	-	-	-	*	-
nonylphenols (unspecified isomers)		NP	-	-	-	-	-	-	-	*	-
Proportion of pyrolysate area (%)			***40.0***	***42.3***	***28.2***	***17.4***	***23.3***	***3.7***	***20.5***	***29.8***	***20.1***
Aliphatic and Cyclic Ketones											
2-butanone	**72**, 57, 50, 43	2b	*	*	**	**	**	t	*	*	***
3-methyl-2-butanone	**86**, 71, 55, 43	M2b	*	-	*	*	*	t	*	*	*
2-pentanone	**86**, 71, 58, 43	2p	*	*	*	*	*	*	*	*	*
3-pentanone	**86**, 71, 57, 29	3p	*	*	*	*	*	*	*	*	*
4-methyl-2-pentanone	**100**, 85, 58, 43	M3p	*	*	*	*	*	*	*	*	*
2-methyl-3-pentanone	**100**, 71, 57, 43	M3p	*	*	*	*	t	*	t	*	t
3-hexanone	**100**, 71, 57, 43	3h	*	*	*	*	*	*	*	*	*
2-hexanone	**100**, 85, 58, 43	2h	-	-	*	-	t	*	t	*	*
methylcyclopentanone	**98**, 70, 69, 55	MC	*	*	*	t	t	-	-	-	-
ethylcyclopentanone	**112**, 84, 56, 55	EC	*	*	*	*	t	-	-	-	-
dimethylcyclopentanone	**112**, 97, 69, 56	dMC	t	t	*	t	t	-	-	-	-
2,3-dimethyl-2-cyclopenten-1-one	**110**, 95, 82, 67	dMC=	**	**	***	**	***	**	-	t	t
trimethyl-2-cyclopenten-1-one	**124**, 109, 96, 81	tMC=	*	**	**	*	*	*	-	t	t
trimethyl-2-cyclopenten-1-one	**124**, 109, 96, 81	tMC=	*	*	**	t	*	*	-	t	t
tetramethyl-2-cyclopenten-1-one	**138**, 123, 95, 67	teMC=	t	t	*	t	t	-	-	-	-
Proportion of pyrolysate area (%)			***3.6***	***3.2***	***6.7***	***4.2***	***4.2***	***3.3***	***1.9***	***1.7***	***4.0***
Other oxygen-containing products											
p-dioxane	**88**, 87, 58, 57	▲	*	-	-	**	-	-	**	*	-
dimethyl-*p*-dioxane	**116**, 101, 72, 59	▲	-	-	-	*	-	-	**	*	-
dimethyl-*p*-dioxane	**116**, 101, 72, 59	▲	-	-	-	*	-	-	*	*	-
p-benzodioxane	**136**, 108, 80, 52	▲	-	-	-	-	-	-	-	**	-
methoxybenzene (anisole)	**108**, 93, 78, 65	A	**	*	*	*	*	-	-	-	-
methylmethoxybenzene	**122**, 121, 107, 77	MA	*	*	-	-	-	-	-	-	-
ethylmethoxybenzene	**136**, 121, 91, 77	EA	**	*	-	-	-	-	-	-	-

acetophenone	**120**, 105, 77, 51		*	*	*	-	*	-	-	-	-
Proportion of pyrolysate area (%)			***1.2***	***1.4***	***< 1.0***	***< 1.0***	***< 1.0***	***nd***	***1.5***	***1.5***	***nd***
Sulfur-containing products											
thiophene	**84**, 58, 57, 45	T	*	*	*	*	*	t	*	*	*
2-methylthiophene	**98**, 97, 53, 45	2MT	**	*	*	*	*	*	*	*	*
3-methylthiophene	**98**, 97, 53, 45	3MT	*	*	*	*	*	*	*	*	*
ethylthiophene	**112**, 97, 53, 45	ET	*	*	*	*	*	*	*	*	*
2,4-dimethylthiophene	**112**, 111, 97, 45	24dMT	*	*	*	*	*	-	*	*	*
3,4-dimethylthiophene	**112**, 111, 97, 45	34dMT	*	*	*	*	*	-	*	*	*
2,3-dimethylthiophene	**112**, 111, 97, 45	23dMT	*	*	*	*	*	-	*	*	*
2,5-dimethylthiophene	**112**, 111, 97, 59	25dMT	t	t	t	*	t	-	*	*	t
propylthiophene	**126**, 97, 53, 45	PT	*	t	t	t	t	-	t	*	t
trimethylthiophenes (unspecified isomers)	**126**	tMT	*	*	t	t	*	-	*	*	t
ethylmethylthiophenes (unspecified isomers)	**126**	EMT	*	*	t	t	t	-	*	*	*
C_4 thiophenes (unspecified isomers)	**140**	C_4T	t	-	t	t	-	-	*	*	t
thiophenol	**110**, 109, 77, 66	TP	-	-	-	-	-	-	*	*	
thioanisole	**124**, 109, 91, 78	TA	-	-	-	***	-	-	*	***	t
4-methylthioanisole	**138**, 123, 91, 45	MTA	-	-	-	-	-	-	*	***	-
2-methylbenzothiazole	**149**, 148, 121, 108	MBT	-	-	-	-	-	-	**	***	-
2,4-diphenylthiophene	**236**, 202, 191, 121	dPT	-	-		*	-	-	-	-	-
Proportion of pyrolysate area (%)			***3.6***	***3.5***	***2.1***	***4.7***	***3.8***	***< 1.0***	***4.4***	***7.5***	***4.3***

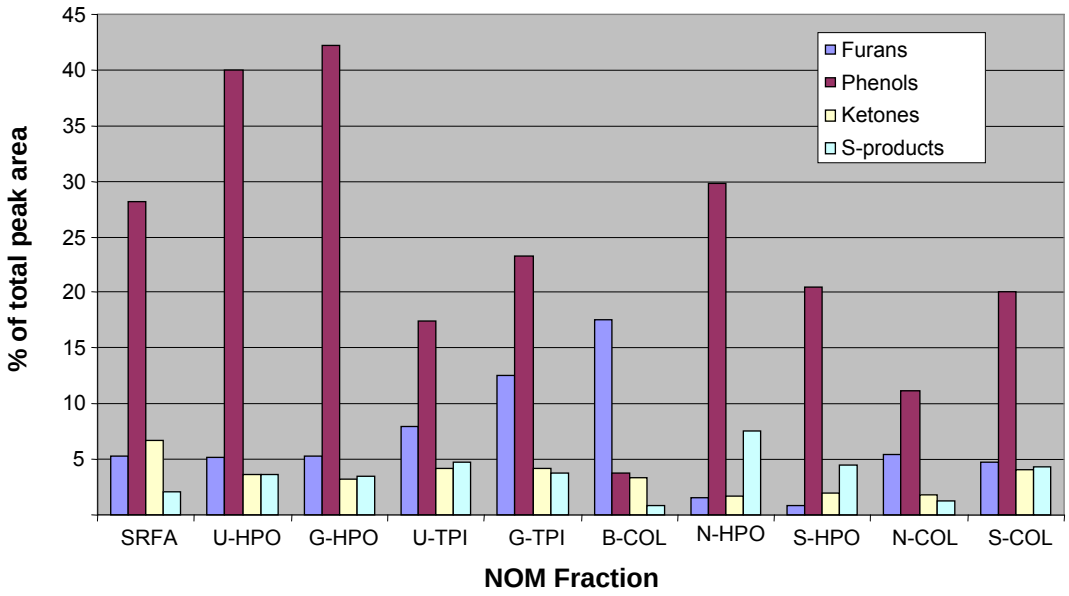

Figure 4.2 Relative abundances of the major O- and S-product groups from 300˚C/72hr MSSV pyrolysis GC-MS of XAD fractions of surface and waste water NOM.

4.3.1.1 Surface water NOM

The alkyl phenols ($\leq C_4$) of the Gartempe and Uruguay HPO fractions accounted for ca. 40 % of the total product signal. Phenolic pyrolysates of river humic substances have been attributed to lignin, tannin and other terrestrial plant sources leached from adjacent soils (e.g. Hedges *et al*., 1985; Malcolm, 1990; Hedges and Oades, 1997). Other O-products of lower concentration included alkyl furans, benzofurans and cyclic ketones indicative of polysaccharide inputs (Saiz-Jimenez and de Leeuw, 1984a; Helleur *et al*., 1985; Pouwels *et al*., 1987), and methoxy aromatics. Alkyl thiophenes were the dominant S-products. The distribution of O- and S- products from G-HPO, U-HPO and Suwannee River fulvic acid (**Fig 4.1a-c**) were generally similar, consistent with a common humic nature.

Compared to the HPO fractions, the TPI fractions of the Gartempe and Uruguay rivers yielded much higher concentrations of alkyl furans and nitrogen-products (see Chapter 5), and lower concentrations alkyl phenols and aromatic hydrocarbons (Chapter 3). Both fractions showed similar concentrations of alkyl thiophenes, benzofurans and aliphatic and cyclic ketones.

The Brittany River colloids (**Fig. 4.1f**) showed distinctively high concentrations of alkyl and acetyl substituted furans with only minor quantities of alkyl phenols, alkyl thiophenes and other aromatic pyrolysates. The low abundance of phenolic and aromatic pyrolysates is consistent with non-humic OM.

4.3.1.2 Waste water effluent OM

MSSV pyrolysis of the HPO fractions of both the Naintré and St. Julien waste water effluents (**Fig. 4.1 d-e**) showed high concentrations of alkyl phenols (29.8 % and 20.5 %, respectively) and alkyl aromatics (see Chapter 3) as well as several other features similar to the data of the HPO fractions of the river waters. The occurrence of alkyl phenols and related products in the HPO effluent OM may reflect humic NOM not removed during potable water treatment. This recalcitrant material may enter wastewater streams from drinking water inputs. Drewes *et al*. (2003) demonstrated that the chemical character of soil/aquifer treated effluent waters resembled that of recalcitrant NOM in drinking water.

The composition of the waste waters did show several significant differences to the river waters. Alkyl furans, benzofurans and cyclic ketones were detected in significantly lower concentrations in the waste waters. The waste water HPO fractions also showed prominent *p*-dioxane and dimethyl-*p*-dioxane products. *p*-benzodioxane was also detected in the N-HPO fraction. None of these dioxane products were detected by flash pyrolysis. These products likely derive from dioxane and dioxolane impurities arising during the manufacture of polyester resins (Romero *et al*., 1998). Polychlorinated dibenzo-*p*-dioxins, formed as industrial byproducts of organo-chlorine manufacture, paper bleaching and in the burning of chlorine-containing substances such as PVC, may also contribute. These compounds are well known endocrine disrupting compounds and have been previously detected in low concentrations in waste waters (Petrovic *et al*., 2002).

Sulfur products were detected in higher concentrations in the HPO fractions of the waste waters than the river sources, although these were not as abundant as N-products (Chapter 5). The major products included alkyl ($\leq C_4$) thiophenes, alkyl ($\leq C_1$) thioanisoles and 2-methylbenothiazole. S-organic inputs to the waste waters

likely include domestic (e.g. sewage) and industrial wastes, and may provide an important bioavailable substrate for the high microbial activity reflected by the high concentrations of protein and amino sugar attributed N-products (Chapter 5). S-pyrolysates were particularly rich in the Naintré HPO fraction. The shorter contact time of the biological treatment at the Naintré treatment plant (*cf.* St Julien; Jarusutthirak, 2002) may result in lower mineralisation of waste water derived S-organics.

The O-product distributions of the COL fractions of the waste and surface waters also showed several distinctive features. The waste waters yielded alkyl thiophenes and alkyl phenols in higher relative abundance and alkyl furans in lower relative abundance than Brittany River. Interestingly, polyphenols from terrestrial plants (e.g. lignin and tannin) are not typically concentrated in the colloidal fractions of NOM, although humic substances may adsorb to mineral surfaces of colloids (Wershaw, 2004). The alkyl phenols of the waste water colloids may reflect a separate pool of phenol structural precursors. It is possible they could derive from algal phlorotannins (van Heemst *et al*., 1996) or the proteinaceous component of treatment microbes (van Heemst *et al*., 1999; Dignac *et al*., 2000).

The distributions of the major O- and S-pyrolysate groups of the NOM fractions and several selected standards representative of potential biological precursors have been compared to help establish their origins and diagenetic or thermal formation pathways. The alkyl- furan, benzofuran, cyclopentenone, phenol and thiophene data are separately discussed below.

4.3.2 Furan distributions of NOM fractions

Alkyl ($\leq C_4$) and acetyl substituted furans were prominent MSSV products of all the surface water NOM fractions. They were detected in highest concentrations in the Brittany River colloids. Summed ion chromatograms highlighting the furan distributions of the Brittany colloids and the HPO and TPI fractions of the Uruguay River are shown in **Figure 4.3**. Major furan pyrolysates of all samples were furan, 2-methylfuran, 2-ethylfuran, 2,5-dimethylfuran, 2-acetylfuran, trimethylfuran and 2-propionylfuran. Little variation in the furan distribution of the TPI and COL

fractions was evident. However, the U-HPO data showed distinctively high concentrations of tetrahydrofuran and slightly higher proportions of 2-ethyl-, trimethyl- and tetramethylfuran. The HPO and COL fractions of both waste water effluents yielded similar furan distributions, but in much lower concentrations (ca. 1 % for HPO and 5 % for COL) relative to the corresponding surface water fractions.

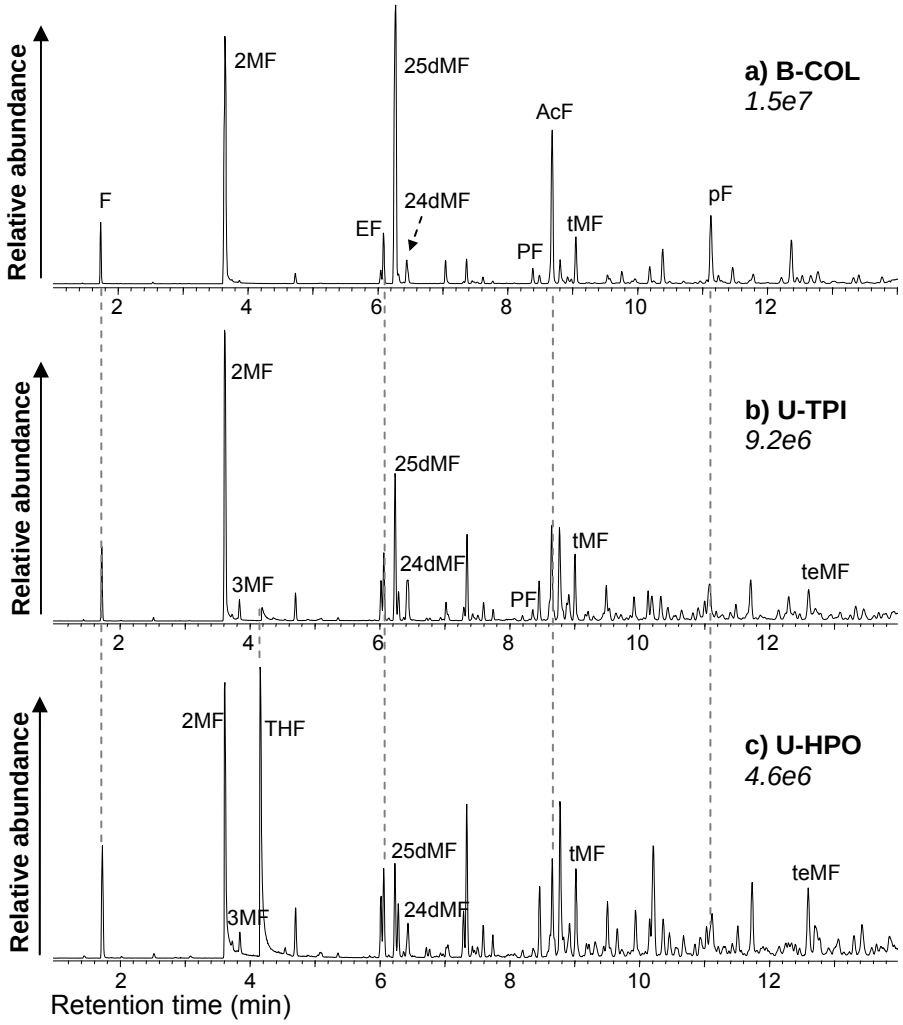

Figure 4.3 Summed *m/z* 68+72+81+82+95+96+109+110+123+124 chromatograms showing the alkyl furan distribution detected by 300˚C/72hr MSSV pyrolysis GC-MS analysis of **a)** Brittany COL, **b)** Uruguay TPI and **c)** Uruguay HPO fractions. Peak assignments correspond to products listed in Table 4.1. Relative abundances of a-c are indicated in italics.

Furans are common pyrolysates of soil and aquatic NOM (e.g. Bruchet, 1985; Saiz-Jimenez and de Leeuw 1984a ; 1986b; Christy *et al*., 1999; Lehtonen *et al*., 2000b; Dignac *et al*., 2005; 2006; Templier *et al*., 2005a). They are typically attributed to polysaccharides (PS) derived from the cellular material of plants and aquatic micro-

organisms (e.g. cellulose, hemicellulose, pectin, amino sugars), as well as simple sugars (e.g. glucose, fructose) of microbial metabolism (Pouwels *et al.,* 1987, Hayes *et al*., 1989; Pastorova *et al*., 1994, Almendros *et al*., 1997, Reeves and Francis, 1997, Paine *et al*., 2008). Carbohydrates and amino sugars are typically concentrated in colloid or TPI fractions of NOM (Rostad *et al*., 1997; Leenheer *et al*., 2000; Leenheer *et al*., 2001a; Jarusutthirak, 2002; Guo *et al*., 2003; Mao *et al*., 2003; Croué *et al*., 2006). This is reflected by the relatively high concentrations of heterocyclic O- and N-products (Chapter 5) in the B-COL, U-TPI and G-TPI fractions (Figure 5.2). Previous ^{13}C-NMR and *Curie* point flash pyrolysis data for Gartempe River (Templier *et al*., 2005a) also showed high occurrences of polysaccharides in the TPI fraction, whilst the HPO fraction contained more substantial input from lignin.

Carbohydrates, a major energy source for microbiota, are rapidly mineralised during early diagenesis (Hedges *et al*., 1985; Stout *et al*., 1988; Hatcher *et al*., 1989a; Almendros *et al*., 1997; Huang *et al*., 1998; Lu *et al*., 2001). Solid state ^{13}C-NMR spectroscopy of artificially matured swamp and soil humic substances showed progressive loss of carbohydrates with increasing humification, which was at least partially attributed to the preferential mineralisation of polysaccharides over lignins and terpenoids (Zech *et al*., 1997; Lu *et al*., 2001). Similarly, declining concentrations of carbohydrate structures have been reported during the coalification of plant biomass in sedimentary systems (Hatcher *et al*., 1981; Hedges *et al*., 1985; Wilson, 1987; Hatcher, 1988). Microbial degradation of carbohydrates would contribute to the lower proportion of furan pyrolysates in the humic HPO fractions of the surface waters.

However, some carbohydrate units may be incorporated into the aromatic or humic structures of NOM (Abbt-Braun *et al*., 1989; Almendros *et al*., 1997; Lu *et al*., 2000; 2001). The AFs of the Uruguay and Gartempe HPO fractions may therefore derive from the macromolecular incorporation of diagenetically altered carbohydrates, as opposed to intact polysaccharides and sugars typically found in the COL fraction. The alteration of plant polysaccharides into polymeric material yielding abundant furan pyrolysates was previously demonstrated during the formation of aquatic NOM from upland soils (Huang *et al*., 1998).

The relatively low furan concentrations in the HPO and COL fractions of both waste water effluents (*cf.* the surface waters) probably relates to limited input of cellulose and other polysaccharide material from terrestrial sources. Additionally, advanced biological treatment of these waters would have contributed to a significant reduction in bioavailable carbohydrates.

High furan concentrations were also detected by flash pyrolysis of the surface water fractions. However, aside from 2-methylfuran and 2,5-dimethylfuran, the major furan products of flash Py, which included furancarboxaldehyde, methylfurancarboxaldehyde, methylfuranone, hydroxydimethylfuranone, methylfurandione, benzofuranone and 1,3-isobenzofurandione, were different to those detected by MSSV Py. Several other PS-derived products were also detected by flash pyrolysis but not MSSV pyrolysis, including acetic acid, 5,6-dihydro-4-methyl-pyran-2-one, 5-hydroxy-2-hydroxymethyl-4-pyrone, 1,4:3,6-dianhydro-α-D-glucopyranose, levoglucosenone and levoglucosan (Helleur *et al*., 1985; Pouwels *et al*., 1987; Dignac *et al*., 2005), some of which are evident in the flash Py data of B-COL shown in **Figure 4.4**. The latter three compounds are indicative of intact carbohydrate structures (Pouwels *et al*., 1987, Pastorova *et al*., 1994).

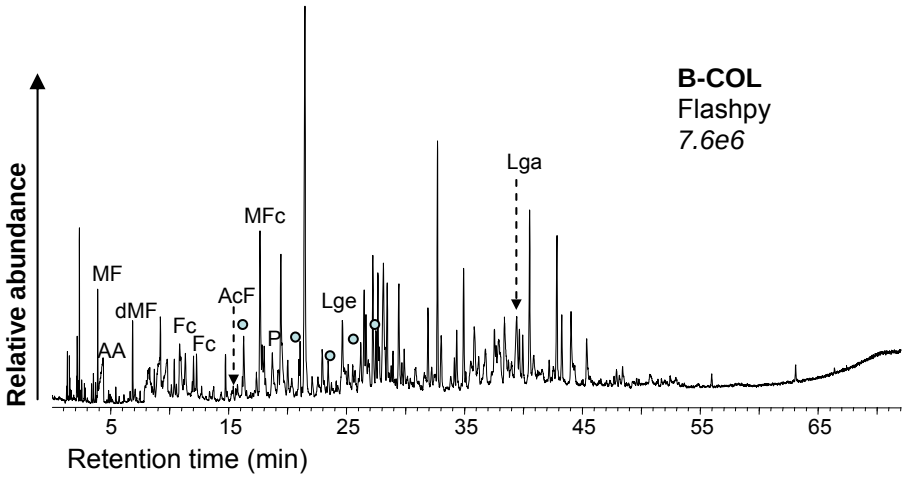

Figure 4.4 TIC obtained by 550˚C/20s flash pyrolysis GC-MS analysis of Brittany colloids. Relative abundance is indicated in italics. AA = acetic acid, Lge = levoglucosenone, Lga = levoglucosan, Fc = furancarboxaldehyde, MFc = methylfurancarboxaldehyde, ∘ = other polysaccharide related products. Additional peak assignments correspond to products listed in Table 4.1.

The different thermal conditions of MSSV and flash pyrolysis no doubt contribute to the different polysaccharide products detected with each approach. Cellulose is prone to two thermal decomposition pathways (Pouwels *et al*., 1989). The very high thermal energies applied by flash pyrolysis favour depolymerisation and production of anhydro sugars such as levoglucosan and levoglucosenone (Pouwels *et al*., 1989; Saiz-Jimenez, 1994; Wershaw, 2004), as well as pyranones, furanones and furans. Lower thermal energies (< 300˚C) promote bond scission, dehydration and formation of CO, CO_2 and char via carbonyl, carboxyl and hydroperoxide intermediates (Wershaw, 2004). The more moderate but confined thermal conditions of MSSV pyrolysis appear to favour the formation of thermodynamically stable alkyl furan products (Templier *et al*., 2005a). Despite the qualitative distinctions both MSSV and flash pyrolysis of the NOM fractions showed quantitatively similar trends with the concentrations of polysaccharide products detected in the order surface COL > surface TPI > waste COL > surface HPO > waste HPO.

4.3.3 Furan distributions of standards

MSSV analyses were conducted on several potential precursors of the carbohydrate structural units of NOM including glucose, N-acetyl-D-glucosamine, cellulose and chitin. Cellulose is a major structural component of wood (Hedges *et al*., 1985). Chitin is a natural polymeric amino sugar present in insect exoskeletons and fungal cell walls (Stankiewicz *et al*., 1996) and is similar in structure to the N-acetyl amino sugars (e.g. peptidoglycans) of microbial cell walls.

The TICs from the MSSV pyrolysis (300˚C/72hr) of cellulose and chitin are shown in **Figure 4.5**. The major cellulose products included the same alkyl and acetyl substituted furans (32 %) detected from the NOM fractions, as well as alkyl cyclopentenones (14 %), cyclopentanones and cyclohexanones (9 %). Low MW aliphatic and alicyclic products (12 %), such as alkyl ($\leq C_3$) substituted butanes, pentanes, hexanes and their corresponding alkenes and also alkyl ($\leq C_4$) cyclopentenes and cyclohexenes were also prominent. Aliphatic products may be attributed to the removal of hydroxy groups from glucose units with concomitant unsaturation and ring opening, as previously observed in pyrolysates of thermally modified carbohydrates (Almendros *et al*., 1997). Several alkyl indanes, thought to

be formed by rearrangement, aromatisation and depletion of oxygen-containing groups (Almendros *et al*., 1997), were also detected.

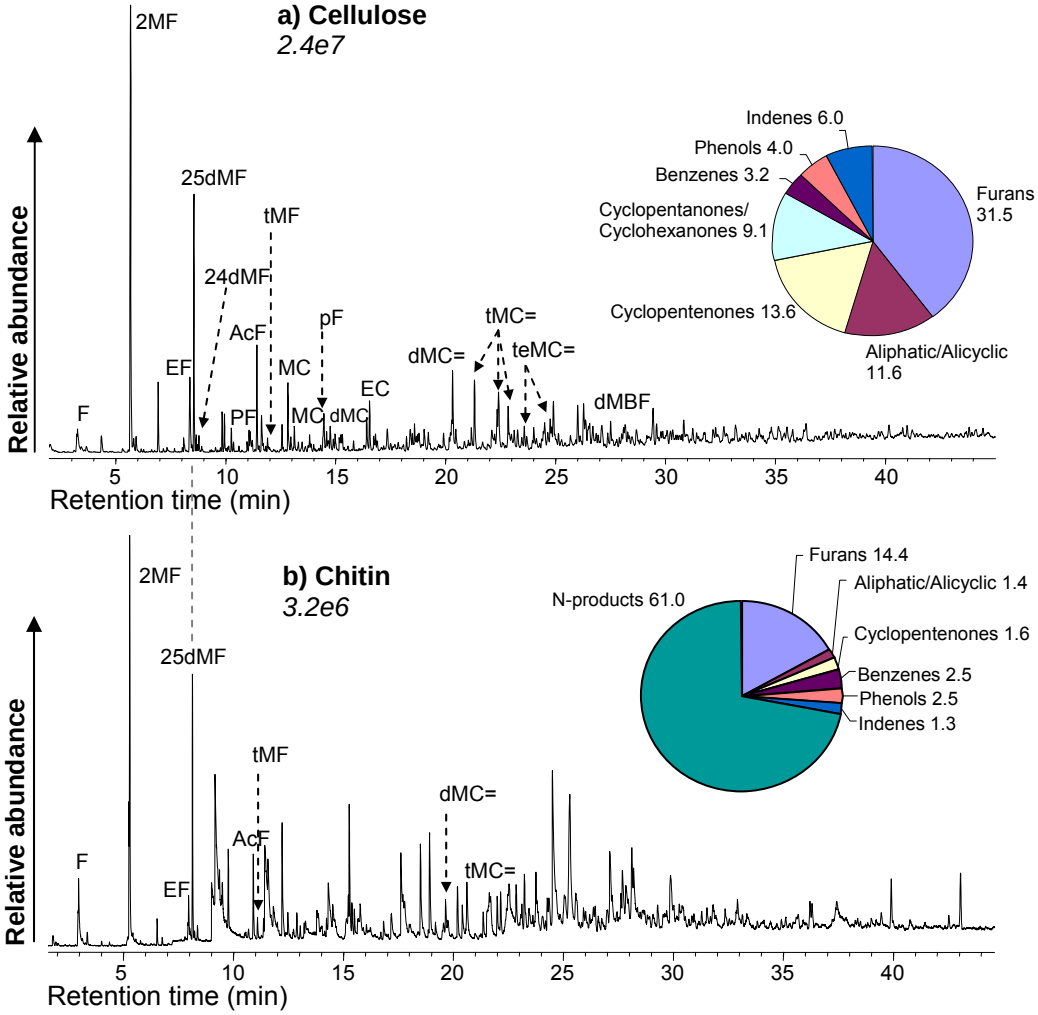

Figure 4.5 Partial TICs and relative abundances of the major O-products detected by 300˚C/72hr MSSV pyrolysis GC-MS of **a)** cellulose and **b)** chitin. Peak assignments correspond to products listed in Table 4.1. Relative peak abundances in italics and a pie chart reflecting relative proportions of major pyrolysate groups are both indicated for a and b.

The MSSV pyrolysate of chitin was dominated by nitrogen-containing products (ca. 60 %), which are discussed in detail in Chapter 5. Alkyl furan products (14.4 %) were also significant; however cyclic ketones and aliphatic products were very minor, suggesting their occurrence in NOM is probably due to cellulose precursors. Alkyl furans were also major MSSV products of the monosaccharides glucose and N-acetyl-D-glucosamine (Appendix 5).

The alkyl furan products from the MSSV analysis of cellulose, chitin and lignin are highlighted in the summed ion chromatograms of **Figure 4.6.** The broad distributions detected from the cellulose and chitin standards (and glucose and N-acetyl-D-glucosamine standards) were very similar to those detected from the NOM fractions, providing convincing evidence that carbohydrates are the major source of these NOM pyrolysates. The low yields of alkyl furans (2 %) observed by MSSV Py of the lignin standard (Fig 4.6c) are likely derived from residual hemicellulose. ^{13}C-NMR and pyrolysis analyses of refractory soil OM have shown that hemicellulose can survive acid treatment by protection from the lignin complex (Quenea *et al*., 2005a).

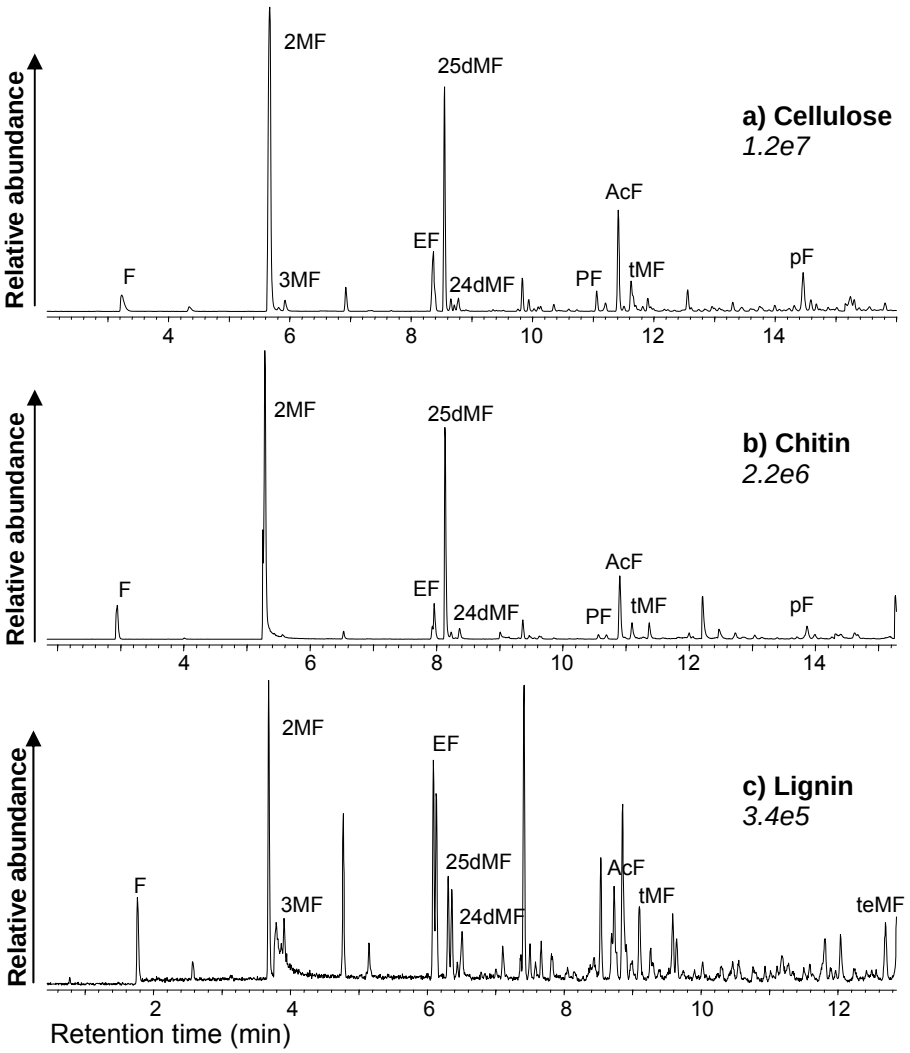

Figure 4.6 Summed *m/z* 68+72+81+82+95+96+109+110+123+124 chromatograms showing the alkyl furan distribution from 300˚C/72hr MSSV pyrolysis GC-MS analysis of **a)** cellulose, **b)** chitin and **c)** lignin. Peak assignments correspond to products listed in Table 4.1. Relative abundances of a-c are indicated in italics.

Tetrahydro furan, which is a component of the lignin structural network (Leenheer *et al*., 2003b), was detected in high concentration from the U-HPO fraction (Fig. 4.3c). However this product was not detected from the lignin standard, suggesting its MSSV Py detection may be dependent on biodegradation to first release this structural unit from the lignin macromolecule. Polycarboxylated tetrahydrofurans may be produced by opening the aromatic moieties of the lignin structure during diagenetic mineralization (Leenheer *et al*., 2003b). Tetrahydro furan was not detected from B-COL, consistent with a limited contribution from lignin.

4.3.4 Benzofurans

The summed ion chromatograms of **Figure 4.7** show the distribution of methyl and dimethyl benzofurans detected from the Suwannee River fulvic acid standard and the G-TPI and B-COL fractions. Flash pyrolysis also yielded alkyl benzofurans but in lower abundance than MSSV Py. The HPO fractions generally produced the highest concentrations of benzofurans. These products were particularly abundant from SRFA, whilst much lower concentrations of the previously discussed alkyl and acetyl furans were detected. In contrast, benzofurans were relatively minor products of the B-COL fraction and the cellulose standard compared to AFs (Figure 4.5).

These results suggest that benzofurans are thermally formed from diagenetically altered polysaccharide structures that are sequestered into HPO NOM fractions. Benzofurans were shown to be major products of humic-like material produced by acid catalysed dehydration of glucose (Almendros *et al*., 1997). They have also been found to be relatively stable pyrolysis products of the residues of thermally treated cellulose and humic substances (Almendros *et al*., 1997; Lu *et al*., 2001). This has been attributed to the transformation of carbohydrates into heterocyclic aromatic structures during heating (Lu *et al*., 2001).

Benzofurans were detected in only trace quantities from the HPO fractions of the waste water effluents and not at all from the colloids. The degradation of carbohydrate precursors during biological treatment would account for the much lower concentrations of these products from the waste waters.

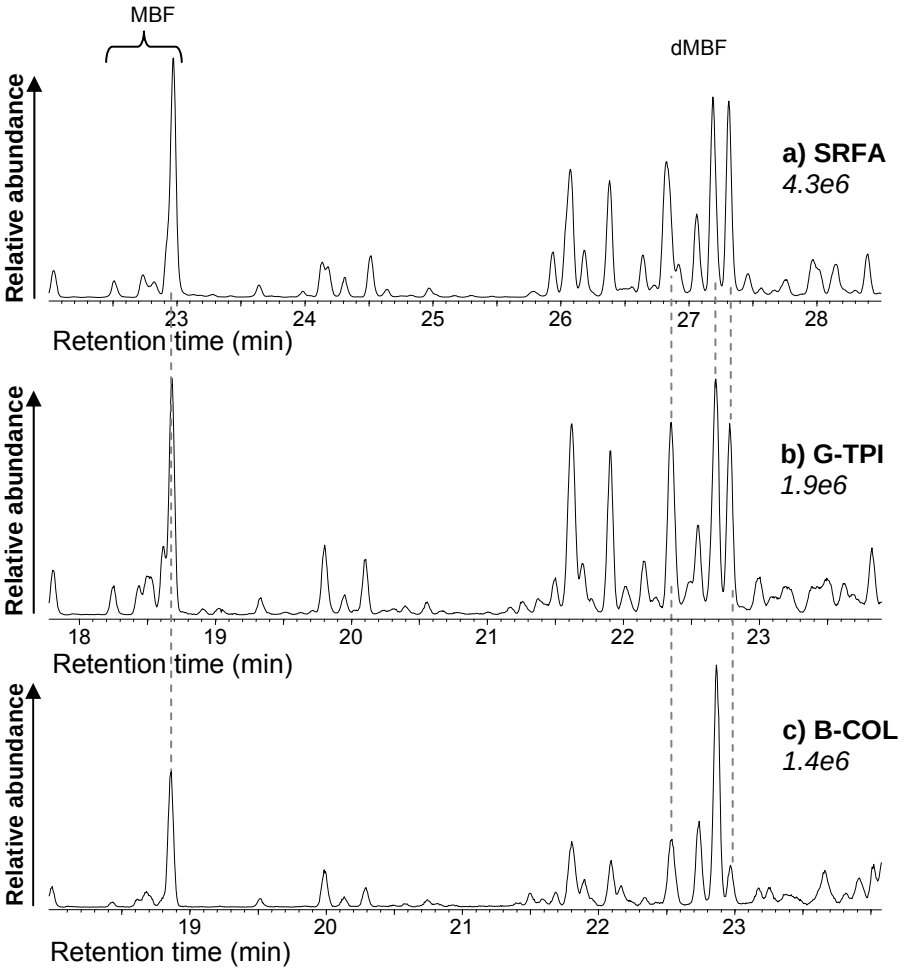

Figure 4.7 Summed *m/z* 131+132+145+146 chromatograms showing the distribution of alkyl (C_1-C_2) benzofurans detected by 300˚C/72hr MSSV pyrolysis GC-MS of **a)** SRFA, **b)** Gartempe TPI and **c)** Brittany COL. Peak assignments correspond to products listed in Table 4.1. Relative abundances of a-c are indicated in italics.

4.3.5 Alkyl cyclopentenones

Alkyl 2-cyclopenten-1-ones were detected in similar concentrations in each of the XAD fractions of the surface waters analysed, but were minor pyrolysates compared to the furans and phenols. The most abundant of these products had 2 to 4 methyl substituents. Flash pyrolysis of the surface water NOM fractions yielded similarly low concentrations of polymethyl cyclopentenones, with the methyl and dimethyl products dominating. Cyclopentenone pyrolysates of soil and aquatic NOM are usually attributed to polysaccharides (e.g. Saiz-Jimenez and de Leeuw, 1984a; Bruchet, 1985; Saiz-Jimenez and De Leeuw, 1986b; Bruchet *et al*., 1990; Reeves and Francis, 1997; Christy *et al*., 1999; van Heemst *et al*., 2000; Page *et al*., 2002; 2003), although they may also derive from other NOM precursors. Cyclisation of

aliphatic polycarboxylic acids represents one alternative formation pathway (Bracewell *et al*., 1980). Guo *et al*. (2003) showed that the abundance of cyclopentenone pyrolysates increased with decreasing molecular size of riverine NOM fractions, whereas furan based carboxaldehyde products decreased, which was attributed to different sources for cyclopentenone and alkyl furan products. It is also possible that the cyclopentenones are products of humified sugars.

The dimethyl to tetramethyl cyclopentenone distributions from the MSSV pyrolysis of cellulose and SRFA are shown in **Figure 4.8**. These distributions were very similar to each other as well as the corresponding polymethyl cyclopentenone distribution of the other surface water NOM samples, providing convincing evidence of a carbohydrate origin for these NOM pyrolysates. Alkyl cyclopentenones were not detected from the COL and HPO fractions of the waste waters, consistent with the quantitative trends observed for the other polysaccharide pyrolysates.

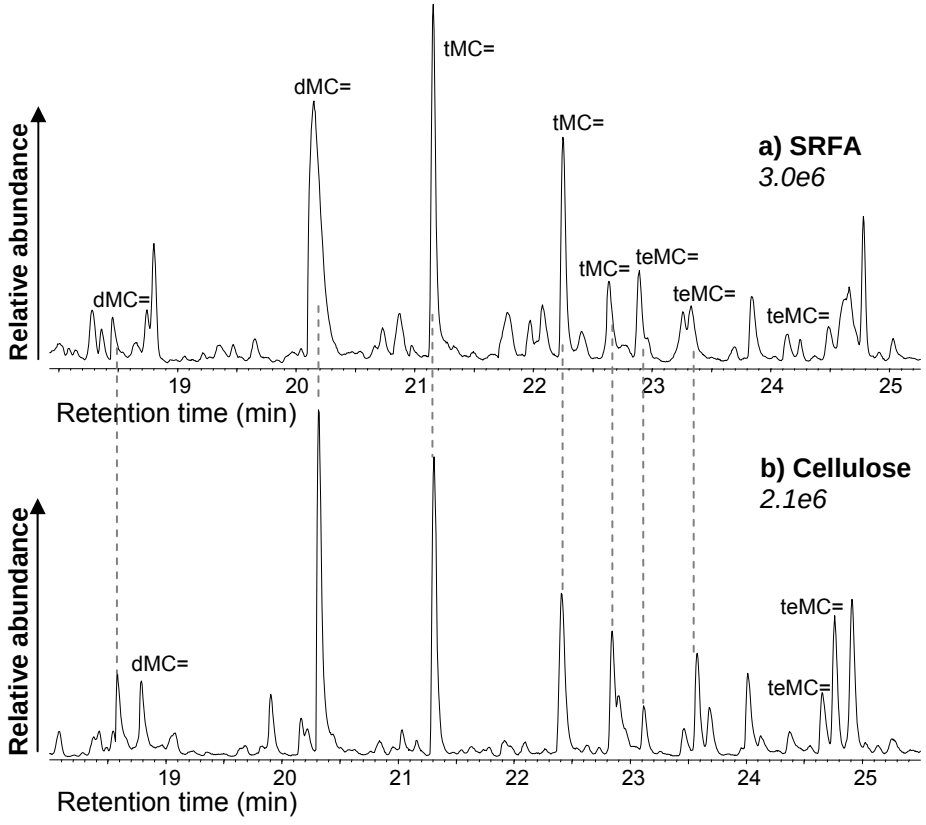

Figure 4.8 Summed *m/z* 67+109+110+123+124+138 chromatograms showing the distribution of alkyl (C_2-C_4) 2-cyclopenten-1-ones detected by 300˚C/72hr MSSV pyrolysis GC-MS analysis of **a)** SRFA and **b)** cellulose. Peak assignments correspond to products listed in Table 4.1. Relative abundances of a-b are indicated in italics.

MSSV pyrolysis of the NOM fractions also yielded several short chain C_4-C_6 aliphatic ketones, including 2-butanone, 3-methyl-2-butanone, 2-pentanone, 3-pentanone, 4-methyl-3-pentanone, 2-methyl-3-pentanone, 3-hexanone and 2-hexanone. These low MW products were not correlated with any specific sources, although several were previously reported to be pyrolysates of thermally treated carbohydrates (Almendros *et al*., 1997). The cellulose standard showed low concentrations of 2-pentanone and 3-hexanone. However, these products were detected in all of the surface and waste water NOM fractions in high concentrations, implying non-carbohydrate origins.

4.3.6 Alkyl phenols

4.3.6.1 Alkyl phenol distributions of surface waters

Alkyl phenols (APs) were the most abundant O-pyrolysates of the HPO and TPI fractions of the surface waters. The AP distribution detected from the HPO fractions of the Uruguay and Gartempe River as well as the SRFA standard are shown in **Figure 4.9**. The low MW alkyl ($\leq C_2$) phenols showed the highest abundances and were able to be assigned by mass spectral comparison with library spectra and literature data (van Heemst *et al*., 1996; Iopollo *et al*., 1992; Iopollo-Armanos *et al*., 1995; Bastow *et al*., 2005). However, the isomeric identities of the C_3 and C_4 alkylated phenols detected in lower concentrations, were difficult to assign on this basis alone. Nevertheless, characteristic mass fragmentation patterns provide some degree of product differentiation, as shown in Table 4.1. The river HPO fractions and the SRFA standard showed very similar AP distributions, suggesting a common origin. The corresponding TPI fractions of Uruguay and Gartempe Rivers showed similar AP distributions, however their abundance was approximately half that of the HPO fractions. The Brittany COL showed very few APs, consistent with the low polyphenolic content of COL fractions.

Much higher concentrations of APs were consistently detected by MSSV Py of the NOM fractions compared to flash pyrolysis. The AP profiles detected by flash pyrolysis of all NOM fractions were similar, and the SRFA data is shown (**Fig. 4.9d)**. Phenol and methyl phenols were prominent flash pyrolysates, but C_2-C_3 substituted phenols were present in much lower abundance and no larger alkyl ($\geq C_4$) phenols

were detected. Similarly, no APs with > C_3 substituents were detected (Templier *et al*., 2005a) by previous *Curie* point pyrolysis of the Gartempe fractions. Nevertheless, the relative AP concentrations of the respective NOM fractions detected by both MSSV and flash Py were consistent, with surface HPO > surface TPI > surface COL.

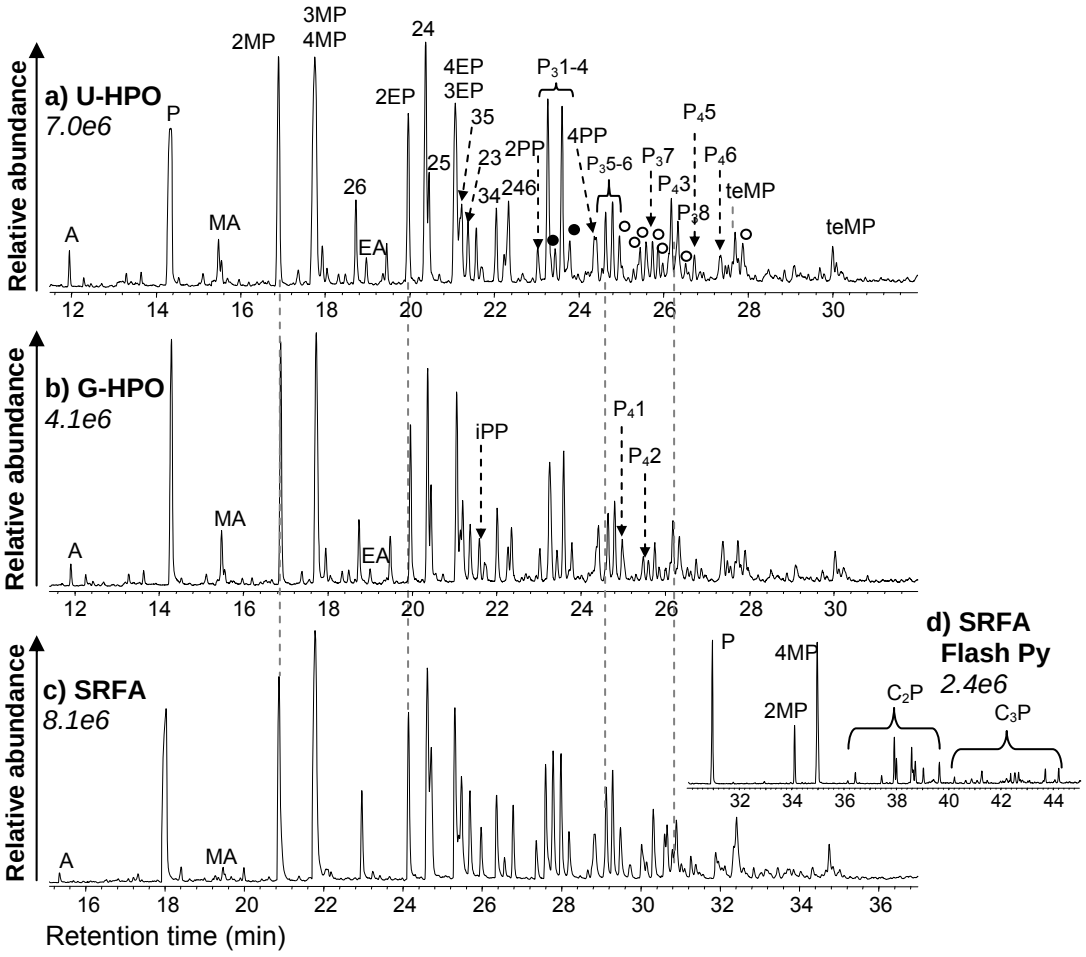

Figure 4.9 Summed *m/z* 94+107+108+121+122+135+136+150 chromatograms showing the distribution of alkyl (≤ C_4) phenols detected by 300˚C/72hr MSSV pyrolysis GC-MS of **a)** Uruguay HPO; **b)** Gartempe HPO; and **c)** SRFA. The inset chromatogram **(d)** shows the alkyl phenol distribution from flash pyrolysis of SRFA. Peak assignments correspond to products listed in Table 4.1. Relative abundances of a-d are indicated in italics.

4.3.6.2 Alkyl phenol distributions of standards

Alkyl phenols are commonly detected products from the flash pyrolysis analysis of aquatic NOM and humic substances, as well as sedimentary OM and crude oils.

They have been attributed to a range of different sources including lignin (Saiz-Jimenez and de Leeuw, 1986b, Bruchet *et al*., 1990; Templier *et al*., 2005a), tyrosine-containing proteins and peptides (Chiavari and Galletti, 1992), hydrolysable and condensed tannins (Galletti and Reeves, 1992), polycarboxylic acids (Bracewell *et al*., 1980) and algal-derived polyphenols (van Heemst *et al*., 1996). However, the capacity to distinguish the origins of phenolic pyrolysates by flash pyrolysis has typically been limited (van Heemst *et al*., 1999). Terrestrially derived vascular plant biopolymers such as lignin and tannin are thought to be a major source of the phenolic structural constituents of refractory humic substances of black waters, such as the Gartempe, Uruguay and Suwannee Rivers (e.g. Hedges *et al*., 1985; Malcolm, 1990; Leenheer, 2004; Templier *et al*., 2005a). To investigate the source diagnostic value of the APs detected by MSSV Py of aquatic NOM fractions, several selected standards representative of potential AP precursors were additionally analysed by MSSV pyrolysis.

4.3.6.2.1 Lignin

The TICs obtained by MSSV pyrolysis (300˚C/72hr) of the lignin and syringic acid standards are show in **Figure 4.10**. Alkyl phenols were major MSSV products of lignin, accounting for ca. 36 % of the pyrolysate signal. Other key products of this sample included methoxy benzenes and tricyclic aromatic hydrocarbons, the latter probably from adsorbed terpenoids. The characteristic methoxyphenol structural units of lignin were absent. Syringic acid, a monomeric sub-structure of biodegraded lignin (Pancost and Boot, 2004), also showed low concentrations of APs but these were relatively minor compared to alkyl methoxybenzenes and methoxyphenols.

The high concentrations of methoxylated phenols and benzenes from syringic acid, and the absence of the former and low concentrations of the latter from the lignin standard were curious. The lignin macromolecule contains a number of methoxylated phenolic units similar to the dimethoxyphenol structure of syringic acid. Like the present syringic acid data, large scale MSSV pyrolysis of pure 2-methoxyphenol (guaiacol) or 2,6-dimethoxyphenol also reported preservation of the methoxy functional groups in the products (Vane and Abbot, 1999). However, the greater structural complexity of the lignin matrix compared to pure methoxyphenol compounds will likely contribute to many secondary interactions and synergistic

effects. Methoxy groups may be more readily reduced in a more hydrogen rich environment.

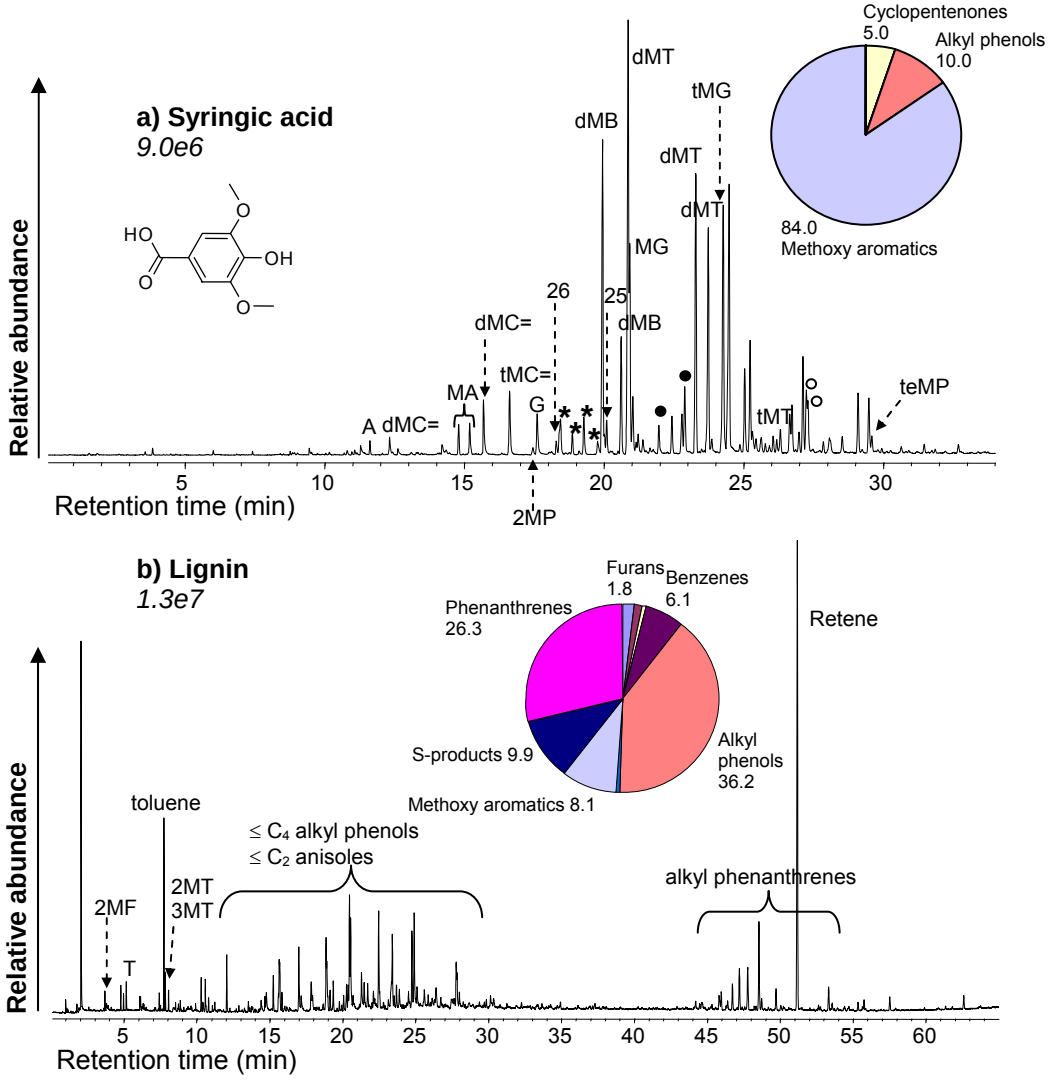

Figure 4.10 Partial TICs detected by 300˚C/72hr MSSV pyrolysis of **a)** syringic acid; and **b)** standard lignin. Relative peak abundances in italics and a pie chart reflecting relative proportions of major pyrolysate groups are both indicated for a and b. ***** = dimethylmethoxybenzenes, G = guaiacol, dMB = dimethoxybenzene, dMT = dimethoxytoluene, tMT = trimethoxytoluene, MG = methylguaiacol, tMG = trimethylguaiacol. Other peak assignments correspond to the products listed in Table 4.1.

The summed ion chromatograms of **Figure 4.11a** highlight the distribution of APs detected from the MSSV pyrolysis of lignin at 300˚C (72hr). The major AP products included 2-methylphenol, 2,6-, 2,4- and 2,5-dimethylphenol, 2,4,6-trimethylphenol.

and several unspecified C_3–C_4 alkyl substituted phenols ($P_3$1, $P_3$5-6 and tetramethylphenol). These products were also detected in high concentrations in the surface water NOM fractions, signifying that lignin is a likely precursor of many of the AP pyrolysates of NOM.

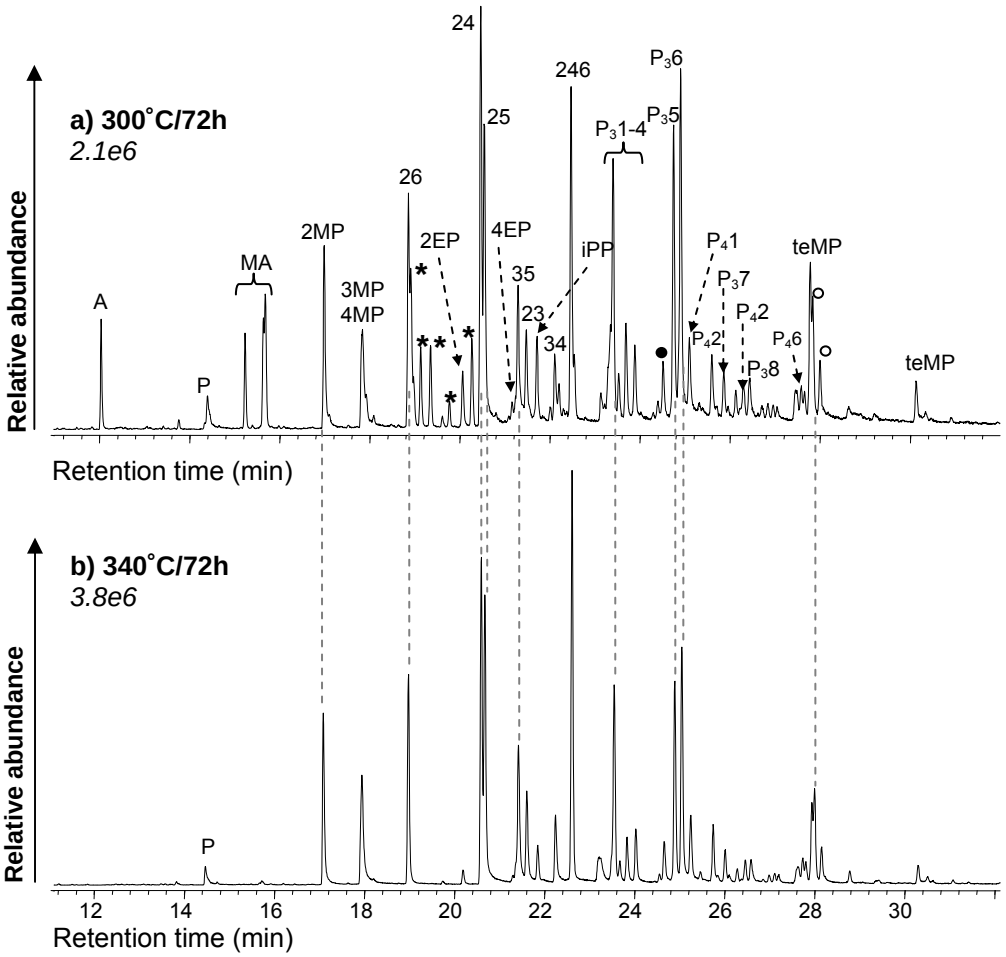

Figure 4.11 Summed *m/z* 94+107+108+121+122+135+136+150 chromatograms showing the distribution of APs detected by MSSV pyrolysis of the lignin standard at **a)** 300˚C/72h and **b)** 340˚C/72h. Peak assignments correspond to products listed in Table 4.1. Relative abundances of a-b are indicated in italics. ***** = C_2 alkyl methoxybenzenes.

The product distributions from the MSSV Py of lignin were very different from those typically detected by flash pyrolysis. Distinctive flash pyrolysates of lignin include methoxyphenols (guaiacols), which are unique indicators of this vascular plant biopolymer (e.g. Hedges and Mann, 1979; Ertel *et al*., 1984), whilst alkyl phenols are generally detected in lower abundance (van Heemst *et al*., 1999).

The flash pyrolysis detection of methoxyphenols in environmental samples provides unequivocal evidence of lignin contribution (e.g. Ertel *et al*., 1984; Ertel and Hedges, 1984; Saiz-Jimenez and de Leeuw; 1986a; 1986b; Opsahl and Benner, 1997; Pancost and Boot, 2004). Lignin input to the Uruguay surface water (HPO) was confirmed by both flash pyrolysis and thermochemolysis (**Figure 4.12**). Characteristic methoxyphenol products included 2-methoxyphenol (guaiacol), 4-ethyl-2-methoxyphenol (ethylguaiacol), 2,6-dimethoxyphenol (syringol), 2-methoxy-4-vinylphenol (4-vinylguaiacol), 2-methoxy-4-propenylphenol (eugenol) and 1,2-dimethoxy-4-propenylbenzene (methyl eugenol). Separate *Curie*-point pyrolysis and TMAH thermochemolysis analyses of the Gartempe HPO fraction by Templier *et al*. (2005a) also confirmed the presence of these lignin sourced pyrolysates. However, direct evidence of lignin biomarkers in aquatic NOM samples is often limited (Leenheer *et al*., 2003a; McIntyre *et al*., 2005). For example, the extensively characterised SRFA has shown limited evidence of lignin products (Leenheer and Rostad, 2004). The relatively high concentrations of the methoxyphenol products of U-HPO reflect exceptionally high lignin concentrations of this NOM.

Some methoxylated aromatics (e.g. anisole, methylanisole and dimethylanisoles) were detected by MSSV pyrolysis of the lignin standard; however these products were present in significantly lower abundance than the APs. Closed system thermal treatment may result in chemical transformations of the lignin structural framework, analogous to the catagenesis of lignin in sedimentary systems. Previous characterisation studies of sedimentary maturity sequences, using ^{13}C-NMR, flash pyrolysis and chemical oxidation, have shown that methoxy phenol structures of lignin are transformed into alkyl phenols with increasing maturation (Hayatsu *et al*., 1986; Hatcher, 1988; Hatcher *et al*., 1988; Stout *et al*., 1988; Bates and Hatcher, 1989; Hartgers *et al*., 1994b).

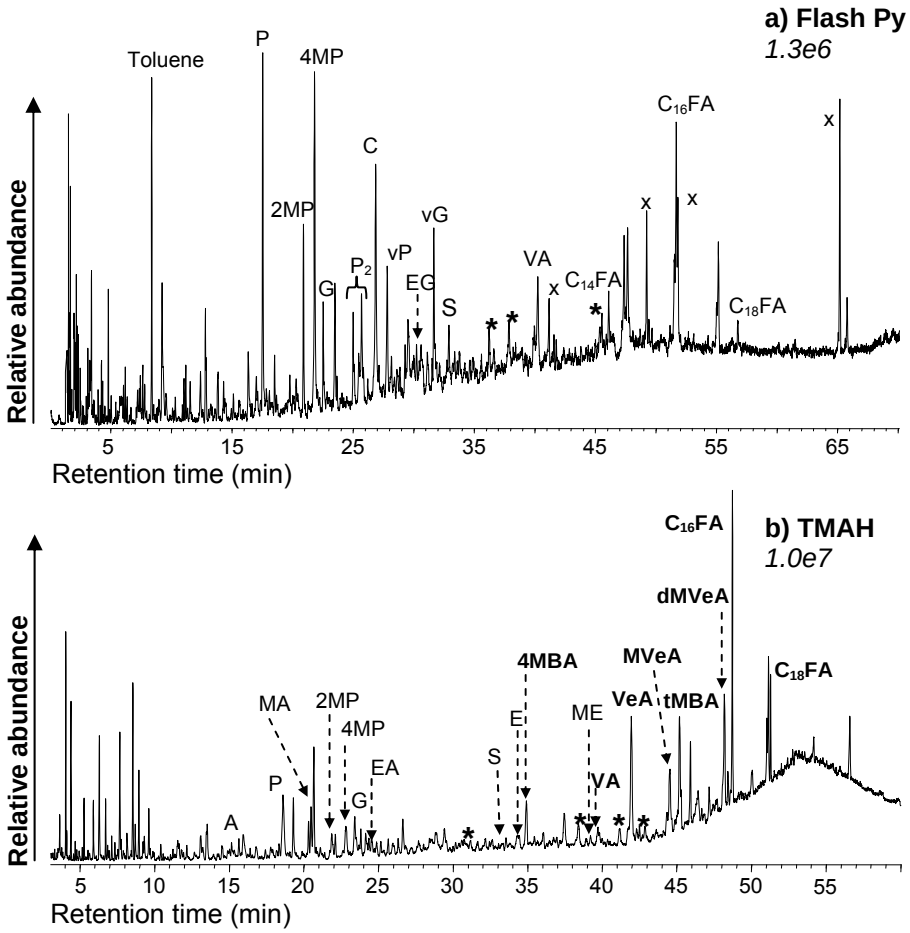

Figure 4.12 TICs from the GC-MS analysis of Uruguay HPO following **a)** 550˚C/20s flash pyrolysis and **b)** TMAH thermochemolysis. Relative abundances of a-b are indicated in italics. G = guaiacol, vP = vinyl phenol, EG = ethylguaiacol, vG = 4-vinylguaiacol , S = syringol, E = eugenol, ME = methyleugenol, C = catechol, 4MBA = 4-methoxybenzoic acid, VA = vanillic acid, VeA = veratric acid, MVeA = 4-methoxyveratric acid, dMVeA = 3,4-dimethoxyveratric acid, tMBA = 3,4,5 trimethoxy-benzoic acid, FA = fatty acids, ***** = methoxy benzylic ketones, x = benzenedicarboxylic acids (possible contaminants). Additional peak assignments correspond to the products listed in Table 4.1. Products in bold were detected as their methyl esters by thermochemolysis.

Coalification involves the diagenetic and catagenetic alteration of sedimentary organic remains of plants by microbial activity, burial, and geothermal heating (Behar and Hatcher, 1995). A number of sequential chemical reactions occur with increasing maturity. With respect to lignin structures, these include thermal cleavage of aryl alkyl ethers, transalkylation, demethylation of methoxyls to form catechols,

subsequent dehydroxylation to form alkyl phenols and both oxidation and reduction of the aromatic side-chain groups to form carboxylic acids and propyl substituents, respectively (Botto, 1987; Hatcher *et al*., 1988; 1989b; Hatcher, 1990; Behar and Hatcher, 1995; Hatcher and Clifford, 1997; Payne and Ortoleva, 2001). Guaiacols and catechols are prominent constituents of thermally immature fossil woods and coals (e.g. less than lignite rank; Hatcher, 1990). However, they are significantly diminished or absent in thermally mature type III kerogens and higher rank bituminous and subbitumous coals, where APs are the dominant products (e.g. Stout *et al*., 1988; Hatcher *et al*., 1988; 1989a; 1992; Sinninghe-Damsté *et al*., 1992b; Hartgers *et al*., 1994b; Hatcher and Clifford, 1997; Almendros *et al*., 1998).

MSSV thermal treatment appears to parallel the natural diagenetic and catagenetic alteration of lignin, resulting in the reduction of methoxy groups and the formation of high concentrations of APs. These structural trends increase with thermal maturity and the 340˚C/72hr MSSV Py of lignin resulted in complete removal of methoxy functional groups and higher concentrations of APs (**Fig. 4.11b**). Similar results have been observed from previous confined pyrolysis studies of extant and naturally coalified fossil woods (Ohta and Venkatesan, 1992; Behar and Hatcher, 1995), immature coals (Mansuy *et al*., 1995; Michels *et al*., 2000) and swamp humic substances (Lu *et al*., 2001). The molecular composition of a lignin derived biofuel, produced by high pressure closed system pyrolysis/solvolysis, has also been shown to include major alkyl (C_1-C_4) phenol products with only minor occurrences of methoxy phenols (Barth and Kleinert, 2008; Kleinert and Barth; 2008a; 2008b).

Whilst APs dominated the MSSV Py data of the lignin standard several alkyl ($\leq C_2$) methoxy benzenes (8 %) were still detected. However, only minor concentrations (< 2 %) of these methoxy aromatics (e.g. A, MA, EA, see Table 4.1) were detected from the U-HPO and G-HPO fractions, in which lignin input was confirmed by flash pyrolysis and thermochemolysis. This discrepancy between the MSSV data of the NOM fractions and the fresh lignin may be attributed to early microbial degradation of lignin derived moieties, which involves demethylation of methoxy groups to form catechols and oxidative degradation of the C_3 side chain to form aromatic carboxylic acids (Saiz-Jimenez and de Leeuw, 1984b; Kirk and Farrell, 1987; Huang *et al*., 1998; Filley *et al*., 2000; Leenheer *et al*., 2003b). The presence of demethoxylated

lignin structures is supported by the detection of catechol in high concentration by flash pyrolysis of U-HPO (**Fig. 4.12a**).In addition to the intact lignin biomarkers detected by flash pyrolysis of U-HPO, several thermochemolysis products also reflected a high degree of microbial degradation of lignin (**Fig. 4.12b**). These included a variety of benzylic ketones (e.g. 4-methoxybenzaldehyde, 3,4-dimethoxybenzaldehyde, 3,4-dimethoxyacetophenone, 3,4,5-trimethoxybenzaldehyde) and methyl esters of aromatic carboxylic acids (e.g. 3- and 4-methoxybenzoic acid, 4-hydroxy-3-methoxybenzoic acid (vanillic acid), 3,4-dimethoxybenzoic acid (veratric acid), 3-(4-methoxyphenyl)-2-propenoic acid (4-methoxycinnamic acid), 3-(3,4-dimethoxyphenyl)-2-propenoic acid (3,4-dimethoxycinnamic acid) and 3,4,5-trimethoxybenzoic acid). Similar distributions of oxidised lignin products were detected by previous thermochemolysis analysis of G-HPO (Templier *et al*., 2005a).

Apart from low concentrations of vanillic acid, phenolic benzenecarboxylic acids were not detected by flash Py analysis of the NOM samples due to thermal decarboxylation of carboxyl groups (Saiz-Jimenez, 1994; del Rio *et al*., 1996). Likewise, these products were not detected by MSSV Py. This may be due to the similar occurrence of thermal decarboxylation (Behar and Hatcher, 1995; Lu *et al*., 2001) or reduction of acidic functional groups to alkyl groups. The latter process is supported by the much high concentrations of alkylated phenols in the MSSV data. The AP products of the riverine HPO fractions may therefore reflect highly modified lignin structures derived from surrounding vascular plant vegetation. It has been shown from various studies that lignin in natural waters is substantially degraded prior to entry into aquatic systems (Frazier *et al*., 2003; Huang *et al*., 1998; Cotrim da Cunha *et al*., 2001), with the structural changes affording solubility to typically insoluble lignin biopolymers (del Rio *et al*., 1998).

Detailed analysis of the MSSV Py, flash Py and thermochemolysis data provides convincing evidence that intact or partially degraded lignin structural moieties are the major source of the high concentrations of APs from the MSSV pyrolysis of the Gartempe and Uruguay HPO fractions. Furthermore, lignin moieties of NOM subject to diagenetic processes may reflect much higher concentrations of AP metabolites than their methoxyphenol structural precursors, in which case the MSSV

Py detection of APs may be a more sensitive indicator of lignin input than unequivocal guaiacol and syringyl based biomarkers.

4.3.6.2.2 Tannin

Plant tannins, natural polyphenolic compounds concentrated in bark and leaf tissues (Hernes and Hedges, 2004), are another potential source of the AP products of surface water NOM. Condensed tannins are polymers and oligomers of three ring flavanols (e.g. quercetin) linked by C–C bonds, while hydrolysable tannin is made up of gallic acid units or its derivatives, often ester-linked to sugars such as glucose (Hernes and Hedges, 2000; Hernes and Hedges, 2004). ^{13}C NMR analysis has identified condensed and hydrolysable tannins in refractory soil OM (Quénéa *et al*., 2005a; Nierop and Filley, 2007), black water humic substances (Leenheer, 2004, Leenheer and Rostad, 2004) and sediments (Wilson and Hatcher, 1987).

Although tannins are more soluble than lignin, they are also more reactive in both biotic and abiotic humification processes (Filley *et al*., 2006) and often undergo oxidative coupling reactions leading to new structures (Wershaw 2004). Tannins can be incorporated into aquatic humic substances via quinone intermediates which can undergo subsequent condensation reactions with proteins and amino acids (Hernes and Hedges, 2000; Leenheer and Rostad, 2004). The ready bioavailability and extensive diagenetic alteration of tannins means they preserve little information about plant source or microbial processes (Lorenz *et al*., 2000). Tannin phenols do not contain methoxy substituents and their aromatic substitution patterns are different to lignin (Leenheer and Rostad, 2004).

MSSV pyrolysis was conducted on several tannin monomers including gallic acid, ellagic acid and quercetin. These standards yielded very few GC-MS detectable products. **Figure 4.13 a-b** shows the TICs obtained by MSSV pyrolysis of quercetin, a flavanol unit present in condensed tannins, at the off-line MSSV temperatures of 300 and 340˚C (72hr). At 300˚C only 2-propanone, 2-butanone, 2-pentanone, benzene, toluene and ethylbenzene were detected. The 340˚C analysis yielded higher concentrations of these products, as well as several additional products including isopropylbenzene, phenol, 4-methylphenol, methylbenzofuran and dimethylbenzofuran. However, these products provide little diagnostic utility. In

comparison, flash pyrolysis of quercetin yielded several characteristic polyphenols including catechol, 4-methylcatechol and 1,3,5-benzenetriol.

These results suggest that the polyphenol structures of tannins are not amenable to characterization by MSSV pyrolysis. Their different structures may contribute to very different thermal behaviour during MSSV pyrolysis compared to lignin. Thus, the contribution of tannin precursors to the AP distributions detected by MSSV Py of the NOM fractions may be minimal. However, it is possible that diagenetically altered tannin structures will have very different MSSV Py behavior than the monomers studied here, particularly if incorporated into a more stable humic form.

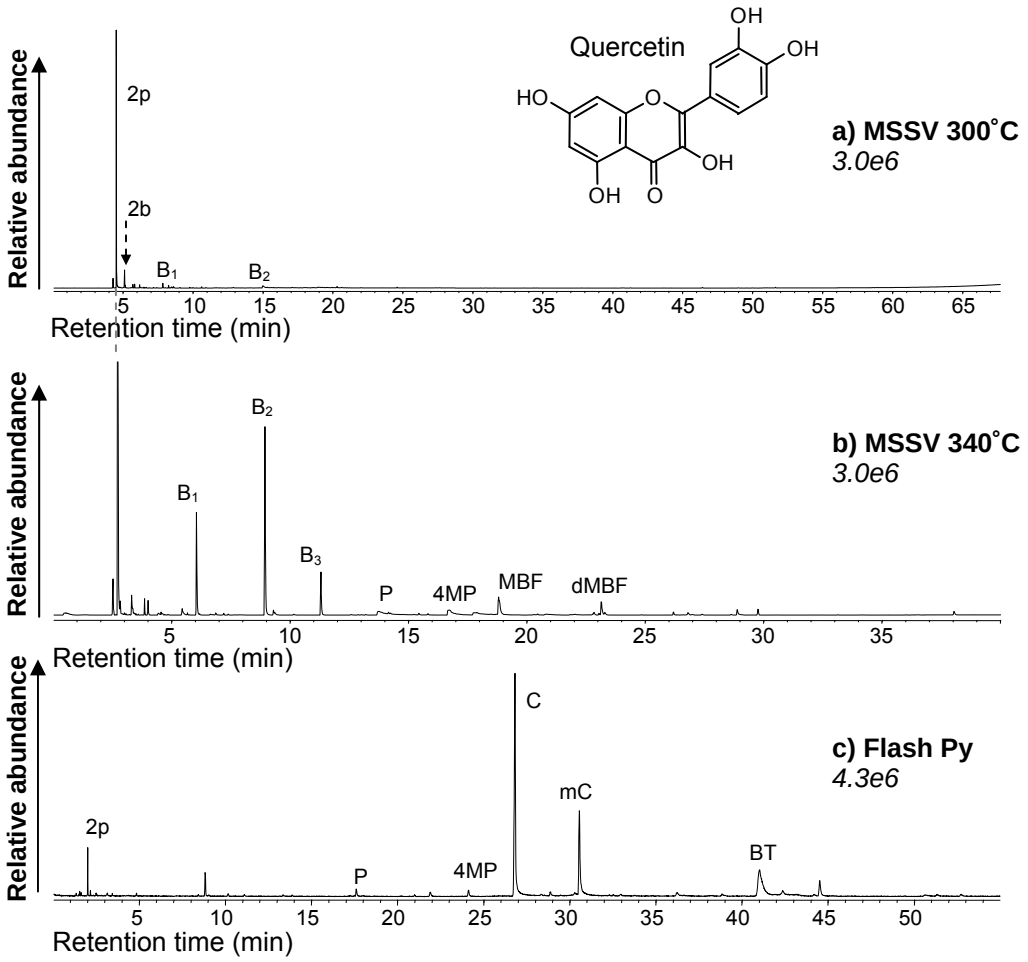

Figure 4.13 TICs from the MSSV pyrolysis (72 hr) of quercetin at **a)** 300˚C, **b)** 340˚C; and **c)** 550˚C/20sec flash pyrolysis of quercetin. B_x = alkyl (≤ C_3) benzenes, 2p = 2-propanone, C = catechol, mC = methyl catechol, BT = 1,3,5-benzenetriol. Other peak assignments correspond to products listed in Table 4.1. Relative abundances of a-c are indicated in italics.

4.3.6.2.3 Amino acid and protein

Proteinaceous material containing the phenolic amino acid tyrosine is another major source of phenolic pyrolysates of aquatic organic matter (Bruchet, 1985; van Heemst *et al*., 1999). The MSSV pyrolysis data of D-tyrosine and bovine serum albumin (BSA) protein are both shown in **Figure 4.14**. Tyrosine comprises ca. 5 % of the amino acid composition of BSA (Stein and Moore, 1949). Phenols accounted for > 96% of the total pyrolysate of tyrosine. The major products of both samples were phenol, 2- and 4-methylphenol and 2- and 4-ethylphenol. A previous flash pyrolysis study of tyrosine also reported predominant phenol and 4-methylphenol (van Heemst *et al*., 1999). BSA also showed low concentrations of several additional C_3 and C_4 APs. Phenolic products accounted for ca. 18 % of the integrated peak area of BSA.

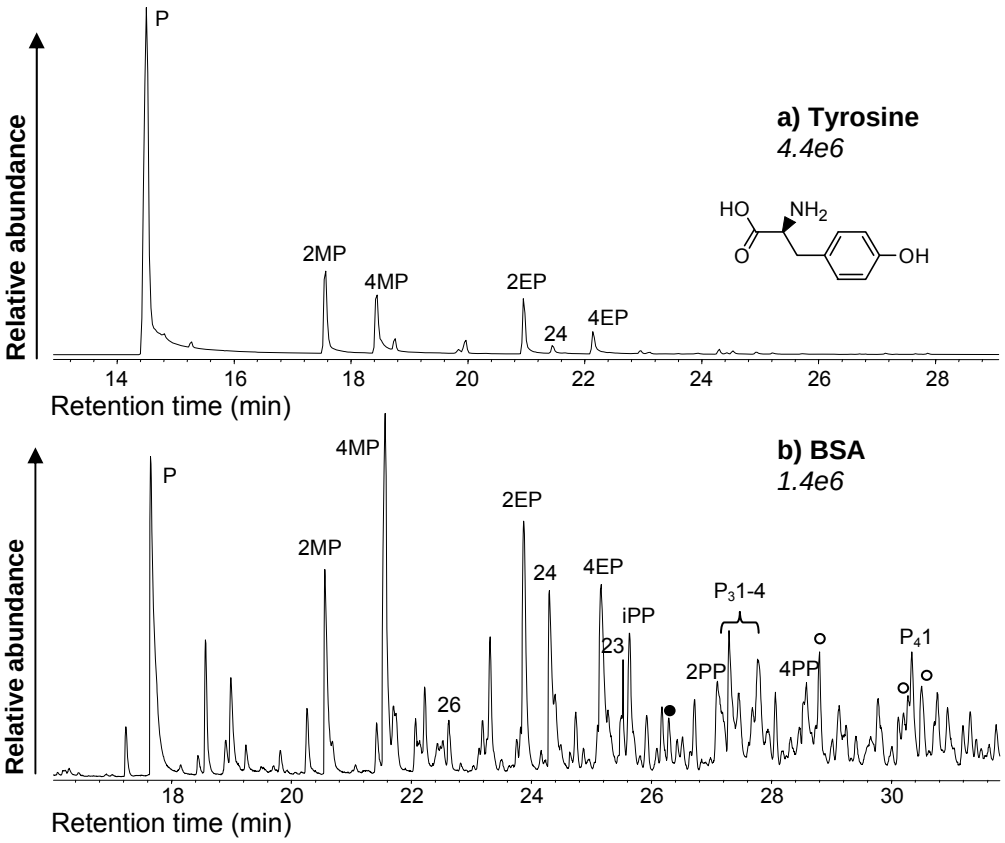

Figure 4.14 Summed *m/z* 94+107+108+121+122+135+136+150 chromatograms showing the distribution of alkyl phenols detected by 300˚C/72hr MSSV pyrolysis of **a)** D-tyrosine; and **b)** BSA protein. Peak assignments correspond to products listed in Table 4.1. Relative abundances of a-b are indicated in italics.

The phenol distributions of these standards contrasts the low concentrations of phenol, 2-ethyl- and 4-ethyl phenol detected from the lignin standard (Fig. 4.11). These were amongst the significant AP products of the river HPO samples, suggesting combined contribution of lignin and proteinaceous sources. Proteins and amino acids are not typically concentrated in the humic material of rivers, but they can be preserved by sequestration or occlusion within recalcitrant humic structures (Knicker and Hatcher, 1997; Zang *et al*., 2000). However the lack of co-occurring nitrogen products of protein precursors in the HPO fractions of the river waters suggests this is unlikely (Chapter 5).

4.3.6.3 Alkyl phenol distributions of waste waters

High concentrations of alkyl phenols were also detected from the MSSV Py analysis of the HPO fractions of the St. Julien and Naintré waste water effluents. Their prevalence in the post treated waste waters suggests their structural precursors are resistant to biological treatment. The summed ion chromatograms of **Figure 4.15** show the AP distribution of these samples. The $\leq C_3$ AP profile of both S-HPO and N-HPO closely resembled the AP distribution of the surface water HPO fractions, although isopropyl phenol was enriched in the Naintré data.

The general similarity of the ($\leq C_3$) AP profiles of the surface (Fig. 4.9) and waste waters may indicate a similar precursory origin from lignin derived humic substances, despite the absence of products containing methoxy functional groups from flash pyrolysis of N-HPO and S-HPO (Jarusutthirak, 2002). Refractory humic substances of drinking water inputs in waste waters have been shown to be recalcitrant to treatment (Namour and Müller, 1998; Drewes *et al*., 2003). Alternatively, phenolic metabolites of algae or treatment biota (van Heemst *et al*., 1996; 1999) may also contribute to the AP products detected in the waste waters.

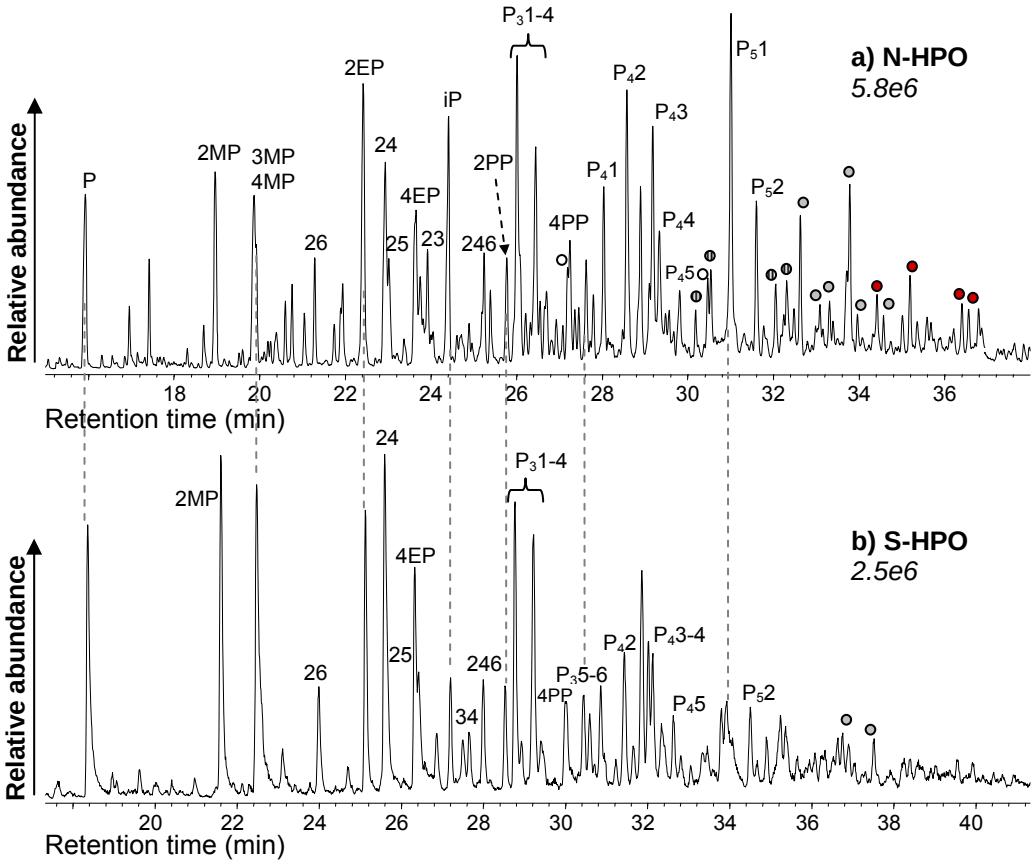

Figure 4.15 Summed *m/z* 94+107+108+121+122+135+136+150+149+ 163+164+177+178+192 chromatograms showing the distribution of alkyl ($\leq C_7$) phenols detected by 300˚C/72hr MSSV pyrolysis GC-MS analysis of **a)** St. Julien HPO and **b)** Naintré HPO. Peak assignments correspond to products listed in Table 4.1. Relative abundances of a-f are indicated in italics.

The N-HPO fraction additionally yielded many extended $C_{4\text{-}10}$ alkyl substituted phenols. The C_4-C_7 APs were detected in relatively high concentration and are highlighted in **Figure 4.15**. Although the specific isomeric identities of these additional products were not assigned, the mass spectra suggest the presence of highly branched alkyl groups, including *sec*-butyl, *tert*-butyl, *tert*-pentyl and di-isopropyl substituents. Furthermore, low relative abundances of several even higher MW APs (C_8-C_{10}) were detected and are highlighted in the summed ion chromatograms of **Figure 4.16**. Several of these products were tentatively assigned as *t*-octylphenol, methyl-*t*-octylphenol, dimethyl-*t*-octylphenol and unspecified isomers of nonylphenol. Octyl- and nonylphenols are components of alkylphenol ethoxylates used as industrial surfactants (Petrovic *et al*., 2002). These chemicals are

of significant health concern because they are endocrine disrupting compounds and are not efficiently degraded in WWTPs (di Corcia *et al*., 1998; Petrovic *et al*., 2002).

Although some of the C_8-C_9 APs can be correlated with industrial surfactants (Petrovic *et al*., 2002), the origins of most of the high MW branched alkyl ($\geq C_5$) phenols of N-HPO are unconfirmed. The $\leq C_7$ AP products may reflect partial microbial degradation of the alkyl side chains of the octyl- and nonylphenols. The high degree of alkyl substitution evident in N-HPO may alternatively reflect a significant refractory alkyl linked macromolecular component. Their exclusive detection from the waste water HPO fractions indicates that they may derive from phenolic metabolites of microbiota (van Heemst *et al*., 1996; 1999). An alternative source may be tyrosine moieties of cross-linked melanoidin-type structures (Dignac *et al*., 2000; van Heemst *et al*., 1999; 2000). Dignac *et al*. (2000) suggested that chemically and biologically refractory OM present in waste water effluents may be formed by recondensation reactions between degraded peptides and carbohydrates, enhanced by the intense activity during biological treatment. Waste water hydrophobic fractions may contain substantially higher protein input from microbial biomass, than surface water humic substances.

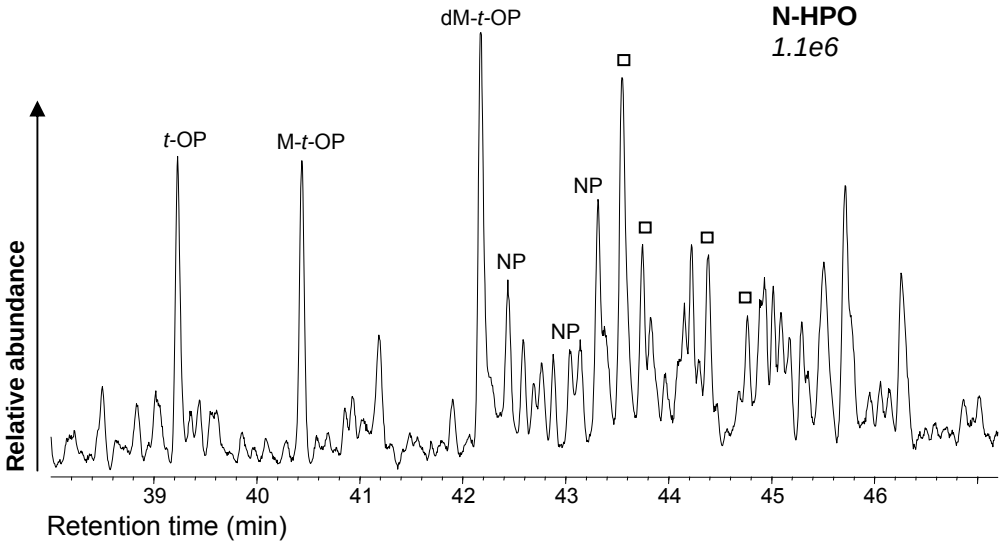

Figure 4.16 Summed *m/z* 135+149+163+206+220+234 chromatograms showing the distribution of C_8-C_{10} alkyl phenols from the 300˚C/72hr MSSV pyrolysis of N-HPO. Relative abundance is indicated in italics. Peak assignments correspond to products listed in Table 4.1. □ = C_{10} APs identified by a molecular ion of *m/z* 234.

No APs with substituents ≥ C_4 were detected from the surface waters and only a few of the C_{5-6} products were present in low concentrations from the S-HPO data. This suggests the high MW alkyl (≥ C_4) phenols reflect an important distinction between the phenolic constituents of the surface and waste waters, as well as between the different waste waters. In contrast, the AP distributions from the flash pyrolysis analyses of all the samples showed little distinction (Jarusutthirak, 2002). The flash pyrolysis data was consistently dominated by the lower MW alkyl (≤ C_2) phenols, and no highly substituted ≥ C_4 alkyl phenols were detected. The milder thermal conditions of MSSV pyrolysis may facilitate the softer macromolecular release of more highly alkylated phenolic structural constituents, analogous to the high concentrations of more highly substituted alkyl aromatic products detected by MSSV Py compared to flash Py (Chapter 3).

4.3.7 Sulfur-containing pyrolysates

Similar proportions of sulfur-containing products (ca. 2-5%) were generally detected from the MSSV pyrolysis of all of the NOM fractions. Exceptions were the Brittany COL (< 1 %) and Naintré waste water HPO fractions (7.5 %%, Figure 5.2) which produced very low and high S-product concentrations, respectively.

Alkyl thiophenes (ATs) were the major S-pyrolysates detected in higher concentrations by MSSV Py than flash Py. Reduced organic S compounds (e.g. thiol, sulfide and thiophene) have been reported to account for more than 50% of the S content of aquatic and soil humic substances (Xia *et al*., 1998). Low MW ATs are often detected from the flash pyrolysis of soil and aquatic humic substances (Saiz-Jimenez and de Leeuw, 1986b, Lu *et al*., 2001) but are not generally associated with any specific precursor. The MSSV distribution of the alkyl (≤ C_4) thiophenes detected from the HPO fractions of the Uruguay surface water and Naintré waste water are shown in **Figure 4.17**. Similar distributions were detected from both samples, however the U-HPO data showed enhanced abundance of 3-methylthiophene, whilst the C_4 ATs were detected only from the N-HPO fraction.

Alkyl thiophenes may derive from the thermal alteration of sulfur-containing amino acids such as cysteine and methionine. High concentrations of ATs were detected by

MSSV pyrolysis of the S-containing amino acid L-cysteine (**Fig. 4.18**), confirming this as a potential precursor.

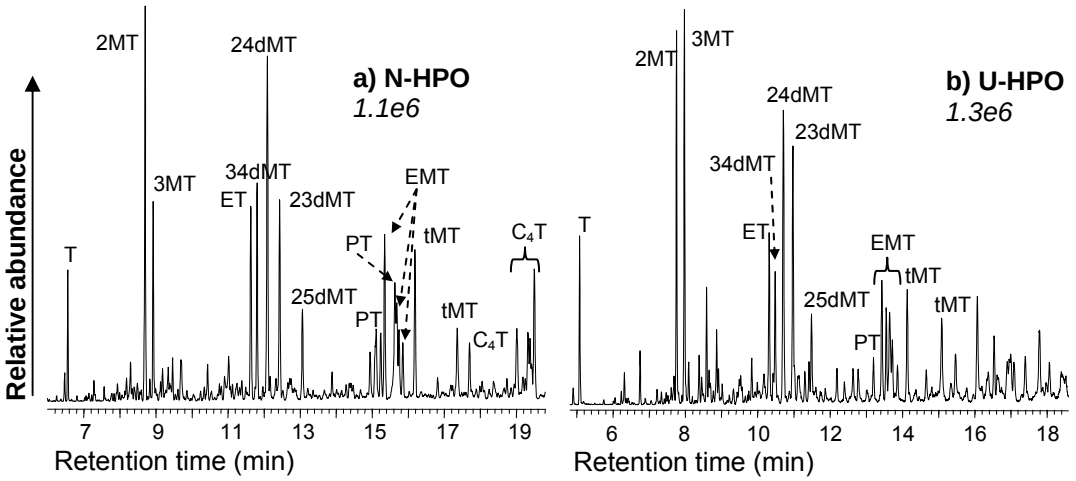

Figure 4.17 Summed *m/z* 97+98+111+112+125+126+140 chromatograms showing the distribution of alkyl thiophenes detected by 300˚C/72hr MSSV pyrolysis of **a)** Naintré HPO; and **b)** Uruguay HPO. Peak assignments correspond to products listed in Table 4.1. Relative abundances of a-b are indicated in italics.

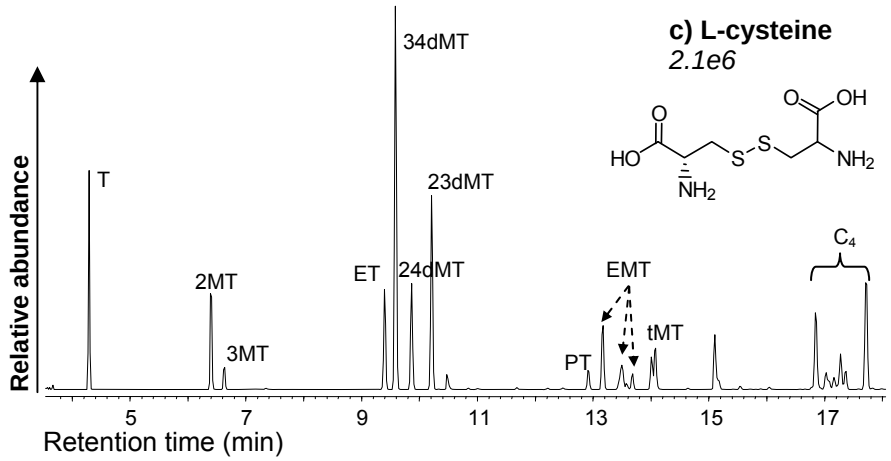

Figure 4.18 Summed *m/z* 97+98+111+112+125+126+140 chromatograms showing the distribution of alkyl thiophenes detected by 300˚C/72hr MSSV pyrolysis of L-cysteine. Peak assignments correspond to products listed in Table 4.1. Relative abundance is indicated in italics.

ATs are also prominent constituents of immature sedimentary macromolecules and type III-S kerogens (Sinninghe Damsté *et al*., 1992; Hartgers *et al*., 1994b

Koopmans et al., 1995; 1996; 1997; 1998; Putschew *et al*., 1998; Zhiguang *et al*., 1998). The occurrence of ATs in geological environments is thought to result from inter- and intramolecular interaction of inorganic sulfur (i.e. H_2S, polysulfides) with functionalised lipids during early diagenesis (Hartgers *et al*., 1994b). The same origin was also attributed to ATs detected in recent marine sediments by flash pyrolysis (Deshmukh *et al*., 2001). Thermal formation of these products during MSSV Py probably accounts for their high concentrations in the waste waters, in which H_2S and biomass are both expected to be at high levels.

With increasing thermal maturity organic sulphides are converted to dibenzothiophenes via thiophene and benzothiophene intermediates (Schmid *et al*., 1987). The dominance of alkylthiophenes and absence of alkylbenzothiophenes in the MSSV pyrolysates of the NOM fractions is consistent with a low level of thermal maturity following 300˚C/72 hrs thermal treatment (Sinninghe Damsté *et al*., 1992b). The distribution patterns of the ATs in the MSSV pyrolysis data of the NOM fractions were also qualitatively similar to those previously reported from flash pyrolysates of immature sulfur rich coals (Sinninghe Damsté *et al*., 1992b).

Several additional S-pyrolysates were detected from the waste water HPO fractions, including thiophenol, thioanisole, methylthioanisole and methylbenzothiazole. These products are highlighted in the summed ion chromatograms of **Figure 4.19.** Thiophenol was also detected in particularly high abundance in the TPI fraction of the Uruguay River. Further investigation is required to establish the thermal formation mechanisms and origins of these S-pyrolysates, but they may correspond to metabolites of sewage organics or pharmaceuticals (Göbel *et al*., 2004), possibly also reflecting an interaction with humic NOM. Whilst MSSV pyrolysis has provided increased access to several S-structural constituents of NOM, their relatively low concentrations and as yet undefined precursory origins remain a challenge to source characterization studies.

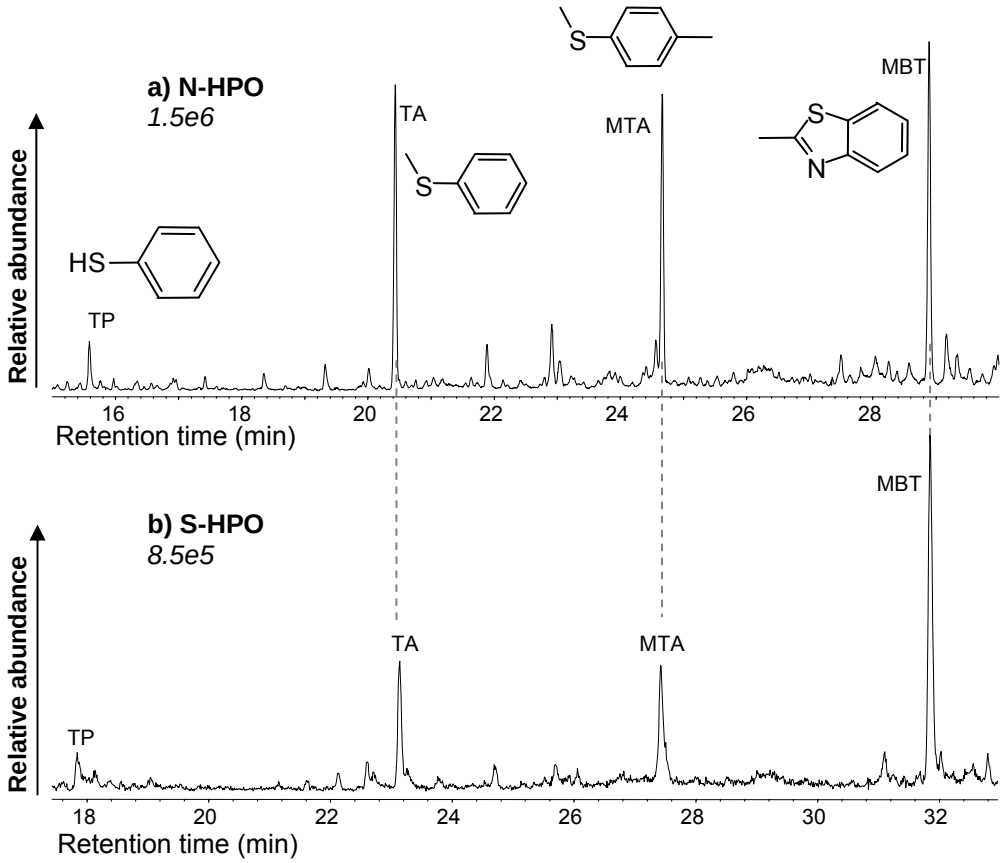

Figure 4.19 Summed *m/z* 110+124+138+149 chromatograms showing the distribution of thiophenol, alkyl (C_1) thioanisoles and methylbenzothiazole detected by 300˚C/72hr MSSV pyrolysis of **a)** Naintré HPO and **b)** St. Julien HPO waste water fractions. Peak assignments correspond to products listed in Table 4.1. Relative abundances of a-b are indicated in italics.

4.4 Conclusions

The O- and S-product distributions detected in high concentrations by MSSV pyrolysis of HPO, TPI and COL fractions of several riverine surface waters (SW) and two waste water (WW) effluents were evaluated. The major O- products included alkyl ($\leq C_4$) and acetyl furans, alkyl ($\leq C_2$) benzofurans, alkyl ($\leq C_{10}$) phenols and low MW cyclic ketones (e.g. alkyl cyclopentenones and cyclopentanones). The prominent S-products included alkyl ($\leq C_4$) thiophenes, alkyl ($\leq C_1$) thioanisoles (C_0-C_1) and low MW alkyl sulfides and thiols. Comparison of the O- and S-product distributions of the NOM samples with several standard materials helped establish more definitive biomolecular origins.

Alky furans (AFs), benzofurans and cyclic ketones, consistently detected by both MSSV and Flash pyrolysis, were attributed to carbohydrate sources following correlation of their high concentrations with several carbohydrate standards, including glucose, cellulose and chitin. In the NOM fractions, AF concentrations followed the order SW COL > SW TPI > SW HPO > WW COL > WW HPO. Their enrichment in the SW COLs confirms the significant contribution of polysaccharide-rich soluble microbial products. The HPO and TPI surface water fractions showed the highest concentrations of alkyl benzofurans and cyclic ketones, thus attributed to diagenetically altered polysaccharide structures sequestered into humic NOM fractions. The reduced concentration of these products in the HPO fraction of the waste waters and the low concentrations of AFs in the COL fractions of the waste waters reveals the rapid biodegradation of carbohydrates during advanced biological treatment.

Alkyl ($\leq C_{10}$) phenols (APs) were the dominant O-pyrolysates of the HPO and TPI fractions of the surface and waste waters. The MSSV AP concentrations followed the general order SW HPO > SW TPI ~ WW HPO > WW COL > SW COL. Flash pyrolysis also consistently yielded APs; however their distribution was dominated by low MW parent and mono-substituted products. The much higher MSSV Py concentrations of more highly substituted phenols carrying greater structural detail allowed for a more comprehensive evaluation of structural origins than previously possible.

In the surface waters, APs were strongly correlated with lignin structural moieties. MSSV pyrolysis of lignin yielded high concentrations and similar distributions of APs to those detected from the NOM fractions. In contrast, MSSV analysis of several tannin standards produced very few GC-MS detectable products, suggesting these precursors are not amenable to the MSSV thermal conditions. The thermally driven formation of APs from methoxyphenol structures of lignin seemed analogous to the transformations of these biochemical precursors during well studied diagenetic processes (e.g. within soils and aquatic sediments) and geothermal heating in subsurface environment (i.e. coals and kerogen). The generation of easily detectable alkyl phenol products of less accessible microbial degradation products of lignin by

MSSV pyrolysis represents an important analytical attribute for NOM characterisation studies.

The $\leq C_3$ AP distributions of both waste waters were very similar to the surface waters, possibly indicating a common lignin source. The Naintré HPO fraction additionally yielded many extended $C_{4\text{-}10}$ alkyl substituted phenols, possibly reflecting a significant refractory alkyl linked macromolecular component of the humic substances from source waters or phenolic metabolites of indigenous or treatment microbiota. Several of the larger alkyl substituted phenols, including alkyl ($\leq C_2$) *tert*-octyl phenols and nonylphenols, indicated the presence of industrial chemicals used in surfactants. Octyl and nonyl phenols are considered endocrine disrupting compounds (EDCs). Additional evidence for the presence of industrial byproducts in the waste waters was evident by the detection of several low MW dioxanes, possibly derived from polychlorinated dibenzo-*p*-dioxins, also considered EDCs. None of the highly substituted $\geq C_4$ alkyl phenol products detected by MSSV pyrolysis were detected by flash pyrolysis of the waste water fractions.

The NOM fractions showed several distinctive S-products in relatively low concentrations (*cf*. O-products) consistent with low organic S levels of aquatic NOM. Alkyl thiophenes (ATs) were detected from all NOM fractions but were present in highest concentrations in the waste waters. These products may derive from S-containing amino acids or may reflect interaction between inorganic sulfides and functionalised humic moieties in these waters or during MSSV thermal treatment. Additional S-pyrolysates, including thiophenol, thioanisole, methylthioanisole and methylbenzothiazole, were also significant products of the waste waters. Their origin remains unclear, but they may be potential indicators of microbial metabolites of sewage organics or pharmaceuticals.

Chapter 5

Thermal release of nitrogen products from aquatic NOM by MSSV pyrolysis

Some of the work in this chapter has been published as:

Berwick, L.J., Greenwood, P.F., Kagi, R.I., Croué, J-P., 2007. Thermal release of nitrogen-organics from natural organic matter (NOM) by micro-scale sealed vessel (MSSV) pyrolysis. Organic Geochemistry 38, 1073-1090.

5.1 Introduction

Organic nitrogen (N) constituents of NOM are efficiently released by the thermal conditions of MSSV pyrolysis. Their sensitive detection by this approach can help to identify N-organic precursors of NOM, including those that may lead to the formation of N-containing disinfection by-products (N-DBPs) during potable water treatment. N-DBPs of drinking waters have attracted considerable attention, as some (e.g. *N*-nitrosodimethylamine, NDMA) may pose a greater health risk than trihalomethanes, haloacetic acids and other commonly regulated DBPs (Shang *et al*., 2000; Najm and Trussel, 2001; Westerhoff and Mash, 2002; Lee *et al*., 2007). DBPs of toxicological significance continue to be a major challenge to water utilities, regulators and policy makers. A better understanding of the structure and origin of nitrogen moieties of NOM, and their behaviour during water treatment processes, will improve the management and quality of potable water resources.

Major organic nitrogen precursors of NOM include proteins, peptides, amino sugars, amino acids, nucleic acids, alkaloids and porphyrins. These are common biochemicals of vascular plant, algal and microbial sources. Freshwater resources may also be impacted by anthropogenic organic N-compounds from agricultural chemicals (e.g. fertilisers) and wastewater effluents. However, the degradation,

incorporation and role of these chemicals during the diagenetic formation of aquatic NOM are not well understood.

The precise structure and origin of organic nitrogen components of aquatic, soil and sedimentary NOM is often ambiguous (Schulten *et al*., 1997; Schulten and Schnitzer, 1998), partly due to the analytical challenges imposed by their low abundance (0.5-10 % by weight but typically at the lower end; Westerhoff and Mash, 2002) and structural functionality. Solid-state ^{13}C- and ^{15}N-NMR spectroscopy has shown that much of the organic nitrogen incorporated during soil humification occurs in the amide form (Knicker *et al*., 1995; 1996; 1997). Flash pyrolysates of proteins, peptides and simple amino acids have shown a variety of aliphatic and aromatic amines, nitriles and N-heterocyclic products, often containing alkyl or other functional group substituents (e.g. Bruchet, 1985; Boon and de Leeuw, 1987; Chiavari and Galletti, 1992; Stankiewicz *et al*., 1996; Basiuk and Douda, 2000). Accordingly, N-pyrolysates are frequently attributed to amino acid and proteinaceous precursors in flash pyrolysis studies of aquatic and soil NOM (e.g. Saiz-Jimenez and de Leeuw, 1986b; Bruchet *et al*., 1990; Templier *et al*., 2005a).

Biodegradation or other diagenetic processes can lead to the alteration of biomolecular nitrogen precursors of terrestrial soil and aquatic NOM, resulting in the incorporation of very different N-structures. N-heterocyclic compounds, including pyrroles, pyridines and pyrrolidines, were identified by flash pyrolysis of diagenetically altered macromolecular soil N intractable to wet chemical (e.g. acid hydrolysis) and other spectroscopic analyses (Schulten *et al*., 1997). Furthermore, chemical degradation and pyrolysis GC-MS studies have indicated that N-heterocycles are also significant contributors to humic substances of aquatic and recent sedimentary environments (Ikan *et al*., 1992; Patience *et al*., 1992; Schulten and Schnitzer, 1998; Schulten and Gleixner, 1999).

To extend the molecular characterisation of the nitrogen constituents of NOM, MSSV pyrolysis was conducted on the hydrophobic (HPO), transphilic (TPI) and colloid (COL) fractions of NOM from several surface waters and two secondary waste water effluents, including some rich in nitrogen or containing specific N-organic functionalities. Comparison of the N-product distributions of NOM with a

variety of standard materials representing potential N-organic precursors was also performed to help improve the source diagnostic value of N-pyrolysates. Flash pyrolysis analyses were conducted to provide a more traditional fast pyrolysis data set for comparative purposes.

5.2 Experimental

5.2.1 NOM samples

XAD resin and colloid fractions of selected surface water and waste water samples characteristic of particular aquatic environments were studied.

5.2.1.1 Surface water NOM

Gartempe River (Vienne, France) and Arroyo Sanchez River (Rio Negro, Uruguay) were selected to represent humic source waters. Detailed descriptions of the collection, fractionation and isolation of the HPO and TPI fractions of these waters were provided in Chapter 3.2.1.1. The colloid fraction of Brittany Reservoir (Brittany, France), representative of a eutrophic surface water environment, was also analysed. This reservoir experiences periodic algal blooms, and is dominated by autochthonous NOM (Lee *et al*., 2006). The HPO (24 %), TPI (26.5 %) and colloid fractions (49.5 %) of the Brittany source water NOM were isolated by 3.5 *kDa* membrane dialysis followed by XAD resin separation (Lee *et al*., 2005), following the same procedure (Leenheer *et al*., 2000) described for the wastewater effluent fractions in Chapter 3.2.1.3.

5.2.1.2 Waste water effluent OM

Isolation of the colloid and XAD resin fractions of Saint Julien (Saint Julien l'Ars, France) and Naintré (Naintré, France) secondary wastewater effluent OM (Ef-OM) was described in Chapter 3.2.1.3.

5.2.2 Representative samples and standards

5.2.2.1 Membrane biofoulant and cultured *Frateuria aurantia*

A membrane filtration biofoulant and an isolate of the acetic acid bacterium *Frateuria aurantia* were selected to be representative of extant microbiota rich in

proteins and polysaccharides. The collection, isolation and general characteristics of the organic fractions of these samples were described in Chapter 2.2.1.

5.2.2.2 Nitrogen standards

The nitrogen-containing model compounds and standards analysed included a protein (bovine serum albumin, BSA), a peptide (pentaglycine), an amino sugar (chitin), amino acids (D-tyrosine, D-tryptophan, L-proline, L-glutamic acid, L-cysteine, L-phenylalanine, L-arginine, L-leucine) and a porphyrin (2,3,7,8,12,13,17,18-octaethyl-21*H*,23*H*-porphine). All were commercially sourced from Sigma-Aldrich and analysed without further purification. A mixture of D-glucose and D-tyrosine was also separately analysed to specifically investigate the potential occurrence of Maillard processes during MSSV pyrolysis.

5.2.3 Molecular analysis

5.2.3.1 MSSV pyrolysis GC-MS

MSSV pyrolysis of < 0.1 - 1 mg of sample was performed according to the procedure described in Chapter 2.2.2.1. All data correspond to MSSV analysis ***I*** (i.e. 300˚C for 72 hr with the MSSV injector at a constant 300˚C). The peptide, protein and porphyrin standards and the Naintré colloid fraction were all studied at several additional temperatures over the range 260 – 340˚C/72 hr. GC-MS analysis of the volatile MSSV pyrolysates was performed using one of two instrument configurations, depending on availability.

1. Hewlett-Packard (HP) 6890 GC coupled to a 5973 mass selective detector (MSD), helium carrier gas at 34 kPa head pressure, 30 m x 0.32 mm i.d. x 0.25 μm DB5-MS capillary column (J&W Scientific).

2. HP 5890 Series II GC coupled to a 5971 MSD, helium carrier gas at 55 kPa head pressure, 30 m x 0.25 mm i.d. x 1 μm phase ZB5-MS capillary column (Phenomenex).

Samples were run with splits of between 20 – 50 mL min^{-1} and one of two GC oven temperature programmes.

1. An initial temperature of 40˚C, 2 minutes isothermal, then programmed at 4˚C min^{-1} to 310˚C with 20 minutes isothermal. In this case the products were

cryogenically trapped for 1 minute at the start of the column using liquid nitrogen prior to commencing the GC-MS analysis.
2. An initial temperature of -20˚C (using liquid CO_2 cryogenic control), 1 min isothermal then increased at 8˚C min^{-1} to 40˚C, then 4˚C min^{-1} to 310˚C, held isothermal for 20 minutes. The latter was used to improve the chromatographic resolution of early eluting components.

Full scan analyses were performed over the range *m/z* 50 – 550 at ca. 4 scans s^{-1} for both instruments. The mass spectrometer was operated in positive ion electron impact mode at 70 eV with a transfer line temperature of 310˚C and a source temperature of 250˚C. Tentative peak identifications were based on GC elution times and mass spectral comparisons with library spectra (Wiley 275 and NIST 05 databases) and previously published data.

5.2.3.2 Flash pyrolysis GC-MS

Flash pyrolysis GC-MS analyses (550˚C/20s) of the sample suite were performed according to the procedure describe in Chapter 3.2.2.2.

5.3 Results and Discussion

5.3.1 Nitrogen-product distributions detected by MSSV and flash pyrolysis

The suite of NOM fractions yielded a wide variety of nitrogen-containing pyrolysates (N-products). The major N-products of MSSV pyrolysis, tentatively identified on the basis of mass spectral interpretation, were low MW alkyl substituted pyrroles ($\leq C_5$), pyridines ($\leq C_4$), pyrazines ($\leq C_3$) and pyridinamines ($\leq C_2$), as well as amine substituted mono-aromatics such as aniline and amino phenols. Condensed N-heterocyclic products, including alkyl quinolines ($\leq C_1$), indoles ($\leq C_4$), carbazoles ($\leq C_3$), β-carbolines ($\leq C_1$) and aminonaphthalenes ($\leq C_1$) were detected in lower concentrations.

The overall N-product distributions detected by MSSV and flash pyrolysis GC-MS of the colloid fraction of the Saint Julien waste water effluent (S-COL) and the membrane filtration biofoulant (BF) are shown in **Figure 5.1**. Both pyrolysis techniques generated rich product distributions, including a variety of N-products. The generally high proportions of N-pyrolysates from these analyses parallel the high organic nitrogen content of S-COL (5.95 %; Jarusutthirak, 2002) and the BF (4.30 %; Croué *et al*., 2003b). MSSV pyrolysis consistently yielded much higher concentrations of N-products than flash pyrolysis from these, and the other TPI and COL fractions analysed in this study, indicating the release of additional N-structural units with the more moderate thermal conditions of the MSSV experiment. The higher MSSV abundance of N-products was particularly pronounced for the biofoulant. N-products were difficult to identify from the flash pyrolysate of this sample due to co-elution or poor quality of mass spectra. The high proportion of structurally polar primary fragments released by fast pyrolysis of extant biomass probably contributes to the complexity of this data.

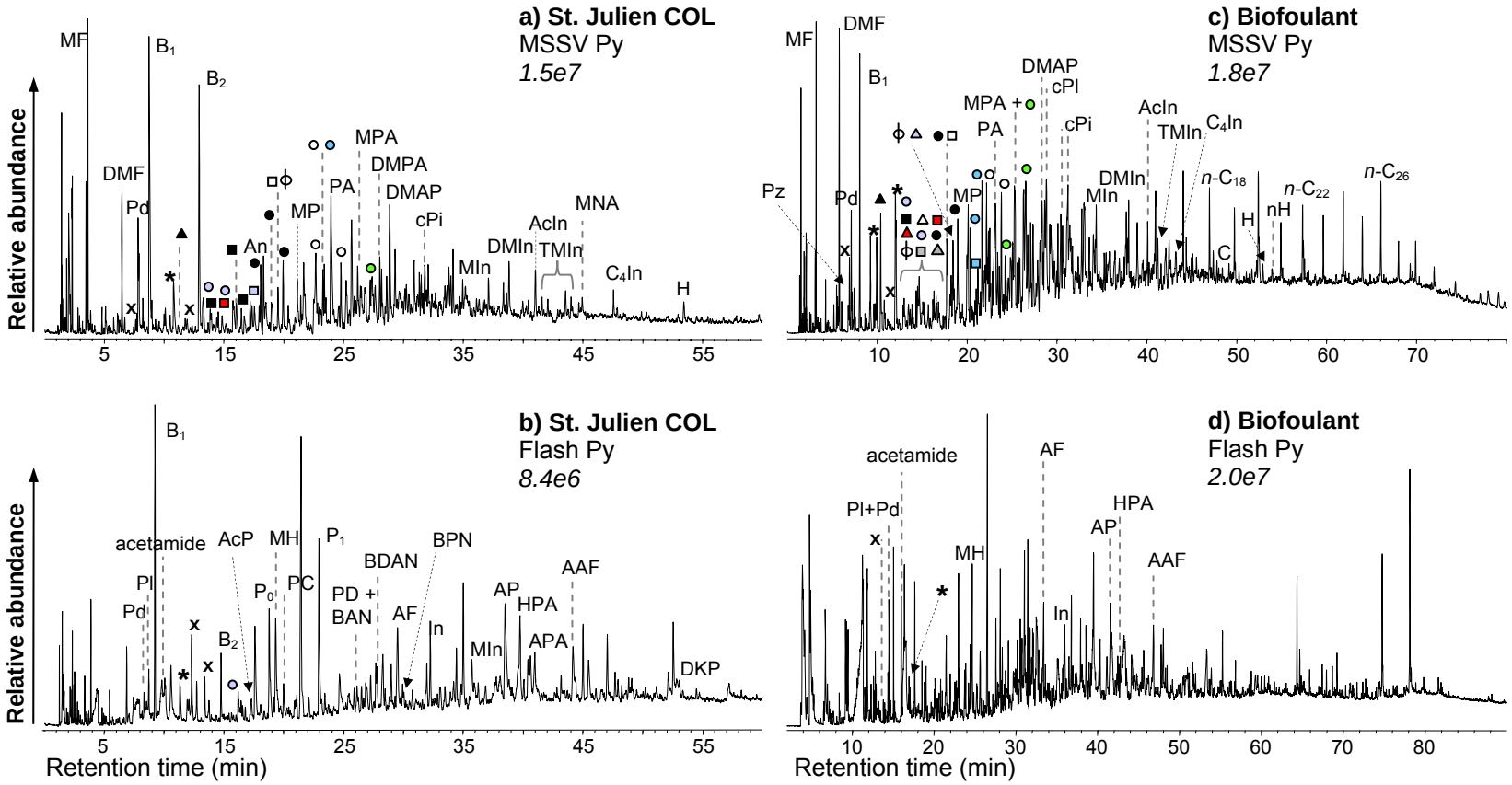

Figure 5.1 TICs obtained by 300˚C/72hr MSSV pyrolysis and 550˚C/20s flash pyrolysis GC-MS analysis of **a-b)** St. Julien colloids and **c-d)** membrane biofoulant. MF = methylfuran; DMF = dimethylfuran; $P_{0\text{-}1}$ = alkyl ($\leq C_1$) phenols; $B_{1\text{-}2}$ = alkyl ($\leq C_2$) benzenes, $n$$C_x$ = *n*-alkanes. Other peak assignments correspond to N-products listed in Table 5.1 or within the text of section 5.3.1. Relative abundances of a-d are indicated in italics.

The flash pyrolysates of both the S-COL fraction and BF did reveal several N-products not detected by MSSV pyrolysis, including acetamides (acetamide, 3-acetamidofuran; AF, 2-acetamidopyridine; AP, *N*-(2,4-dihydroxyphenyl)-acetamide; HPA, *N*-(3-aminophenyl)-acetamide; APA, and 3-acetamido-5-acetylfuran; AAF), aromatic nitriles (e.g. benzeneacetonitrile; BAN, 1,2-benzenediacetonitrile; BDAN, and benzenepropanenitrile; BPN) and oxygenated N-heterocyclic compounds (e.g. methyl hydantoin; MH, *N*-acetylpyrrole; AcP, pyrrole-2-carboxaldehyde; PC, 2,5-pyrrolidinedione; PD). This demonstrates the complementary N-organic structural data that can be obtained using the two methods.

5.3.2 N-product distributions of surface and waste water NOM

The different N-product profiles detected by MSSV pyrolysis of the surface and waste water fractions reflect variation in the nature and abundance of their N-precursors. TICs from the MSSV pyrolysis of selected samples, including Gartempe River hydrophobic (G-HPO) and transphilic (G-TPI) fractions, Brittany reservoir colloids (B-COL) and Naintré wastewater colloids (N-COL), are shown in **Figure 5.2**. The major N-products identified are listed in **Table 5.1**. The relative abundances of all N-products detected by MSSV pyrolysis of each of the NOM fractions are provided in **Figure 5.3**. These values were calculated as described in Chapter 3.3.2 (pg 71). The N-product distributions and semi-quantitative data of the various samples will be referred to in detail in the following sub sections.

5.3.2.1 HPO and TPI fractions of surface water NOM

Alkyl pyridines and pyrroles were the only N-products detected from the HPO fractions of the Arroyo Sanchez (data not shown) and Gartempe Rivers (Fig. 5.2 a). These products accounted for a relatively minor proportion of the total pyrolysates (ca. 4.2 % and 3.4 % respectively), with alkyl phenols detected in much higher concentrations (see Chapter 3 and 4). A high proportion of phenolic products, attributed to lignin precursory input, was also previously reported from *Curie*-point pyrolysis of the G-HPO fraction (Templier *et al*., 2005a). Flash pyrolysis of both surface water HPO fractions produced slightly higher concentrations of N-products than MSSV Py, possibly indicating the presence of thermally resistant N-moieties.

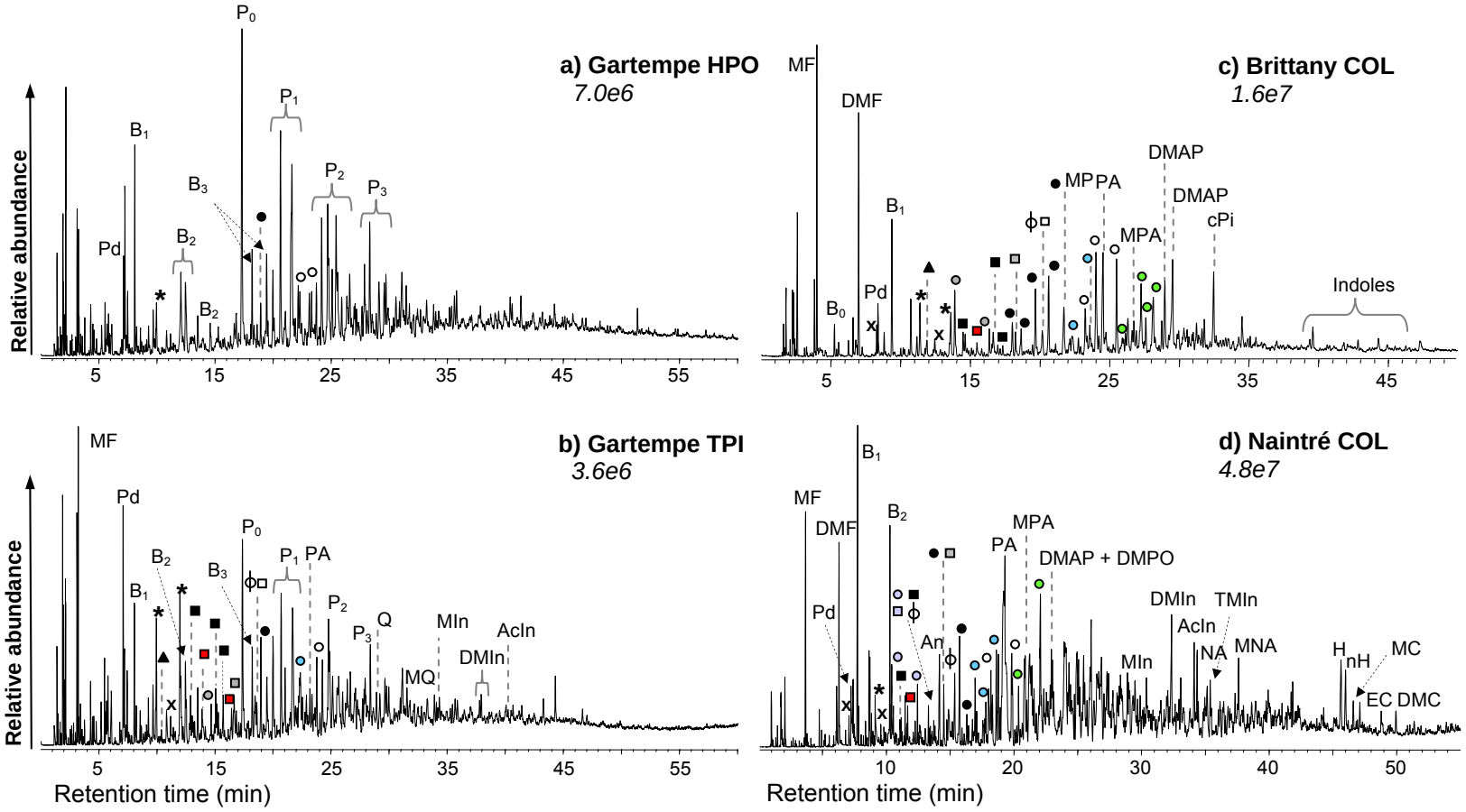

Figure 5.2 TICs obtained by 300˚C/72hr MSSV pyrolysis GC-MS analysis of **a)** Gartempe HPO, **b)** Gartempe TPI, **c)** Brittany colloids and **d)** Naintré waste water colloids. MF = methylfuran; DMF = dimethylfuran; $P_{0\text{-}3}$ = alkyl ($\leq C_3$) phenols; $B_{0\text{-}3}$ = alkyl ($\leq C_3$) benzenes. Other peak assignments correspond to N-products listed in Table 5.1. Relative abundances of a-d are indicated in italics.

Table 5.1 Major nitrogen products detected by 300˚C/72hr MSSV pyrolysis GC-MS analyses of aquatic NOM fractions.

Compound Identification	MW	Peak Label
Pyrrole	67	Pl
Pyrazine	80	Pz
Pyridine	79	Pd
Methylpyrroles	81	x
Methylpyrazines	94	▲
Methylpyridines	93	*
Ethylpyrroles	95	●
Ethylpyrazines	108	▲
Ethylpyridines	107	■
Dimethylpyrroles	95	●
Dimethylpyrazines	108	△
Dimethylpyridines	107	■
Ethylmethylpyrroles	109	ϕ
Ethylmethylpyridines	121	□
Ethylmethylpyrazines	122	△
Trimethylpyrroles	109	●
Trimethylpyridines	121	□
Aniline	93	An
1-methyl-2-pyrrolidinone	99	MP
Ethyldimethylpyrroles	123	●
Tetramethylpyrroles	123	○
C_4 pyridines	135	□
Pyridinamine	94	PA
Methylpyridinamine	108	MPA
C_5 pyrroles	137	●
Dimethylpyridinol	123	DMPO
Dimethyl pyridinamine	122	DMPA
Dimethyl aminophenols	137	DMAP
1-(1-cyclopenten-1-yl)-pyrrolidine	137	cPl
1-(1-cyclopenten-1-yl)-piperidine	151	cPi
Quinoline	129	Q
Methylquinoline	143	MQ
Indole	117	In
Methylindole	131	MIn
Ethylindole	145	EIn
Dimethylindoles	145	DMIn
3-acetylindole	159	AcIn
Trimethylindoles	159	TMIn
1-naphthalenamine	143	NA
2-methyl-1-naphthalenamine	157	MNA
C_4 indoles	173	C_4In
Carbazole	167	C
Methylcarbazoles	181	MC
1-methyl-9H-Pyrido[3,4-b]indole (harman)	182	H
9H-Pyrido[3,4-b]indole (β-carboline)	168	nH
2-ethylperimidine	195	EP
Dimethylcarbazoles	195	DMC
Ethylcarbazoles	195	EC
Trimethylcarbazoles	209	TMC
Aminocarbazole	182	AC

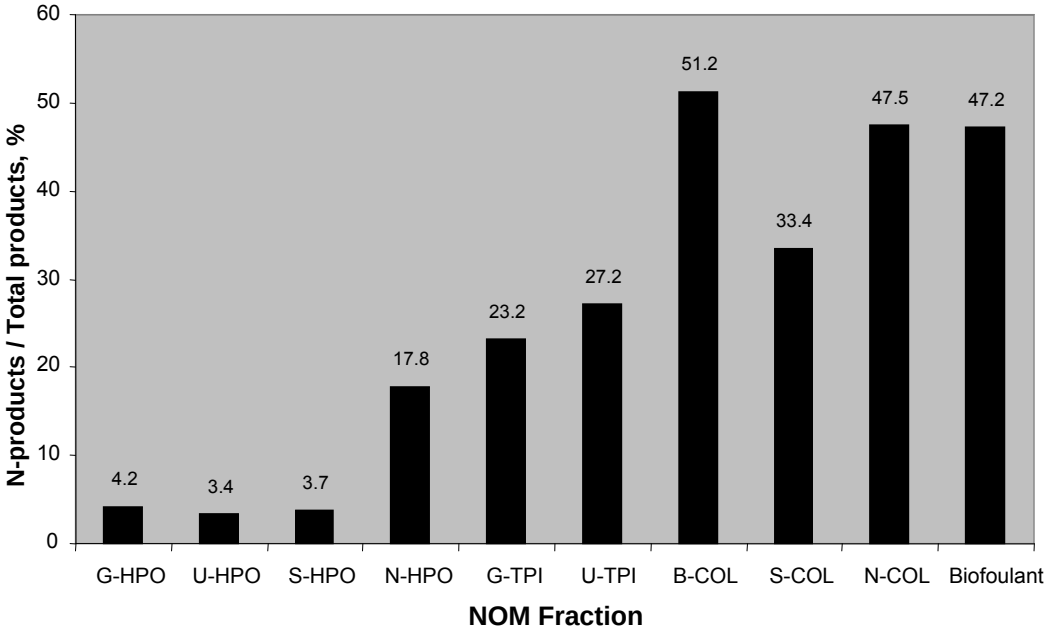

Figure 5.3 Proportion of N-products in the total pyrolysates detected by 300˚C/72hr MSSV pyrolysis GC-MS of several NOM fractions and the biofoulant.

Amide was the only nitrogen form detected by ^{15}N-NMR spectroscopic analysis of the G-HPO fraction (Templier *et al*., 2005b). The low concentration of N-pyrolysates from this sample suggests that amide moieties are relatively recalcitrant to thermal degradation. The high thermal resistance of certain amide components of plants (peptides) and algae (algaenans) has been established by characterisation studies of sedimentary OM (sed-OM) using ^{15}N-NMR and pyrolysis techniques (Derenne *et al*., 1991; 1993; Knicker *et al*., 1996a; 1996b). Interestingly, ^{13}C- and ^{15}N-NMR studies have shown that protein-derived amides (Knicker *et al*., 1996; 1997) represent most of the organic nitrogen incorporated during humification in soil and sed-OM. During diagenesis, peptides and proteins are generally rapidly degraded or mineralised by microbial and/or enzymatic degradation; however, part of their nitrogen can be incorporated into a recalcitrant organic form (Knicker and Skjemstad, 2000). Intact proteinaceous material has been identified in humic acids (Zang *et al*., 2000), ancient sediments (Knicker *et al*., 1996) and fossil remains (Poinar and Stankiewicz, 1999). The preservation of proteins in humic acids has been linked to sequestration by encapsulation or occlusion within non-extractable humic structures (Knicker and Hatcher, 1997; Zang *et al*., 2000). The seemingly intractable response of these structural precursors to most wet chemical and

pyrolysis methods means analytical characterisation may quantitatively under represent the nitrogen component of humic fractions of NOM.

MSSV pyrolysis of the TPI fractions of the surface waters yielded much higher concentrations of N-products than their HPO fractions (23.2% for G-TPI and 27.2 % for U-TPI), despite the similar nitrogen contents (e.g. G-HPO – 1.9 % N, G-TPI – 2.6 % N). The higher N-pyrolysate concentration of G-TPI (**Fig. 5.2b**) parallels the more significant amide, amine and pyrrole structural moieties of this sample previously identified using ^{15}N-NMR analysis (Templier *et al*., 2005b). The ability of amino acid and peptide groups, major functionalities of N-organic NOM precursors, to form hydrogen bonds with surrounding water molecules contributes to the hydrophilic character of NOM (Westerhoff and Mash, 2002). Hence, organic nitrogen is concentrated in the more polar HPI and TPI fractions (Croué *et al*., 2003a). Flash pyrolysis of the G-TPI and U-TPI fractions showed significantly fewer N-products than MSSV pyrolysis. Nevertheless, higher concentrations of N-products from the TPI compared to the HPO fractions were consistently observed by both MSSV and flash pyrolysis.

5.3.2.2 Colloid fractions of surface water NOM

N-products were detected in highest concentration from the Brittany River colloid fraction (**Fig. 5.2c**), accounting for ca. 52 % of the total pyrolysate area. Colloid fractions of NOM typically contain high organic N content (Sigleo *et al*., 1982; Rostad *et al*., 1997; Croué *et al*., 2006). Soluble microbial products (SMPs), including proteins, peptides, amino acids, amino sugars and carbohydrates, derived from the decomposition of cellular material of aquatic micro-organisms, have been shown to concentrate in colloids (Rostad *et al*., 1997; Leenheer *et al*., 2000; Leenheer *et al*., 2001a; Jarusutthirak, 2002; Croué *et al*., 2006). The Brittany reservoir experiences periodic algal blooms (Lee *et al*., 2006) and N-heterocycles such as pyrroles and indoles have been shown to be enriched in fossil algal sediments (Knicker *et al*., 1996). SMPs, which are enriched in N-organic precursors, are a more likely source of the high concentrations of N-heterocyclic pyrolysates of B-COL than the typically low quantities of organic N released from plant degradation.

5.3.2.3 Waste water effluent OM

Different concentrations of N-pyrolysates were detected from the HPO fractions of the Naintré and St. Julien waste water effluents. N-HPO yielded significantly higher concentrations of N-products (ca. 17.8 %) compared to S-HPO (ca. 3.7%), which showed a similar proportion of N-products to the surface water fractions. The colloid fractions yielded much higher overall abundances of N-products, but again these were higher from N-COL (47.5 %) than S-COL (33.4 %). The organic nitrogen content of the Naintré HPO (4.0 %) and COL (6.6 %) fractions was shown to be higher than the St. Julien HPO (2.8 %) and COL (5.9%) fractions (Jarusutthirak, 2002). The extended biological treatment (i.e. anoxic/aerobic processes) employed at the St. Julien WWTP would be expected to result in increased microbial degradation of N-organic precursors.

The major difference between the N-product distributions of the waste water (e.g. N-COL shown in **Fig 5.2d**) and surface water colloids (i.e. B-COL) was the much higher proportion of higher MW N-products, including alkyl indoles, carbazoles and β-carbolines, from the waste waters.

The MSSV pyrolysis distribution of several N-product classes of selected TPI and COL NOM fractions were investigated in more detail and were correlated with corresponding data from a variety of potential N-organic NOM precursors. The low MW N-heterocyclic products, prominent from all fractions, and higher MW N-products, generally more abundant from the waste water effluents, will be separately discussed.

5.3.3 Low MW N-heterocyclic products of NOM fractions

Low MW heterocyclics were the most abundant N-pyrolysates of all the NOM fractions studied. The summed ion chromatograms of **Figure 5.4** highlight the distribution of several of the major products detected by MSSV and flash pyrolysis of the G-TPI and B-COL surface water fractions, and the membrane biofoulant. Similar distributions of N-heterocyclic products were also detected in high abundance from the St. Julien (**Fig. 5.1a**; Berwick *et al*., 2007) and Naintré waste water colloids (**Fig. 5.13b**). The major MSSV products were alkyl (C_1-C_5) pyrroles, alkyl ($\leq C_4$) pyridines, alkyl ($\leq C_3$) pyrazines and alkyl pyridinamines ($\leq C_2$).

The G-TPI (**Fig. 5.4a**) and U-TPI (Appendix 6) samples showed a slightly higher proportion of alkyl pyridines, whilst alkyl pyrroles and pyridinamines were proportionally more abundant from the Brittany colloids and the membrane biofoulant (**Fig. 5.4b**). Similar N-heterocyclic products were detected from the biofoulant (**Fig. 5.4c**) and B-COLs. Previous FTIR and ^{13}C-NMR spectroscopy and pyrolysis GC-MS studies have shown that colloids are major contributors to the OM that irreversibly fouls ultra- and nano-filtration membranes (Speth *et al*., 1998; Howe and Clark, 2002; Croué *et al*., 2003b; Makdissy *et al*., 2004; Park *et al*., 2006). One significant distinction between these samples was the higher abundance of alkyl pyrazines from the biofoulant. This may reflect minor contribution of additional N-precursors to the foulant material or the occurrence of secondary processes involving other structural components, such as the Maillard reaction which is discussed further in section 5.3.5.

The summed ion data of **Figure 5.4** clearly shows the much higher concentrations of N-heterocyclic products detected by MSSV pyrolysis compared with flash pyrolysis of NOM. Additional GC detectable N-containing fragments are accessed with the more moderate thermal conditions of the MSSV experiment. Flash pyrolysis generated only the $\leq C_2$ alkyl pyrroles and pyridines in relatively low concentrations. The higher concentrations of more highly substituted alkyl (C_3-C_5) pyrroles and alkyl (C_2-C_3) pyridines detected by MSSV Py may reflect the release of less altered alkyl heterocycles from the macromolecular matrix. In contrast, many alkyl substituents may not survive the excessive thermal energy of flash pyrolysis, in which the parent and mono-methylated products were dominant. Higher MSSV Py concentrations of more highly substituted alkyl naphthalenes and alkyl phenols were similarly recognized in Chapter 3 and 4.

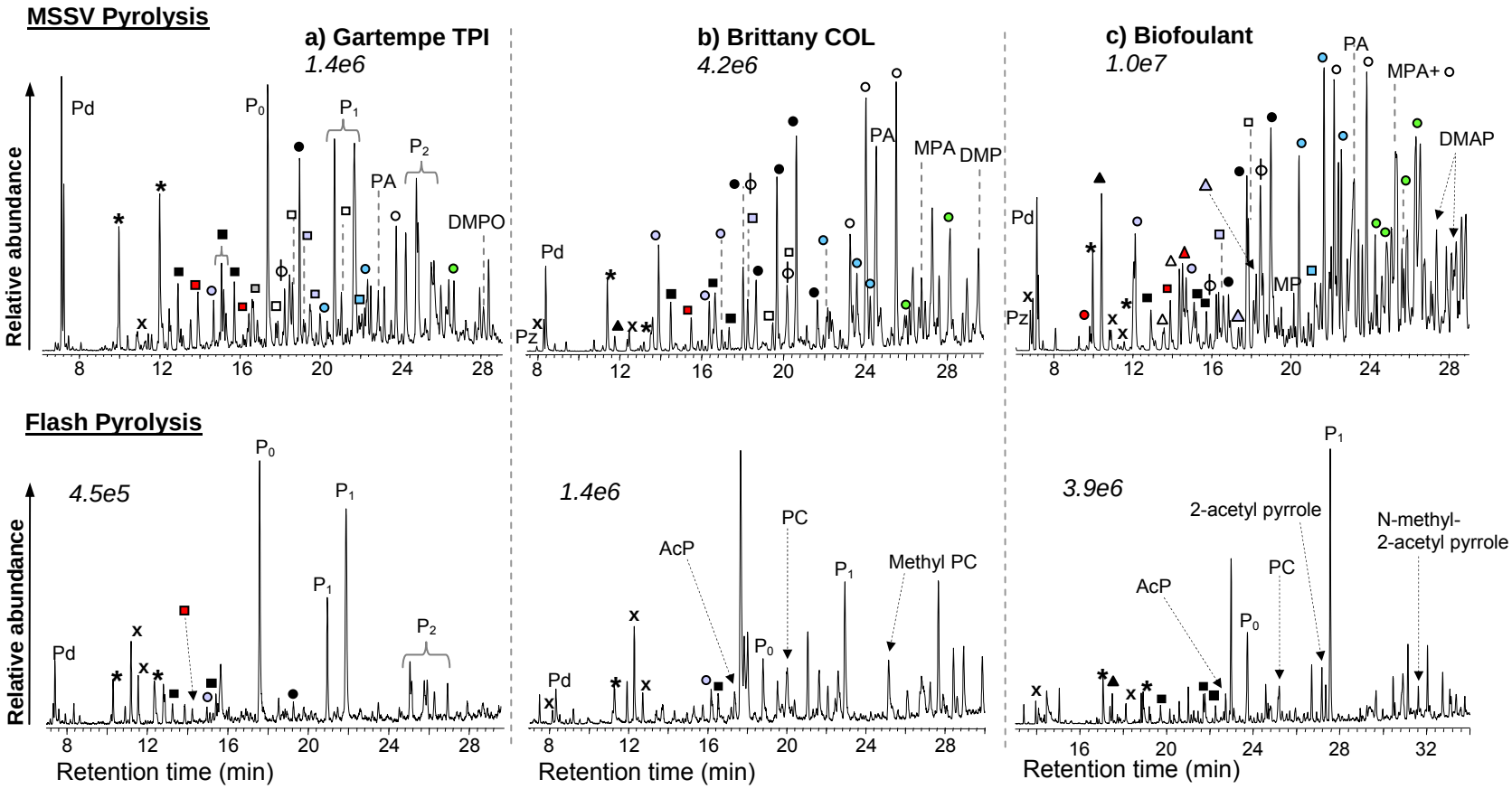

Figure 5.4 Summed *m/z* 79+80+93+94+106+107+108+109+120+121+122+123 chromatograms showing the distribution of low MW N-heterocyclic products detected by 300˚C/72hr MSSV pyrolysis and 550˚C/20sec flash pyrolysis GC-MS analysis of **a)** Gartempe TPI; **b)** Brittany colloids and **c)** membrane bio-foulant. $P_{0\text{-}2}$ = alkyl ($\leq C_2$) phenols. Other peak assignments correspond to N-products listed in Table 5.1. Relative abundances are indicated in italics.

The flash pyrolysis data did include low concentrations of several oxygenated N-heterocycles not detected by MSSV pyrolysis, including *N*-acetylpyrrole (AcP), 2-acetylpyrrole, *N*-methyl-2-acetylpyrrole, pyrrole-2-carboxaldehyde (PC), methyl hydantoin (MH), 2,5-pyrrolidinedione (PD), and 2-acetamido pyridine (AP). Several of these were previously observed in flash pyrolysates of a range of amino acids, peptides, proteins (Chiavari and Galletti, 1992; Basiuk and Douda, 2000; 2001) and model melanoidins (Tehrani *et al*., 2002). The oxygen group of these products may be vulnerable to the closed MSSV pyrolysis conditions.

5.3.4 Low MW N-heterocyclic products of representative standards

MSSV pyrolysis was conducted on a variety of standards representative of potential N-organic precursors of NOM to improve the diagnostic value of low MW N-heterocyclic products. The standards included a protein, a peptide, a porphyrin, chitin and several amino acids. Partial TICs showing the distribution of low MW N-heterocyclic products from these standards are given in **Figure 5.5**. N-heterocycles were detected from all standards but subtle variations in the isomeric distribution and abundance of these products was evident. The relative abundances of the major N-product classes detected from the peptide, protein and chitin standards are shown in **Figure 5.6** and are discussed in further detail in the following sub sections dedicated to the different standard types.

5.3.4.1 Amino acids

Only a few of the amino acids analysed by MSSV pyrolysis produced appreciable concentrations of the low MW alkylated heterocyclic N-products common to the NOM fractions. L-glutamic acid (**Fig. 5.5a**) yielded high concentrations of pyrrole and alkyl (C_1-C_4) pyrroles, while the major N-products of L-cysteine and L-arginine were alkyl pyridines and pyridinamines, respectively. Many of the dominant MSSV products of the amino acids were not detected in the aquatic NOM fractions. For example, the amino acid proline, structurally related to pyrrole, generated a broad range of N-products (Appendix 7) but very low concentrations of the alkyl substituted pyrroles prominent from the NOM fractions.

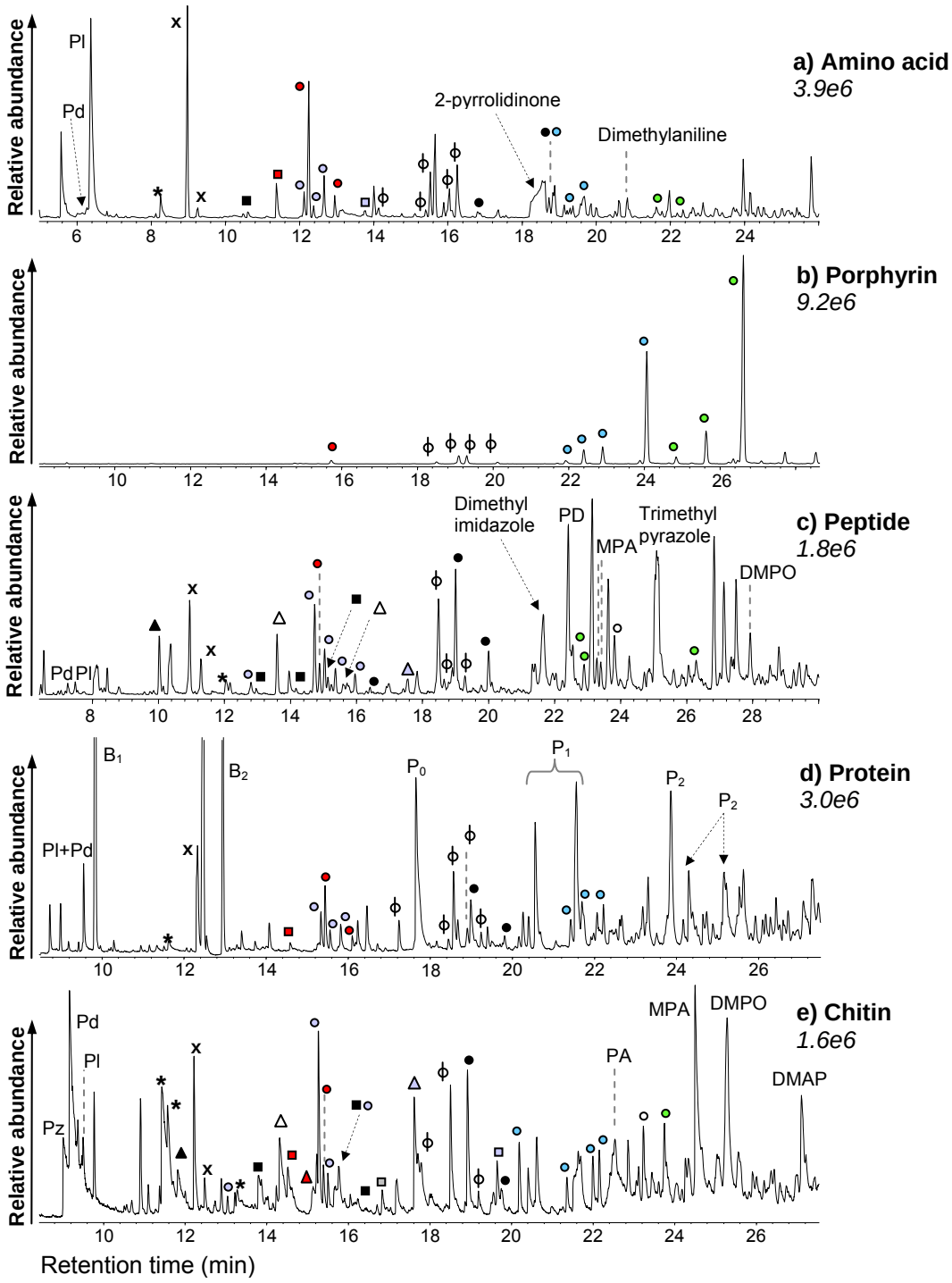

Figure 5.5 Partial TICs obtained by 300˚C/72hr MSSV pyrolysis GC-MS analysis of **a)** L-glutamic acid; **b)** porphyrin (2,3,7,812,13, 17,18-octaethyl-21*H*,23*H*-porphine); **c)** pentaglycine); **d)** BSA protein; and **e)** chitin. B_1-B_2 = alkyl benzenes $P_{0\text{-}2}$ = alkyl ($\leq C_2$) phenols. Other peak assignments correspond to N-products listed in Table 5.1. Relative abundances of a-e are indicated in italics.

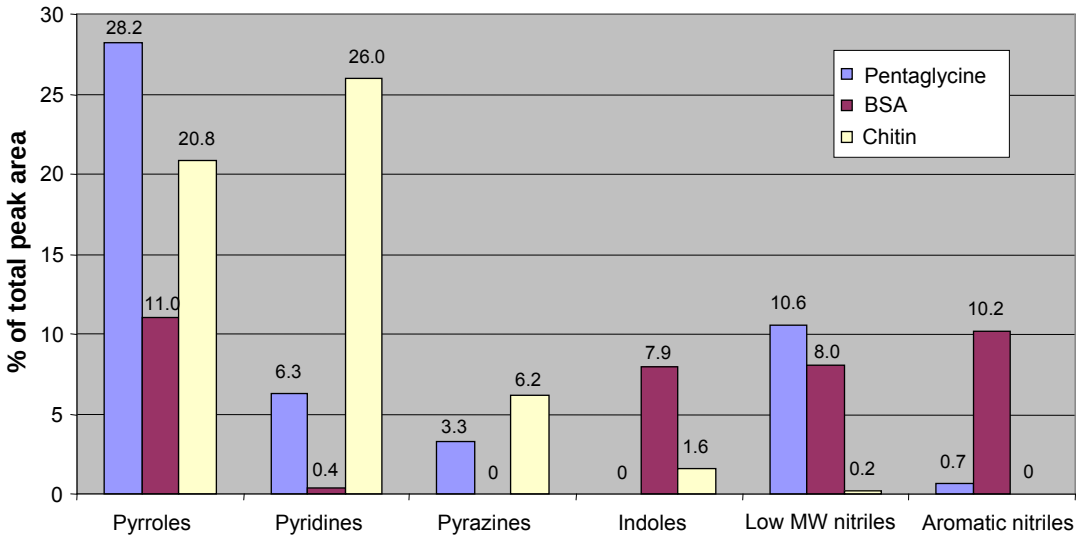

Figure 5.6 Relative abundances of major nitrogen product classes detected by 300˚C/72hr MSSV pyrolysis GC-MS of pentaglycine, BSA protein and chitin.

Amino acids are therefore not thought to contribute significantly to the abundant N-heterocyclic products characteristic of the NOM fractions. Since free amino acids are susceptible to rapid biodegradation (Westerhoff and Mash, 2002) they are typically present in very low concentrations in aquatic NOM (typically < 5% of DOC; Thurman, 1985; Westerhoff and Mash, 2002).

5.3.4.2 Peptides and proteins

Several low MW N-heterocyclic pyrolysates were detected by MSSV pyrolysis of the pentaglycine peptide and BSA protein standards (**Fig. 5.5 c-d**). Similar, alkyl (C_1-C_3) pyrrole rich distributions were observed for both the peptide and protein samples. Proteinaceous material is therefore a likely source of the prominent alkyl pyrrole products of NOM. Pentaglycine (**Fig 5.5c**) showed a broader distribution of N-heterocycles than the protein (**Fig 5.5d**), including several additional pyrolysates such as alkyl pyrazines, pyrrolidinedione, dimethylimidazole, trimethylpyrazole, methylpyridinamines and dimethylpyridinol. The much higher concentrations of low MW N-heterocyclic products of pentaglycine, reflected in the semi-quantitative data of **Figure 5.6**, may be due to more efficient thermal breakdown and rearrangement of the amide bonds of the structurally simpler peptide than the protein.

The thermal conversion of proteinaceous amide functionalities to N-heterocyclic structures such as pyrroles and imidazoles has been demonstrated by ^{15}N-NMR analysis of thermally treated biomass (Knicker *et al*., 1996; Knicker and Skjemstad, 2000). Thermal oxidation studies of peat have also demonstrated the progressive formation of N-heterocyclics with increasing temperature. This was ascribed to the thermal degradation of other labile N-structures, as well as newly synthesized structures (Almendros *et al*., 2003). Furthermore, organic nitrogen in mature sediments and petroleum is predominantly present as heterocyclic aromatic structures derived via diagenetic and catagenetic alteration of proteinaceous biological source materials (Baxby *et al*., 1994).

Besides the alkyl pyrroles, the only other low MW N-heterocyclic products of BSA were pyridine, methyl pyridine and ethyl pyridine (**Fig 5.5d**). These were very minor products compared to other aromatic products such as toluene, ethylbenzene, alkyl phenols and aromatic nitriles (e.g. benzonitrile, benzeneacetonitrile, benzenepropanenitrile), which likely derive from specific amino acid constituents of the protein. Alkyl (C_1-C_2) benzenes, aromatic nitriles and alkyl phenols were major MSSV products of the aromatic amino acids phenylalanine (Chapter 3.3.4) and tyrosine (see section 5.3.4 and Figure 5.7a), respectively.

Low concentrations of alkyl pyrroles were also the only low MW N-heterocycles detected from the MSSV pyrolysis of the F. *aurantia* bacterial isolate (Berwick *et al*., 2007). This protein rich biomass did produce other significant N-pyrolysates, including long-chain *n*-alkyl nitriles, aromatic nitriles and alkyl indoles. *n*-Alkyl nitriles may originate from the dehydration of amides formed either as primary pyrolysis products, or as secondary products by reaction of fatty acids with NH_3 (Simoneit *et al*., 2003). *n*-Alkyl nitriles have also previously been identified in pyrolysates of non-hydrolysable amide containing biomacromolecules from the outer cell walls of green algae (Derenne *et al*., 1993), but were not detected from the NOM fractions. The thermal resistance of these amides has been established using ^{15}N-NMR and pyrolysis techniques (Derenne *et al*., 1991; 1993). This may account for the relatively low concentrations of low MW N-products detected from F. *aurantia*. Extraction of the lipid component of the bacterial isolate may facilitate an improved characterisation of the proteinaceous component.

5.3.4.3 Amino sugars

Chitin is a naturally occurring water soluble polymer of N-acetylglucosamine found in fungal cell walls and arthropod exoskeletons. It is studied here as a representative of polymeric N-acetyl amino sugars (e.g. peptidoglycan) present in microbial and algal cell walls. Chitin produced the highest proportion of low MW N-heterocyclic products of all the samples studied (**Fig. 5.6**). Alkyl pyridines were detected in much higher abundance from chitin than the peptide and protein samples (Fig. 5.6). Alkyl pyridines have also previously been detected by flash pyrolysis of chitin (Stankiewicz *et al*., 1996). Other major N-products of chitin included alkyl pyrroles, pyrazines, pyridinamines and dimethylpyridinol. All of these products were common to the colloid NOM fractions and biofoulant. Correlation of the N-heterocyclic profiles indicates that amino sugars are significant N-organic constituents of these NOM samples.

Separate flash pyrolysis analyses of the colloid fractions and BF revealed high concentrations of acetamide products (**Fig. 5.1b and d**; see Chapter 5.3.1), which also derive from N-acetyl amino sugars (Stankiewicz *et al*., 1996). These precursors have been shown through ^{13}C-NMR and FTIR spectral characterisation to dominate colloidal NOM fractions (Rostad *et al*., 1997; Leenheer *et al*., 2001a; Mao *et al*., 2003) and membrane biofoulants (Croue *et al*., 2006). The BF also yielded several other microbially derived products including hopanes, *n*-alkanes and monomethyl alkanes and the significance of these products was discussed in Chapter 2.

Several other prominent N-products of the colloid fractions and BF were also detected from the amino sugar, but not the other standards (data not shown). These products were difficult to unequivocally identify from their mass spectra alone, however several were tentatively identified as aminophenols, alkyl pyridinols and cyclopentenyl and cyclohexenyl substituted pyrrolidines and piperidines. Some of these products (e.g. DMAP, DMPO, cPi, cPl; Table 5.1) are evident in the NOM data of Figure 5.1-5.4. Further investigation of these MSSV products may provide additional diagnostic information regarding the occurrence of amino sugars in NOM samples.

The broad range and high concentrations of N-heterocyclic products identified by MSSV pyrolysis of the protein, peptide and amino sugar standards provides strong evidence that these natural precursors, or their diagenetic products, are major sources of the low MW N-pyrolysates detected from the NOM fractions.

5.3.4.4 Porphyrins

Several of the alkyl pyrrole products of NOM could also reflect intact structural units derived form porphyrins, which are tetrapyrrole ring structures present in higher plants, algae and bacteria. MSSV pyrolysis of a standard porphyrin, 2,3,7,8,12,13,17,18-octaethyl-21*H*,23*H*-porphine (**Figure 5.5b**), yielded a very different pyrrole distribution to the other standard materials, characterised by high concentrations of methyl ethyl substituted analogues (e.g. ethylmethyl, ethyldimethyl, diethylmethyl) over a narrower MW range (C_3-C_6). Significantly, the alkyl substitution patterns of the pyrrole products are consistent with those of the original precursor (i.e. ethyl substituted), indicating minimal degradation or rearrangement of the alkyl side chains to polymethylated isomers during MSSV pyrolysis. In contrast, the alkyl pyrrole distribution detected by flash pyrolysis (Appendix 8) of the porphyrin showed several polymethylated products as well as other secondary N-products such as alkyl anilines, bearing little obvious structural relationship to the parent compound.

The MSSV pyrolysates of the TPI and COL NOM fractions and the BF also contained much higher concentrations of C_4-C_5 pyrroles than the protein and peptide standards. Highly substituted alkyl (C_1-C_6) pyrroles, previously identified from flash pyrolysis of kerogens, were attributed to tetrapyrrole pigments of chlorophyll (Sinninghe-Damsté *et al.*, 1992a). The prominent higher MW pyrroles of the NOM fractions may have a similar tetrapyrrole origin. Unlike the N-heterocyclic products of the amino acid, amino sugar and protein standards, which are attributed to secondary alteration during MSSV thermal treatment, the alkyl pyrrole pyrolysates of porphyrins largely represent primary structural units directly released from the macromolecular network.

Further research is required to unequivocally distinguish the primary or secondary nature of the N- products of NOM, many of which may not reflect indigenous N-

structural moieties. Heterocyclic aromatics for example can form by auto-condensation reactions between liberated NH_3 and aromatic components (Knicker *et al*., 1996) or as by-products of Maillard reactions (Coleman and Chung, 2002; Tehrani *et al*., 2002). The N-organic standards studied here represent only basic structural units of potential NOM precursors, hence, interpretations based on the data from their isolated analyses should be considered with caution. The pyrolysates identified from individual standards and model systems may not be representative of bulk NOM samples, since synerginistic relationships from interacting chemical species are negligible.

5.3.5 Maillard reaction

The Maillard reaction occurs by random condensation of reducing sugars and compounds possessing a free amino group such as amino acids (Maillard, 1912), producing high MW, refractory macromolecules called melanoidins (Maillard, 1917). There has been considerable interest and debate about the occurrence of this process in natural environments and its potential role in the formation of humic substances (Maillard, 1917; Yamamoto and Ishiwatari, 1992; Ikan *et al*., 1992). Whilst amino acids and simple sugars are abundant microbial metabolites of polysaccharides and proteins, both of which were major precursors of the COL and BF samples (Croué *et al*., 2003b), Maillard reactions may not be favoured by the ambient and sub surface temperatures of recent environments.

^{15}N-NMR analysis of synthetically prepared melanoidins has revealed secondary amide, pyrrole and pyridine N signals (Benzing-Purdie *et al*., 1983). Furthermore, thermal degradation of such heteropolymers (Boon *et al*., 1984; Coleman and Chung, 2002; Tehrani *et al*., 2002; Adams *et al*., 2003) has been shown to include several of the lower MW N-heterocyclic products (e.g. alkyl pyrroles, pyridines and pyrazines) common to the MSSV pyrolysates of the BF, NOM and waste water fractions. Therefore, these N-heterocyclic products may represent indigenous units of melanoidin type structures formed by Maillard reactions in aquatic environments, with the MSSV thermal conditions favouring their thermal release. The high proportions of highly alkyl substituted (e.g. $\geq C_2$) N-heterocyclic products of the NOM fractions may reflect cross-linking alkyl units of melanoidins.

Highly substituted N-heterocyclic products were previously identified in flash pyrolysates of model melanoidins formed by the reaction of several amino acids with glucose and rhamnose (Coleman and Chung, 2002). The presence of condensed and cross-linked melanoidin structures has also been previously postulated in refractory fractions of soil OM (Benzing-Purdie and Ripmeester, 1983; Poirier *et al*., 2000; 2002), estuarine DOM (van Heemst *et al*., 2000) and recent sediments (Patience *et al*., 1992; Peulve *et al*., 1996). Similarly, Dignac *et al*. (2000) suggested that chemically and biologically refractory OM present in waste water effluents could be products of melanoidin like structures, their formation enhanced by the intense biological activity during treatment. However, further research is required to investigate this potentially rare evidence of the environmental occurrence of melanoidins, as low MW N-heterocycles were also common MSSV pyrolysates of several of the standard materials.

In addition to high MW humic-like melanoidins, the Maillard reaction also produces volatile low MW N-organic compounds (Coleman and Chung, 2002; Tehrani *et al*., 2002). The recent identification of alkyl pyrazines in buried plant remains helped confirm the occurrence of Maillard processes during sedimentary diagenesis (Evershed *et al*., 1997). The BF pyrolysate also showed high concentrations of alkyl pyrazines, possibly formed as secondary byproducts of Maillard reactions promoted by the thermal conditions of the MSSV experiment.

To investigate the potential formation of low MW N-heterocycles by Maillard reactions during closed system MSSV pyrolysis, separate analyses were performed on the amino acid D-tyrosine, the carbohydrate D-glucose and a 1:1 mixture of both. D-tyrosine was selected because this amino acid did not yield any N-heterocyclic products from its individual analysis, compared with some of the other amino acids discussed in section 5.3.4.1 (e.g. L-glutamic acid). The major MSSV products of D-tyrosine and glucose (Fig. 5.7a, c) were alkyl ($\leq C_2$) phenols and alkyl furans, respectively. The MSSV pyrolysate from the tyrosine/glucose mixture (Fig. 5.7b) largely showed a combination of the products observed from the analysis of the individual samples. Similar molar quantities of each compound were analysed, however the phenolic products of tyrosine dominated the mixture data. Typical N-heterocyclic Maillard reaction products such as pyrazines, pyridines and oxazoles

(Tehrani *et al*., 2002) were not detected, providing no evidence that Maillard processes are promoted by MSSV pyrolysis (300˚C/72hrs).

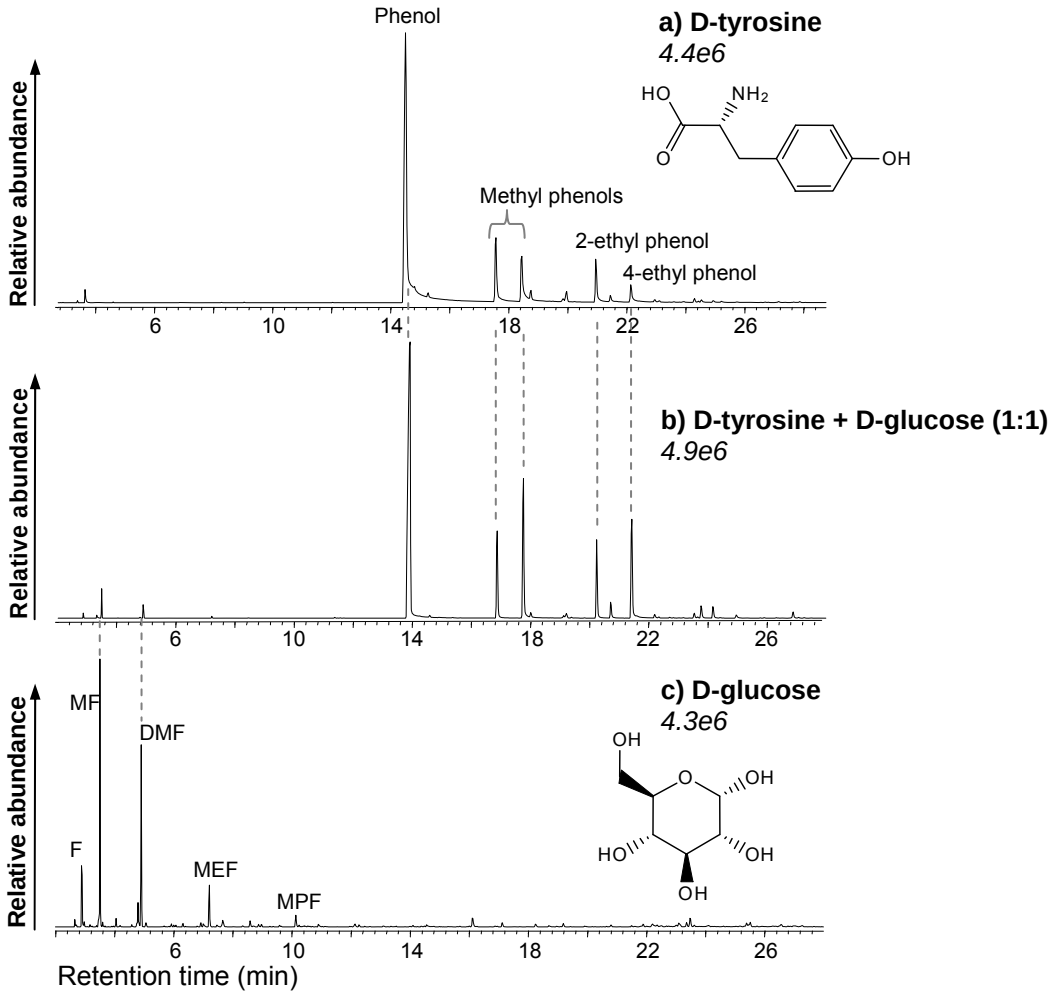

Figure 5.7 Partial TICs obtained by 300˚C/72hr MSSV pyrolysis GC-MS analysis of **a)** D-tyrosine; **b)** D-tyrosine + D-glucose (1:1) and **c)** D-glucose. F = furan, M = methyl-, DM = dimethyl-, ME = methylethyl- MP = methylpropyl-. Relative abundances of a-c are indicated in italics.

Several other glucose and amino acid (e.g. proline, phenylalanine, glycine) mixtures were also analysed over a range (260-340˚C/72hrs) of MSSV temperatures. None of these analyses showed evidence for the generation of heterocyclic N-products in addition to those from the individual precursors. These results suggest that the N-pyrolysates detected from the NOM fractions are not formed by secondary reactions between carbohydrates and amino acids during thermal treatment. However, more

robust assessment of this issue will require investigation of other starting materials over a wide range of thermal conditions.

5.3.6 Higher MW N-pyrolysates of NOM fractions

In addition to the dominant low MW heterocyclic N-products several higher MW heterocyclic products, including alkyl indoles, carbazoles and β-carbolines, were also detected by MSSV pyrolysis of the NOM fractions. These were detected in highest abundance from the colloid fraction of the Naintré wastewater effluent, which had both the highest DOC (14.4 mg L^{-1}) and organic nitrogen (6.6 %) concentration of all the samples analysed.

Alkyl (C_1-C_4) indoles were prominent MSSV products of all the TPI and COL fractions, as well as the biofoulant. The summed ion chromatograms of **Figure 5.8** show the distribution of alkyl indoles in the colloid fractions of the Brittany river and the two waste waters. The alkyl indole profiles for all fractions were similar, with C_1-C_3 alkyl indoles and 3-acetylindole detected in highest abundance. Parent indole was also detected but in significantly lower concentration compared to the alkyl substituted products. Flash pyrolysis of the same NOM fractions yielded indole and methylindole in low abundance; but no higher alkylated indoles. Indole, 3-methylindole and 3-ethylindole were previously detected by flash pyrolysis of the amino acid tryptophan (Chiavari and Galletti, 1992), which contains an indole nucleus with functionalised carboxylic acid and amine substituents (see Figure 5.11a).

MSSV pyrolysis of the waste water colloids and biofoulant also yielded the naturally occurring indole alkaloids 9H-pyrido[3,4-β]indole (β-carboline) and 1-methyl-9H-pyrido[3,4-β]indole (harman), as shown in **Figure 5.9**. These compounds were not detected by flash pyrolysis of any of the NOM fractions.

Alkyl ($\leq C_3$) carbazoles and amino carbazole (Fig. 5.9), which also possess an indole nucleus, were similarly detected only from the wastewater colloids and biofoulant. The summed ion chromatograms of **Figure 5.10** show the alkyl carbazole distribution detected from the N-COL fraction. Similar distributions were detected from the S-COL and BF data, but in lower concentrations due to the lower DOC and

nitrogen content of these samples. The major products for each sample were the parent carbazole and isomers of methyl-, dimethyl- and ethylcarbazole.

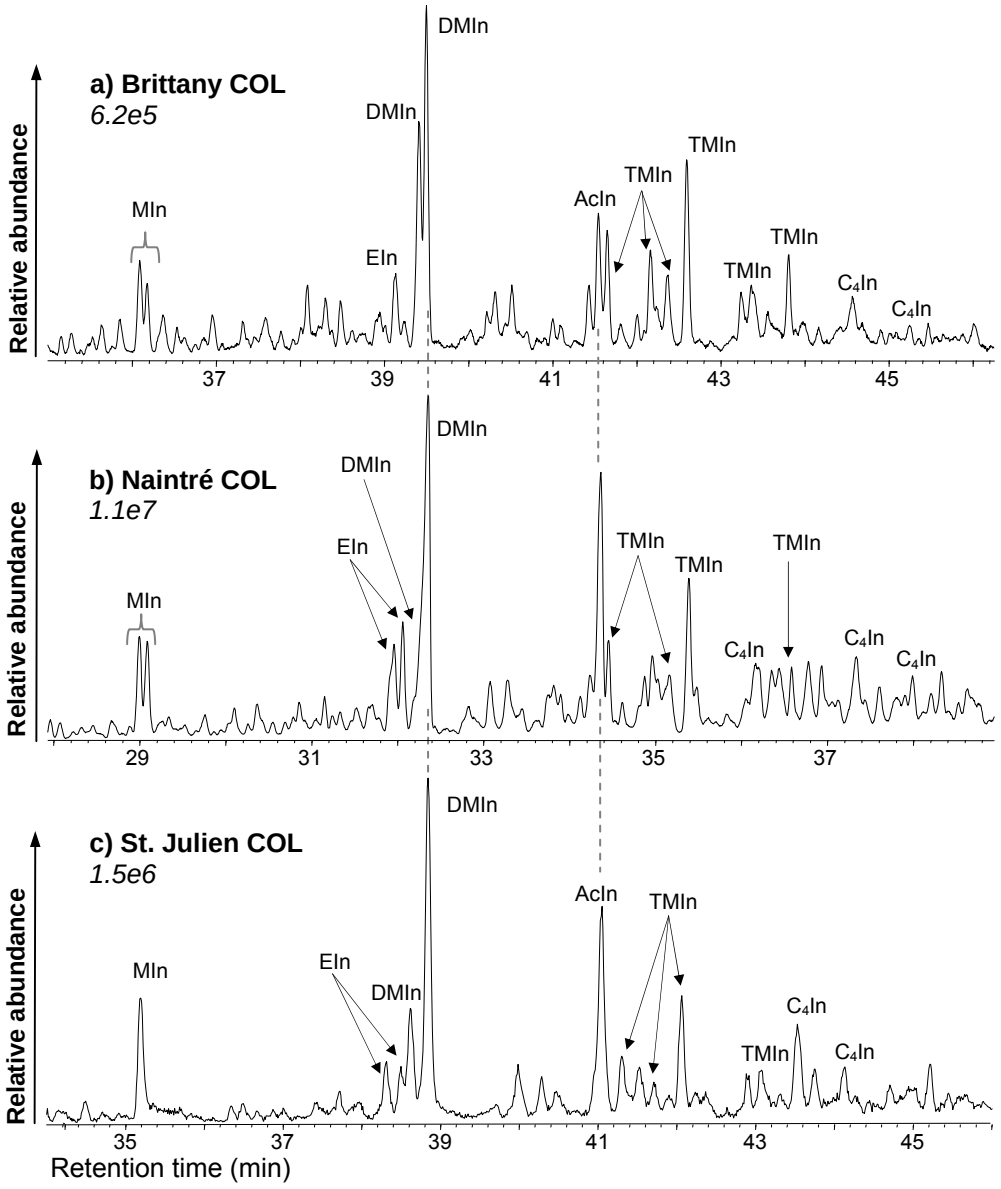

Figure 5.8 Partial summed *m/z* 130+144+145+158+159 chromatograms showing the alkyl indole distribution detected by 300˚C/72hr MSSV pyrolysis GC-MS analysis of **a)** Brittany colloids, b) Naintré colloids, and **c)** St. Julien colloids. Relative abundances of a-c are indicated in italics. Peak assignments correspond to N-products listed in Table 5.1.

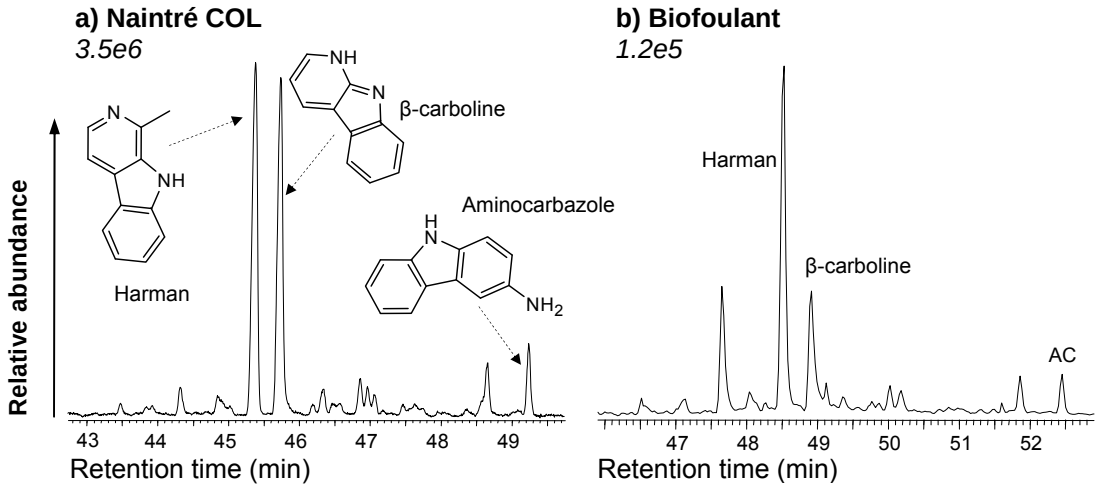

Figure 5.9 Partial summed *m/z* 168+182 chromatograms showing indole alkaloids detected by 300˚C/72hr MSSV pyrolysis GC-MS analysis of **a)** Naintré colloids and **b)** Biofoulant. Peak assignments correspond to N-products listed in Table 5.1. Relative abundances of a-c are indicated in italics.

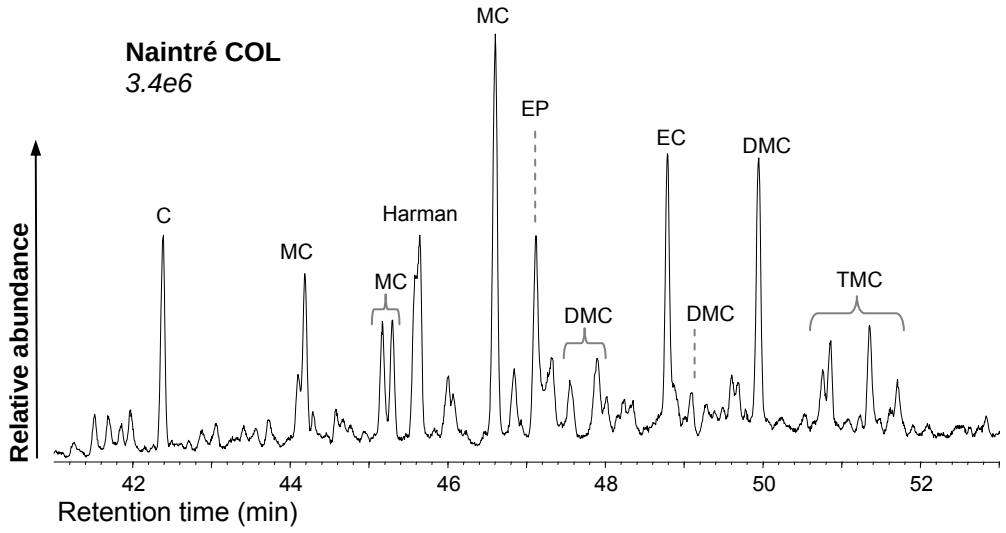

Figure 5.10 Partial summed *m/z* 167+180+181+194+195+209 chromatograms showing alkyl carbazoles detected by 300˚C/72hr MSSV pyrolysis GC-MS analysis of Naintré colloids. Peak assignments correspond to products listed in Table 5.1. Relative abundance is indicated in italics.

Alkyl carbazoles are well known petroleum hydrocarbons (Clegg *et al*., 1998; Bennett *et al*., 2004). However their presence has been rarely reported in recent environmental settings such as aquatic NOM and soils (Bennett *et al*., 2004). Flash pyrolysis of the wastewater fractions and BF did not detect any carbazole products,

which suggests they are not amenable to detection prior to geological diagenesis or artificial thermal maturation by approaches such as MSSV pyrolysis.

The alkyl indole and carbazole distributions detected by MSSV pyrolysis of the NOM fractions were similar to those reported recently by hydropyrolysis analyses of algal and bacterial biomass and immature sedimentary OM (Bennett *et al*., 2004). In addition to a tryptophan origin (see 5.3.7), Bennett *et al*. (2004) also attributed indoles and carbazoles to macromolecularly bound indole alkaloid constituents of plants, algae and bacteria (Zeng *et al*., 1999). These products were only released as solvent extractable products following hydropyrolysis treatment (Bennett *et al*., 2004). The moderate thermal conditions of MSSV may release similar N-structural moieties from bound and functionalised alkaloid constituents of the waste water Ef-OM, analogous to the release of hopane (Chapter 2) and aromatic (Chapter 3) biomarkers of bound bacterial and higher plant terpenoids. The distinctive *β*-carboline and carbazole products of the waste water colloids may be potential molecular markers for waste water impact into natural waters. Alkaloids may be significant contributors to the formation of toxic N-containing disinfection by-products during potable water treatment. Recent research has shown that indole moieties can form toxic aromatic nitrosamine DBPs on reaction with chloramines (Bull, R., 2007, personal communication). Hence an analytical capacity to detect the aquatic occurrence of alkaloids will be valuable for assessing DBP formation potential.

The wastewater effluents also yielded other condensed aromatic N-products including naphthalenamine, methylnaphthalenamine (Appendix 9) and ethyl perimidine (see Fig. 5.10), the origins of which remain unclear.

5.3.7 Higher MW N-products of standards

MSSV pyrolysis was conducted on D-tryptophan, bovine serum albumin (BSA) protein and the cultured Frateuria *aurantia* bacterium, which represent potential precursors of the higher MW heterocyclic products of the NOM fractions. The major pyrolysates of tryptophan (**Fig. 5.11a**) were indole, methylindole and ethylindole, with lower quantities of dimethylindole and 3-acetylindole. The product distribution was very similar to that obtained by larger scale closed system anhydrous pyrolysis

of tryptophan (Bennett *et al*., 2004). MSSV pyrolysis of tryptophan also produced β-carboline and harman (**Fig. 5.12**), which were prominent pyrolysates of the waste water NOM fractions.

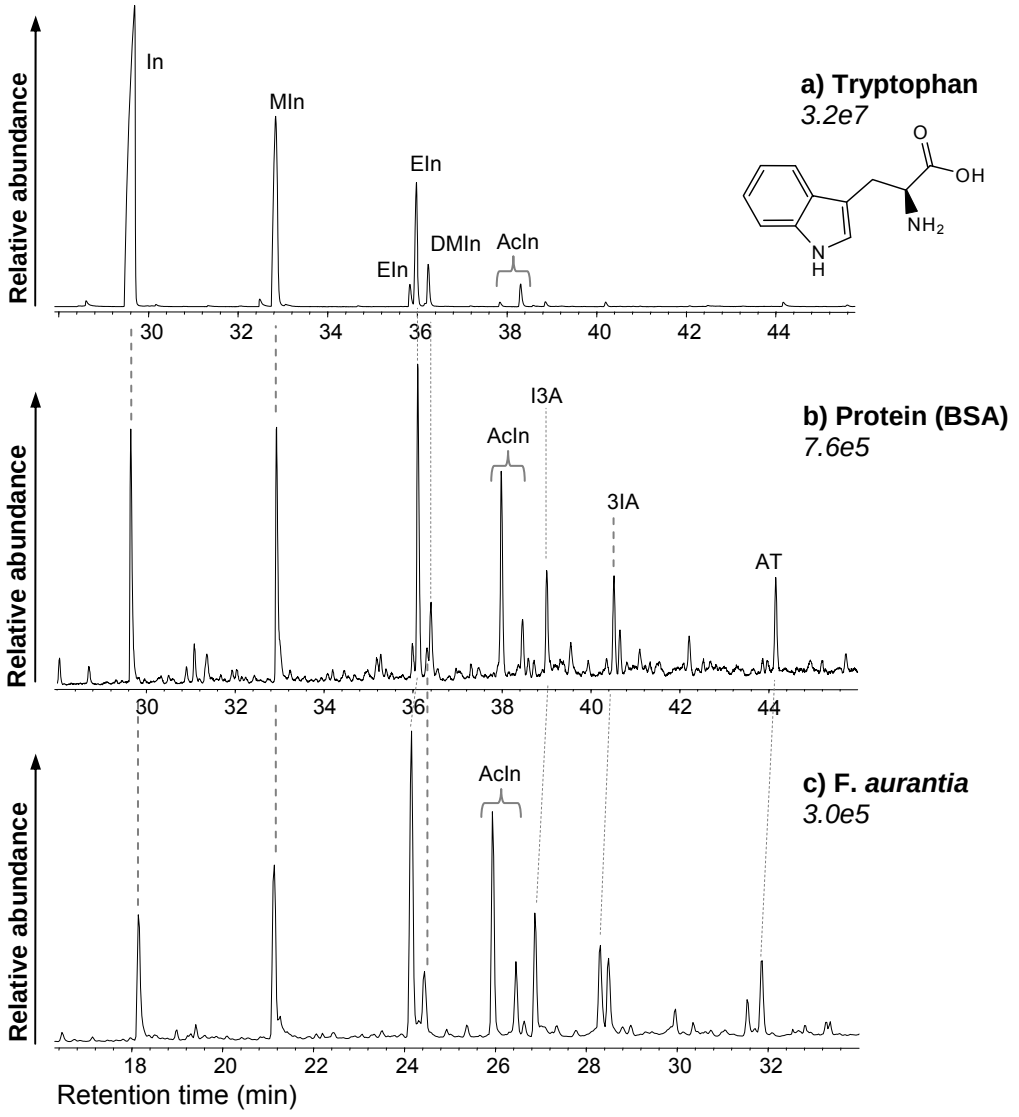

Figure 5.11 Partial TICs **(a)** and summed *m/z* 117+130+144+145+158+159 chromatograms **(b-c)** showing the distribution of alkyl indoles obtained by 300˚C/72hr MSSV pyrolysis GC-MS analysis of **a)** D-tryptophan (amino acid); **b)** BSA (protein) and **c)** F. *aurantia* isolate bacteria. I3A = indole-3-acetaldehyde, 3IA = 3-indolylacetone; AT = *N*-acetyl-D-tryptophan. Other peak assignments correspond to N-products listed in Table 5.1. Relative abundances of a-c are indicated in italics.

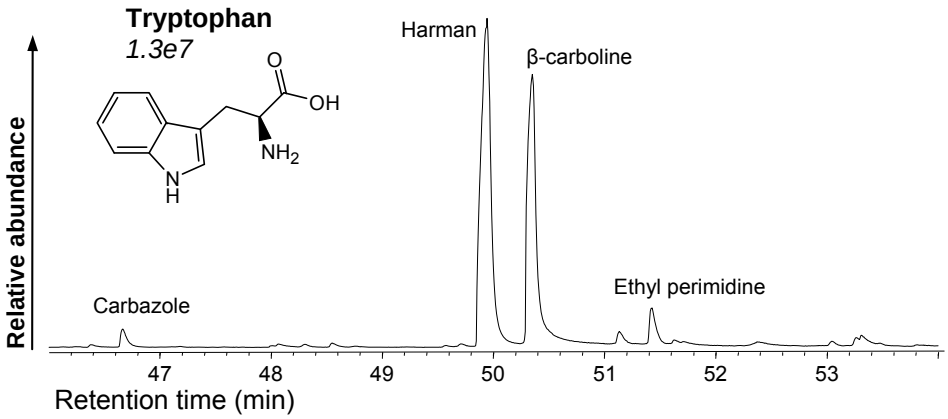

Figure 5.12 Summed *m/z* 168+182 chromatograms showing indole derivatives detected by 300˚C/72hr MSSV pyrolysis GC-MS analysis of D-tryptophan. Relative abundance is indicated in italics.

The occurrence of these effluent OM products could therefore be attributed to cyclisation of tryptophan structural moieties, as well as naturally occurring indole alkaloids, as discussed previously. The high abundance of indole related products in the waste waters is consistent with previous studies (Dignac *et al*. 2000), which have shown that the dominant amino acids in waste water effluents usually differ from natural waters, and include higher concentrations of tryptophan.

MSSV pyrolysis of BSA protein and F. *aurantia* (**Fig. 5.11 b-c**) also yielded high concentrations of indole, methylindole and ethylindole. Several oxygenated indole derivatives, including 3-acetylindole, indole-3-acetaldehyde (I3A), 3-indolylacetone (3IA) and (tentatively) N-acetyl-D-tryptophan (AT), were also identified in high abundance. Only 3-acetylindole was detected in the river and waste water fractions. The precursors of the other indole derivatives may be vulnerable to early diagenetic processes leading to loss of the oxygen functional groups.

Interestingly, MSSV analysis of NOM showed a more significant contribution from the more highly substituted alkyl indoles, which were not detected from any of the standards analysed. This could be due to early diagenetic transformation of tryptophan moieties of proteinaceous materials, or may reflect different biological sources such as alkaloids. Alternatively the higher degree of alkyl substitution may reflect cross-linking units in NOM macromolecules, consistent with the co-

occurrence of highly alkylated low MW N-heterocycles such as pyrroles and pyridines.

The prominent alkyl carbazoles detected from the waste water colloids and BF were not detected in significant abundance from any of the standards selected for this study. Tryptophan (**Fig. 5.12**) and BSA yielded only parent carbazole in low concentration and no substituted carbazoles. Therefore it is likely that the alkyl carbazole pyrolysates of the waste waters and BF derive from other source precursors such as alkaloids as suggested by Bennett *et al*. (2004).

5.3.8 Effect of temperature on N-pyrolysate distributions

The Naintré waste water colloid fraction was studied over a range of off-line MSSV temperatures to monitor the thermal behaviour of several major N-organic products, including alkyl pyrroles and alkyl indoles. The MSSV distribution of alkyl pyrroles, pyridines and pyrazines detected at 260, 300 and 340˚C (72h) are shown in **Figure 5.13**. Similar product distributions were evident at all temperatures. Aniline, pyridinamine and methyl pyridinamine were consistently detected in high relative abundance. The alkyl (C_2-C_5) pyrroles and alkyl (C_1-C_3) pyridines increased moderately in relative abundance with higher pyrolysis temperatures. However, the general thermal stability of the heterocyclic N-product profile suggests that the MSSV thermal parameters do not greatly influence their generation.

The porphyrin and peptide (pentaglycine) standards were also studied over the same MSSV temperature range. The distribution of alkyl pyrroles detected at 260, 300 and 340˚C (72h) are shown in **Figure 5.14**. These were the only products from the porphyrin over the displayed retention time window and were clearly revealed by the TIC data. Selected ions were used to highlight the alkyl pyrrole profile of the peptide. The two standards show very different alkyl pyrrole distributions.

The abundance of alkyl pyrroles detected from the porphyrin increased dramatically with pyrolysis temperature. Only a few of these products, comprising mainly ethyldimethylpyrroles (C_4) and diethylmethylpyrroles (C_5), were detected in low concentration at 260˚C, indicating that the thermal conditions were too mild to significantly release alkyl pyrroles from the porphyrin. At 300˚C there was a

significant increase in the overall abundance of these same C_4 and C_5 alkyl pyrroles. At 340˚C a much broader range of alkyl pyrroles were detected, probably due to secondary fragmentation and isomeric rearrangement. The C_4 and C_5 analogues were still most abundant, but increased concentrations of the C_2 and C_3 alkyl pyrroles were also evident. These lower MW products are likely formed by degradation of the alkyl side-chains of the higher MW pyrroles.

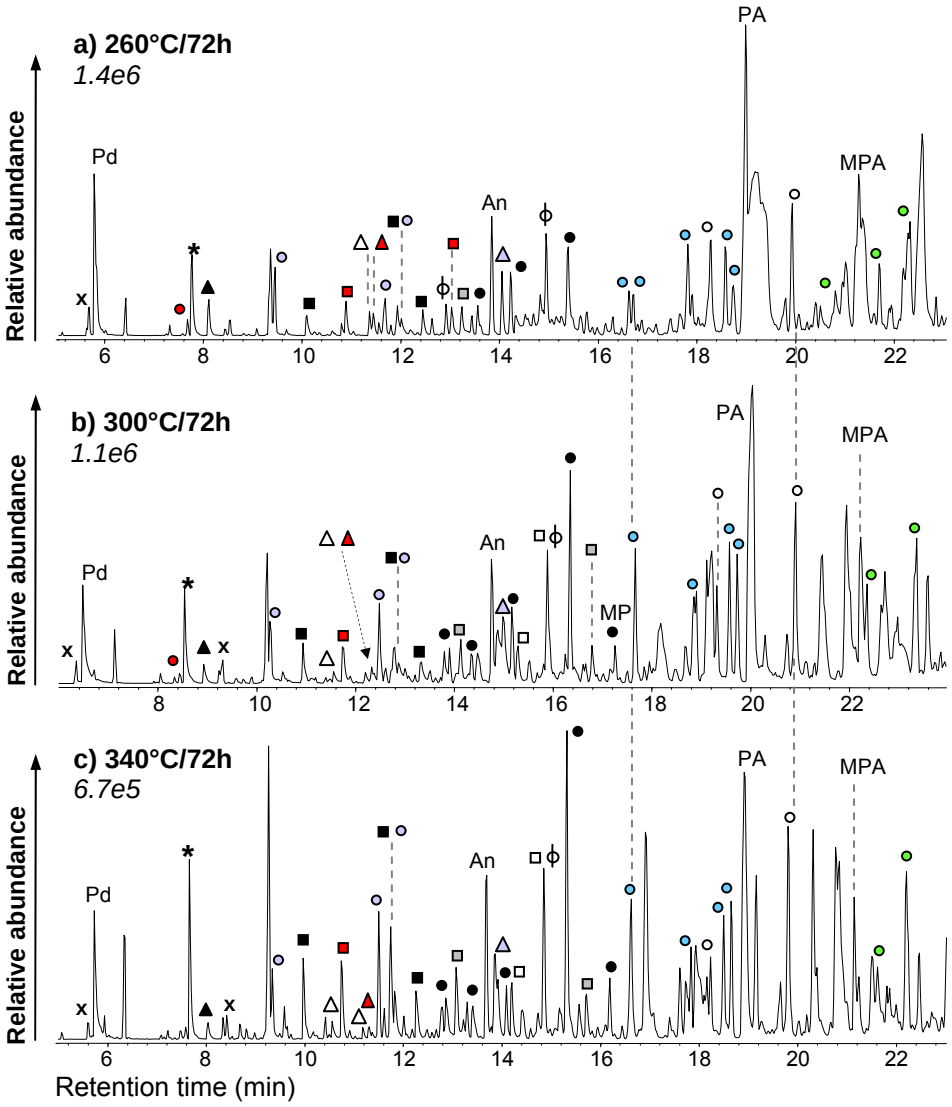

Figure 5.13 Summed *m/z* 79+80+93+94+106+107+108+109+120+121+122+123 chromatograms showing the distribution of alkyl pyrroles, pyridines and pyrazines detected by MSSV pyrolysis of Naintré colloids at **a)** 260˚C/72h; **b)** 300˚C/72h and **c)** 340˚C/72h. Peak assignments correspond to N-products listed in Table 5.1. Relative abundances of a-c are indicated in italics.

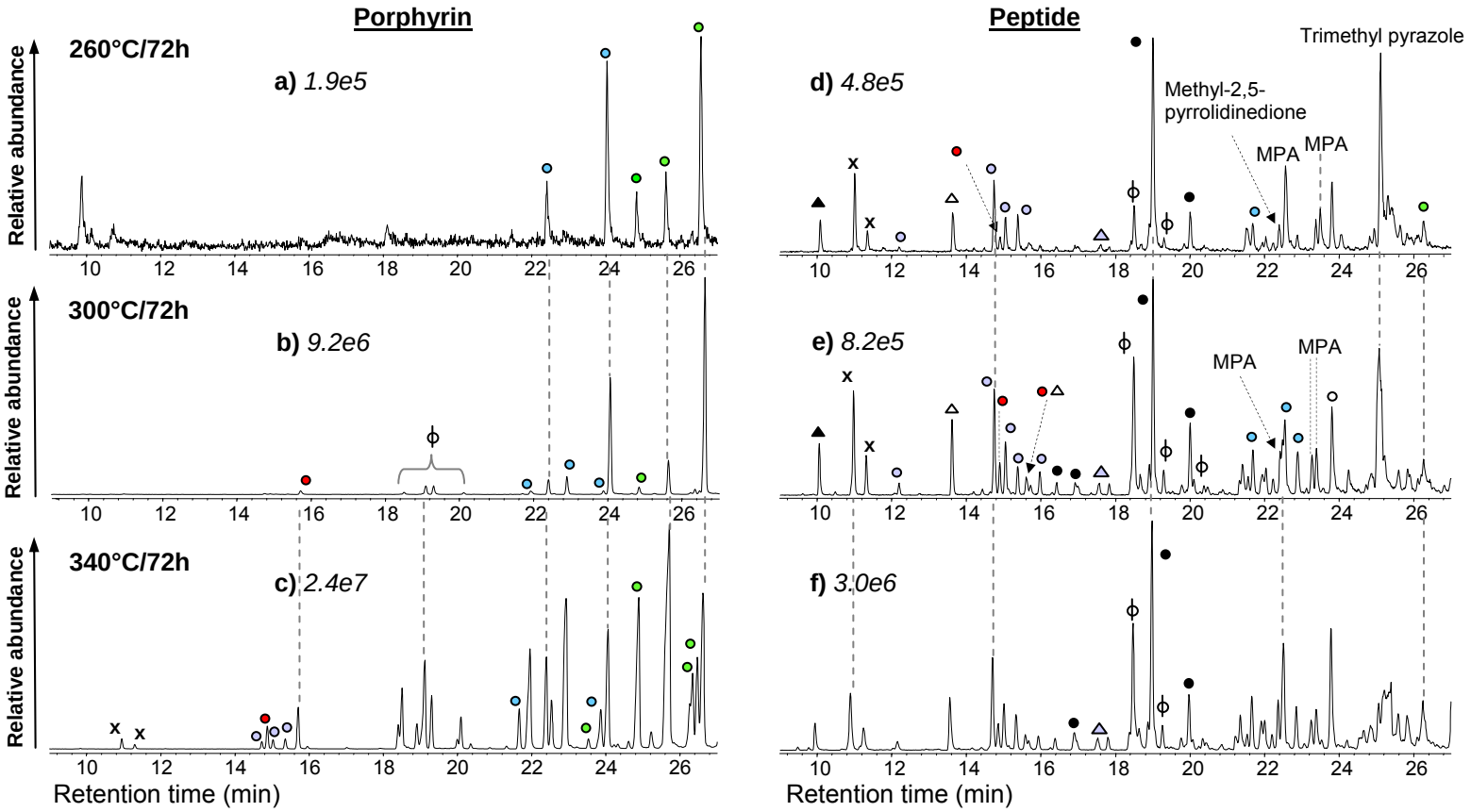

Figure 5.14 TICs **(a-c)** and summed *m/z* 80+94+108+109+122+123 chromatograms **(d-f)** showing the distribution of alkyl pyrroles detected by MSSV pyrolysis of a standard porphyrin (2,3,7,812,13,17,18-octaethyl-21*H*,23*H*-porphine) and peptide at 260˚C/72h, 300˚C/72h and 340˚C/72h. Peak assignments correspond to N-products listed in Table 5.1. Relative abundances of a-f are indicated in italics.

The isomeric distributions of the alkyl pyrrole products of pentaglycine were also relatively stable over the 260-340˚C temperature range (**Fig. 5.14d-f**), consistent with the N-COL data. There was an increase in concentration of all pyrrole products at higher temperatures, but their isomeric distribution remained largely unchanged. Trimethylpyrrole (retention time ca. 19 minutes) was consistently the most abundant product. From 260 to 300˚C there was a notable increase in the relative abundance of ethylmethylpyrrole and a slight increase in the higher MW pyrroles. However, little further change was evident at the highest temperature of 340˚C. Preservation of the isomeric integrity of the alkyl pyrrole distribution may reflect the high thermal stability of these products. In contrast, the thermal profiles of other pentaglycine products do change with temperature. For example, trimethyl pyrazole and several amide products including acetamide, methyl acetamide, propanamide and methyl propanamide were all detected at 260˚C and 300˚C but not 340˚C, indicating thermal degradation or structural alteration of these products at the higher temperature.

Although the product distributions showed some dependence on thermal conditions, many constant features allowed consistent distinction of the two precursors irrespective of temperature. For example, under all MSSV conditions, 2,5-dimethylpyrrole and ethylpyrrole were the dominant C_2 pyrrole isomers from pentaglycine and the porphyrin, respectively. Pentaglycine also yielded major trimethyl- and tetramethylpyrrole products at all three temperatures, whilst polymethylated C_3 and C_4 pyrroles were not detected from the porphyrin over the temperature range studied.

The thermal profile of the alkyl indole products of the N-COL fraction (**Fig. 5.15**) showed a similar trend to the lower MW heterocyclic products. The same products were consistently detected at all temperatures, however there were some notable quantitative differences. The major products at 260˚C were methylindole, ethylindole, dimethylindole and acetylindole, with lower abundances of oxygenated products such as indole-3-acetaldehyde, 3-indolylacetone and N-acetyltryptophan. At 300˚C the methyl, dimethyl and acetylindole products remain dominant, however there was a notable decrease in the abundance of ethylindole and the oxygenated derivatives. The 340˚C analysis showed a relative enrichment of the dimethylindole isomers, concomitant with a further reduction of the ethyl and acetyl substituted

products. This data reflects the relatively high thermal stability of dimethyl indoles, consistent with previously published hydropyrolysis results, which showed enhanced abundances of 2,3-dimethyl indole in sedimentary OM of higher thermal maturity (Bennett *et al*., 2004). The sedimentary occurrence of this compound was attributed to direct derivation from an alkaloid precursor or to secondary rearrangement of tryptophan-derived molecules during early diagenesis (Bennett *et al*., 2004).

The summed ion chromatograms of **Figure 5.16** display the thermal profile of the indole pyrolysates of the protein (BSA) standard. Again, the distribution of products exhibited relatively minor variation with increasing thermal severity. Indole, methylindole and ethylindole were the most abundant products across the entire temperature range. However, the oxygen-containing derivatives of indole (indole-3-acetaldehyde, 3-indolylacetone and N-acetyl tryptophan) showed a decrease in abundance with increasing pyrolysis temperature but were still detectable from the 340˚C analysis. These products were only detected in significant concentrations from the 260˚C pyrolysate of the N-COL fraction, possibly reflecting the lower concentrations of tryptophan moieties in the Ef-OM or microbial alteration into more thermally susceptible metabolites. In contrast to the thermal behaviour of the O-indole products, the relative abundance of dimethylindole was shown to increase with temperature, providing further evidence for the high thermal stability of this product.

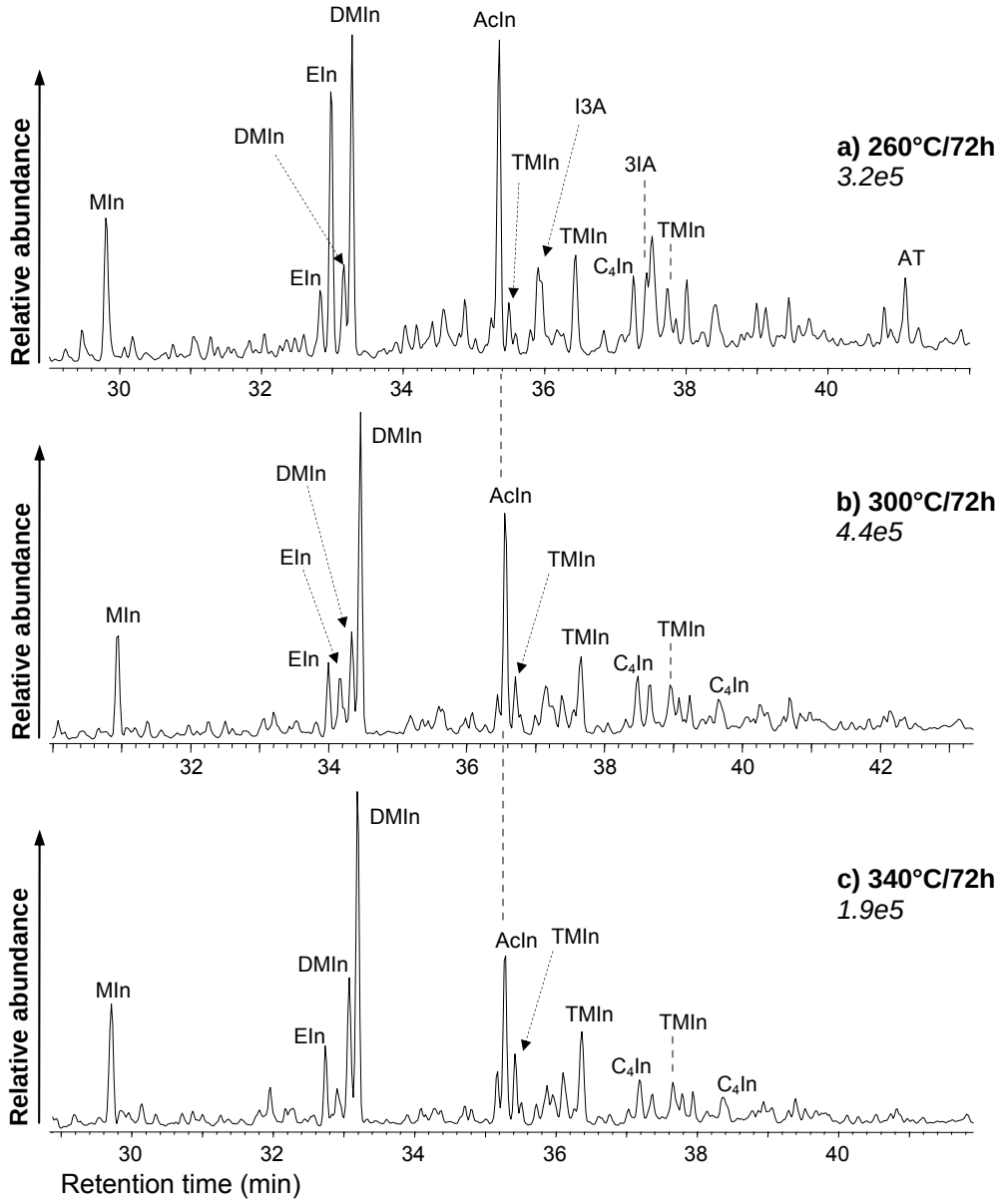

Figure 5.15 Summed *m/z* 130+144+145+158+159 chromatograms showing the distribution of alkyl indoles detected by MSSV pyrolysis of Naintré colloids at **a)** 260˚C/72h; **b)** 300˚C/72h and **c)** 340˚C/72h. I3A = indole-3-acetaldehyde, 3IA = 3-indolylacetone, AT = *N*-acetyl-D-tryptophan. Other peak assignments correspond to N-products listed in Table 5.1. Relative abundances of a-c are indicated in italics.

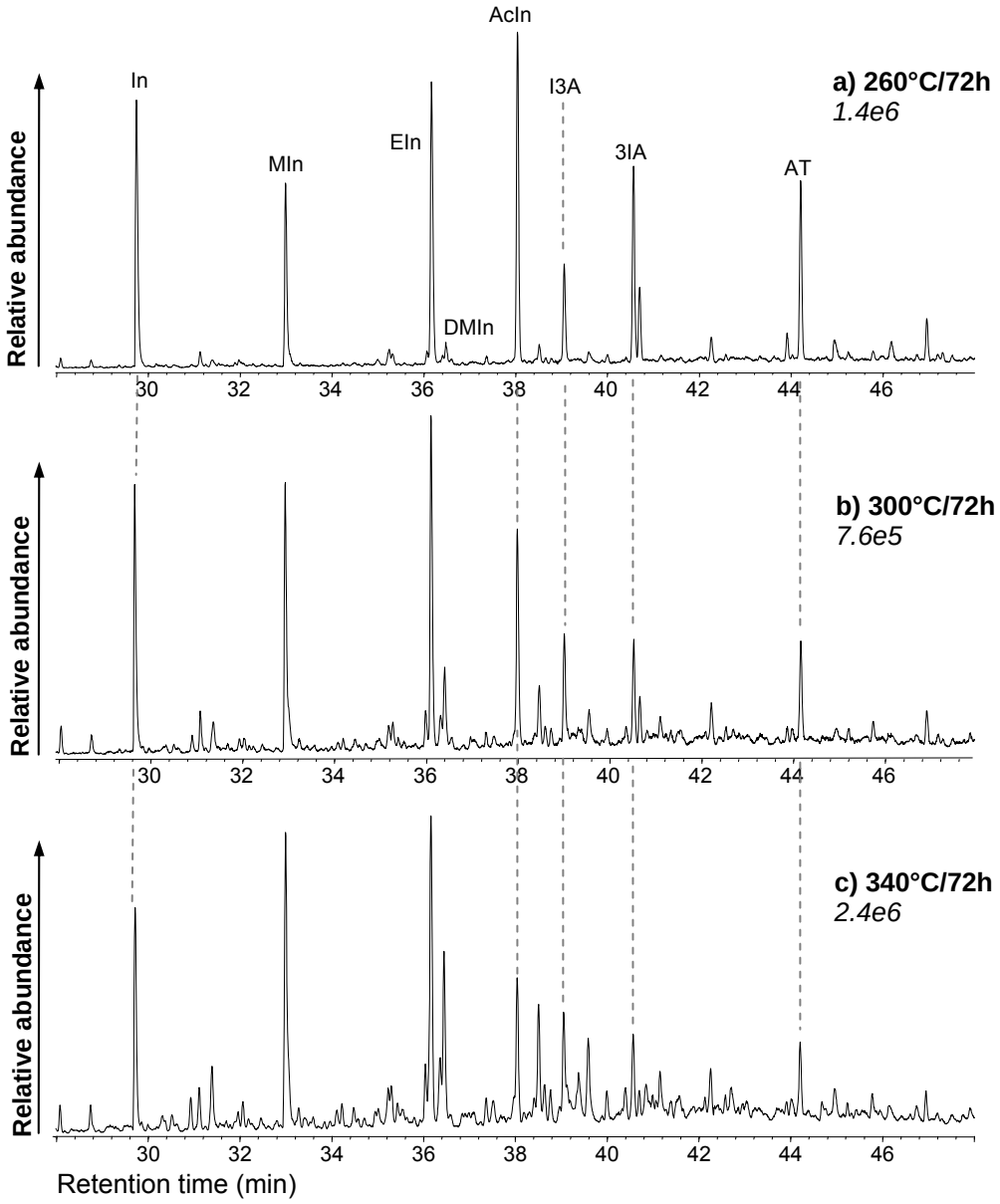

Figure 5.16 Summed *m/z* 117+130+144+145+158+159 chromatograms showing the distribution of indoles detected by MSSV pyrolysis of BSA protein at **a)** 260˚C/72h; **b)** 300˚C/72h and **c)** 340˚C/72h. I3A = indole- 3-acetaldehyde, 3IA = 3-indolylacetone, AT = *N*-acetyl-D-tryptophan. Other peak assignments correspond to N-products listed in Table 5.1. Relative abundances of a-c are indicated in italics.

5.4 Conclusions

MSSV pyrolysis has proved very effective at thermally releasing polar N functionalities of immature biochemicals present in aquatic NOM. The relatively moderate thermal conditions of MSSV pyrolysis yielded much higher concentrations of GC-MS detectable N-pyrolysates compared to flash pyrolysis, which may underestimate the N-organic contribution of NOM. A broad distribution of alkylated pyrroles, pyridines, pyrazines and indoles were detected from the transphilic and colloid fractions of the surface and waste waters, but few N-organic products were detected from the HPO fractions studied.

Corresponding MSSV pyrolysis analyses of a suite of N-containing standards afforded many of the same products detected from the NOM samples. Characterisation of the distinctive N-product profiles of these standards showed potential for establishing their contributions in complex environmental macromolecules. For example, the amino sugar standard (chitin) revealed very similar product distributions, including high concentrations of alkyl pyrroles, pyridines and pyrazines, to those observed in the Gartempe TPI and Brittany COL fractions as well as the membrane filtration biofoulant, providing strong evidence that amino sugars are significant N-organic precursors of these samples. On the other hand, higher MW N-pyrolysates, including β-carbolines and alkyl carbazoles, were detected only from the waste water effluents. These products were correlated with specific amino acid (e.g. tryptophan) or alkaloid precursors and may be potential molecular markers for waste water impact into natural waters.

It should be noted that the N-organic standards studied here represent only basic structural units of potential NOM precursors. Hence, there remains some ambiguity about the precise MSSV formation mechanisms of the N-pyrolysates of NOM. Mechanistic definition of complex pyrolytic pathways remains a significant analytical challenge. Notwithstanding this, some of the N-product relationships identified in this study allow greater inference of potential N-precursors than previously possible.

Further investigation is required to more accurately identify and distinguish the primary structural or thermally induced origins of many of the N-organic products reported here. Several low MW heterocyclic N-products detected from the colloid and transphilic NOM fractions may reflect melanoidin structures formed by Maillard reactions occurring naturally in freshwater aquatic environments or during biological waste water treatment. Analysis of representative mixtures of amino acids and carbohydrates did not suggest that these products were artefacts of the closed-system MSSV pyrolysis process.

Preliminary studies here showed that the N-product distributions from the analysis of colloidal NOM were relatively stable at different MSSV temperatures (260 – 340˚C/72hr). Additionally, the N-products of peptide, porphyrin and protein standards were consistently different over the MSSV temperature range investigated, allowing their clear distinction and demonstrating the utility of the MSSV approach for the characterisation of N-organic moieties of NOM over a broad range of thermal analytical conditions. The sensitive detection of N-pyrolysates by MSSV pyrolysis holds promise for the improved characterisation of the N-organic moiety of NOM, which should be useful for determining the structural precursors of N-containing disinfection by-products (N-DBPs) produced during potable water treatment.

Chapter 6

Isolation and characterisation of NOM from a pristine source water (North Pine Dam, Brisbane, Queensland)

6.1 Introduction

Treated potable water from North Pine (NP) Dam, located on the North Pine River in Pine Rivers Shire (Queensland) is supplied to the northern areas of Brisbane and adjacent Shires. NP Dam, along with Wivenhoe and Somerset Dams, is responsible for the supply of potable water to more than 1.2 million people in south east Queensland and is also used for power generation, irrigation and recreation. NP Dam was one of several source waters selected as part of a wider CRC study (2.5.1.3) on advanced analytical characterisation of NOM in selected Australian source waters. NP is a high quality source water, characterised by low colour and low dissolved organic carbon concentration (< 5 mg L^{-1}), compared with many organic rich surface and ground water sources of other Australian cities (e.g. Perth and Adelaide).

In this study, XAD resin fractions of NOM from the NP Dam were isolated and holistically characterised using MSSV pyrolysis GC-MS and several other more established analytical techniques to provide insight into the structure and source of the NOM in this major potable resource. An integrated analytical approach is typically used for chemical structural elucidations of complex macromolecules like aquatic NOM. The quantitative distribution of molecular weights (MW) by size exclusion chromatography (SEC) and carbon structural environments and functional groups by ^{13}C nuclear magnetic resonance (^{13}C-NMR) and Fourier transform infrared (FTIR) spectroscopy can be integrated with the molecular speciation information identified by analytical pyrolysis and thermochemolysis GC-MS (González-Vila *et al*., 2001). A major objective of this case study was to evaluate the

practical capacity of MSSV pyrolysis to provide additional structural information to complement the more established characterisation tools.

6.2 Experimental

6.2.1 Description of site and sample collection

The NP Dam impounds the NP River to form Lake Samsonvale in Pine Rivers Shire, approximately 30 km north of Brisbane, Queensland. Water is released from the Dam to the adjacent water treatment plant operated by Brisbane Water and provides potable water for Brisbane and the broader regions of Pine Rivers, Redcliffe and Caboolture. The drainage basin of the Lake Samsonvale catchment covers an area of 348 km^2 and comprises 70 km^2 of mixed forest; 100 km^2 of grassland and pasture; and 6 km^2 of cropping land (SEQWater and Brisbane Water, 2006). Mean annual rainfall is 1175 mm however this is subject to extreme annual and seasonal variation. There are extensive grasslands within the Lake Samsonvale catchment, which are lightly grazed, with a small area used for cropping. The intensity of rural industry (e.g. cattle feedlots, dairying and an abattoir) is less than in the catchments of the other two major Brisbane reservoirs (SEQWater and Brisbane Water, 2006). Lake Samsonvale is also used for recreation including fishing, canoeing and sailing.

NP Dam has a surface area of 21.6 km^2, storage capacity of 215,000 ML and an average depth of 9.4 m (Littlejohn, 2004). The dam is a concrete gravity type, with a steel gated spillway, and earth and rock fill abutments. Water is drawn from the dam through an outlet tower on the face of the dam. Outlets, guarded by screens and valves, are provided at several depths so that the best quality source water can be taken from the reservoir and supplied to the treatment plant (SEQ water and Brisbane Water, 2006). An aeration system improves water quality through destratification, which means the temperature-based layers of water are mixed so that uniform temperatures are achieved over the depth of the lake (Littlejohn, 2004). This can help overcome some of the problems associated with eutrophication of still waters. For example, accumulation of dissolved nutrients can contribute to algal and cyanobacterial blooms and deterioration of water quality.

Approximately 93 L of water from the NP Dam was collected in five 20 L polyethylene containers in July 2005. The sample was vacuum-filtered using pre-washed 0.5 μm glass fibre filters (43 mm, Whatman) to remove particulate material, and the filtrate (DOC 4.8 mg L^{-1}) was transferred to a 100 L pre-cleaned stainless steel drum. The sample was refrigerated at 4˚C prior to concentration, fractionation and analysis.

6.2.2 Isolation and fractionation procedure

6.2.2.1 Pre-concentration by reverse osmosis and rotary evaporation

The filtered sample was pre-concentrated approximately 5-fold prior to XAD fractionation using a combination of reverse osmosis (RO) and rotary evaporation (RE). Reduction of the raw water volume to suit the column capacity of the XAD system allowed the sample to be singularly processed, without the need for time-consuming resin regeneration and cleaning procedures between sample aliquots. RO was performed at 414 kPa, with the retentate recycled through the system until the required volume was reached. Pre-concentration of the raw water (4.8 mg L^{-1} DOC) from 93 L to 17.3 L by RO and rotary evaporation resulted in a final DOC concentration of 25.1 mg L^{-1}, corresponding to ca. 97 % recovery. This is consistent with previous reports stating that DOC recovery by RO is generally greater than 90 percent (Croué, 2004).

6.2.2.2 XAD resin fractionation

A 300 mL superimposed XAD-8/XAD-4 (Amberlite) resin system was employed with a column capacity of 19.8 L. The XAD resins were thoroughly cleaned prior to NOM fractionation by consecutive rinses with 2 L Milli-Q water (MQ; Elga) and 2 L MQ/acetonitrile (25:75 % v/v). The XAD-4 resin required additional elution of 1.5 L sodium hydroxide (NaOH, 0.1 M), followed by a second wash with the MQ/acetonitrile mixture (1.5 L) to remove residual DOC. The resins were then finally eluted with MQ water until the DOC concentration was below 0.2 mg L^{-1} (XAD-8 = 0.17 mg L^{-1}; XAD-4 = 0.19 mg L^{-1}). Dilute hydrochloric acid (0.1 M, 1 L) was eluted through each resin prior to introduction of the sample.

Following pre-concentration of the raw water, the NP sample was acidified to pH 2 with 1 M hydrochloric acid to condition for XAD separation. The sample was

peristaltically pumped through XAD-8 resin to isolate the adsorbed HPO fraction whilst the eluent containing the transphilic (TPI) and hydrophilic (HPI) fractions was collected in 5 L pre-annealed glass bottles. The eluent was then pumped through XAD-4 resin to isolate the adsorbed TPI fraction, whilst the HPI fraction passed through. DOC analyses were performed on aliquots of the XAD-8 and XAD-4 eluents. The HPO, TPI and HPI fractions accounted for 64.5, 11.5 and 24 % of the DOC, respectively.

Prior to elution of the adsorbed NOM fractions the resins were rinsed with MQ water (800 mL, adjusted to pH 2 with formic acid) and MQ/acetonitrile (200 mL, 25/75 % v/v). The fractions were then desorbed with MQ/acetonitrile (1.5 - 2 L, 25/75 % v/v) and collected in 2 L pre-annealed glass bottles. Acetonitrile was removed by rotary evaporation and the fractions were lyophilized (freeze-dried) to yield solid HPO (390 mg) and TPI (101 mg) fractions.

6.2.3 Bulk characterisation of raw and fractionated water

6.2.3.1 Ultraviolet absorbance

Ultraviolet/visible (UV/Vis) absorbance at 254 and 400 nm was measured on the raw water, pre-concentrated water, and XAD resin eluents using a Shimadzu Pharmaspec UV-1700 UV-Visible spectrophotometer. The absorbance at 400 nm was converted to total colour units (TCU) by calibration with colour standards.

6.2.3.2 Dissolved organic carbon concentration

Water samples (40 mL) were filtered in duplicate using separate pre-washed glass fibre filters and collected in annealed glass vials. Analysis was performed with a Shimadzu Total Organic Carbon Analyser (TOC-Vws) using a non-purgable organic carbon (NPOC) method. The NPOC parameters included 3 to 5 injections of 2.5 mL sample (with a maximum standard deviation of 0.05 mg L^{-1}), with 2 washes. Phosphoric acid solution (75 µL, 17 % w/v) was added and the sample sparged with nitrogen gas for 3 minutes. Persulfate oxidiser solution (1.5 mL, 12 % w/v) was added and the sample irradiated with UV light to oxidise organic carbon. The resulting carbon dioxide was detected using an infrared detector and calibrated against potassium hydrogen phthalate standards.

6.2.3.3 High performance size exclusion chromatography

High performance size exclusion chromatography (HP-SEC) with dual UV_{254} and organic carbon detection (OCD) of the filtered raw and pre-concentrated waters, and the XAD resin eluents was performed according to a previously described method (Allpike *et al*., 2005). Briefly, water samples (up to 1.8 mL) were injected into an Agilent 1100 LC system equipped with a Toyopearl HW-50S SEC column (25 cm × 2 cm i.d., particle size 30 µm, pore size 12.5 nm), with on-line UV (254 nm) detection using a diode array detector. A phosphate buffer (10 mM of Na_2HPO_4 and KH_2PO_4; pH 6.85) was used as the mobile phase at a flow rate of 1 mL min^{-1}. Polystyrene sulfonate (PSS) standards with molecular weights of 81800, 35300, 15200, 6530, 4400, 2220, 1290, 840 and 208 Da were used for apparent molecular weight (AMW) calibration.

After passing through the UV detector, the column effluent passed through a wet chemical treatment process to oxidise organic carbon to CO_2. First, H_3PO_4 (20% w/v; 10 µL min^{-1}) was added to the effluent stream using a syringe pump (Harvard Apparatus Pump 22). It was then passed through a Sievers TOC degassing module with a vacuum pump connected in a counter-flow direction to remove CO_2 produced by inorganic carbon compounds reacting with H_3PO_4. Subsequently, $Na_2S_2O_8$ (20 g L^{-1}; 10 µL min^{-1}) was introduced to the flow stream using a syringe pump, which then passed through a clear silica capillary (120 cm) adjacent to a medium pressure mercury vapour UV lamp (170 W, < 190 to > 400 nm, length = 120 cm). The chemical oxidant and UV lamp combined to oxidise the organic carbon present in the flow stream to CO_2. Helium (5 mL min^{-1}) was added to the flow stream, which then passed through two membrane separators in series (Genie 170, A+ Corporation) fitted with hydrophobic membranes (polytetrafluoroethylene, 0.45 µm pore size; Alltech) through which the gaseous CO_2/He mixture passed while the liquid was rejected.

The gaseous CO_2/He mixture was then introduced via a fused silica capillary (100 µm I.D., 200 µm O.D. × 2.5 m) into a Balzers ThermoStar GSD300 mass spectrometer operating in single ion mode (*m/z* 44) at a sampling frequency of 0.8 Hz, dwell time 1 s, and source voltage of 1500 V. The capillary was inserted into an open polyether ether ketone plastic tube (20 cm × ~1.4 mm i.d.) attached to the

outlet of the second membrane separator, so that a portion of the gaseous CO_2/He mixture was drawn into the capillary by the action of the mass spectrometer vacuum. Excess gas was vented. Data collection and processing was performed using Balzers Quadstar 422 software (Version 5.02).

6.2.4 Molecular characterisation of HPO and TPI fractions

6.2.4.1 Elemental analysis

Elemental analysis was conducted on the freeze-dried HPO and TPI fractions by Chemical and Micro Analytical Services (CMAS) Pty. Ltd (Victoria, Australia). Percentage concentrations of carbon, hydrogen, nitrogen, oxygen, sulphur and ash (representing the inorganic component) were determined.

6.2.4.2 Fourier transform infrared spectroscopy

Fourier transform infrared (FTIR) spectra of the NOM fractions were acquired in the transmission mode using a Bruker IFS-66 spectrometer. Approximately 1 mg of freeze-dried material was ground, mixed with 250 mg of potassium bromide (dried at 100˚C) and pressed into a small disc. FTIR analysis was performed by collecting 4 background scans followed by 4 scans of the sample. All FTIR spectra were scanned between 4000 and 700 cm^{-1} and data analysis performed with OPUS software. Detector resolution was maintained at 4 cm^{-1} for all analyses.

6.2.4.3 Solid state ^{13}C-nuclear magnetic resonance spectroscopy

Solid-state ^{13}C cross polarization (CP) magic angle spinning (MAS) NMR analyses were conducted by Dr. Ron Smernik at the University of Adelaide (South Australia). The spectra were obtained at a ^{13}C frequency of 50.3 MHz on a Varian Unity 200 spectrometer. The samples were packed in a 7 mm diameter cylindrical zirconia rotor with Kel-F end-caps and spun at 5000 ± 100 Hz in a Doty Scientific MAS probe. The spectra were acquired using a 1 ms contact time and a 1 s recycle delay. Between 24000 and 61000 scans were collected, representing a total run time of 7 to 17 hours. The free induction decays were acquired with a sweep width of 40 kHz; 1216 data points were collected over an acquisition time of 15 ms. The FID was zero-filled to 32768 data points and processed with a 50 Hz Lorentzian line broadening and a 0.01 s Gaussian broadening. The chemical shift was externally referenced to the methyl resonance of hexamethylbenzene at 17.36 ppm. Spectra

were corrected for background signal by subtracting the signal of an empty rotor under the same acquisition conditions.

Several potential issues associated with the quantitative interpretation of solid-state ^{13}C CPMAS NMR spectra of complex organic materials such as NOM include long-spin lattice relaxation times, strong C-H and N-H dipolar interactions, chemical shift anisotropy, spectral alterations by paramagnetic materials and poor quantitation at high fields (Hatcher *et al*., 2001). Most quantitation issues can be addressed using a technique known as spin counting (Smernik and Oades, 2000a; 2000b). This involves calibrating the strength of the NMR signal of the sample against that of a reference known to give a quantitative signal. Glycine was used for this purpose and the details of the technique are described in Smernik and Oades (2000a, 2000b). The output is the 'NMR observability' (C_{obs}), which is the proportion of potential NMR signal that is actually detected for the sample. If the NMR observability is close to 100%, then it can safely be assumed that the NMR spectrum is quantitative, and that the distribution of NMR chemical shifts accurately reflects the distribution of carbon types.

6.2.4.4 MSSV pyrolysis GC-MS

MSSV pyrolysis of 0.5 - 1 mg of the two samples was separately performed according to the procedure described in Chapter 2.2.2.1. All data correspond to MSSV analysis **I** at an off-line pyrolysis temperature of 300˚C for 72 hr. GC-MS analysis of the volatile MSSV pyrolysates was performed using an HP 6890 GC coupled to an HP 5973 mass selective detector (MSD), with a 40 m x 0.32 mm i.d. x 0.25 μm DB5-MS capillary column (J&W Scientific). Analyses were performed with a split of 30 mL min^{-1} using helium carrier gas at 42 kPa head pressure. The GC oven was held at -20˚C (using liquid CO_2 cryogenic control) for 1 minute, then increased at 8˚C min^{-1} to 40˚C, then 4˚C min^{-1} to a final temperature of 310˚C, held isothermal for 20 minutes. Full scan acquisition was performed over the range m/z 50 – 550 at ca. 4 scans s^{-1}. An electron energy of 70 eV, source temperature of 250˚C and transfer line of 310˚C was used. Tentative peak identifications were based on correlation of GC elution position and mass spectral data with previously published data and the Wiley 275 and NIST 05 mass spectral libraries.

6.2.4.5 Flash pyrolysis GC-MS

NOM samples (0.5 – 1 mg) were loaded into pre-annealed quartz tubes and flash pyrolysis was conducted at 600˚C/20 seconds using a Chemical Data Systems analytical Pyroprobe 5250 fitted with a pyrolysis autosampler. The pyrolysis chamber was held at 300˚C. GC-MS analysis was performed using an HP 6890 GC coupled to an HP 5973 MSD, with a 60 m x 0.25 mm i.d. x 0.25 μm DB5-MS capillary column (J&W Scientific). Helium carrier gas was used at 131 kPa head pressure with a split of 30 mL min^{-1}. The GC oven temperature programme and mass spectral parameters were the same as used for MSSV pyrolysis.

6.2.4.6 Thermochemolysis GC-MS

The NOM samples (ca. 1 mg) were loaded into pre-annealed quartz tubes sealed at one end. Tetramethylammonium hydroxide (Sigma-Aldrich) was added as a methanolic solution (5 μL, 25% w/w) and the open end plugged with pre-cleaned glass wool. Pyrolysis was performed at 650˚C for 20 seconds using a Chemical Data Systems 160 Pyroprobe, with the pyrolysis chamber held at 150˚C. The products were cryo-focused for 1.5 minutes at the start of the GC column using liquid nitrogen prior to analysis. A HP 5890 Series II gas chromatograph coupled to a 5971 MSD was used for GC-MS analysis of the pyrolysis products. Analyses were performed with a split of 20 ml min^{-1} using helium carrier gas at 55 kPa and a 30 m x 0.25 mm x 1 μm phase ZB5-MS (Phenomenex) capillary column. The GC oven was initially held at 40˚C for 2 minutes, then heated at a rate of 4˚C min^{-1} to a final 310˚C and held isothermal for 25 minutes. After a 3-minute solvent delay, full scan mass spectra (*m/z* 50 –550 at ca. 4 scans sec^{-1}) were acquired with relatively standard mass spectral conditions (e.g. electron energy 70 eV; transfer line = 310˚C).

6.3 Results and Discussion

6.3.1 DOC distribution

The XAD resin distribution of NP source water DOC is shown in **Table 6.1**. The HPO, TPI and HPI (determined by difference) fractions accounted for approximately 65 %, 12 % and 24 % of the DOC, respectively. These values are generally consistent with XAD compositions of previously studied surface water (e.g. Templier *et al*., 2005a). **Table 6.1** shows the fraction recovery and total DOC recovery for the XAD isolation protocol. 75 % of the adsorbed HPO fraction was recovered from the XAD-8 resin by elution with MQ/acetonitrile, indicating that some strongly adsorbed material was retained. Combined with the ca. 97 % recovery of the TPI fraction the total DOC recovery was 60 % of the ca. 450 mg of original source water DOC. This provided sufficient quantities of organic material for a variety of chemical analyses.

Table 6.1 DOC distribution and percentage recovery of NP HPO, TPI and HPI fractions.

Sample	NP-HPO	NP-TPI	NP-HPI
% of DOC	***64.5***	***11.5***	***24***
Net weight of fraction, mg	390	101	-
% organic carbon*	53.5	48.1	-
Net mass organic C, mg	208.7	48.6	-
Calculated wt. organic C, mg	278.4	49.9	-
Percent recovery of fraction	75	97	0
Total recovery of DOC, %	***60***		

* From elemental analysis (section 6.3.4.1)

The dissolved organic carbon, UV_{254} absorbance, SUVA and colour measurements for the NP raw water, concentrated source water (CSW) and the XAD resin eluents are shown in **Table 6.2**. UV_{254} absorbance is often used as a surrogate measure for aromatic constituents of NOM such as lignin, tannin and humic substances (Clesceri *et al*., 1998). Specific UV absorbance (SUVA), the ratio of UV_{254} absorbance to DOC concentration, has been shown to strongly correlate with the aromatic carbon content of aquatic NOM (Croué *et al*., 1999; Weishaar *et al*., 2003).

Table 6.2 Basic water quality characteristics of raw water, concentrated water and XAD resin eluents.

	Raw	CSW	XAD-8 eluent	XAD-4 eluent
DOC, mg L^{-1}	4.8	25.1	8.9	6.0
UV_{254}, cm^{-1}	0.086	0.458	0.094	0.058
SUVA, m^{-1} L mg^{-1}	1.8	1.8	1.0	0.96
Colour, TCU	5.7	44.5	3.2	0.7

The NP raw water showed a much lower SUVA value than several of the surface black waters previously characterized in this study (e.g. Gartempe River SUVA = 4.4 m^{-1}.L.mg C^{-1}; Lavaud *et al*., 2008). In general, SUVA values show a direct correlation with the concentration of HPO material (Croué *et al*., 1999); however the low SUVA of NP conflicts with the high abundance of its HPO fraction. This suggests a significant difference in the aromatic character of the humic component of pristine and black water sources, with the former more aliphatic in nature. This trend was also noted for the terpenoid rich ground water analysed in Chapter 3, which showed relatively low SUVA (1.2 m^{-1}.L.mg C^{-1}) but high HPO content (Lavaud *et al*., 2008). The low colour of the NP source water is also consistent with a relatively minor contribution of aromatic carbon.

6.3.2 High performance size-exclusion chromatography

HP-SEC with UV_{254} absorbance and OCD was used to gain insight into the MW distribution of NP NOM. **Figure 6.1** shows the HP-SEC-UV_{254} and OCD chromatograms of the apparent MW distribution of the CSW and the XAD resin eluents. The MW distribution of the concentrate was consistent with the raw water, indicating no significant MW fractionation on pre-concentration. The majority of the DOC had intermediate MWs between 800 – 10000 Da. Organic constituents of this size are generally attributed to humic and fulvic acid-type structures (Abbt-Braun and Frimmel, 1999). The XAD-8 eluent showed a large reduction in both DOC and UV_{254} absorbance in the high MW region of this intermediate band, indicating a significant proportion of 3000 – 10000 *Da* organic constituents in the HPO fraction. This is consistent with the adsorption of high MW aromatic structures onto XAD-8

resin. The XAD-4 eluent also showed a further small reduction in DOC and UV signal of the 3000 – 10000 Da region.

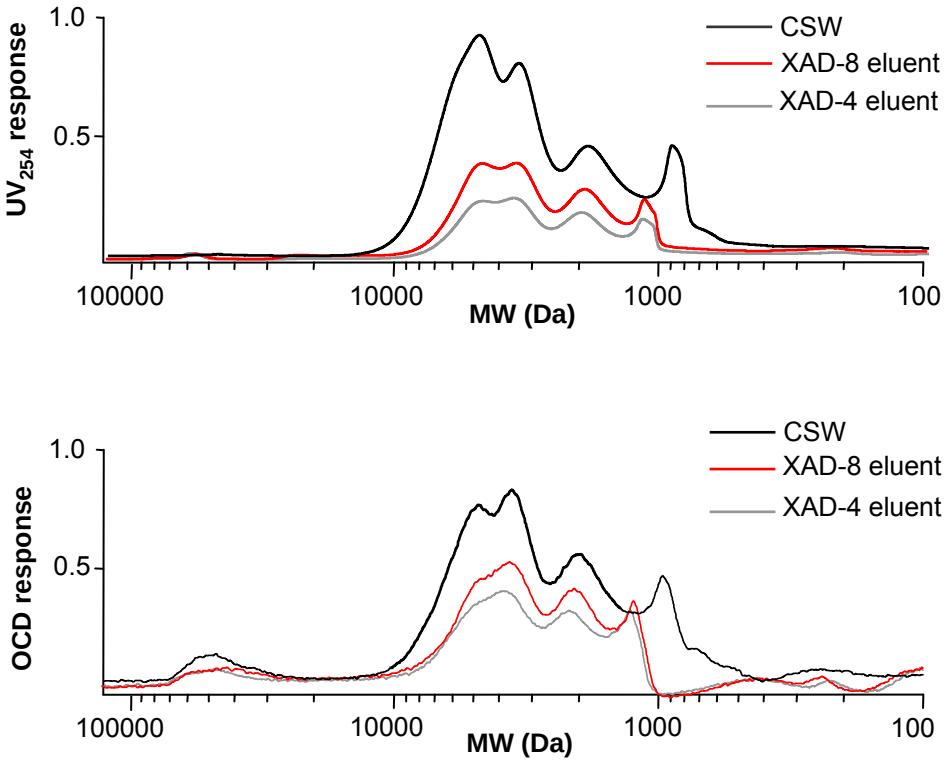

Figure 6.1 HPSEC-UV_{254} and HPSEC-OCD chromatograms of concentrated NP source water (CSW) and XAD resin eluents.

In comparison, the abundance and aromatic content of the low MW (< 3000 Da) SEC fractions were only slightly reduced, attributed to inefficient XAD resin adsorption of low MW (< 3000 Da) hydrophilic organic acids (Croue *et al*., 2000). Interestingly, the lowest MW fraction of the XAD eluants appeared at a higher MW (1000 – 1500 Da) than the concentrate (< 1000 Da). This may be due to interactions between the higher MW material of the concentrate and the stationary phase of the SEC column, which upon removal during the isolation procedure causes an apparent shift to higher MW.

6.3.3 Characterisation of XAD resin fractions

6.3.3.1 Elemental composition

The elemental composition of the NP HPO and TPI fractions, presented in Table 6.3, were generally similar to those of other aquatic NOM fractions and humic substances (e.g. Croue *et al*., 2000; McIntyre *et al*., 2005; Templier *et al*., 2005a). Both organic-rich fractions contained very low low ash contents (< 2 %). Ash contains heteroatom (e.g. P, S, N), halogen (e.g. Cl, Br) and metal species and provides a general indication of total inorganic content.

Table 6.3 Elemental composition and atomic ratios of NP HPO and TPI fractions.

Mass %	NP-HPO	NP-TPI
Carbon	53.5	48.1
Hydrogen	5.9	5.6
Oxygen	36.8	38.7
Nitrogen	2.3	4.3
Sulfur	0.8	0.7
Ash	1.2	2
H/C	1.3	1.4
O/C	0.5	0.6
C/N	27.1	13.1

The atomic ratios of O/C, H/C and C/N are often used for basic characterisation of the chemical character and terrestrial versus microbial source of humic substances (Steelink, 1985). The H/C ratio provides an indication of the aromatic/aliphatic character of the sample (Abbt-Braun and Frimmel, 1999). H/C values greater than one were measured for both fractions, reflecting high aliphatic content, possibly indicative of substantial algal or bacterial input. Belzile *et al*. (1997) reported that humic substances originating primarily from aquatic organisms in lake sediments have H/C values greater than one. NP Dam is subject to periodic cyanobacterial blooms (Littlejohn, 2004, Burford *et al*., 2007) which are a ready source of aliphatic biomolecules. Humic substances derived from vascular plant material generally have H/C ratios less than one (Bourbonniere and Meyers, 1978), refecting the lower contribution from terrigenous sources to NP NOM.

The XAD resin fractions of NP showed only minor variation in H/C composition, with slightly higher aromatic character measured for the HPO fraction. The UV_{254} data from Table 6.2 supports this observation, with the HPO fraction accounting for approximately 80 % of the UV_{254} absorbance of the raw source water. Similarly, only slight variation was observed in the O/C ratios. The lower O/C ratio of the HPO fraction is consistent with a higher proportion of aromatic and alicyclic hydrocarbon constituents of humic material (Lu *et al*., 2000), whilst the slightly higher value of the TPI fraction indicates a higher abundance of O-containing functional groups including O-alkyl, carboxylic acid and carbonyl carbon (Belzile *et al*., 1997; Lu *et al*., 2000).

A major distinction between the two fractions was the higher organic nitrogen concentration of the TPI fraction, reflected by the much lower C/N value. The ability of amino acid and peptide groups, major N-organic precursors of NOM, to form hydrogen bonds with surrounding water molecules contributes to the hydrophilic character of NOM (Westerhoff and Mash, 2002). Hence, organic nitrogen is generally concentrated in the more polar (i.e. hydrophilic or transphilic) fractions of NOM (Croué *et al*., 2003a). A C/N ratio > 20, as observed for the HPO fraction, is more typical of vascular land plants (Lu *et al*., 2000). The lower C/N ratio of the TPI fraction may reflect more significant contribution from nonvascular aquatic plant material (C/N in the range 2-10; Lu *et al*., 2000) or microbial biomass.

6.3.3.2 Fourier transform infrared spectroscopy

The FT-IR spectra of the NP HPO and TPI fractions (**Figure 6.2**) were very similar. Specific infra-red absorbance bands can be assigned to various functional groups (Silverstein and Webster, 1997). The intense, broad absorption at 3600 – 3250 cm^{-1} is due to hydrogen bonded hydroxyl groups of carbohydrates, carboxylic acids, phenols or alcohols (Silverstein and Webster, 1997). The partially resolved band at 3000 – 2800 cm^{-1} and the bands at 1460 cm^{-1} and 1380 cm^{-1} are characteristic of C-H stretching and symmetric and asymmetric bending of methyl and methylene groups, respectively.

Carboxylic acid functional groups of fulvic acids exhibit a broad band at 2750 – 2500 cm^{-1} (Leenheer and Rostad, 2004). The very prominent band centred at ca.

1720 cm^{-1} is indicative of C=O stretching due to the presence of carboxylic, ketonic, aldehydic or ester carbonyl groups. The bands at 1650 and 1560 cm^{-1} probably represent the combined contribution of the amide I (N-C=O; 1660 cm^{-1}) and amide II bands (N=C-O; 1540 - 1550 cm^{-1}) and N-H bending vibrations of amines (1650 – 1580 cm^{-1}). These signals are more pronounced for the TPI isolate indicating a higher contribution of proteinaceous or amino sugar structures (Leenheer and Rostad, 2004). Aromatic carbons (1600 and 1580 cm^{-1}) and aromatic carbonyl groups (1660 – 1630 cm^{-1}) can also give moderate bands in this region. The small absorbance at 900 – 700 cm^{-1} is also indicative of aromatic carbon (Leenheer and Rostad, 2004).

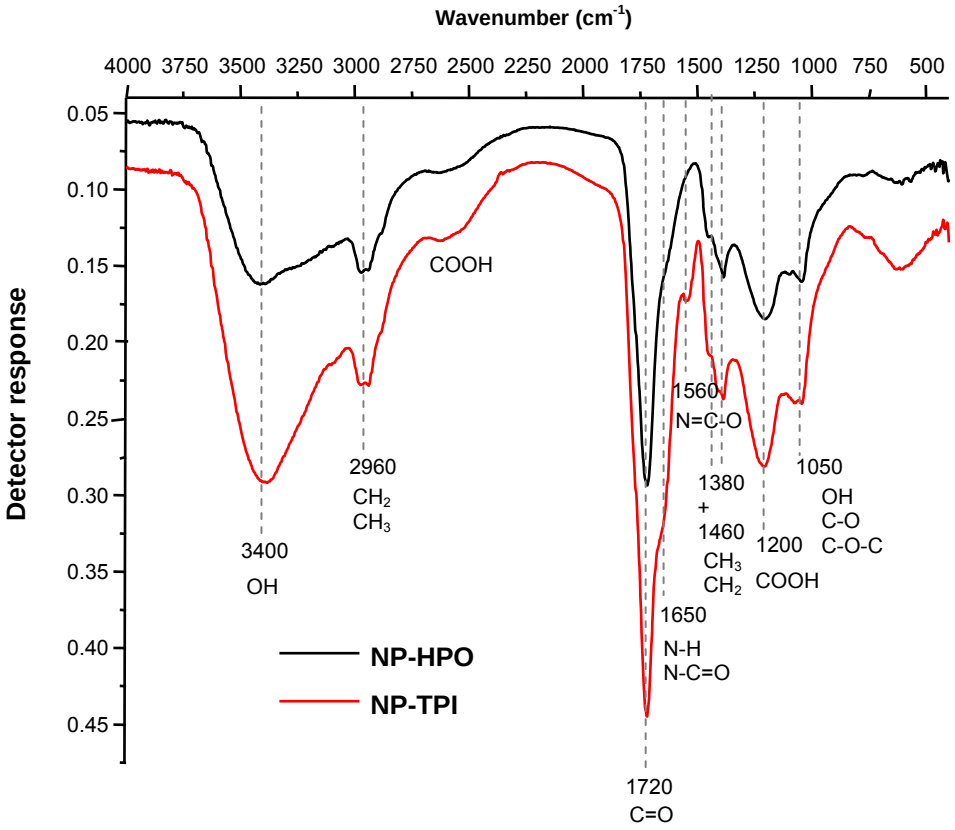

Figure 6.2 FTIR spectra of North Pine HPO and TPI fractions.

The HPO and TPI spectra also show several strong absorbance bands centered at 1000 – 1200 cm^{-1} assigned to O-H of alcohols (1000 – 1200 cm^{-1}), C-O stretching and O-H deformations of carboxylic acids (~1200 cm^{-1}), C-O stretching of esters (~1100 cm^{-1}), or C-O-C stretching of ethers (~1100 cm^{-1}; Silverstein and Webster, 1997). Overall, FTIR spectroscopy provided limited distinction between the HPO and TPI samples, with the major difference being a higher proportion of N and O

functional group signals from the TPI fraction, reflecting the higher concentration of more polar structural moieties in this fraction.

6.3.3.3 Cross polarization magic angle spinning ^{13}C-NMR spectroscopy

The solid state ^{13}C CPMAS NMR spectra of the NP HPO and TPI fractions (**Figure 6.3**) showed similar qualitative features, but noteworthy distinctions were evident on closer scrutiny. The NMR spectra were integrated over four spectral regions attributed to the following functionalities: 0 – 45 ppm assigned to alkyl carbon bonded to hydrogen; 45 – 110 ppm to O-alkyl carbons or N-alkyl carbons (e.g. carbohydrates, amines, alcohols); 110 - 165 ppm to aromatic and unsaturated C (Malcolm, 1990); and 165 – 185 ppm to carbonyl C in carboxylic acids, amides and esters (Croué *et al*., 2000; Hatcher *et al*., 2001; Keeler *et al*., 2006). The proportions of these carbon types in the two fractions are shown in **Table 6.4**. The results of spin counting showed that the observable carbon was 72 and 79 % for the HPO and TPI fractions respectively, indicating quantitative reliability.

Aliphatic carbon was the most abundant integral region of the HPO fraction, but can be overestimated using CPMAS due to a higher efficiency of magnetisation transfer from hydrogen to carbon in CH_2 groups compared with other carbon types (Wilson, 1987; Poirier *et al*., 2000; Quénéa *et al*., 2005a). The aliphatic region of both spectra can be separated into methyl carbons at 20 ppm, branched alkyl and quaternary aliphatic carbons at 42 ppm (McIntyre *et al*., 2005; Leenheer *et al*., 2003a; 2004), possibly indicative of highly branched and ring structures of terpenoids (Leenheer *et al*., 2003a), and methylene carbons at 30 ppm (González-Vila *et al*., 2001).

The major peak in the O-alkyl region of the HPO spectrum occurred at 76 ppm. The O-alkyl signal was more abundant for the TPI fraction (Table 6.4) and was centred at 72 ppm. This is indicative of oxygen linked aliphatic carbons of alcohols (van Heemst *et al*., 2000), ethers and esters (Leenheer and Rostad, 2004) or polysaccharides (Lu *et al*., 2000; Templier *et al*., 2005a, Quénéa *et al*., 2005a). The small shoulder at 106 ppm of the broad O-alkyl region is more prominent for the TPI fraction and is attributed to anomeric carbon of carbohydrates (Pastorova *et al*., 1994, McIntyre *et al*., 2005).

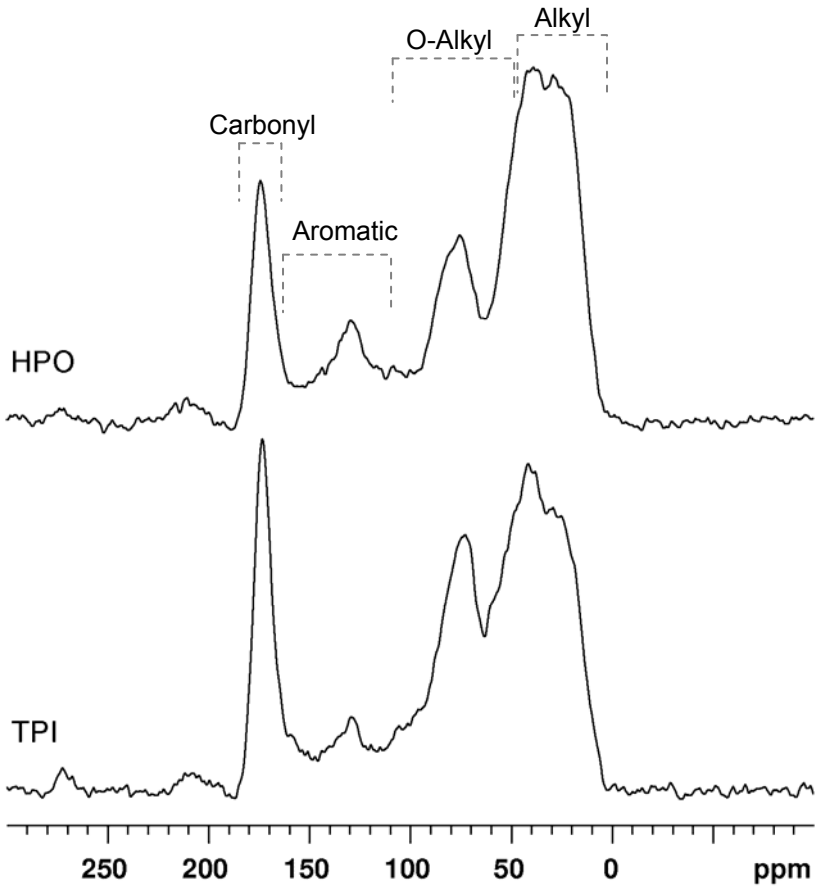

Figure 6.3 Solid state ^{13}C CPMAS NMR spectra of North Pine HPO and TPI NOM fractions (ppm is chemical shift in parts per million).

Table 6.4 Proportion of carbon types in the solid state ^{13}C CPMAS NMR spectra of the NP HPO and TPI fractions. % = percentage of total signal.

Sample	Carbonyl 185 - 165 ppm	Aromatic 165 - 110 ppm	O-alkyl 110 - 45 ppm	Alkyl 45 - 0 ppm
NP-HPO	11.4%	12.8%	33.4%	42.3%
NP-TPI	15.0%	10.4%	40.6%	34.1%

Aromatic C and unsaturated C contribute to the aryl signal intensities at 130 ppm. This spectral region was more abundant for the HPO fraction. A small shoulder at 156 ppm of the TPI spectrum corresponds to carbons bonded to phenolic OH groups found in lignin (McIntyre *et al*., 2005). The small shoulder at 58 ppm in the O-alkyl region corresponding to methoxy groups of lignin (Hatcher *et al*., 1980) is also

slightly more prominent for the TPI spectrum. However, the low abundance of this signal indicates only minor contribution from lignin-derived methoxy aromatics.

Carbonyl C of carboxylic acid, amide and esters at 172 ppm are significant components of both fractions but higher abundances were observed for the TPI fraction. Carboxylic acid groups may be formed by microbial oxidation of lignin side-chains (Saiz-Jimenez and de Leeuw, 1984b; Kirk and Farrell, 1987; Huang *et al*., 1998; Filley *et al*., 2000). The small spectral region from 190 – 220 ppm observed in similar abundance for both fractions corresponds to aldehydic and ketonic carbon. ^{13}C-NMR signals corresponding to amide and amine groups of proteins (C-N, 40-55 ppm and 160-190 ppm; Leenheer and Rostad, 2004) overlap those produced by alkyl, methoxyl and carbonyl structures (Gonzalez *et al*., 2003), so are not easily determined. However, a small shoulder peak at 52 ppm, more prominent for the TPI fraction, is likely caused by C-N linkages of amines and amides (Leenheer *et al*., 2004).

The high aliphatic, moderate carboxylic, and relatively low aromatic content identified by ^{13}C-NMR spectroscopy of both NP fractions may reflect a major contribution from terpenoid hydrocarbons. The HPO and TPI NMR spectra were very similar to those previously reported in the corresponding fractions of the Great Salt Lake (Leenheer *et al*., 2004), which were attributed to terpenoid precursors derived from primary production of algae and secondary production of bacteria. ^{13}C-NMR studies have characterised terpenoid-derived NOM fractions of landfill leachates, groundwaters and surface waters by high alicyclic ring structures and low numbers of carbon per rings, indicative of fused structures, with extensive methyl, branched alkyl, hydroxyl and carboxyl substitution (Leenheer, 2004, Leenheer and Rostad, 2004; Leenheer e*t al*., 2004). Low methoxy and aromatic content, both features of the NP NOM, distinguishes terpenoid derived NOM from tannin and lignin derived NOM (Leenheer *et al*., 2004; McIntyre *et al*., 2005).

^{13}C-NMR analysis revealed that the NP TPI fraction is richer in the more polar carbonyl and O-alkyl carbon, indicating a greater contribution from carbohydrate, alcohol, carboxylic acid, ester or amide functional groups. Methoxy phenolic structures of lignin were present in low quantities for both fractions, but were also

slightly enriched for the TPI fraction. Conversely, the HPO fraction was richer in the less polar aromatic and alkyl carbon. Lower quantities of oxygenated aliphatic carbon and enrichment of aromatic carbon has been associated with an increasing degree of humification involved in microbial and chemical degradation during diagenesis (Lu *et al*., 2000). However, the overall abundance of aromatic carbon is much lower than typically found in highly humic surface waters such as Suwannee River (Leenheer *et al*., 2003a) and Gartempe River (Templier *et al*., 2005a). This suggests that the HPO/humic materials of pristine water sources derive from alternative sources (i.e. terpenoids) or diagenetic processes to black waters, consistent with the differences in SUVA and elemental composition discussed previously.

6.3.4 MSSV pyrolysis GC-MS

The total ion chromatograms obtained by MSSV pyrolysis GC-MS of the NP HPO and TPI fractions are shown in **Figure 6.4**. **Table 6.5** comprises a list of the 100 most abundant MSSV products of each fraction and an indication of their relative abundance. The identified products were grouped into 10 major compound classes, which accounted for ca. 80-90% of the total MSSV product yield. These are semi-quantitatively compared in **Figure 6.5**. The values express the summed percentage of the total integrated pyrolysate area of each product group and were calculated as described in Chapter 3.3.2 (pg 71). The same semi-quantitative data of the flash pyrolysis analysis of each fraction is also shown in Figure 6.5 for comparison. MSSV pyrolysis yielded much higher product concentrations than flash pyrolysis, although several qualitative aspects of the product distributions of each method were similar.

Many qualitative similarities were evident in the MSSV pyrolysate distributions of the HPO and TPI fractions. The main distinction was the significantly higher abundance of aromatic hydrocarbons from the HPO fraction, and an enrichment of nitrogen-containing pyrolysates from the TPI fraction. The isomeric distribution, structural significance and possible sources of several prominent product classes were evaluated in further detail.

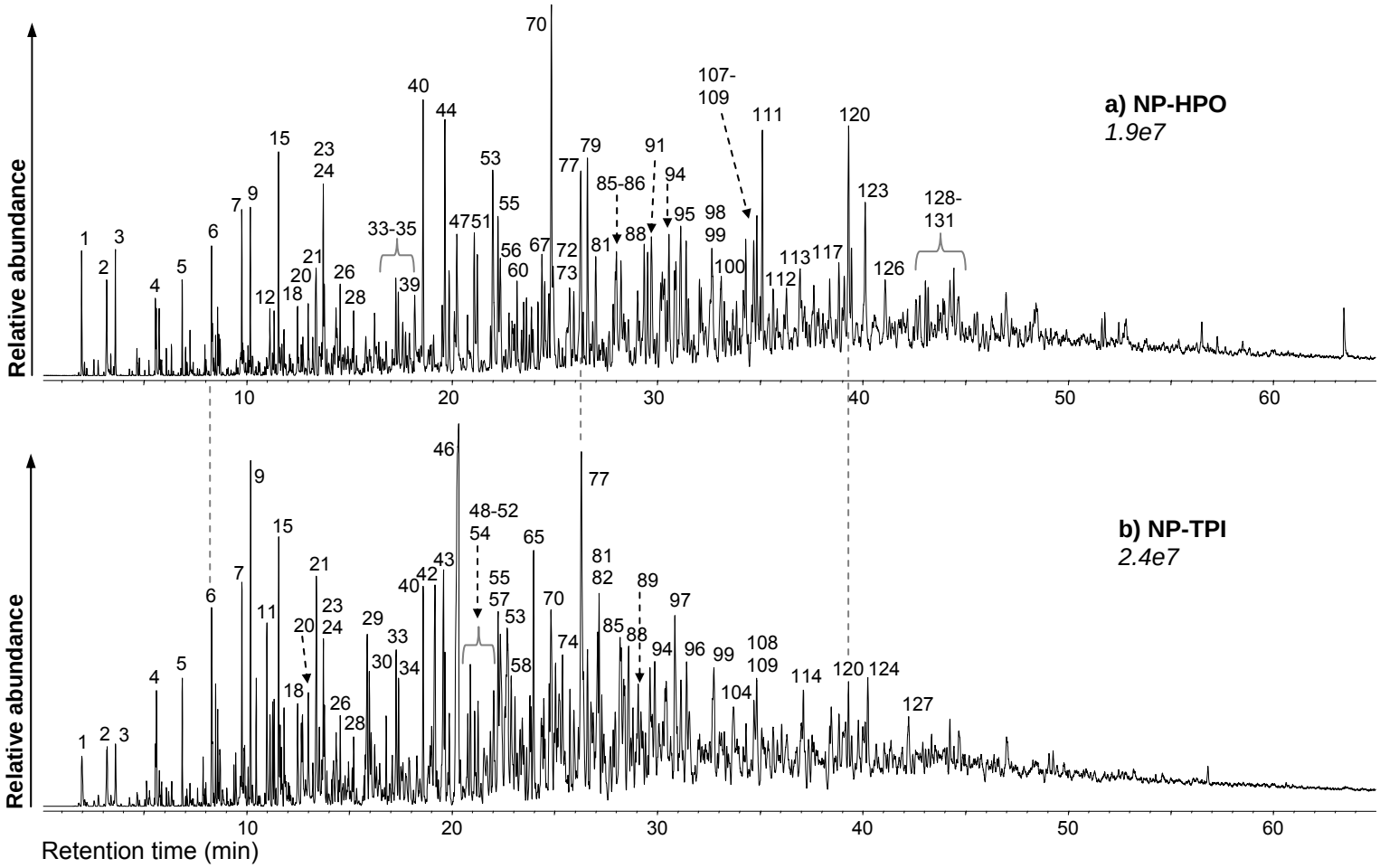

Figure 6.4 TICs obtained by 300°C/72hr MSSV pyrolysis GC-MS analysis of **a)** NP HPO; and **b)** NP TPI fractions. Peak assignments correspond to products listed in Table 6.5. Relative abundances of a-b are indicated in italics.

Table 6.5 Products detected by MSSV pyrolysis GC-MS of NP HPO and TPI fractions. The 100 most abundant products of each fraction are listed. A semi-quantitative indication of the relative abundance of each product is given as a percentage of the total peak area: * = < 0.5 %, ** = 0.5 – 1.5 %, *** = > 1.5 %, nd = not detected. A = low MW aliphatics, CA = cycloaliphatics, F = furans, B = benzenes, K = ketones, P = phenols, N = nitrogen-products, I = indenes, Na = naphthalenes, O = other.

Peak	Identification	Compound Class	HPO	TPI	Peak	Identification	Compound Class	HPO	TPI
1	1-butene	A	**	*	25	dimethylpyridine + dimethylheptadiene	N + A	nd	*
2	acetone	O	**	*	26	1,2 dimethylbenzene	B	**	*
3	2-methylbutene	A	*	*	27	ethylpyridine	N	nd	*
4	methylfuran	F	*	**	28	methylpropylfuran	F	*	*
5	methylcyclopentene	CA	*	*	29	dimethylpyrrole	N	*	**
6	dimethylcyclopentene	CA	**	**	30	ethylpyrrole + dimethylpyridine	N	nd	**
7	dimethylcyclopentene	CA	**	**	31	dimethylpyrrole + dimethylpyridine	N	nd	*
8	pyrrole	N	nd	*	32	dimethylpyridine	N	nd	*
9	toluene	B	**	**	33	1-methyl-3-ethylbenzene	B	*	**
10	methylheptane	A	*	*	34	1-methyl-4-ethylbenzene	B	*	**
11	methylheptene + methyleneheptane	A	*	**	35	1,3,5-trimethylbenzene	B	*	*
12	dimethylcyclohexene	CA	*	*	36	aniline	N	*	*
13	methylheptane	A	*	*	37	1-methyl-2-ethylbenzene	B	*	nd
14	acetylfuran	F	nd	*	38	trimethylpyrrole	N	*	*
15	trimethylcyclopentene	CA	**	**	39	phenol	P	**	*
16	ethylpyrrole	N	nd	*	40	1,2,4-trimethylbenzene	B	***	**
17	trimethylfuran	F	*	**	41	trimethylpyridine	N	*	**
18	methylethylcyclopentene + trimethylfuran	CA + F	**	**	42	ethylmethylpyrrole	N	*	**
19	methylpyrrole	N	nd	*	43	trimethyl pyrrole	N	*	***
20	tetramethylcyclopentene	CA	*	**	44	1,2,3-trimethyl benzene	B	***	**
21	ethylbenzene	B	**	**	45	1-methyl-4-isopropylbenzene (*p*-cymene)	B	**	**
22	dimethylpyrrole	N	nd	*	46	2-ethyl hexanol	O	*	***
23	1,3 dimethylbenzene	B	**	**	47	2,3-dimethyl-2-cyclopenten-1-one + trimethylcyclohexanone	K	**	nd
24	1,4 dimethylbenzene	B	*	*					

Peak	Identification	Compound Class	HPO	TPI	Peak	Identification	Compound Class	HPO	TPI
48	1,3-diethyl benzene	B	*	**	78	dimethylindane	I	*	nd
49	ethyldimethylpyrrole	N	nd	**	79	dimethylindane + C_5 benzene + 3,4-dimethyl phenol	I + B + P	***	**
50	1,4-diethylbenzene	B	nd	**	80	trimethylindane	I	*	nd
51	2-methylphenol	P	**	**	81	2,4,6-trimethylphenol	P	**	**
52	trimethyl-2-cyclopenten-1-one	K	**	*	82	ethyldimethylpyrrolidinedione	N	nd	**
53	3- and 4-methylphenol + dimethylethylbenzene	P + B	***	***	83	2-propylphenol + trimethylindane	I + P	**	nd
54	ethyldimethylpyrrole + trimethylpyridine	N	nd	**	84	C_3 phenol	P	*	nd
55	ethyldimethylbenzene + methylphenylcyclopropane	B	**	**	85	C_5 benzene + C_3 phenol	B + P	**	***
56	trimethyl-2-cyclopenten-1-one	K	**	nd	86	C_3 phenol + trimethylindane	I	**	nd
57	ethyldimethylpyrrole	N	*	***	87	2-methyl-4-isopropyl-2-cyclohexenone	K	*	nd
58	ethyldimethylpyrrole	N	*	**	88	trimethylphenol	P	**	**
59	2,4-dimethylacetophenone	B	*	nd	89	C_3 phenol + diethylpyrrolidinedione	P + N	*	*
60	2,6-dimethylphenol	P	**	**	90	trimethylphenol	P	**	**
61	ethylpyrrolidinedione	N	nd	*	91	dimethylindane + C_5 benzene + C_4 phenol	I + B + P	**	*
62	1,2,4,5-tetramethylbenzene	B	**	*	92	hexamethylbenzene	B	**	nd
63	1,2,3,5-tetramethylbenzene	B	*	*	93	trimethylindane	I	*	nd
64	ethyltrimethylpyrrole	N	nd	*	94	trimethylphenol + diethylphenol	P	**	**
65	tetramethylpyrrole	N	*	**	95	trimethylindane + C_3 phenol	I + P	**	nd
66	isopropyldimethylbenzene	B	*	nd	96	dihydro trimethyl indene	I	**	**
67	methylindane + 2-ethylphenol	I + P	**	**	97	C_4 phenol	P	*	**
68	isopropyldimethylbenzene	B	**	nd	98	C_4 phenol	P	**	**
69	methyl indane	I	**	**	99	C_4 phenol	P	**	**
70	1,2,3,4-tetramethylbenzene + 2,4-dimethylphenol	B	***	***	100	trimethylindene + trimethyltetralin	I + Na	**	*
71	ethyl trimethyl pyrrole	N	nd	**	101	trimethylindene	I	*	nd
72	4-ethylphenol	P	*	nd	102	trimethyltetralin	Na	*	*
73	3,5-dimethyl phenol	P	**	*	103	2,3-dihydro-trimethyl-1H-inden-1-one	I	**	nd
74	2,3-dimethyl phenol	P	*	**	104	methylindole	I	nd	**
75	ethyltrimethylpyrrole	N	nd	**	105	trimethyltetralin	Na	*	nd
76	ethyltrimethylpyrrole	N	nd	**	106	2,3-dihydro-trimethyl-1H-inden-1-one	I	*	*
77	dimethylindane + ethyltrimethylpyrrole	I + N	***	***	107	2,7-dimethylnaphthalene	Na	**	*

Peak	Identification	Compound Class	HPO	TPI
108	1,3- + 1,7-dimethylnaphthalene	Na	**	**
109	1,6-dimethylnaphthalene	Na	**	**
110	tetramethylphenol	P	*	nd
111	diphenylmethane	B	**	nd
112	trimethyltetralin	Na	**	nd
113	diphenylethane + tetramethyltetralin	B + Na	**	nd
114	dimethylindole	N	nd	**
115	di-*tert*-butylphenol	P	**	nd
116	1,3,6-trimethylnaphthalene	Na	**	*
117	1,4,6- + 1,3,5-trimethylnaphthalene	Na	**	*
118	trimethylnaphthalene	Na	*	nd
119	dimethyl diisopropyl benzene	B	**	nd
120	1,2,7-trimethylnaphthalene	Na	***	*
121	1,6,7- + 1,2,6-trimethylnaphthalene	Na	**	nd
122	trimethylindole	N	nd	*
123	1,2,5-trimethylnaphthalene	Na	**	nd
124	trimethylindole	N	nd	**
125	trimethylindole	N	nd	*
126	C_4 naphthalene	Na	**	nd
127	C_4 indole	N	nd	**
128	C_4 naphthalene	Na	*	nd
129	C_4 naphthalene	Na	**	nd
130	C_4 naphthalene	Na	*	nd
131	C_4 naphthalene	Na	*	nd

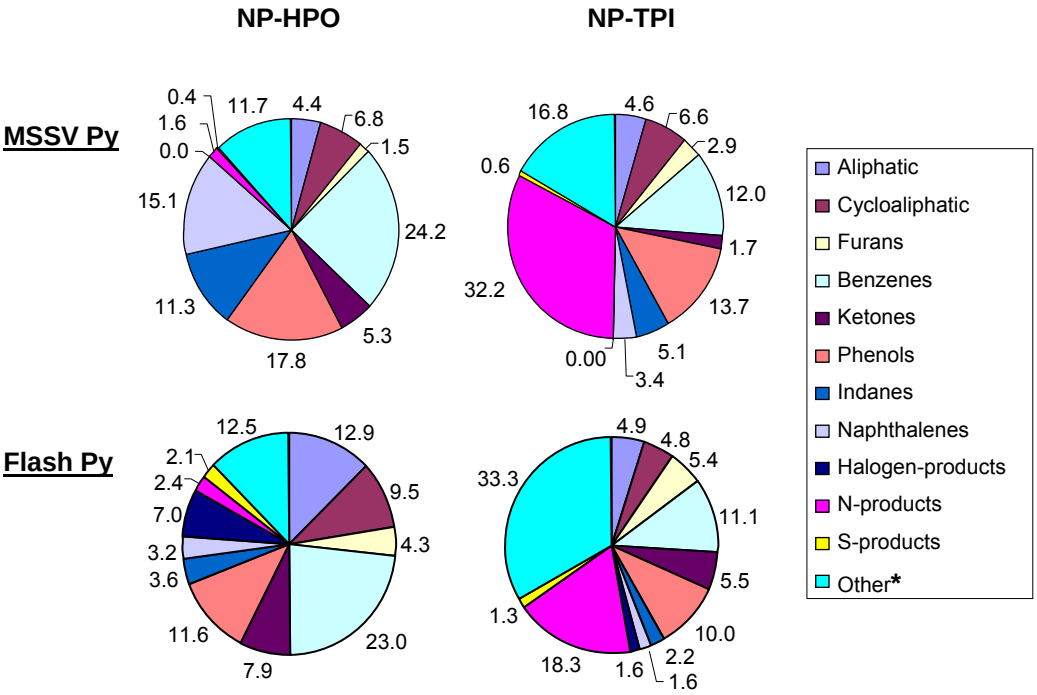

Figure 6.5 Relative proportions of major product classes detected by MSSV pyrolysis and flash pyrolysis of NP HPO and TPI NOM fractions. Other***** = identified peaks not classified into one of the 10 product groups, or peaks that could not be identified due to low abundance and/or poor mass spectra.

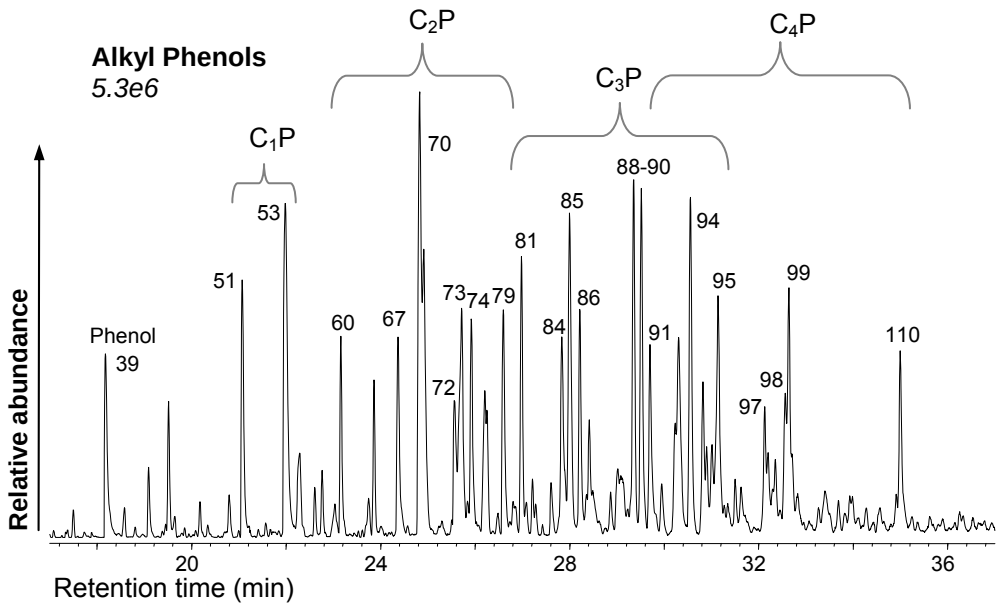

Figure 6.6 Summed *m/z* 94+107+108+121+122+135+136+150 chromatograms showing the distribution of alkyl ($\leq C_4$) phenols from the MSSV pyrolysis GC-MS analysis of NP HPO. Peak assignments correspond to products listed in **Table 6.5**. Relative abundance is indicated in italics.

6.3.4.1 Hydrophobic fraction

Alkyl substituted benzenes and polycyclic aromatic hydrocarbons (PAHs) were the most abundant MSSV pyrolysates of the HPO fraction, accounting for ca. 68 % of the total integrated pyrolysate area. The major products were alkyl ($\leq C_6$) benzenes, alkyl ($\leq C_4$) phenols, alkyl (C_1-C_4) naphthalenes and partially hydrogenated PAHs, including alkyl (C_1-C_3) indanes and alkyl (C_1-C_3) tetrahydronaphthalenes (tetralins). This product distribution was very different to the HPO fractions of the surface black waters studied in previous chapters (e.g. Uruguay, Gartempe Rivers), showing higher concentrations of aromatic hydrocarbons (e.g. alkyl naphthalenes) and lower relative abundances of phenols. These same pyrolysate features were also noted from the MSSV analysis of terpenoid derived ground water NOM (see Chapter 3.3.2.2, Lavaud *et al*., 2008).

6.3.4.1.1 Alkyl phenols

Alkyl ($\leq C_4$) phenols (APs) were prominent products of the NP HPO fraction. The AP distribution is shown in the summed ion chromatograms of **Figure 6.6** and the product list of **Table 6.5**. Parent and monomethyl phenols were also prominent flash pyrolysates; however the higher MW alkyl ($\geq C_2$) phenols were detected in much lower concentration. APs are very common pyrolysates of aquatic and terrestrial humic substances and are often attributed to intact or partially degraded lignin structures, as discussed in Chapter 4 (e.g. Saiz-Jimenez and de Leeuw, 1986b; Bruchet *et al*., 1990; Templier *et al*., 2005a). Several of the prominent AP isomers, including 2-methylphenol (51), 2,6-, 2,4- and 2,5-dimethylphenol (60, 70), 2,4,6-trimethylphenol (81), ethylmethylphenol (84) and unspecified trimethylphenol isomers (89-90), were also detected in high abundance from the corresponding MSSV pyrolysis (300˚C/72hr) of a lignin standard (Chapter 4). Lignin is therefore a likely precursor of some of the AP pyrolysates of the HPO fraction.

However, methoxyphenol pyrolysates, which are unequivocal indicators of lignin (Hedges and Mann, 1979; Ertel *et al*., 1984; Saiz-Jimenez and de Leeuw, 1986a; Opsahl and Benner, 1997), were not detected by either flash or MSSV pyrolysis, consistent with the low methoxy content detected by ^{13}C-NMR. This contrasts with the riverine black waters studied in Chapter 4 (e.g. Gartempe, Uruguay), which yielded several prominent methoxyphenol products. This may indicate more

substantial contribution from *p*-coumaryl (i.e. non-methoxylated) lignin units, which are characteristic of non-woody (i.e. grass) tissues (Ertel *et al*., 1984; Challinor, 1995; Pancost and Boot, 2004; Quénéa *et al*., 2006). This would be consistent with the surrounding vegetation of the NP catchment, which has been largely cleared or modified for grazing, agriculture and rural residential subdivisions (SEQWater and Brisbane Water, 2006).

The broad MSSV distribution of APs from the HPO fraction likely reflects contribution from other sources. The low colour of the NP source water and the relatively low aromatic C content detected by NMR suggests only minor input from plant tannins. Lehtonen *et al*. (2000b) attributed AP pyrolysates of lake humic substances to carbon-carbon bound alkyl aromatic networks, as opposed to phenolic-carboxylic acid structures characteristic of degraded lignin. The origins of these APs were attributed to algal derived compounds, including tyrosine moieties of proteins and selectively preserved phenolic biomolecules (phlorotannins). van Heemst *et al*. (1996) demonstrated that APs were major flash pyrolysis products of algal phlorotannins. Sediment accumulation in NP Dam can lead to increased nutrient inputs resulting in algal blooms. This is a significant problem for this source water (Burford *et al*., 2007). De-stratification of NP Dam has not been successful at controlling the levels of toxic cyanobacteria (Littlejohn, 2004), and it was closed in August 1995 due to excessive cyanobacterial levels. Therefore, phenolic biomolecules of aquatic algae may contribute to the AP distribution of the NP fractions (van Heemst *et al*., 2000). APs have been postulated to be more strictly bound macromolecular components than esterified or acidic lignin phenols not containing alkyl groups (Lehtonen *et al*. 2000a). The softer thermal release of covalently bound APs by MSSV pyrolysis may partially preserve their alkyl substitution patterns and contribute to the higher concentrations of more highly substituted alkyl (C_2-C_4) phenols than were evident by flash pyrolysis. The high alkyl substitution is consistent with the high content of methyl and branched alkyl groups detected by ^{13}C-NMR spectroscopy.

In addition to grass lignin and phenolic compounds derived from algae, diagenetically modified terpenoids also likely contribute to the AP distribution. As discussed previously (section 6.3.3.3), the NMR spectral characteristics of NP HPO

resembled HPO fractions of the Great Salt Lake, which were found to be derived from algal and bacterial terpenoids (Leenheer *et al*., 2004). Model structures of this fraction proposed by Leenheer *et al*. (2004) were based on alicyclic ring structures extensively substituted with alkyl, carboxyl and hydroxyl groups. Thermal release and aromatisation of alkyl and hydroxyl substituted aliphatic ring structures to form APs may occur during MSSV pyrolysis. This origin would be consistent with the relatively low aromatic content and high aliphatic hydroxyl group (O-alkyl) content detected by ^{13}C-NMR spectroscopy. The occurrence of the (tentatively identified) monoterpene C_4 APs thymol and carvacrol may also indicate the presence of phenolic higher plant terpenoids.

6.3.4.1.2 Alkyl naphthalenes and other polycyclic aromatic hydrocarbons

High concentrations of PAHs, including alkyl (C_1-C_5) naphthalenes (ANs), alkyl (C_1-C_3) indanes (dihydroindenes) and alkyl (C_1-C_4) tetrahydronaphthalenes (tetralins), were detected from the MSSV pyrolysis of North Pine HPO. Flash pyrolysis yielded very low concentrations of these products. The AN and hydroaromatic distributions are shown in **Figure 6.7**. The high concentration of these products contrasts with their much lower abundance in the HPO fraction of the black water Gartempe River, reflecting an important difference in the structural characteristics of humic substances from pristine and black water sources.

Chapter 3 provided a comprehensive investigation of the distribution of ANs from several likely NOM precursors, including lignin, terpenoids, aromatic amino acids and proteins. ANs were strongly correlated with higher plant terpenoids due to their high concentrations in the HPO fraction of terpenoid rich ground water, and in the MSSV pyrolysates of extant bark samples of *Pinus radiata* and *Wandoo eucalyptus*. Several of the major AN products of these samples, including 1,6-dimethylnapthalene (109), 1,2,5-, 1,2,7-, 1,6,7- and 1,2,6-trimethylnapthalene (120, 121, 123), methylisopropylnaphthalene (126), tetramethylnaphthalene (131) and cadalene (C) were also detected in high abundance from the NP HPO fraction. ANs, as well as alkyl benzenes and alkyl phenanthrenes, were recently reported as major flash pyrolysis products of the HPO fraction of a municipal landfill leachate (Leenheer *et al*., 2003a) and were also attributed to highly branched terpenoids from plant resin acids (Leenheer *et al*., 2003a).

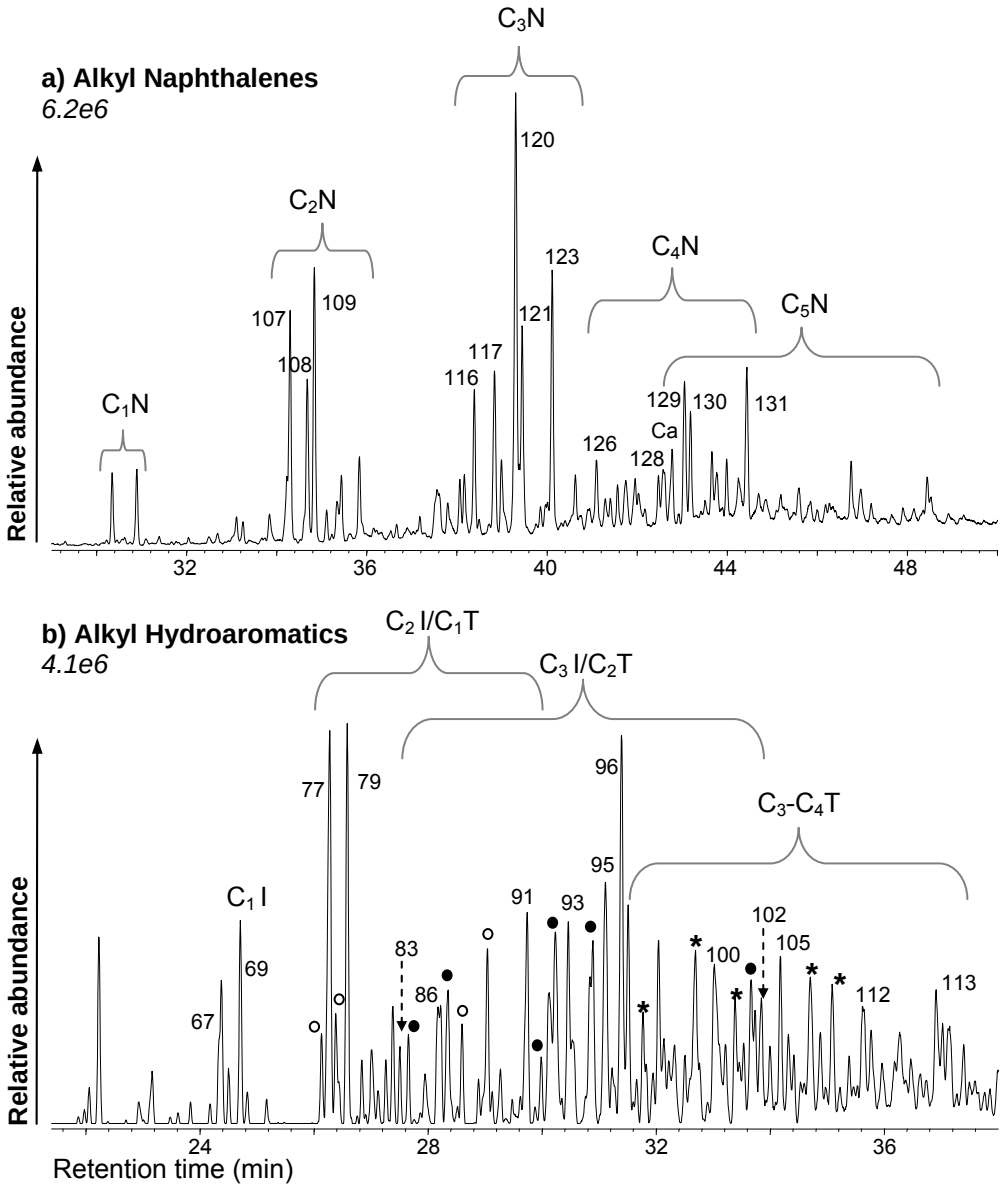

Figure 6.7 Summed **(a)** *m/z* 142+156+170+184+198+133+134+148 and **(b)** *m/z* 117+131+132+145+146+159+160+174 chromatograms showing the distribution of alkyl naphthalenes (C_xN, x = number of alkyl carbons) and alkyl indanes (I) and tetralins (T) from the MSSV pyrolysis GC-MS analysis of NP HPO. Relative abundances of a-b are indicated in italics. Peak assignments correspond to products listed in Table 6.5. Additional hydroaromatics (non-integrated peaks): ∘ = $C_2I + C_1T$, • = C_3I/C_2T, * = C_3T.

Many cyclic aliphatic higher plant terpenoids undergo aromatisation during natural or artificial maturation (Hayatsu et al., 1990; van Aarssen et al., 2000). A high aliphatic 13C-NMR signal was measured for NP HPO and aromatisation of alicyclic terpenoids during MSSV thermal treatment may contribute to the high

concentrations of aromatic hydrocarbon products. Straight chain aliphatics such as fatty acids are readily mineralised by microbial activity; however branched and cyclic aliphatic terpenoid molecules are refractory to aerobic degradation processes (McDonald et al., 2004). The lack of significant amounts of long chain aliphatic pyrolysates by MSSV pyrolysis, flash pyrolysis and thermochemolysis (Chapter 6.3.5) suggests the high alkyl carbon content detected by NMR probably reflects highly branched and cyclic aliphatic structures of terpenoids (Lu *et al*., 2003).

Naturally occurring terpenoids occur in an extremely wide variety of structural configurations and may be subject to alteration during diagenesis or MSSV thermal treatment. As such, it is difficult to unequivocally correlate individual AN pyrolysates to specific terpenoid precursors. Nevertheless, possible terpenoid sources may be inferred for several abundant AN products. Trimethylnaphthalenes (TMNs) dominated the AN distribution of the NP HPO fraction. High concentrations of TMNs have previously been reported in immature sediments rich in higher plant terpenoids (Püttman and Villar, 1987; Strachan *et al*., 1988; Almendros *et al*., 1998). 1,2,5-TMN and 1,2,7-TMN, the most abundant isomers of NP HPO, are diagenetic products of oleanane type pentacyclic triterpenoids such as β-amyrin, which are specific to flowering plants (Strachan *et al*., 1988, Watson *et al*., 2005). 1,2,5-TMN may also form from bicyclic diterpenoids and resins common in conifers, or the compound onocerane, which has been found in a variety of vascular plants (Pearson and Obaje, 1999; Watson *et al*., 2005).

1,6-dimethylnaphthalene, the most abundant C_2 isomer of NP HPO, can derive from sesquiterpenoids of essential oils and plant resins (Simoneit, 1985; van Aarssen *et al*., 1991). The sesquiterpenoids cadalene (Ca) and methylisopropylnaphthalene (126) were also detected in low concentration. Tetramethylnaphthalenes (TeMNs) may derive from oxygenated triterpenoids (e.g. arborene and fernene) or from bicyclanes (Bastow, 1998). Alternatively, co-occurrence of 1,2,5-TMN and 1,2,5,6-TeMN (tentatively peak 131) in extracts and flash pyrolysates of immature brown coal have been attributed to C-ring cleavage of bacterial hopanoids (Püttman and Villar, 1987; Sinninghe Damste *et al*., 1992b).

Although their specific isomeric identities were not determined, the general detection of high concentrations of hydroaromatics including C_1-C_4 tetrahydronaphthalenes (tetralins) and C_1-C_3 dihydroindenes (indanes) in the HPO fraction provides further evidence of a significant contribution of plant terpenoids. Except for the methyl indanes, hydroaromatics were not detected by flash pyrolysis. Confined gold tube pyrolysis has shown that plant resins yield a range of hydronaphthalenics (Michels *et al*., 2000), which are very efficient hydrogen donors and contribute significantly to the generation of petroleum hydrocarbons from humic substances in coal (Hayatsu *et al*., 1990; Michels *et al*., 2000). Hydroaromatics probably represent intermediates in the aromatisation of alicyclic terpenoid structural moieties (Wakeham, 1980; Simoneit *et al*., 1986; Hayatsu *et al*., 1987). However, alkyl indanes may also be produced by the MSSV thermal alteration of polysaccharides such as cellulose, as discussed in Chapter 4.3.3.

6.3.4.1.3 Alkyl benzenes

Alkyl ($\leq C_5$) benzenes (ABs) were major products of the NP HPO fraction. Their isomeric distribution is shown in **Figure 6.8**. Flash pyrolysis similarly yielded high concentrations of ABs but mostly with alkyl substituents $\leq C_3$. No C_5-C_6 ABs were detected and the C_4 products were present in very low abundance. Low MW ABs ($\leq C_3$) offer limited source diagnostic value as they are ubiquitous pyrolysates of aquatic NOM and can derive from a variety of biomolecular sources.

The ABs of the NP HPO fraction likely include both primary alkyl-linked aromatic structures (e.g. Schulten *et al*., 1987; Schulten, 1996 a,b), as well as secondary products from the thermal alteration of other NOM moieties. MSSV reduction of aromatic carboxylic acid groups may be one possible route to ABs. ^{13}C-NMR analysis showed that NP HPO contained moderate carboxyl content. Thermochemolysis of this fraction also detected several aromatic carboxylic acids (as methyl esters; Chapter 6.3.5). Chemical reduction using *n*-butylsilane has proven effective for converting polycarboxylic acid constituents of aquatic fulvic acids to their corresponding ABs (Nimmagadda *et al*., 2006; 2007a). The thermal conditions of MSSV pyrolysis may favour a similar conversion.

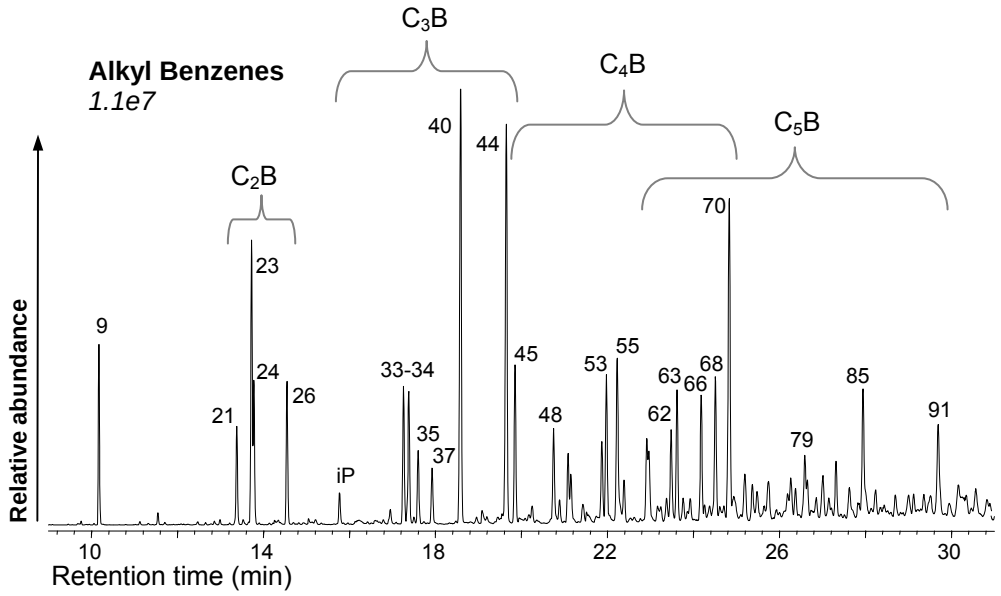

Figure 6.8 Summed *m/z* 91+105+106+119+120+133+134+148 chromatograms showing the distribution of C_1-C_5 alkyl benzenes from the MSSV pyrolysis GC-MS analysis of North Pine HPO. Peak assignments correspond to products listed in **Table 6.5**. Relative abundance is indicated in italics.

However, the very high concentration of ABs is inconsistent with the relatively low aromatic C content detected by ^{13}C-NMR spectroscopy. This suggests that secondary cyclisation and/or aromatisation of aliphatic and alicyclic terpenoids may be a significant source of ABs, analogous to the thermal formation pathway proposed for the dominant AN pyrolysates. Higher plant terpenoids, carotenoids and alkaloids are potentially significant precursors of sedimentary ABs (Hartgers *et al*., 1994 a,b; Hoefs, 1995; Clegg *et al*., 1997). Furthermore, Schulten and Gleixner (1999) isotopically correlated alkyl benzene pyrolysates of some aquatic humic acids with natural terpenes (Schmidt *et al*., 1995). Several of the prominent ABs detected from NP HPO, including isopropylbenzene (iP), *p*-cymene (peak 45) and isopropyldimethylbenzenes (peaks 66 and 68), were previously observed in the other NOM fractions studied and were correlated with terpenoid constituents of higher plants (Chapter 3.3.3.2 b). The high abundance of 1,2,3,4- and 1,2,3,5-tetramethylbenzene (peaks 63 and 70) may also indicate contribution from bacterial or algal carotenoids (Hartgers *et al*., 1994 b,c; Brown *et al*., 2000; Pedentchouk *et al*., 2004).

6.3.4.1.4 Furans and cyclic ketones

MSSV pyrolysis of NP HPO (Fig 6.4) also yielded several cyclic oxygen-containing products including alkyl furans, benzofurans, and cyclic ketones. These products were detected in lower relative abundance than the alkyl phenolic and aromatic hydrocarbon products. The prominent furans were methylfuran (4), dimethylfuran, acetylfuran (14), trimethylfurans (17, 18) methylpropylfuran (28) and dimethyl benzofurans. The major ketone products were polymethyl (C_1-C_4) substituted cyclopentanones and cyclopenten-1-ones (47, 52, 56), trimethylcyclohexanones and methylisopropylcyclohexenone (87). Major sources of furans and cyclic ketones include carbohydrates such as simple sugars (e.g. glucose, fructose), polysaccharides (e.g. cellulose, hemicellulose and pectin), and their microbial metabolites (e.g. Pouwels *et al*., 1987; Pastorova *et al*., 1994, Almendros *et al*., 1997, Reeves and Francis, 1997, Paine *et al*., 2008). The furan and cyclic ketone products detected from NP HPO were also detected by MSSV pyrolysis of the cellulose standard (Chapter 4.3.3). Flash pyrolysis yielded slightly higher proportions of furans, however this may be due to the much lower concentrations of other pyrolysates such as APs and ANs. Cyclic ketones were detected in similar relative abundance by both pyrolysis methods.

Pyrolysates indicative of unaltered polysaccharides, such as levoglucosan, levoglucosenone or 1,4:3,6-dianhydro-α-D-glucopyranose (Pouwels *et al*., 1987, Pastorova *et al*., 1994), were not detected by either MSSV or flash pyrolysis. ^{13}C-NMR similarly showed little evidence of intact polysaccharide input, with very low signal intensity in the O-alkyl region (106 ppm) for anomeric carbon of carbohydrates. Carbohydrates are a major energy source for micro-organisms, and are rapidly and preferentially mineralised (*cf* lignins and terpenoids) during early diagenesis (Hedges *et al*., 1985; Almendros *et al*., 1997; Huang *et al*., 1998; Lu *et al*., 2001). Whilst the contribution to the NP HPO fraction may be minimal, carbohydrate occurrence in complex environmental samples may be underestimated using pyrolytic techniques due to excessive thermal degradation and formation of non-diagnostic pyrolysates (Gauthier *et al*., 2003). Furthermore, diagenetically altered carbohydrates may be incorporated into resistant heterocyclic and aromatic structures within the humic fraction of NOM (Abbt-Braun *et al*., 1989; Almendros *et al*., 1997; Lu *et al*., 2000; 2001).

6.3.4.1.5 Low MW aliphatic products

Low MW aliphatics were also prominent MSSV products from the NP HPO fraction. These included C_4-C_8 branched alkanes and alkenes, and alkyl (C_1-C_4) cyclopentenes and cyclohexenes. Flash pyrolysis also generated high concentrations of low MW aliphatics displaying a range of unsaturation and alkyl substitution. The high concentration of these pyrolysates is consistent with the high aliphatic carbon signal measured by ^{13}C-NMR analysis. Monoterpenes from algal, bacterial and higher plant sources, or their microbial metabolites, are likely to contribute to the high yields of low MW aliphatic products. Several monoterpenes including camphene and methylisopropylcyclohexenes (menthenes) were also tentatively identified. Recent chemical reduction studies of terpenoid derived fulvic acids from Antarctic locations (Nimmagadda and McRae, 2007b) also identified several terpene hydrocarbons (e.g. camphene, myrcene, limonene and pinene).

Alkyl cyclopentenes (peaks 5-7, 15, 18, 20; Fig. 6.4) were detected in particularly high concentration. These products were also detected in high abundance by MSSV pyrolysis of the cellulose standard (Chapter 4.3.3), suggesting their occurrence in the NP NOM may be due to carbohydrate structural precursors. Almendros *et al*. (1997) also identified unsaturated aliphatic products in the pyrolysates of thermally treated carbohydrates. However, the low concentration of carbohydrate-derived furan products suggests an alternative origin. Alkyl substituted alicyclic products have been attributed to small cyclic polycarboxylic acids on the basis of chemical reduction analyses of aquatic, soil and peat fulvic acids (Nimmagadda *et al*., 2007a).

6.3.4.2 Transphilic fraction

MSSV pyrolysis of the NP TPI fraction showed similar concentrations of alkyl phenols and low MW aliphatic and cycloaliphatic products to the HPO fraction, whilst aromatic hydrocarbons (e.g. benzenes, naphthalenes, indanes) were detected in much lower abundance. Conversely, alkyl furans and nitrogen-containing products (N-products) were more abundant from the TPI fraction, consistent with the higher O-alkyl, amide and amine signals of the ^{13}C-NMR and FTIR data. The same trends were generally evident from the corresponding flash pyrolysis data, except that higher proportions of low MW aliphatic products were detected from the HPO fraction by flash pyrolysis.

6.3.4.2.1 Nitrogen-containing products

N-products accounted for more than 30 % of the total pyrolysate area of the NP TPI data, indicating a significant contribution from N-organic precursors such as amino acids, proteins and amino sugars. This is consistent with the higher organic nitrogen content and lower C/N ratio of the TPI fraction (Table 6.3), and the higher proportions of amide and amine functional groups measured by both FTIR and ^{13}C-NMR. Flash pyrolysis also detected higher concentrations of N-products in the TPI fraction, although their total abundance was much lower than the MSSV data, and typically showed less alkyl substitution.

The major N-products detected by MSSV pyrolysis of NP TPI were alkyl substituted heterocyclic aromatics including alkyl ($\leq C_3$) pyridines, alkyl ($\leq C_5$) pyrroles, alkyl (C_2-C_4) pyrrolidinediones and alkyl (C_1-C_4) indoles. The summed ion chromatograms of **Figure 6.9** selectively reveal the distributions of alkyl pyrroles and pyridines. The high concentrations of heterocyclic N-products probably represent primary or secondary pyrolysates of degraded peptides and proteins autochthonously derived from aquatic algae or bacteria. The prominent amide and amine FTIR signals of NP TPI indicate proteinaceous input. Low MW alkyl ($\leq C_3$) pyrroles (peaks 8, 16, 19, 22, 29, 30, 31, 38, 42, 43, 49), were also detected in high concentrations by MSSV pyrolysis of the pentaglycine (peptide) and albumin protein standards investigated in Chapter 5.3.4.2. Alkyl indoles (104, 114, 122, 124, 125, 127), which likely derive from tryptophan-containing peptides and proteins (Chiavari and Galletti, 1992), were also prominent in the TPI fraction. Alkylated pyrrolidinediones (61, 82, 89) have also been previously detected in protein pyrolysates (Boon and de Leeuw, 1987).

The flash pyrolysis data also included low concentrations of several protein-derived N-products not detected by MSSV. These included benzonitrile (Tsuge and Matsubara, 1985), methylbenzonitrile, 2-methyl-1*H*-isoindole-1,3(2*H*)-dione, hexahydropyrrolo[1,2-α]pyrazine-1,4-dione and 2,5-diketopiperazine. The latter two compounds have been attributed to intact proteins (Bruchet *et al*., 1990; Chiavari and Galletti, 1992; Voorhees *et al*., 1994; Basiuk and Douda, 2000; Douda and Basiuk, 2000; Sharma *et al*., 2005), possibly indicating the presence of low amounts of intact

proteinaceous material sequestered within the macromolecular structure (Knicker and Hatcher, 1997; Zang *et al*., 2000).

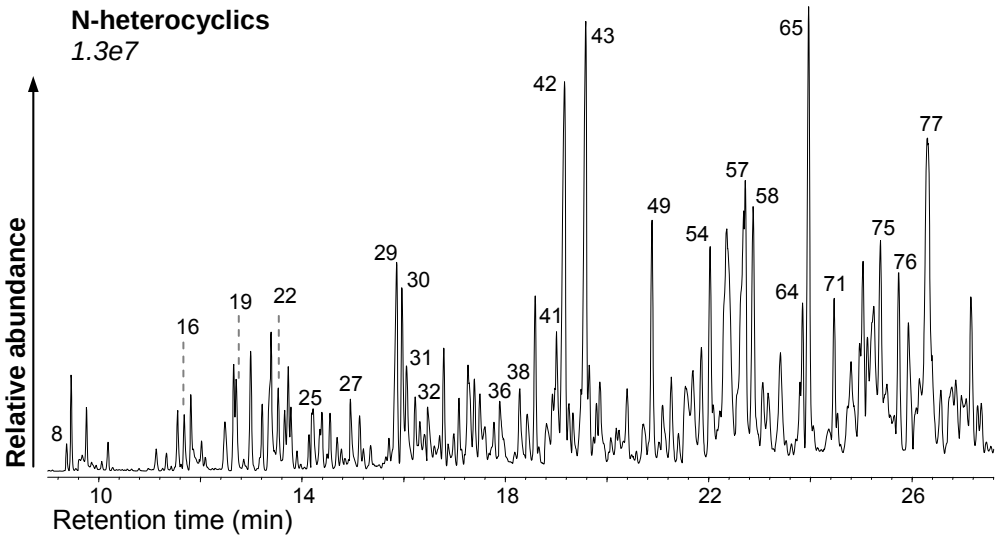

Figure 6.9 Summed *m/z* 79+80+93+94+106+107+108+109+120+121+122+123 chromatograms showing the distribution of alkyl pyrroles and pyridines from the MSSV pyrolysis GC-MS analysis of the NP TPI fraction. Peak assignments correspond to products listed in Table 6.5. Relative abundance is indicated in italics.

However, most of the major N-heterocyclic products probably represent pyrolysis fragments of diagenetically degraded proteinaceous material, rather than intact proteins. ^{13}C-NMR spectroscopy, chemical degradation and pyrolysis-mass spectrometric data have indicated that N-heterocycles are significant components of humic substances from soil, aquatic and recent sedimentary environments (Ikan *et al*., 1992; Patience *et al*., 1992; Schulten and Schnitzer, 1998; Schulten and Gleixner, 1999; Westerhoff and Mash, 2002; Mao *et al*., 2007). Melanoidin type structures formed by the cross-linking of heavily degraded proteins and polysaccharides, derived from both terrestrial and aquatic algal and bacterial sources, may also be significant structural precursors of N-heterocyclic pyrolysates of the TPI fraction (Patience *et al*., 1992; Peulve *et al*., 1996; van Heemst *et al*., 1999; 2000; Garcette-Lepecq *et al*., 2000; Poirier *et al*., 2000), as discussed in Chapter 5.3.5.

Thermal degradation of refractory N-acetylaminosugar polymers (e.g. peptidoglycan) derived from the decomposition of bacterial and algal cell walls may also contribute to the abundant N-pyrolysate distributions. Like the protein standards, MSSV pyrolysis of the amino sugar standard chitin yielded high concentrations of low MW N-heterocyclic products (Chapter 5.3.4.3). Alkyl pyridines were particularly prominent and several of these were detected from the NP TPI fraction (peaks 25, 27, 30, 31, 32, 41, 54). Structural models proposed by Leenheer (2004) and Leenheer *et al*. (2004) of TPI NOM fractions isolated from various surface waters included significant contributions from amino sugars. However, characteristic acetamide products of aminosugars (Stankiewicz *et al*., 1996; Steinbrecht and Stankiewicz, 1999) were not identified by either flash or MSSV pyrolysis, suggesting that peptidic N is a more significant precursor of the N-pyrolysates of the TPI fraction.

The MSSV pyrolysis detection of higher MW alkyl (C_4-C_5) pyrroles (54, 57, 58, 64, 65, 71, 75-77) in the NP TPI fraction may also reflect the presence of tetrapyrrole porphyrin pigments (e.g. chlorophyll) derived from land plants or photosynthetic aquatic organisms. MSSV pyrolysis of a porphyrin standard (Chapter 5.3.4.4) yielded a very distinctive distribution of pyrrole products, dominated by C_4-C_6 alkyl substituents. Degradation products of porphyrins have previously been identified as aquatic NOM constituents, although they are typically concentrated in hydrophilic base fractions (Leenheer, 2004).

6.3.5 Thermochemolysis GC-MS

The TICs obtained by tetramethylammonium hydroxide (TMAH) thermochemolysis GC-MS analysis of the NP HPO and TPI fractions are presented in **Figure 6.10**. Thermochemolysis with TMAH promotes the methylation of carboxylic acid and hydroxy functional groups (Challinor, 1989). A list of the unique TMAH products is shown in **Table 6.6**. Both fractions showed similar methyl esters of aliphatic and aromatic carboxylic acids that were not detected by either flash or MSSV pyrolysis. The detection of carboxylic acid TMAH products is consistent with the moderate carboxyl group content of both fractions measured by ^{13}C-NMR analysis.

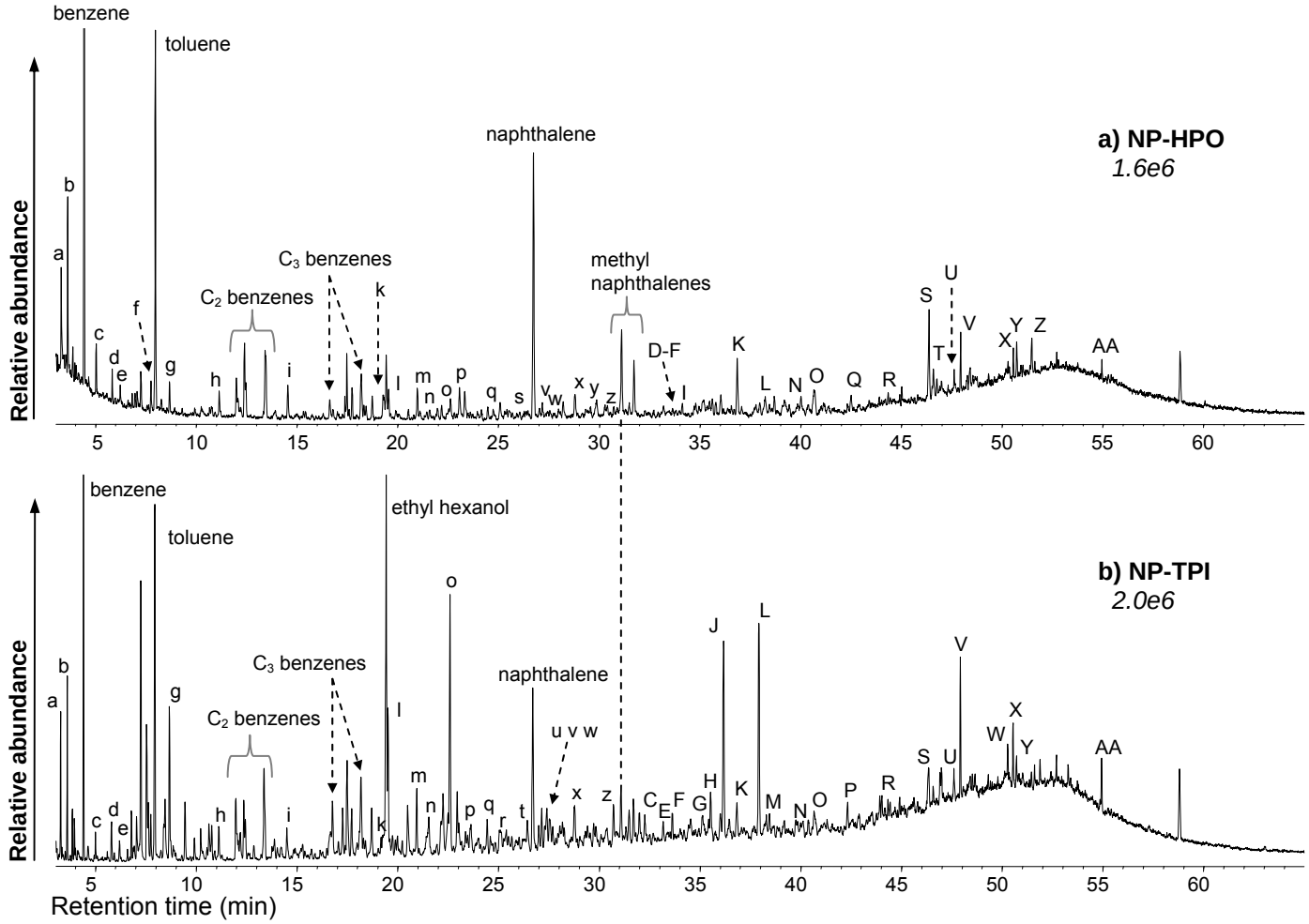

Figure 6.10 TICs obtained by TMAH thermochemolysis GC-MS analysis of NP HPO and TPI fractions. Peak assignments correspond to products listed in Table 6.6. Relative abundances of a-b are indicated in italics.

Table 6.6 Products detected by TMAH thermochemolysis of NP HPO and TPI fractions. A semi-quantitative indication of the relative abundance of each product is given as a percentage of the total peak area: * = < 0.5 %, ** = 0.5 – 1.5 %, *** = > 1.5 %, nd = not detected.

Peak	Identification	HPO	TPI	Peak	Identification	HPO	TPI
a	2-propenoic acid, methyl ester	***	**	B	1-(4-hydroxy-3-methoxyphenyl)ethanone (acetovanillone)	*	nd
b	propanoic acid, methyl ester	***	**	C	3-methoxybenzoic acid, methyl ester	nd	*
c	2-methyl-propanoic acid, methyl ester	**	*	D	3,4-dimethylbenzoic acid, methyl ester	*	*
d	2-methyl-2-propenoic acid, methyl ester	**	*	E	1,2,4-trimethoxybenzene	*	*
e	butanoic acid, methyl ester	**	*	F	3-methoxy-4-methylbenzoic acid, methyl ester	*	*
f	2-butenoic acid, methyl ester	**	**	G	4-*t*-butyl-1,2-dimethoxybenzene	nd	**
g	2-methoxy-propanoic acid, methyl ester	**	***	H	2-methyl-1H-isoindole-1,3(2H)-dione	nd	**
h	3-methyl-2-butenoic acid, methyl ester	**	**	I	biphenyl	**	*
i	methoxybenzene	**	**	J	1,2-benzenedicarboxylic acid, dimethyl ester	*	***
j	2-methoxy toluene	**	nd	K	biphenylene	***	**
k	3- and 4-methoxytoluene	**	*	L	1,4-benzenedicarboxylic acid, dimethyl ester	**	***
l	butanedioic acid, dimethyl ester	**	***	M	dodecanoic acid, methyl ester	*	*
m	methylbutanedioic acid, dimethyl ester	**	**	N	3,5-dimethoxybenzoic acid, methyl ester	**	*
n	3-ethyl-2-hydroxy-2-cyclopenten-1-one	*	**	O	3,4-dimethoxybenzoic acid, methyl ester	**	**
o	benzoic acid, methyl ester	**	***	P	decanedioic acid, dimethyl ester	nd	*
p	dimethylmethoxybenzene	**	*	Q	benzophenone	**	nd
q	1,2-dimethoxybenzene	*	**	R	tetradecanoic acid, methyl ester	*	*
r	2-methylpentanedioic acid, dimethyl ester	*	*	S	phenanthrene	***	**
s	2-methylbenzoic acid, methyl ester	*	*	T	anthracene	**	nd
t	dimethoxy benzenamine	nd	**	U	hexadecenoic acid, methyl ester	**	*
u	3-ethyl-1,3-dimethyl-2,5-pyrrolidinedione	*	*	V	hexadecanoic acid, methyl ester	**	**
v	4-methylbenzoic acid, methyl ester	*	**	W	octadecenoic acid, methyl ester	nd	*
w	2,3-dimethoxytoluene	*	**	X	octadecanoic acid, methyl ester	*	**
x	3,4-dimethoxytoluene + quinoline	**	**	Y	pyrene	**	*
y	2,4-dimethylbenzoic acid, methyl ester	*	nd	Z	fluoranthene	**	nd
z	3,5-dimethylbenzoic acid, methyl ester	*	**	AA	1,2-benzenedicarboxylic acid, diisooctyl ester	*	**
A	4-ethylbenzoic acid, methyl ester	*	*				

The methyl esters of low MW saturated and unsaturated aliphatic acids (e.g. 2-propenoic acid, propionic acid, methyl propanoic/propenoic acid, butanoic acid, butenoic acid) and diacids (e.g. butanedioic acid, methyl butanedioic acid and methyl pentanedioc acid) were detected in relatively high abundance. These are common thermochemolysis products of NOM (del Rio *et al*., 1998; Templier *et al*., 2005a) and are usually attributed to cross linking units between phenolic structures of humic macromolecules (Martin *et al*., 1995b). These products may be related to some of the abundant low MW aliphatic products detected by MSSV pyrolysis. Diacids such as succinic (butanedioic acid) and maleic acid are natural metabolic products of animal, vegetable and microbial cells (Templier *et al*., 2005a). The alkyl cyclopenten1-ones detected in low abundance by MSSV pyrolysis may derive from these aliphatic dicarboxylic acids by pyrolytic cyclisation reactions (Bracewell *et al*., 1980). Fatty acid methyl esters (FAMEs) were present in moderate proportions, with the most prominent being saturated and unsaturated C_{16} and C_{18} products (U, V, W, X; Table 6.6), which are generally attributed to microbial sources (Dignac *et al*., 2006).

Several aromatics containing methoxy and carboxylic acid (methyl esters) substituents were detected in slightly higher relative abundance from the HPO fraction. A few of these products, including acetovanillone (B), 3-methoxymethylbenzoate (C), and 3,5- and 3,4-dimethoxymethylbenzoate (N, O), are biomarkers of microbially degraded lignin. Several other methoxy aromatic products, including methoxybenzene (i), methoxytoluenes (j, k), dimethoxytoluenes (w, x), 1,2-dimethoxybenzene, 1,2,4 trimethoxybenzene (E) and 3-methoxy-4-methylbenzoic acid (F), may also derive from diagenetically or thermally altered lignin. However, this cannot be confirmed due to the inability of the TMAH approach to distinguish between pre-existing methoxy functionalities and those produced by methylation of hydroxy groups during the derivatisation procedure (Filley *et al*., 1999). As such, several different precursory structures may give identical thermochemolysis products. 1,2-dimethoxy benzene, for example, may be produced by methylation of the guaiacyl (2-methoxyphenol) moiety of lignin, but can also result from methylation of 1,2-dihydroxybenzene (catechol) derived from plant tannins or algal polyphenols such as phlorotannins (van Heemst *et al*., 1996; 1999). Nevertheless, the low overall abundance of methoxy aromatic TMAH

products is consistent with the low contribution of lignin to the NP NOM observed by ^{13}C-NMR spectroscopy, MSSV and flash pyrolysis. In contrast, the corresponding thermochemolysis data of the black water HPO fractions of Arroyo Sanchez River (Chapter 4) and Gartempe River (Templier *et al*., 2005a) showed high concentrations of methoxyphenol lignin markers.

An interesting feature of the thermochemolysis data of both fractions was the detection of several alkyl substituted benzoic acids (methyl esters), including 2- and 4-methylbenzoic acid (s, v), 2,4-, 3,4- and 3,5-dimethylbenzoic acid (y, z) and 4-ethylbenzoicacid (A). The origin of alkyl benzenecarboxylic acids is unclear, but given the lack of phenolic or methoxy group substitution it is unlikely that they are related to lignin. Lehtonen *et al.* (2000a; 2000b) suggested that alkyl substituted benzoic acids and methoxy aromatics derive from resistant alkyl aromatic networks, as opposed to ester or ether bound aromatic constituents. This source is consistent with the alkyl aromatic network proposed for some of the alkyl phenolic MSSV products.

The TPI fraction additionally yielded dimethyl esters of 1,2- and 1,4-benzenedicarboxylicacid (J, L) and the diisooctyl ester of 1,2-benzenedicarboxylic acid (AA). These are ubiquitous plasticiser compounds and may reflect contamination from the plastic containers used for sampling and storage (Leenheer and Rostad, 2004; Lehtonen *et al*., 2000a; Kaiser *et al*., 2003). Flash pyrolysis detected very high concentrations of the same diisooctyl phthalic acid ester.

Several of the major aromatic hydrocarbon pyrolysates detected by MSSV and flash pyrolysis, including parent and alkylated benzenes ($\leq C_3$) and naphthalenes ($\leq C_1$), were also detected in high abundance by TMAH thermochemolysis. Other parent PAHs, including biphenyl (I), biphenylene (K), phenanthrene (S), anthracene (T), pyrene (Y) and fluoranthene (Z), were detected only by thermochemolysis and were particularly prominent from the HPO fraction. These may be combustion products of natural fires or fossil fuels. The low phenanthrene/anthracene ratio (<15; Wise *et al*., 1988) and high fluoranthene/pyrene ratio (>1; Sicre *et al*., 1987) is consistent with their production during the combustion of fossil fuels from recreational boating activities (Deshmukh *et al*., 2001), and subsequent incorporation into the HPO

fraction. However, the reason that these products were not detected by MSSV and flash pyrolysis is presently unclear, but may relate to a structural recalcitrance which the TMAH reagent is able to uniquely access.

6.4 Conclusions

Comprehensive characterisation of the North Pine HPO and TPI fractions, isolated by XAD resin fractionation, was performed by MSSV pyrolysis and a variety of other established analytical techniques. The hydrophobic fraction accounted for ca. 65 % of the source water DOC. This fraction appears highly refractory due to the very low abundance of pyrolysates characteristic of unaltered polysaccharides, proteins, lignin and lipids by MSSV pyrolysis, flash pyrolysis and thermochemolysis. The ^{13}C NMR spectra of this fraction indicated the presence of aliphatic and alicyclic structures substituted with methyl, branched alkyl, hydroxyl and carboxyl groups. These features are characteristic of diagenetically modified terpenoid precursors of higher plants, algae and bacteria.

MSSV pyrolysis of the hydrophobic fraction yielded high concentrations of alkyl aromatic hydrocarbon pyrolysates (e.g. benzenes, naphthalenes, hydroaromatics), likely derived from the aromatisation of alicylic terpenoid precursors. The high degree of alkyl substitution of the MSSV pyrolysates correlates well with the NMR spectra. Alkyl phenols were prominent MSSV products and may also reflect hydroxyl substituted alicyclic ring structures, as well as covalently bound phenolic metabolites of aquatic algae. The low aromatic and methoxy content detected by NMR, and the limited detection of diagnostic methoxyphenol pyrolysates by thermochemolysis was not consistent with the high lignin input characteristic of the black water humic substances studied in previous chapters. However, non-methoxylated phenols of grass lignins may contribute to the NP NOM, given that the catchment has been largely cleared for agriculture and grazing. The holistic characterisation data thus reflect important differences in the structural characteristics of humic substances from pristine and black water sources.

The NP TPI fraction accounted for only 11.5 % of the source water DOC.
The MSSV data of this fraction showed many similar features to the HPO fraction but also included high concentrations of alkyl substituted N-pyrolysates. Degraded proteinaceous precursors and cross-linked melanoidin type macromolecules were postulated as the major source of these products. Both the FTIR and NMR data also confirmed the presence of amide and amine functional groups characteristic of proteinaceous materials.

MSSV pyrolysis provided more comprehensive molecular-level characterisation of the isolated fractions than flash pyrolysis and complemented well the ^{13}C-NMR and FTIR spectral data. In particular, high concentrations of pyrolysates characteristic of aliphatic terpenoid and organic nitrogen structures were obtained by MSSV analysis, where previously such constituents of NOM and other immature organic materials have proved elusive to analysis. Flash pyrolysis and thermochemolysis provided limited information regarding these quantitatively significant precursor classes. The capacity of MSSV pyrolysis to assist and extend the compositional characterisation of NOM with important additional structural information was clearly demonstrated by the present NP case study, despite the significant differences in the structure and source of this material compared to the NOM fractions studied in detail in the preceding chapters.

Chapter 7

Conclusions

This PhD project reports the first detailed application and evaluation of micro-scale sealed vessel (MSSV) pyrolysis (Py) GC-MS for the molecular characterisation of aquatic natural organic matter (NOM). MSSV pyrolysis contributed significantly to the structural and source characterisation of a suite of NOM fractions from several diverse aquatic environments, providing additional and complementary molecular information to contemporary NOM characterisation methods such as flash pyrolysis, thermochemolysis, and FT-IR and ^{13}C-NMR spectroscopy. The high abundances and rich product distributions of MSSV Py included many products not detected by flash pyrolysis, highlighting the effectiveness of this approach in the release of additional structural fragments amenable to detection by GC-MS. The milder thermal regime and closed system conditions of MSSV pyrolysis can facilitate the partial reduction of a variety of polar structural constituents of aquatic NOM that are not amenable to chromatographic analysis using conventional flash pyrolysis.

A significant outcome of this work was the demonstration of the importance of terpenoid OM in several different aquatic environments. A variety of source-specific terpenoid biomarkers were detected by MSSV pyrolysis of several NOM fractions isolated from surface, ground and waste waters. These included hopane biomarkers of bacterial terpenoids, aromatic hydrocarbon biomarkers (e.g. *p*-cymene, cadalene, retene) of higher plant terpenoids, sterane biomarkers of eukaryote steroids and high MW nitrogen-containing products (e.g. carbazoles and β-carbolines), tentatively attributed to alkaloid constituents of plants, algae and bacteria. Corresponding flash pyrolysis and thermochemolysis analyses of the same samples failed to detect these important products. Terpenoids derived from both allochthonous and autochthonous sources have been proposed as significant precursors of aquatic NOM, however diagnostic information about these types of contributors has until now been very limited.

Many of the product classes detected in high abundance by MSSV Py lacked the well defined precursory origins of the aforementioned terpenoid biomarkers. These included a broad range of alkyl aromatic hydrocarbons (e.g. benzenes, naphthalenes, tetralins), and oxygen-, sulfur- and nitrogen-containing heteroatomic compounds (e.g. alkylated furans, phenols, cyclic ketones, thiophenes, pyrroles, pyridines, indoles). The distributions of these specific product classes were comprehensively investigated in Chapters 3-5. Their detection now contributes to a more holistic interpretation of NOM structural character. Separate MSSV Py analyses of a suite of standards, representing potential biochemical precursors of NOM, facilitated source assignment of many pyrolysates, including several previously unexplained thermal degradation products of NOM. This information will be valuable for future analytical pyrolysis studies of NOM. In addition to the aforementioned terpenoid biomarkers, some of the NOM products providing evidence of a particular precursor included:

- alkyl aromatic hydrocarbon products of plant and algal terpenoids
- long-chain alkyl benzene products of industrial surfactants
- alkyl phenol products of lignin, tyrosine-containing proteins and alkyl phenol ethoxylate surfactants
- alkyl furan products of polysaccharides and simple sugars
- alkyl thiophene products of S-containing amino acids (e.g. cysteine)
- alkyl dioxane products of dioxane and dioxolane pollutants from polyester resin manufacture
- alkyl pyridine and pyrrole products of peptides, proteins and amino sugars
- alkyl indole products of tryptophan-containing proteins and N-alkaloids
- alkyl ethyl pyrrole products of porphyrin pigments

Several of the major MSSV products were also detected by flash pyrolysis, however the higher abundance and broader isomeric distributions evident in the MSSV data allowed for a more comprehensive structural characterisation than previously possible. The sensitive molecular speciation of MSSV Py afforded compositional and source distinction of NOM from different aquatic environments. In particular, the more highly alkyl substituted pyrolysates, which are of potentially greater source

diagnostic value, were better preserved by MSSV Py. Large substituents may not survive the excessive thermal energy of flash pyrolysis.

This PhD study has clearly demonstrated that MSSV Py can be a valuable component of the analytical protocol for aquatic NOM characterisation. MSSV analysis ***I*** provided significant molecular detail suitable for standard characterisation purposes. MSSV analysis ***II*** facilitated fast pyrolysis of the residue from analysis ***I*** and could be used as an alternative to flash pyrolysis. MSSV pyrolysis (***I or II***) also offers the advantages of low cost, low sample requirements and operational simplicity. Its practical application to the water industry should have wide utility, extending from determination of structural features and biochemical origins - including the identification of anthropogenic and microbial inputs, to assessing the effectiveness of drinking water treatment processes and the fate of organic constituents through the entire potable water system, including treatment plants and distribution networks.

Despite the still immature development status of this technique, the present research has identified several specific applications to which it can presently make a significant contribution. These include:

- Terpenoid constituents of NOM were particularly well defined by MSSV pyrolysis and this finding has significant implications for the potable water industry. Terpenoids are resistant to aerobic degradation processes, can readily infiltrate groundwater aquifers, with little removal by soil/aquifer treatment, and are difficult to remove by coagulation/flocculation. An analytical method sensitive to these compounds will be useful for establishing the extent of their removal by treatment processes.

- The high sensitivity of MSSV pyrolysis to the detection of N-pyrolysates, which are historically under-represented by flash pyrolysis, holds promise for the improved characterisation of the N-organic moiety of NOM. This should be useful for determining the structural precursors of toxic N-containing disinfection by-products (N-DBPs) formed during potable water treatment.

- MSSV pyrolysis can significantly aid the organic characterisation of waste water effluent OM (Ef-OM). A variety of unique molecular features indicative of anthropogenic sources (e.g. dioxins and large alkyl substituted phenols of industrial by-products, steranes of human faecal pollution, S-products of sewage organics or pharmaceuticals) and recalcitrant biochemicals of source water NOM (e.g. alkyl aromatics of terpenoids and aliphatic biopolymers of algae, alkyl phenols of lignin-derived humic substances) and microbial communities (e.g. N-heterocyclic products of proteins and amino sugars, carbazoles and B-carbolines of algal or microbial alkaloids) were detected from separate fractions of two Ef-OM samples by MSSV pyrolysis. The same level of compositional information was not evident by flash pyrolysis. MSSV Py can thus be a useful tool in assessing the effectiveness of waste water treatment, and monitoring the persistence of recalcitrant chemicals in secondary effluents and the reservoirs to which they are discharged.

- The analytical capability of MSSV Py for the compositional characterisation of membrane biofoulants was obvious, with the detection of many additional pyrolysates compared to flash pyrolysis. The identification of hopane biomarkers, monomethyl- and *n*-alkanes, and high concentrations of N-containing products unequivocally established the microbial origin of the foulant. In addition, high abundances of long chain alkyl benzenes revealed the incorporation of surfactant compounds used in membrane cleaning processes. The detailed structural appraisal of bio-foulant samples afforded by MSSV Py has interesting industrial applications, but would have gone undetected by flash pyrolysis.

Ongoing research is required to fully establish the MSSV Py technique alongside other contemporary thermal degradation approaches like flash pyrolysis and thermochemolysis. In particular, the largely undefined MSSV pyrolysis behavior of functionalised NOM moieties and their biochemical precursors remains on ongoing challenge. A better understanding of the mechanistic processes associated with MSSV Py is required for realisation of the full characterisation potential of this approach. The utility of MSSV pyrolysis would be extended by the following targeted research and development:

- Analysis of a much larger range of NOM samples and potential biochemical precursors to continue investigating the mechanistic formation of pyrolysates during off-line thermal treatment.
- Analysis of mixtures of different standards to investigate important synergistic effects between environmentally occurring organic compounds.
- The use of internal and/or external standards to assist quantitative measurement of pyrolysate yields and a robust assessment of precursory contributions. Potential quantitative endeavours include installation of a gas-sampling loop, mass balance calculations of pyrolysate residues, or calibration of GC-MS response factors using model compounds as external standards to establish orders of magnitude in the concentrations of GC amenable products.
- Continued investigation of optimal thermal conditions for targeting the different biomolecular constituents of NOM.
- Preparative scale MSSV Py, in combination with offline extraction and separation procedures (e.g. column chromatography), permitting improved GC resolution of products and application of additional molecular characterisation approaches such as chemical derivatisation and compound specific isotope analysis.

References

Abbott, G.D., Bashir, F.Z., Sugden, M.A., 2001. Kerogen-bound and free hopanoic acids in the Messel oil shale kerogen. Chirality 13, 510-516.

Abbt-Braun, G., Frimmel, F.H., 1999. Basic characterisation of Norwegian NOM samples - similarities and differences. Environment International 25, 161-180.

Abbt-Braun, G., Frimmel, F.H., Schulten, H-R., 1989. Structural investigations of aquatic humic substances by pyrolysis-field ionization mass spectrometry and pyrolysis-gas chromatography/mass spectrometry. Water Research 23, 1579-1589.

Abbt-Braun, G., Lankes, U., Frimmel, F.H., 2004. Structural characterisation of aquatic humic substances – The need for a multiple method approach. Aquatic Science 66, 151-170.

Adams, A., Tehrani, K.A., Kersiene, M., Venskutonis, R., De Kimpe, N., 2003. Characterisation of model melanoidins by the thermal degradation profile. Journal of Agricultural and Food Chemistry 51, 4338-4343.

Aiken, G. R., 1985. Isolation and concentration techniques for aquatic humic substances. In: Humic Substances in Soil, Sediment, and Water, Aiken, G. R., McKnight, D. M., Wershaw, R. L., MacCarthy, P., (Eds.), John Wiley & Sons, New York, 1985, pp 363-385.

Aiken, 2002. Organic matter in ground water. In: Aiken, G.R., Kuniansky, E.L., (Eds.), U.S. Geological Survey Artificial Recharge Workshop Proceedings, Sacramento, California, April 2-4, 2002.

Alexander, R., Kagi, R.I., Rowland, S.J., Sheppard, P.N., Chirila, T.V., 1985. The effects of thermal maturation on distributions of dimethylnaphthalenes and trimethylnaphthalenes in some ancient sediments and petroleums. Geochimica et Cosmochimica Acta 49, 385-395.

Alexander, R., Kagi, R.I., Sheppard, P.N., 1983. Relative abundance of dimethylnaphthalene isomers in crude oils. Journal of Chromatography 267, 367-372.

Alexander, R., Larcher, A.V., Kagi, R.I., Price, P.L., 1992. An oil-source correlation study using age specific plant-derived aromatic biomarkers. In: Biological

Markers in Sediments and Petroleum, Moldowan, J.M., Albrecht, P., Philp, R.P., (Eds.), Prentice-Hall Englewood Cliffs, N.J. pp 201-221.

Allpike, B.P., Heitz, A., Joll, C.A., Kagi, R.I., Abbt-Braun, G., Frimmel, F.H., Brinkmann, T., Her, N., Amy, G., 2005. Size exclusion chromatography to characterise DOC removal in drinking water treatment. Environmental Science and Technology 39, 2334-2342.

Almendros, G., Dorado, J., González-Vila, F.J., Martin, F., 1997. Pyrolysis of carbohydrate-derived macromolecules: its potential in monitoring the carbohydrate signature of geopolymers. Journal of Analytical and Applied Pyrolysis 40-41, 599-610.

Almendros, G., González-Vila, F.J., Martin, F., Sanz, J., Álvarez-Ramis, C., 1998. Appraisal of pyrolytic techniques on different forms of organic matter from a Cretaceous basement in Central Spain. Organic Geochemistry 28, 613-623.

Almendros, G., Knicker, H., Gonzalez-Vila, F.J., 2003. Rearrangement of carbon and nitrogen forms in peat after progressive thermal oxidation as determined by solid-state ^{13}C and ^{15}N-NMR spectroscopy. Organic Geochemistry 34, 1559-1568.

Amon, R.M.W., Benner, R., 1996. Bacterial utilisation of different size classes of dissolved organic matter. Limnology and Oceanography 41, 41-51.

Amy, G., 1993. Using NOM characterisation for the evaluation of treatment. Proceedings of Workshop on NOM in Drinking Water: Origin, Characterisation and Removal Conference, Chamonix, France, September 19-22.

Amy, G., Cho, J., 1999. Interactions between natural organic matter (NOM) and membranes: Rejection and fouling. Water Science and Technology 40, 131-139.

Anderson, K.B., Winans, R.E., 1991. Nature and fate of natural resins in the geosphere. 1. Evaluation of pyrolysis-gas chromatography/mass spectrometry for the analysis of natural resins and resinites. Analytical Chemistry 63, 2901-2908.

Aoustin, E., Schafer, A.I., Fane, A.G., Waite, D.T. 2001. Ultrafiltration of natural organic matter. Separation and Purification Technology 22-23, 63-78.

Audino, M., Alexander, R., Kagi, R.I., 1996. Ethylmethylnaphthalenes in crude oils. Polycyclic Aromatic Compounds 8, 93-103.

Barth, T., 1999. Similarities and differences in hydrous pyrolysis of biomass and source rocks. Organic Geochemistry 30, 1495-1507.

Barth, T., Kleinert, M., 2008. Motor fuels from biomass pyrolysis. Chemical Engineering Technology 31, 773-781.

Basiuk, V.A., Douda, J., 2000. Pyrolysis of poly-glycine and poly-L-alanine: Analysis of less volatile products by gas chromatography/Fourier transform infrared spectroscopy/mass spectrometry. Journal of Analytical and Applied Pyrolysis 55, 235-246.

Basiuk, V.A., Douda, J., 2001. Analysis of less volatile products of poly-L-valine pyrolysis by gas chromatography/Fourier transform infrared spectroscopy/mass spectrometry. Journal of Analytical and Applied Pyrolysis 60, 27-40.

Bastow, T.P., 1998. Sedimentary processes involving aromatic hydrocarbons. PhD Thesis. Curtin University of Technology, Perth, Western Australia.

Bastow, T.P., Singh, R.K., van Aarssen, B.G.K., Alexander, R., Kagi, R.I., 2001. 2-Methylretene in sedimentary material: a new higher plant biomarker. Organic Geochemistry 32, 1211-1217.

Bastow, T.P., van Aarssen, B.G.K., Kagi, R.I., Alexander, R., 2005. Origins of alkylphenols in crude oils: Hydroxylation of alkylbenzenes. Organic Geochemistry 36, 991-1001.

Bastow, T.P., van Aarssen, B.G.K., Alexander, R., Kagi, R.I., 1999. Biodegradation of aromatic land-plant biomarkers in some Australian crude oils. Organic Geochemistry 30, 1229-1239.

Bates, A.L., Hatcher, P.G., 1989. Solid-state ^{13}C NMR studies of a large fossil gymnosperm from the Yallourn Open Cut, Latrobe Valley, Australia. Organic Geochemistry 14, 609-617.

Baxby, M., Patience, R.L., Bartle, K.D., 1994. The origin and diagenesis of sedimentary organic nitrogen. Journal of Petroleum Geology 17, 211-230.

Behar, F., Hatcher, P.G., 1995. Artificial coalification of a fossil wood from brown coal by confined system pyrolysis. Energy and Fuels 9, 984-994.

Behar, F., Lewan, M.D., Lorant, F., Vandenbroucke, M., 2003. Comparison of artificial maturation of lignite in hydrous and nonhydrous conditions. Organic Geochemistry 34, 575-600.

Belzile, N., Joly, H.A., Li, H., 1997. Characterisation of humic substances extracted from Canadian lake sediments. Canadian Journal of Chemistry 75, 14-27.

Bennett, B., Abbott, G.D., 1999. A natural pyrolysis experiment – hopanes from hopanoic acids? Organic Geochemistry 30, 1509-1516.

Bennett, B., Lager, A., Russell, C.A., Love, G.D., Larter, S.R., 2004. Hydropyrolysis of algae, bacteria, archaea and lake sediments: Insights into the origin of nitrogen compounds in petroleum. Organic Geochemistry 35, 1427-1439.

Benzing-Purdie, L., Ripmeester, J.A., 1983. Melanoidins and soil organic matter: Evidence of strong similarities revealed by ^{13}C CP-MAS NMR. Soil Science Society American Journal 47, 56-61.

Benzing-Purdie, L.M., Ripmeester, J.A., Preston, C.M., 1983. Elucidation of the nitrogen forms in melanoidins and humic acids by nitrogen-15 cross-polarization-magic angle spinning nuclear magnetic resonance. Journal of Agricultural and Food Chemistry 31, 913-915.

Berwick, L.J., Greenwood, P.F., Kagi, R.I., Croué, J-P., 2007. Thermal release of nitrogen-organics from natural organic matter (NOM) by micro-scale sealed vessel (MSSV) pyrolysis. Organic Geochemistry 38, 1073-1090.

Bishop, A.N., Love, G.D., McAulay, A.D., Snape, C.E., Farrimond, P., 1998. Release of kerogen-bound hopanoids by hydropyrolysis. Organic Geochemistry 29, 989-1001.

Blumer, M., Youngblood, W.W., 1975. Polycyclic aromatic hydrocarbons in soils and recent sediments. Science 188, 53-55.

Boon, J.J., de Leeuw, J.J., 1987. Amino acid sequence information in proteins and complex proteinaceous material revealed by pyrolysis-capillary gas chromatography-low and high resolution mass spectrometry. Journal of Analytical and Applied Pyrolysis 11, 313-327.

Boon, J.J., de Leeuw, J.W., Rubinsztain, Y., Aizenshtat, Z., Ioselis, P., Ikan, R., 1984. Thermal evaluation of some model melanoidins by *Curie* point pyrolysis-mass spectrometry and gas chromatography-mass spectrometry. Organic Geochemistry 6, 805-811.

Botto, R.E., 1987. Solid ^{13}C NMR tracer studies to probe coalification. Energy and Fuels 1, 228-230.

Bourbonniere, R.A., Meyers, P.A., 1978. Characterization of sedimentary humic matter by elemental and spectroscopic methods. Canadian Journal of Spectroscopy 23, 35-41.

Bracewell, J.M., Robertson, G.W., Williams, B.L., 1980. Pyrolysis-mass spectrometry studies of humification in a peat and peaty podzol. Journal of Analytical and Applied Pyrolysis 2, 53-62.

Brown, S.D., Chiavari, G., Ediger, V., Fabbri, D., Gaines, A.F., Galletti, G. Karayigit, A.I., Love, G.D., Snape, C.E., Sirkecioglu, O., Toprak, S., 2000. Black Sea sapropels: relationship to kerogens and fossil fuel precursors. Fuel 79, 1725-1742.

Bruchet, A.,1985. Applications de la technique de pyrolyse-cg-sm a l'etude des matieres organiques non volatiles des eaux naturelles ou en cours de traitement. PhD Thesis, University of Poitiers, France.

Bruchet, A., Rousseau, C. and Mallevialle, J., 1990. Pyrolysis-GC-MS for investigating high-molecular weight THM precursors and other refractory organics. Journal of the American Water Works Association 82, 66-74.

Burford, M.A., Johnson, S.A., Cook, A.J., Packer, T.V., Taylor, B.M., Townsley, E.R., 2007. Correlations between watershed and reservoir characteristics, and algal blooms in subtropical reservoirs. Water Research 41, 4105-4114.

Busetti, F., Linge, K.L., Blythe, J.W., Heitz, A., 2008. Rapid analysis of iodinated X-ray contrast media in secondary and tertiary treated wastewater by direct injection liquid chromatography-tandem mass spectrometry. Journal of Chromatography A 1213, 200-208.

Cabaniss, S.E., Madey, G., Leff, L., Maurice, P.A., Wetzel, R., 2005. A stochastic model for the synthesis and degradation of natural organic matter. Part 1. Data structures and reaction kinetics. Biogeochemistry 76, 319-347.

Cabaniss, S.E., Zhou, Q., Maurice, P.A., Chin, Y., Aiken, G., 2000. A log- normal distribution model for the molecular weight of aquatic fulvic acids. Environmental Science and Technology 34, 1103-1109.

Cardoza, L.A., Korir, A.K., Otto, W.H., Wurrey, C.J., Larive, C.K., 2004. Applications of NMR spectroscopy in environmental science. Progress in nuclear magnetic resonance spectroscopy 45, 209-238.

Carter, W., Suffet, I., 1982. Binding of DDT to dissolved humic materials. Environmental Science and Technology 16, 735-740.

Challinor, J.M., 1989. A pyrolysis-derivatisation-gas chromatography technique for the structural elucidation of some synthetic polymers. Journal of Analytical and Applied Pyrolysis 16, 323-333.

Challinor, J.M., 1991. The scope of pyrolysis methylation reactions. Journal of Analytical and Applied Pyrolysis, 20, 15-24.

Challinor, J.M., 1995. Characterisation of wood by pyrolysis derivatisation-gas chromatography/mass spectrometry. Journal of Analytical and Applied Pyrolysis 35, 93-107.

Challinor, J.M., 2001. Review: the development and applications of thermally assisted hydrolysis and methylation reactions. Journal of Analytical and Applied Pyrolysis 61, 3-34.

Chefetz, B., Salloum, M.J., Deshmukh, A.P., Hatcher, P.G., 2002. Structural components of humic acids as determined by chemical modifications and Carbon-13 NMR, pyrolysis-, and thermochemolysis-gas chromatography mass spectrometry. Soil Science Society of America Journal 66, 1159-1171.

Chiavari, G., Galletti, G.C., 1992. Pyrolysis-gas chromatography/mass spectrometry of amino acids. Journal of Analytical and Applied Pyrolysis 24, 123-137.

Chin, Y., Aiken, G., O'Loughlin, E., 1994. Molecular weight, polydispersity, and spectroscopic properties of aquatic humic substances. Environmental Science and Technology 28, 1853-1858.

Christy, A.A., Bruchet, A., Rybacki, D., 1999. Characterisation of natural organic matter by pyrolysis/GC-MS. Environment International 25, 181-189.

Cho, J., Amy, G., Pellegrino, J., 1999. Membrane filtration of natural organic matter: initial comparison of rejection and flux decline characteristics with ultrafiltration and nanofiltration membranes. Water Research 33, 2517-2526.

Chow, C.W.K., van Leeuwen, J., Drikas, M., Fabris, R., Spark, K.M., Page, D.W., 1999. The impact of the character of natural organic matter in conventional treatment with alum. Water Science and Technology 40, 97-104.

Clapp, C.E., Hayes, M.H.B., 1999. Sizes and shapes of humic substances. Soil Science 164, 777-789.

Clegg, H., Horsfield, B., Stasiuk, L., Fowler, M., Vliex, M., 1997. Geochemical characterisation of organic matter in Keg River Formation (Elk point group,

Middle Devonian), La Crete Basin, Western Canada. Organic Geochemistry 26, 627-643.

Clegg, H., Horsfield, B., Wilkes, H., Sinninghe Damsté, J., Koopmans, M.P., 1998. Effect of artificial maturation on carbazole distributions, as revealed by the hydrous pyrolysis of an organic-sulphur-rich source rock (Ghareb Formation, Jordan). Organic Geochemistry 29, 1953-1960.

Clesceri, L.S., Greenerg, A.E. and Eaton, A.D., (Eds.), 1998. Standard Methods for the Examination of Water and Wastewater. American Public Health Association, Washington D.C.

Coble, P.G., 1996. Characterization of marine and terrestrial DOM in seawater using excitation-emission matrix spectroscopy. Marine Chemistry 51, 325-346.

Coleman, W.M., Chung, H.L., 2002. Pyrolysis GC-MS analysis of Amadori compounds derived from selected amino acids with glucose and rhamnose. Journal of Analytical and Applied Pyrolysis 63, 349-366.

Cooke, M.P., Talbot, H.M., Farrimond, P., 2008. Bacterial populations recorded in bacteriohopanepolyol distributions in soils from Northern England. Organic Geochemistry, *In Press*.

Coolen, M.J.L., Talbot, H.M., Abbas, B.A., Ward, C., Schouten, S., Volkman, J.K., Sinninghe Damsté, J.S., 2008. Sources for sedimentary bacteriohopanepolyols as revealed by 16s rDNA stratigraphy. Environmental Microbiology 10, 1783-1803.

Cotrim da Cunha, L., Serve, L., Gadel, F., Blazi, J-L., 2001. Lignin-derived phenolic compounds in the particulate organic matter of a French Mediterranean river: seasonal and spatial variations. Organic Geochemistry 32, 305-320.

Croué, J-P., 2004. Isolation of humic and non-humic NOM fractions: Structural characterisation. Environmental Monitoring and Assessment 92, 193-207.

Croué, J-P., Benedetti, M.F., Violleau, D., Leenheer, J.A., 2003a. Characterisation and copper binding of humic and nonhumic organic matter isolated from the South Platte River: Evidence for the presence of nitrogenous binding site. Environmental Science and Technology 37, 328-336.

Croué, J-P., Debroux, J., Aiken, G., Leenheer, J.A. and Amy, G., 1999. Natural organic matter: structural characteristics and reactive properties in formation and control of disinfection by-products in drinking water. In: Formation and

Control of Disinfection By-products in Drinking Water, Singer, P.C. (Ed.), American Water Works Association.

Croué, J-P., Gallard, H., Ambonguilat, S., Greenwood, P., Berwick, L., Boyd, L., Grice, K., 2006. Characterisation of colloids isolated from surface waters. Proceedings of Combined Australian Organic Geochemists/Natural Organic Matter Users Conference, Perth, Western Australia, 12-15th February 2006, p 25-26.

Croué, J-P., Grasset, L., Bacle, S., Jacquemet, V., 2003b. Nanofiltration membrane autopsy of a full scale unit: Characterisation of the organic and inorganic constituents of the foulants. Proceedings of American Water Works Association Membrane Technology Conference, Atlanta, United States, 2-5th March 2003.

Croué, J-P., Korshin, G.V., Benjamin, M., 2000. Characterisation of natural organic matter in drinking water. American Water Works Association Research Foundation, Denver, pp 1-324.

Croué, J.P., Martin, B., Simon, P., Legube, B., 1993. Les matiéres hydrophobes et hydrophiles des eaux de retenues: extraction, caractérisation et quantification. Water Supply 11, 51-62.

Davidson, W.A., 1995. Hydrogeology and Groundwater Resources of the Perth Region, Western Australia, *Bulletin 142* (Ed. by G.S.o.W. Australia), pp. 257. National Library of Australia.

de Leeuw, J.W., Baas, M., 1993. The behaviour of esters in the presence of tetramethylammonium salts at elevated temperatures; flash pyrolysis or flash chemolysis. Journal of Analytical and Applied Pyrolysis 26, 175-184.

de Leeuw, J.W., van Bergen, P.F., van Aarssen, B.G.K., Gatellier, J-P., Sinninghe Damsté, J.S., Collinson, M.E., Ambler, R.P., Macko, S., Curry, G.B., Eglington, G., Maxwell, J.R., 1991. Resistant biomacromolecules as major contributors to kerogen. Philosophical Transactions: Biological Sciences 333, 329-337.

del Rio, J.C., González Vila, F.J., Martin, F., Verdejo, T., 1994. Characterisation of humic acids from low-rank coals by ^{13}C NMR and pyrolysis-methylation. Formation of benzenecarboxylic acid moieties during the coalification process. Organic Geochemistry 22, 885-891.

del Rio, J.C., Hatcher, P.G., 1998. Analysis of aliphatic biopolymers using thermochemolysis with tetramethylammonium hydroxide (TMAH) and gas chromatography-mass spectrometry. Organic Geochemistry 29, 1441-1451.

del Rio, J.C., Martin, F., González-Vila, F.J., 1996. Thermally assisted hydrolysis and alkylation as a novel pyrolytic approach for the structural characterization of natural biopolymers and geomacromolecules. Trends in Analytical Chemistry 75, 70-79.

del Rio, J.C., McKinney, D.E., Knicker, H., Nanny, M.A., Minard, R.D., Hatcher, P.G., 1998. Structural characterization of bio- and geo-macromolecules by off-line thermochemolysis with tetramethylammonium hydroxide. Journal of Chromatography A 823, 433-448.

Derenne, S., Largeau, C., Casadevall, E., Berkaloff, C., Rousseau, B., 1991. Chemical evidence of kerogen formation in source rocks and oil shales via selective preservation of thin resistant outer walls of microalgae: Origin of ultralaminae. Geochimica et Cosmochimica Acta 55, 1041-1050.

Derenne, S., Largeau, C., Taulelle, F., 1993. Occurrence of non-hydrolysable amides in the macromolecular constituent of *Scenedesmus quadricauda* cell wall as revealed by ^{15}N-NMR: Origin of *n*-alkylnitriles in pyrolysates of ultralaminae-containing kerogens. Geochimica et Cosmochimica Acta 57, 851-857.

Deshmukh, A.P., Chefetz, B., Hatcher, P.G., 2001. Characterisation of organic matter in pristine and contaminated coastal marine sediments using solid-state ^{13}C NMR, pyrolytic and thermochemolytic methods: a case study in the San Diego harbor area. Chemosphere 45, 1007-1022.

Diallo, M.S., Simpson, A.J., Gassman, P., Faulon J-L., Johnson, J.H., Goddard, W.A., Hatcher, P.G., 2003. 3-D structural modelling of humic acids through experimental characterization, computer assisted structure elucidation and atomistic simulations. 1. Chelsea soil humic acid. Environmental Science and Technology 37, 1783-1793.

di Corcia, A., Costantino, A., Crescenzi, C., Marinoni, E., Samperi, R., 1998. Characterization of recalcitrant intermediates from the biotransformation of the branched alkyl side chain of nonylphenol ethoxylate surfactants. Environmental Science and Technology 32, 2401-2409.

Diekmann, V., Schenk, H.J., Horsfield, B., 2000. Assessing the overlap of primary and secondary reactions by closed- versus open-system pyrolysis of marine kerogens. Journal of Analytical and Applied Pyrolysis 56, 33-46.

Diekmann, V., Schenk, H.J., Horsfield, B., Welte, D.H., 1998. Kinetics of petroleum generation and cracking by programmed-temperature closed-system pyrolysis of Toarcian Shales. Fuel 77, 23-31.

Dignac, M-F., Ginestet, P., Rybacki, D., Bruchet, A., Urbain, V., Scribe, P., 2000. Fate of wastewater organic pollution during activated sludge treatment: nature of residual organic matter. Water Research 34, 4185-4194.

Dignac, M-F., Houot, S., Derenne, S., 2006. How the polarity of the separation column may influence the characterization of compost organic matter by pyrolysis-GC/MS. Journal of Analytical and Applied Pyrolysis 75, 128-139.

Dignac, M-F., Houot, S., Francou, C., Derenne, S., 2005. Pyrolytic study of compost and waste organic matter. Organic Geochemistry 36, 1054-1071.

Domalgalski, J.L, Orem, W.H., Eugster, H.P., 1989. Organic geochemistry and brine composition in the Great Salt, Mono, and Walker Lakes. Geochimica et Cosmochimica Acta 53: 2857-2872.

Douda, J., Basiuk, V.A., 2000. Pyrolysis of amino acids: Recovery of starting materials and yields of condensation products. Journal of Analytical and Applied Pyrolysis 56, 113-121.

Douglas, A.G., Sinninghe Damsté, J.S., Fowler, M.G., Eglinton, T.I., de Leeuw, J.W., 1991. Unique distributions of hydrocarbons and sulphur compounds released by flash pyrolysis from the fossilised alga *Gloeocapsomorpha prisca*, a major constituent in one of four Ordovician kerogens. Geochimica et Cosmochimica Acta 55, 275-291.

Drewes, J.E., Reinhard, M., Fox, P., 2003. Comparing microfiltration-reverse osmosis and soil-aquifer treatment for indirect potable reuse of water. Water Research 37, 3612-3621.

Drikas, M., Chow, C., Cook, D., 2003. The impact of recalcitrant organic character on disinfection stability, trihalomethane formation and bacterial regrowth: An evaluation of magnetic ion exchange (MIEX®) and alum coagulation. Journal of Water Supply: Research and Technology-AQUA 52, 475-487.

Eganhouse, R.P., Blumfield, D.L., Kaplan, I.R., 1983. Longchain alkylbenzenes as molecular tracers of domestic wastes in the marine environment. Environmental Science and Technology 17, 523-530.

Eglite, L., Rozenbaha, I., Odham, G., Jarnberg, U., Klavins, M., 2003. Reductive degradation of humic substances. Latvijas Kimijas Zurnals, 283-291.

Engelhaupt, E., Bianchi, T.S., Wetzel, R.G., Tarr, M.A., 2002. Photochemical transformations and bacterial utilization of high molecular-weight dissolved organic carbon in a southern Louisiana tidal stream (Bayou Trepagnier). Biogeochemistry 62, 39-58.

Ertel, J.R., Caine, J.M., Thurman, E.M., 1993. Biomarker compounds as source indicators for dissolved fulvic acids in a bog. Biogeochemistry 22, 195-212.

Ertel, J.R., Hedges, J.I., 1984. The lignin component of humic substances: Distribution among soil and sedimentary humic, fulvic, and base-insoluble fractions. Geochimica et Cosmochimica Acta 48, 2065-2074.

Ertel, J.R., Hedges, J.I., Perdue, E.M., 1984. Lignin signature of aquatic humic substances. Science 223, 485-487.

Evershed, R.P., Bland, H.A., van Bergen, P.F., Carter, J.F., Horton, M.C., Rowley-Conway, P.A., 1997. Volatile compounds in archaeological plant remains and the Maillard reaction during decay of organic matter. Science 278, 432-433.

Fabbri, D., Helleur, R., 1999. Characterization of the tetramethylammonium hydroxide thermochemolysis products of carbohydrates. Journal of Analytical and Applied Pyrolysis 49, 277-293.

Fabris, R., Chow, C.W.K., Drikas, M., Eikebrokk, M., 2008. Comparison of NOM character in selected Australian and Norwegian drinking waters. Water Research 42, 4188-4196.

Farrimond, P., Griffiths, T., Evdokiadis, E., 2002. Hopanoic acids in Mesozoic sedimentary rocks: their origin and relationship with hopanes. Organic Geochemistry 33, 965-977.

Farrimond, P., Love, G.D., Bishop, A.N., Innes, H.E., Watson, D.F., Snape, C.E., 2003. Evidence for rapid incorporation of hopanoids into kerogen. Geochimica et Cosmochimica Acta 67, 1383-1394.

Faure, P., Jeanneau, L., Lannuzel, F., 2006a. Analysis of organic matter by flash pyrolysis-gas chromatography-mass spectrometry in the presence of Na-

smectite. When clay minerals lead to identical molecular signature. Organic Geochemistry 37, 1900-1912.

Faure, P., Schlepp, L., Mansuy-Huault, L., Elie, M., Jardé, E., Pelletier, M., 2006b. Aromatisation of organic matter induced by the presence of clays during flash pyrolysis-gas chromatography-mass spectrometry (PyGC-MS). A major analytical artefact. Journal of Analytical and Applied Pyrolysis 75, 1-10.

Fievre, A., Solouki, T., Marshall, A.G., Cooper, W.T., 1997. High-resolution Fourier transform ion cyclotron resonance mass spectrometry of humic and fulvic acids by laser desorption/ionization and electrospray ionization. Energy Fuels 11, 554-560.

Filley, T.R., Minard, R.D., Hatcher, P.G., 1999. Tetramethylammonium hydroxide (TMAH) thermochemolysis: proposed mechanisms based upon the application of ^{13}C-labeled TMAH to a synthetic model lignin dimer. Organic Geochemistry 30, 607-621.

Filley, T.R., Hatcher, P.G., Shortle, W.C., Praseuth, R.T., 2000. The application of ^{13}C-labeled tetramethylammonium hydroxide (^{13}C-TMAH) thermochemolysis to the study of fungal wood degradation. Organic Geochemistry 31, 181-198.

Filley, T.R., Nierop, K.G.J., Wang, Y., 2006. The contribution of polyhydroxyl aromatic compounds to tetramethylammonium hydroxide lignin-based proxies. Organic Geochemistry 37, 711-727.

Franzmann, P.D., Heitz, A., Zappia, L.R., Wajon, J.E., Xanthis, K., 2001. The formation of malodorous oligosulphides in treated groundwater: The role of biofilms and potential precursors. Water Research 35, 1730-1738.

Frazier, S.W., Nowack, K.O., Goins, K.M., Cannon, F.S., Kaplan, L.A., Hatcher, P.G., 2003. Characterization of organic matter from natural waters using tetramethylammonium hydroxide thermochemolysis GC-MS. Journal of Analytical and Applied Pyrolysis 70, 99-128.

Frimmel, F.H., 1994. Photochemical aspects related to humic substances. Environment International 20, 373-385.

Frimmel, F.H., 1998. Impact of light on the properties of aquatic natural organic matter. Environment International 24, 559-571.

Gadel, F., Bruchet, A., 1987. Application of pyrolysis-GC-MS to the characterisation of humic substances resulting from decay of aquatic plants in sediments and waters. Water Research 21, 1195-1206.

Galletti, G.C., Modafferi, V., Poiana, M., Bocchini, P., 1995. Analytical pyrolysis and thermally assisted hydrolysis-methylation of wine tannin. Journal of Agriculture and Food Chemistry 43, 1859-1863.

Galletti, G.C., Reeves, J.B., 1992. Pyrolysis/gas chromatography/ion-trap detection of polyphenols (vegetable tannins): Preliminary results. Organic Mass Spectrometry 27, 226-230.

Gallois, N., Templier, J., Derenne, S., 2007. Pyrolysis-gas chromatography–mass spectrometry of the 20 protein amino acids in the presence of TMAH. Journal of Analytical and Applied Pyrolysis 80, 216-230.

Garcette-Lepecq, A., Derenne, S., Largeau, C., Bouloubassi, I., Saliot, A., 2000. Origin and formation pathways of kerogen-like organic matter in recent sediments off the Danube delta (northwestern Black Sea). Organic Geochemistry 31, 1663-1683.

Gauthier, A., Derenne, S., Largeau, C., Dupont, L., Guillon, E., Dumonceau, J., Aplincourt, M., 2003. Comparative study of ligno-cellulosic material from wheat straw and of pure and mixed standard compounds via solid state ^{13}C NMR spectroscopy, conventional pyrolysis and TMAH thermochemolysis. Journal of Analytical and Applied Pyrolysis 67, 277-293.

Gimeno, R.A., Altelaar, A.F.M., Marcé, R.M., Borrull, F., 2002. Determination of polycyclic aromatic hydrocarbons and polycylic aromatic sulfur heterocycles by high-performance liquid chromatography with fluorescence and atmospheric pressure chemical ionization mass spectrometry detection in seawater and sediment samples. Journal of Chromatography A 958, 141-148.

Göbel, A., McArdell, C., Suter, M.J.F, Giger, W., 2004. Trace determination of macrolide and sulfonamide antimicrobials, a human sulfonamide metabolite, and trimethoprim in wastewater using liquid chromatography coupled to electrospray tandem mass spectrometry. Analytical Chemistry 76, 4756-4764.

Gonzalez, J.A., González-Vila, F.J., Almendros, G., Zancada, M.C., Polvillo, O., Martin, F., 2003. Preferential accumulation of selectively preserved biomacromolecules in the humus fractions from a peat deposit as seen by

analytical pyrolysis and spectroscopic techniques. Journal of Analytical and Applied Pyrolysis 68-69, 287-298.

González-Vila, F.J., del Rio, J.C., Martin, F., Verdejo, T., 1996. Pyrolytic alkylation-gas chromatography-mass spectrometry of model polymers. Further insights into the mechanism and scope of the technique. Journal of Chromatography A 750, 155-160.

González-Vila, F.J., Lankes, U., Lüdemann, H-D., 2001. Comparison of the information gained by pyrolytic techniques and NMR spectroscopy on the structural features of aquatic humic substances. Journal of Analytical and Applied Pyrolysis 58-59, 349-359.

Greenwood, P.F., Leenheer, J.A., McIntyre, C., Berwick, L., Franzmann, P., 2006. Bacterial biomarkers thermally released from dissolved organic matter. Organic Geochemistry 37, 597-609.

Grice, K., Schouten, S., Blokker, P., Derenne, S., Largeau, C., Nissenbaum, A., Sinninghe-Damsté, J.S., 2003. Structural and isotopic analysis of kerogens in sediments rich in free sulfurised *Botryococcus braunii* biomarkers. Organic Geochemistry 34, 471-482.

Gros, M., Petrovic, M., Barcelo, D., 2006. Development of a multi-residue analytical methodology based on liquid chromatography–tandem mass spectrometry (LC–MS/MS) for screening and trace level determination of pharmaceuticals in surface and wastewaters. Talanta 70, 678–690.

Grosse, S., Letzel, T., 2007. Liquid chromatography/atmospheric pressure ionization mass spectrometry with post-column liquid mixing for the efficient determination of partially oxidized polycyclic aromatic hydrocarbons. Journal of Chromatography A 1139, 75–83.

Guo, L., Lehner, J.K., White, D.M., Garland, D.S., 2003. Heterogeneity of natural organic matter from the Chena River, Alaska. Water Research 37, 1015-1022.

Haitzer, M., Aiken, G.R., Ryan, J.N., 2002. Binding of mercury(II) to dissolved organic matter: The role of the mercury-to-DOM concentration ratio. Environmental Science and Technology 36, 3564-3570.

Hall, P.A., Watson, A.F.R., Garner, G.V., Hall, K., Smith, S., Waterman, D., Horsfield, B., 1999. An investigation of micro-scale sealed vessel thermal extraction-gas chromatography-mass spectrometry (MSSV-GC-MS) and

micro-scale sealed vessel pyrolysis-gas chromatography-mass spectrometry applied to a standard reference material of an urban dust/organics. The Science of the Total Environment 235, 269-276.

Han, Z., Kruge, M.A., 1999. Chemistry of maceral and groundmass density fractions of torbanite and cannel coal. Organic Geochemistry 30, 1381-1401.

Hartgers, W.A., Sinninghe-Damsté, J.S., de Leeuw, J.W., 1992. Identification of C_2-C_4 alkylated benzenes in flash pyrolysates of kerogens, coals and asphaltenes. Journal of Chromatography 606, 211-220.

Hartgers, W.A., Sinninghe-Damsté, J.S., de Leeuw, J.W., 1994a. Geochemical significance of alkylbenzene distributions in flash pyrolysates of kerogens, coals and asphaltenes. Geochimica et Cosmochimica Acta 58, 1759-1775.

Hartgers, W.A., Sinninghe-Damsté, J.S., de Leeuw, J.W., Ling, Y., Dyrkacz, G.R., 1994b. Molecular characterisation of flash pyrolysates of two carboniferous coals and their constituting maceral fractions. Energy and Fuels 8, 1055-1067.

Hartgers, W.A., Sinninghe-Damsté, J.S., Requejo, A.G., Allan, J., Hayes, J.M., Ling, Y., Xie, T., Primack, J., de Leeuw, J.W., 1994c. A molecular and carbon isotopic study towards the origin and diagenetic fate of diaromatic carotenoids. Organic Geochemistry 22, 703-725.

Hatcher, P.G., 1988. Dipolar-dephasing ^{13}C NMR studies of decomposed wood and coalified xylem tissue: Evidence for chemical structural changes associated with defunctionalisation of lignin structural units during coalification. Energy and Fuels 2, 48-58.

Hatcher, P.G., 1990. Chemical structural models for coalified wood (vitrinite) in low rank coal. Organic Geochemistry 16, 959-968.

Hatcher, P.G., Breger, I.A., Earl W. L., 1981. Nuclear magnetic resonance studies of ancient buried wood. I. Observations on the origin of coal to the brown coal stage. Organic Geochemistry 3, 49-55.

Hatcher, P.G., Clifford, D.J., 1994. Flash pyrolysis and in situ methylation of humic acids from soil. Organic Geochemistry 21, 1081-1092.

Hatcher, P.G., Clifford, D.J., 1997. The organic geochemistry of coal: from plant materials to coal. Organic Geochemistry 27, 251-274.

Hatcher, P.G., Dria, K.J., Kim, S., Frazier, S.W., 2001. Modern analytical studies of humic substances. Soil Science 166, 770–794.

Hatcher, P.G., Faulon, J-L., Wenzel, K.A., Cody, G.D., 1992. A structural model for lignin-derived vitrinite from high-volatile bituminous coal (coalified wood). Energy and Fuels 6, 813-820.

Hatcher, P.G., Lerch, H.E., Kotra, R.K., Verheyen, T.V., 1988. Pyrolysis g.c.-m.s. of a series of degraded woods and coalified logs that increase in rank from peat to subbituminous coal. Fuel 67, 1069-1075.

Hatcher, P.G., Lerch, H.E., Verheyen, T.V., 1989a. Organic geochemical studies of the transformation of gymnosperm xylem during peatification and coalification to subbitumous coal. International Journal of Coal Geology 13, 65-97.

Hatcher, P.G., Minard, R.D., 1996. Comparison of dehydrogenase polymer (DHP) lignin with native lignin from gymnosperm wood by thermochemolysis using tetramethylammonium hydroxide (TMAH). Organic Geochemistry 24, 593–600.

Hatcher, P.G., Vanderhart, D.L., Earl, W.L., 1980. Use of solid state ^{13}C NMR in structural studies of humic acids and humin from Holocene sediments. Organic Geochemistry 2, 87-92.

Hatcher, P.G., Wilson, M.A., Vassallo, A.M., Lerch, H.E, 1989b. Studies of angiospermous wood in Australian brown coal by nuclear magnetic resonance and analytical pyrolysis: new insights into the early coalification process. International Journal of Coal Geology 13, 99-126.

Hautevelle, Y., Michels, R., Lannuzel, F., Malartre, F., Trouiller, A., 2006b. Confined pyrolysis of extant land plants: A contribution to palaeochemotaxonomy. Organic Geochemistry 37, 1546-1561.

Hautevelle, Y., Michels, R., Malartre, F., Trouiller, A., 2006a. Vascular plant biomarkers as proxies for palaeoflora and palaeoclimatic changes at the Dogger/Malm transition of the Paris Basin (France). Organic Geochemistry 37, 610-625.

Hayatsu, R., Botto, R.E., Scott, R.G., McBeth, R.L., Winans, R.E., 1986. Evaluation of lignin and cellulose contributions to low-rank coal formation by alkaline cupric oxide oxidation. Fuel 65, 821-826.

Hayatsu, R., Botto, R.E., Scott, R.G., McBeth, R.L., Winans, R.E., 1987. Thermal catalytic transformation of pentacyclic triterpenoids: Alteration of geochemical fossils during coalification. Organic Geochemistry 11, 245-250.

Hayatsu, R., McBeth, R.L., Neill, P.H., Xia, Y., Winans, R.E., 1990. Terpenoid biomarkers in Argonne premium coal samples and their role during coalification. Energy and Fuels 4, 456-463.

Hedges, J.I., 1988. Polymerization of humic substances in natural environments. In: Humic Substances and Their Role in the Environment, Frimmel, F.H., Christman, R.F. (Eds.), Dahlem Konferenzen, West Berlin, pp. 45-58.

Hedges, J.I., Cowie, G.L., Ertel, J.R., Barbour, R.J., Hatcher, P.G., 1985. Degradation of carbohydrates and lignins in buried woods. Geochimica et Cosmochimica Acta 49, 701-711.

Hedges, J.I., Eglington, G., Hatcher, P.G., Kirchman, D.L., Arnosti, C., Derenne, S., Evershed, R.P., Kögel-Knabner, I., de Leeuw, J.W., Littke, R., Michaelis, W., Rullkötter, J., 2000. The molecularly uncharacterised component of non-living organic matter in natural environments. Organic Geochemistry 31, 945-958.

Hedges, J.I., Mann, D.C., 1979. The lignin geochemistry of marine sediments from the southern Washington coast. Geochmica et Cosmochimica Acta 43, 1809-1818.

Hedges, J.I., Oades, J.M., 1997. Comparative organic geochemistries of soils and marine sediments. Organic Geochemistry 27, 319-361.

Heitz, A., Blythe, J., Allpike, B.P., Joll, C.A. and Kagi, R.I., 2002. Plastic tastes in drinking water: factors affecting the chemistry of bromophenol formation. Water Science and Technology 2, 179-184.

Heitz, A., Kagi, R.I., Alexander, R., 2000. Polysulfide sulfur in pipewall biofilms: Its role in the formation of swampy odour in distribution systems. Water Science and Technology, 41, 271-278.

Helleur, R.J., Hayes, E.R., 1985. Analysis of polysaccharide pyrolysate of red algae by capillary gas chromatography-mass spectrometry. Journal of Analytical and Applied Pyrolysis 8, 333-347.

Hem, L., Efraimsen, H., 2001. Assimilable carbon in molecular weight fractions of natural organic matter. Water Research 35, 1106-1110.

Her, N., Amy, G., Foss, D., Cho, J., Yoon, Y., Kosenka, P., 2002. Optimisation of method for detecting and characterizing NOM by HPLC-size exclusion chromatography with UV and on-line DOC detection. Environmental Science and Technology 36, 1069-1076.

Hernes, P.J., Hedges, J.I., 2000. Determination of condensed tannin monomers in environmental samples by capillary gas chromatography of acid depolymerization extracts. Analytical Chemistry 72, 5115-5124.

Hernes, P.J., Hedges, J.I., 2004. Tannin signatures of barks, leaves, cones, and wood at the molecular level. Geochimica et Cosmochimica Acta 68, 1293-1307.

Hoefs, M.J.L., van Heemst, J.D.H., Gelin, F., Koopmans, M.P., van Kaam-Peters, H.M.E., Schouten, S., de Leeuw, J.W., Sinninghe-Damsté, J.S., 1995. Alternative biological sources for 1,2,3,4-tetramethylbenzene in flash pyrolysates of kerogen. Organic Geochemistry 23, 975-979.

Horsfield, B., 1990. Evaluating kerogen type according to source quality, compositional heterogeneity and thermal lability. Review of Palaeobotany and Palynology 65, 357-365.

Horsfield, B., Bharati, S., Larter, S.R., Leistner, F., Littke, R., Schenk, H.J., Dypvik, H., 1992. On the atypical petroleum-generating characteristics of alginate in the Cambrian Alum Shale. In: Early Organic Evolution: Implications for Mineral and Energy Resources, Schidlowski, M., Golubic, S., Kimberley, M.M., McKirdy, D.M., Trudinger, P.A., (Eds.). Springer-Verlag Berlin and Heidelberg GmbH and Co., 257-266.

Horsfield, B., Disko, U., Leistner, F., 1989. The micro-scale simulation of maturation: outline of a new technique and its potential applications. Geologische Rundschau 78, 361-374.

Horsfield, B., Dueppenbecker, S.J., 1991. The decomposition of Posidonia shale and Green River shale kerogens using microscale sealed vessel pyrolysis. Journal of Analytical and Applied Pyrolysis 20, 107-123.

Howe, R.F., Lu, X.Q., Hook, J., Johnson, W.D., 1997. Reaction of aquatic humic substances with aluminium: an ^{27}Al NMR study. Marine and Fresh Water Research 48, 377-383.

Howe, K.J., Clark, M.M., 2002. Fouling of micro-filtration and ultra-filtration membranes by natural waters. Environmental Science and Technology, 36, 3571-3576.

Huang, Y., Eglington, G., van der Hage, E.R.E., Boon, J.J., Bol, R., Ineson, P., 1998. Dissolved organic matter and its parent organic matter in grass upland soil horizons studied by analytical pyrolysis techniques. European Journal of Soil Science 49, 1-15.

Huber, S.A., Frimmel, F.H., 1994. Direct gel chromatographic characterisation and quantification of marine dissolved organic carbon using high-sensitivity DOC detection. Environmental Science and Technology 28, 1194-1197.

Hudson, N., Baker, A., Reynolds, D., 2007. Fluorescence analysis of dissolved organic matter in natural, waste and polluted waters – a review. River Research and Applications 23, 631-649.

Hunt, A.P., Parry, J.D. and Hamilton-Taylor, J., 2000. Further evidence of elemental composition as an indicator of the bioavailability of humic substances to bacteria. Limnology and Oceanography 45, 237-241.

Hwang, C.J., Krasner, S.W., Sclimenti M.J., Amy, G.L., Dickenson, E., Bruchet, A., Prompsy, C., Filippi, G., Croué, J-P., Violleau, D., 2001. Polar NOM: Characterisation, DBPs, Treatment. Report 90877, AWWA Research Foundation, Denver, Colorado.

Ikan, R., Ioselis, P., Rubinsztain, Y., Aizenshtat, Z., Miloslavsky, I., Yariv, S., Pugmire, R., Anderson, L.L., Woolfenden, W.R., Kaplan, I.R., Dorsey, T., Peters, K.E., Boon, J.J., de Leeuw, J.W., Ishiwatari, R., Morinaga, S., Yamamoto, S., Macihara, T., Muller-Vonmoos, M., Rub, A., 1992. Chemical, isotopic, spectroscopic and geochemical aspects of natural and synthetic humic substances. The Science of the Total Environment 117/118, 1-12.

Ikeya, K., Yamamoto, S., Watanabe, A., 2004. Semiquantitative GC/MS analysis of thermochemolysis products of soil humic acids with various degrees of humification. Organic Geochemistry 35, 583-594.

Iopollo, M., Alexander, R., Kagi, R.I., 1992. Identification and analysis of C_0-C_3 phenols in some Australian crude oils. Organic Geochemistry 18, 603-609.

Iopollo-Armanios, M., Alexander, R., Kagi, R.I., 1995. Geosynthesis of organic compounds: I. Alkylphenols. Geochimica et Cosmochimica Acta 59, 3017-3027.

Jarusutthirak, C., 2002. Fouling and flux decline of reverse osmosis (RO), nanofiltration (NF), and ultrafiltration (UF) membranes associated with effluent organic matter (EfOM) during wastewater reclamation/reuse. PhD Thesis, Department of Civil, Environmental and Architectural Engineering, University of Colorado.

Johnsen, S., Gribbestad, I.S., 1988. Influence of humic substance on the formation of chlorinated polycyclic aromatic hydrocarbons during chlorination of polycyclic aromatic hydrocarbon polluted water. Environmental Science and Technology 22, 978-981.

Joll, C., Couton, D., Heitz, A., Kagi, R.I., 2004. Comparison of reagents for off-line thermochemolysis of natural organic matter. Organic Geochemistry 35, 47-59.

Joyeux, C., Fouchard, S., Llopiz, P., Neunlist, S., 2004. Influence of the temperature and the growth phase on the hopanoids and fatty acids content of Frateuria aurantia (DSMZ 6220). Microbial Ecology 47, 371-379.

Kaiser, E., Simpson, A.J., Dria, K.J., Sulzberger, B., Hatcher, P.G., 2003. Solid-state and multidimensional solution-state NMR of solid phase extracted and ultrafiltered riverine dissolved organic matter. Environmental Science and Technology 37, 2929-2935.

Kalbitz, K., Schwesig, D., Schmerwitz, J., Kaiser, K., Haumaier, L., Glaser, B., Ellerbrock, R., Leinweber, P., 2003. Changes in properties of soil-derived dissolved organic matter induced by biodegradation. Soil Biology and Biochemistry 35, 1129-1142.

Keeler, C., Kelly, E.F., Maciel, G.E., 2006. Chemical-structural information from solid-state ^{13}C NMR studies of a suite of humic materials from a lower montane forest soil, Colorado, USA. Geoderma 130, 124-140.

Kelleher, B.P, Simpson, A.J., 2006. Humic substances in soils: Are they really chemically distinct? Environmental Science and Technology 40, 4605-4611.

Kim, S., Simpson, A.J., Kujawinski, E.B., Freitas, M.A., Hatcher, P.G., 2003. High resolution electrospray ionization mass spectrometry and 2D solution NMR for the analysis of DOM extracted by C18 solid phase disk. Organic Geochemistry 34, 1325-1335.

Kirk, T.K., Farrell, R.L., 1987. Enzymatic ‘‘combustion’’: the microbial degradation of lignin. Annual Review of Microbiology 41, 465-505.

Kleinert, M., Barth, T., 2008a. Phenols from lignin. Chemical Engineering Technology 31, 736-745.

Kleinert, M., Barth, T., 2008b. Towards a lignincellulosic biorefinery: direct one-step conversion of lignin to hydrogen-enriched biofuel. Energy and Fuels 22, 1371-1379.

Knicker, H., Almendros, G., González -Vila, F.J., Ludemann, H.D., Martin, F., 1995. ^{13}C and ^{15}N-NMR analysis of some fungal melanins in comparison with soil organic matter. Organic Geochemistry 11/12, 1023-1028.

Knicker, H., Almendros, G., González -Vila, F.J., Martin, F., Ludemann, H-D., 1996a. ^{13}C and ^{15}N-NMR spectroscopic examination of the transformation of organic nitrogen in plant biomass during thermal treatment. Soil Biology and Biochemistry 28, 1053-1060.

Knicker, H., Hatcher, P.G., 1997. Survival of protein in an organic-rich sediment – possible protection by encapsulation in organic matter. Naturwissenschaften 84, 231-234.

Knicker, H., Hatcher, P.G., González-Vila, F.J., 2002. Formation of heteroaromatic nitrogen after prolonged humification of vascular plant remains as revealed by nuclear magnetic resonance spectroscopy. Journal of Environmental Quality 31, 444-449.

Knicker, H., Lüdemann, H.-D., 1995. N-15 and C-13 CPMAS and solution NMR studies of N-15 enriched plant material during 600 days of microbial degradation. Organic Geochemistry 23, 329-341.

Knicker, H., Scaroni, A.W., Hatcher, P.G., 1996b. ^{13}C and ^{15}N-NMR spectroscopic investigation on the formation of fossil algal residues. Organic Geochemistry 24, 661-669.

Knicker, H., Skjemstad, J.O., 2000. Nature of organic carbon and nitrogen in physically protected organic matter of some Australian soils as revealed by solid-state ^{13}C and ^{15}N-NMR spectroscopy. Australian Journal of Soil Research 38, 113-127.

Koch, B.P., Dittmar, T., 2006. From mass to structure: an aromaticity index for high-resolution mass data of natural organic matter. Rapid Communications in Mass Spectrometry 20, 926-932.

Kögel-Knabner, I., 1997. ^{13}C and ^{15}N NMR spectroscopy as a tool in soil organic matter studies. Geoderma 80, 243-270

Koopmans, M.P., Carson, F.C., Lewan, M.D., Sinninghe-Damste, J.S., 1998. Biomarker generation from Type II-S kerogens in claystone and limestone during hydrous and anhydrous pyrolysis. Organic Geochemistry 29, 1395-1402.

Koopmans, M.P., de Leeuw, J.W., Lewan, M.D., 1996. Impact of dia- and catagenesis on sulphur and oxygen sequestration of biomarkers as revealed by artificial maturation of an immature sedimentary rock. Organic Geochemistry 25, 391-426.

Koopmans, M.P., Reiss, C., de Leeuw, J.W., Lewan, M.D., 1997. Sulphur and oxygen sequestration of *n*-C_{37} and *n*-C_{38} unsaturated ketones in an immature kerogen and the release of their carbon skeletons during early stages of thermal maturation. Geochimica et Cosmochimica Acta 61, 2397-2408.

Koopmans, M.P., Sinninghe-Damsté, J.S., Lewan, M.D., de Leeuw, J.W., 1995. Thermal stability of thiophene biomarkers as studied by hydrous pyrolysis. Organic Geochemistry 23, 583-596.

Korshin, G.V., Li, C-W., Benjamin, M.M., 1997. Monitoring the properties of natural organic matter through UV spectroscopy: A consistent theory. Water Research 31, 1787-1795.

Koster, J., Volkman, J.K., Rullkotter, J., Scholz-Bottcher, B.M., Reithmeier, J., Fischer, U., 1999. Mono-, di- and trimethyl-branched alkanes in cultures of the filamentous cyanobacterium *Calothrix scopulorum*. Organic Geochemistry 30, 1367-1379.

Kralert, P.G., Alexander, R., Kagi, R.I., 1995. An investigation of polar constituents in kerogen and coal using pyrolysis-gas chromatography-mass spectrometry with in situ methylation. Organic Geochemistry 23, 627-639.

Kruge, M.A., Mukhophadyay, P.K., Lewis, C.F.M., 1998. A molecular evaluation of contaminants and natural organic matter in surface sediments from western Lake Ontario. Organic Geochemistry 29, 1797-1812.

Kruge, M.A., Permanyer, A., 2004. Application of pyrolysis-GC/MS for rapid assessment of organic contamination in sediments of Barcelona harbor. Organic Geochemistry 35, 1395-1408.

Kujawinski, E.B., del Vecchio, R., Blough, N.V.,. Klein, G.C., Marshall, A.G., 2004. Probing molecular-level transformations of dissolved organic matter: Insights on photochemical degradation and protozoan modification from electrospray ionization Fourier transform ion cyclotron resonance mass spectrometry. Marine Chemistry 92, 23-37.

Kujawinski, E.B., Freitas, M.A., Zang, X., Hatcher, P.G., Green-Church, K.B., Jones, R.B., 2002. The application of electrospray ionization mass

spectrometry (ESI MS) to the structural characterization of natural organic matter. Organic Geochemistry 33, 171-180.

Landais, P., Michels, R., Elie, M., 1993. Are time and temperature the only constraints to the simulation of organic matter maturation? Organic Geochemistry 22, 617-630.

Landais, P., Monthioux, M., 1988. Closed system pyrolysis: An efficient technique for simulating natural coal maturation. Fuel Processing Technology 20, 123-132.

Lapen, A. J., Seitz, W.R. 1982. Fluorescence polarisation studies of the conformation of soil fulvic acid. Analytica Chimica Acta 134, 31–38.

Larter, S.R., Senftle, J.T., 1985. Improved kerogen typing for petroleum source rock analysis. Nature 318, 277-280.

Lavaud, A., Berwick, L., Chabbi, A., Greenwood, P., Croué, J-P., 2008. Isolation and characterization of groundwater (Lysimetric plate collected water) NOM: Comparison with surface water NOM. *Proceedings* of 4th IWA Specialist Conference: Natural Organic Matter Research Conference: from Source to Tap, Bath, UK, June 2-4 2008.

Lee, N., Amy, G., Croué, J-P., 2006. Low pressure membrane (MF/UF) fouling associated with allochthonous versus autochthonous natural organic matter. Water Research 40, 2357-2368.

Lee, N., Amy, G., Croué, J-P., Buisson, H., 2005. Morphological analyses of natural organic matter (NOM) fouling of low-pressure membranes (MF/UF). Journal of Membrane Science 261, 7-16.

Lee, W., Westerhoff, P., Croué, J-P., 2007. Dissolved organic nitrogen as a precursor for chloroform, dichloroacetonitrile, N-nitrosodimethylamine, and trichloronitromethane. Environmental Science and Technology 41, 5485-5490.

Leenheer, J.A., 1981. Comprehensive approach to preparative isolation and fractionation of dissolved organic carbon from natural waters and wastewaters. Environmental Science and Technology 15, 578-587.

Leenheer, J.A., 2004. Comprehensive assessment of precursors, diagenesis, and reactivity to water treatment of dissolved and colloidal organic matter. Water Science and Technology: Water Supply 4, 1-9.

Leenheer, J.A., Croué, J-P., 2003. Characterising dissolved aquatic organic matter: Understanding the unknown structures is key to better treatment of drinking water. Environmental Science and Technology A-Pages 37, 18A – 26A.

Leenheer, J.A., Croué, J-P., Benjamin, M., Korshin, G.V., Hwang, C.J., Bruchet, A., Aiken, G.R., 2000. Comprehensive isolation of natural organic matter from water for spectral characterizations and reactivity testing. In: ACS Symposium Series 761: Natural Organic Matter and Disinfection By-Products: Characterization and Control in Drinking Water, Barrett, S.E., Krasner, S.W., Amy, G.L., (Eds.), American Chemical Society, Washington DC.

Leenheer, J.A., Huffman, E.W.D., 1976. Classification of organic solutes in water using macroreticular resins. Journal of Research of the U.S. Geological Survey 4, 737-751.

Leenheer, J.A., Nanny, M.A., McIntyre, C., 2003a. Terpenoids as major precursors of dissolved organic matter in landfill leachates, surface water and groundwater. Environmental Science and Technology 37, 2323-2331.

Leenheer, J.A., Noyes, T.I., 1984. A filtration and column-adsorption system for onsite concentration and fractionation of organic substances from large volumes of water. US Geological Survey Water Supply Paper 2230, US Government Printing Office, Washington DC, 16p.

Leenheer, J.A., Noyes, T.I., 1989. Derivatization of humic substances for structural studies. In: Humic Substances II - In Search of Structure, Hayes, M.H.B., MacCarthy, P., Malcolm, R.L., Swift, R.S. (Eds.), Wiley, Chichester, pp 257-280.

Leenheer, J.A., Noyes, T.I., Rostad, C.E., Davisson, M.L., 2004. Characterization and origin of polar dissolved organic matter from the Great Salt Lake. Biogeochemistry 69, 125-141.

Leenheer, J.A., Rostad, C., 2004. Tannins and terpenoids as major precursors of Suwannee River fulvic acid. U.S. Geological Survey Scientific Investigations Report 2004, 16p.

Leenheer, J.A., Rostad, C.E., Barber, L.B., Schroeder, R.A., Anders, R., Davisson, M.L., 2001a. Nature and chlorine reactivity of organic constituents from reclaimed water in groundwater, Los Angeles County, California. Environmental Science and Technology 35, 3869-3876.

Leenheer, J.A., Rostad, C.E., Gates, P.M., Furlong, E.T., Ferrer, I., 2001b. Molecular resolution and fragmentation of fulvic acid by electrospray ionisation/multistage tandem mass spectrometry. Analytical Chemistry 73, 1461-1471.

Leenheer, J.A., Wershaw, R.L., Brown, G.K. and Reddy, M.M., 2003b. Characterization and diagenesis of strong-acid carboxyl groups in humic substances. Applied Geochemistry 18, 471-482.

Leenheer, J.A., Wershaw, R.L., Reddy, M.M., 1995. Strong-acid carboxyl group structures in fulvic acid from the Suwannee River, Georgia. 2. Major structures. Environmental Science and Technology 29, 399-405.

Leenheer, J.A., Wilson, M.A., Malcolm, R.L., 1987. Presence and potential significance of aromatic-ketone groups in aquatic humic substances. Organic Geochemistry 4, 273-280.

Lehtonen, T., Peuravuori, J., Pihlaja, K., 2000a. Degradation of TMAH treated aquatic humic matter at different temperatures. Journal of Analytical and Applied Pyrolysis 55, 151-160.

Lehtonen, T., Peuravuori, J., Pihlaja, K., 2000b. Characterisation of lake-aquatic humic matter isolated with two different sorbing solid techniques: tetramethylammonium hydroxide treatment and pyrolysis-gas chromatography/mass spectrometry. Analytica Chimica Acta 424, 91-103.

Lehtonen, T., Peuravuori, J., Pihlaja, K., 2004. Degradative analysis of aquatic fulvic acid: CuO oxidation versus pyrolysis after tetramethylammonium hydroxide treatments in air and helium atmospheres. Analytica Chimica Acta 511, 349-356.

Lewan, M.D., 1985. Evaluation of petroleum generation by hydrous pyrolysis experimentation. Philosophical Transactions of the Royal Society of London Series A 315, 123-132.

Lewan, M.D., 1993. Laboratory simulation of petroleum formation: Hydrous pyrolysis. In: Organic Geochemistry, Principles and Applications – Topics in Geobiology, Engel, M.H., Macko, S.A. (Eds.), Plenum Publishing Corporation, New York, pp. 419-444.

Lewan, M.D., 1997. Experiments on the role of water in petroleum formation. Geochimica et Cosmochimica Acta 61, 3691-3723.

Lewan, M.D., Winters, J.C., McDonald, J.H., 1979. Generation of oil-like pyrolysates from organic-rich shales. Science 203, 897-899.

Littlejohn, C.L., 2004. Influence of artificial destratification on limnological processes in Lake Samsonvale (North Pine Dam), Queensland, Australia. PhD Thesis, Griffith University, Brisbane, Australia.

Lorenz, K., Preston, C.M., Raspe, S., Morrison, I.K., Feger, K.H., 2000. Litter decomposition and humus characteristics in Canadian and German spruce ecosystems: information from tannin analysis and ^{13}C CPMAS NMR. Soil Biology and Biochemistry 32, 779-792.

Love, G.D., Bowden, S.A., Jahnke, L.L., Snape, C.E., Campbell, C.N., Day, J.G., Summons, R.E., 2005. A catalytic hydropyrolysis method for the rapid screening of microbial cultures for lipid biomarkers. Organic Geochemistry 36, 63-82.

Love, G.D., McAulay, A., Snape, C.E., Bishop, A.N., 1997. Effect of process variables in catalytic hydropyrolysis on the release of covalently-bound aliphatic hydrocarbons from sedimentary organic matter. Energy and Fuels 11, 522-531.

Love, G.D., Snape, C.E., Carr, A.D., Houghton, R.C., 1995. Release of covalently bound biomarkers in high yields from kerogen via catalytic hydropyrolysis. Organic Geochemistry 23, 981-986.

Lu , X.Q., Hanna, J.V., Johnson, W.D., 2000. Source indicators of humic substances: an elemental composition, solid state ^{13}C CP/MAS NMR and Py-GC/MS study. Applied Geochemistry 15, 1019-1033.

Lu , X.Q., Hanna, J.V., Johnson, W.D., 2001. Evidence of chemical pathways of humification: a study of aquatic humic substances heated at various temperatures. Chemical Geology 177, 249-264.

Lu, X.Q., Johnson, W.D., 1997. The reaction of aquatic humic substances with copper(II) ions: an ESR study of complexation. The Science of the Total Environment 203, 199-207.

Lu, X.Q., Johnson, W.D., Hook, J., 1998. Reaction of vanadate by aquatic humic substances: an ESR and 51 V NMR study. Environmental Science and Technology 32, 2257-2263.

Lu, X.Q., Maie, N., Hanna, J.V., Childers, D.L., Jaffé, R., 2003. Molecular characterisation of dissolved organic matter in freshwater wetlands of the Florida Everglades. Water Research 37, 2599-2606.

Mackenzie, A.S., Brassel, S.C., Eglington, G., Maxwell, J.R., 1982. Chemical fossils: The geological fate of steroids. Science 217, 491-504.

Mackenzie, A.S., Patience, R.L., Maxwell, J.R., Vandenbroucke, M., Durand, B., 1980. Molecular parameters of maturation in the Toarcian shales, Paris Basin, France – I. Changes in the configurations of acyclic isoprenoid alkanes, steranes and triterpanes. Geochimica et Cosmochimica Acta 44, 1709-1721.

Maillard, L.C., 1912. Reaction of amino acids on sugars: Melanoidin formation through a methodologic way. Comptes Rendus de l'Académie des Sciences 156, 148-149.

Maillard, L.C., 1917. Identité des matiéres humiques de synthése avec les matiéres humiques naturelles. Annales de Chimie (Paris) 7, 113-152.

Makdissy, G., Croué, J-P., Amy, G., Buisson, H., 2004. Fouling of a polyethersulfone membrane by natural organic matter. Water Science and Technology: Water Supply 4, 205-212.

Malcolm, R.L., 1990. The uniqueness of humic substances in each of soil, stream and marine environments. Analytica Chimica Acta 232, 19-30.

Malcolm, R.L., MacCarthy, P., 1992. Quantitative evaluation of XAD-8 and XAD-4 resins used in tandem for removing organic solutes from water. Environment International 18, 597-607.

Malcolm, R.L., McKnight, D.M., Averett, R.C., 1989. History and description of the Okefenokee Swamp – origin of the Suwannee River. In: Humic Substances in the Suwannee River, Georgia: Interactions, Properties and Proposed Structures, US Geological Survey Water-Supply Paper 2373.

Mansuy, L., Bourezgui, Y., Garnier-Zarli, E., Jardé, E., Réveillé, V., 2001. Characterization of humic substances in highly polluted river sediments by pyrolysis-methylation-gas chromatography-mass spectrometry. Organic Geochemistry 32, 223-231.

Mansuy, L., Landais, P., Ruau, O., 1995. Importance of the reacting medium in artificial maturation of a coal by confined pyrolysis. 1. Hydrocarbons and polar compounds. Energy and Fuels 9, 691-703.

Mao, J., Cory, R.M., McKnight, D.M., Schmidt-Rohr, K., 2007. Characterization of a nitrogen-rich fulvic acid and its precursor algae from solid state NMR. Organic Geochemistry 38, 1277-1292.

Mao, J-D., Hundal, L.S., Schmidt-Rohr, K., Thompson, M.L., 2003. Nuclear magnetic resonance and diffuse-reflectance infrared Fourier transform spectroscopy of biosolids-derived biocolloidal organic matter. Environmental Science and Technology 37, 1751-1757.

Martin, F., del Rio, J.C., González-Vila, F.J., Verdejo, T., 1995a. Thermally assisted hydrolysis and alkylation of lignins in the presence of tetra-alkylammonium hydroxides. Journal of Analytical and Applied Pyrolysis 35, 1-13.

Martin, F., del Rio, J.C., González-Vila, F.J., Verdejo, T., 1995b. Pyrolysis derivatization of humic substances 2. Pyrolysis of soil humic acids in the presence of tetramethylammonium hydroxide. Journal of Analytical and Applied Pyrolysis 35, 75-83.

Martin, F., González-Vila, F.J., del Rio, J.C., Verdejo, T., 1994. Pyrolysis derivatization of humic substances 1. Pyrolysis of fulvic acids in the presence of tetramethylammonium hydroxide. Journal of Analytical and Applied Pyrolysis 28, 71-80.

McDonald, S., Bishop, A.G., Prenzler, P.D., Robards, K., 2004. Analytical chemistry of freshwater humic substances. Analytica Chimica Acta 527, 105-124.

McIntyre, C.P., Batts, B.D., Jardine, D.J., 1997. Electrospray mass spectrometry of groundwater organic acids. Journal of Mass Spectrometry 32, 329-330.

McIntyre, C., McRae, C., Batts, B., Piccolo, A., 2005. Structural characterisation of groundwater hydrophobic acids isolated from the Tomago Sand Beds, Australia. Organic Geochemistry 36, 385-397.

McIntyre, C., McRae, C., Jardine, D.R., Batts, B.D., 2002. Identification of compound classes in soil and peat fulvic acids as observed by electrospray ionisation tandem mass spectrometry. Rapid Communications in Mass Spectrometry 16, 1604-1609.

McKinney, D.E., Carson, D.M., Clifford, D.J., Minard, R.D., Hatcher, P.G., 1995. Off-line thermochemolysis versus flash pyrolysis for the in situ methylation of lignin: is pyrolysis necessary? Journal of Analytical and Applied Pyrolysis 34, 41-46.

McKinney, D.E., Hatcher, P.G., 1996. Characterisation of peatified and coalified wood by tetramethylammonium hydroxide (TMAH) thermochemolysis. International Journal of Coal Geology 32, 217-228.

Meredith, W., Russel, C.A., Snape, C.E., Fabbri, D., Vane, C.H., Love, G.D., 2004. The thermal desorption of hydropyrolysis oils from silica to facilitate rapid screening by GC-MS. Organic Geochemistry 35, 73-89.

Meredith, W., Sun, C-G., Snape, C.E., Sephton, M.A., Love, G.D., 2006. The use of model compounds to investigate the release of covalently bound biomarkers via hydropyrolysis. Organic Geochemistry 37, 1705-1714.

Michels, R., Burkle, L., Mansuy, L., Langlois, E., Ruau, O., Landais, P., 2000. Role of polar compounds as source of hydrocarbons and reactive medium during artificial maturation of Mahakam coal. Energy and Fuels 14, 1059-1071.

Miles, J., 2005. Characterisation studies to investigate the origin of aquatic biopolymers. Chemistry Honours Dissertation, Department of Applied Chemistry, Curtin University of Technology, Perth, Western Australia.

Monthioux, M., Landais, P., Monin, J-C., 1985. Comparison between natural and artificial maturation series of humic coals from the Mahakam delta, Indonesia. Organic Geochemistry 8, 275-292.

Murphy, E.M., Zachara, J.M. and Smith, S.C., 1990. Influence of mineral-bound humic substances on the sorption of hydrophobic organic compounds. Environmental Science and Technology 24, 1507-1516.

Murray, I.P., Love, G.D., Snape, C.E., Bailey, N.J.L., 1998. Comparison of covalently-bound aliphatic biomarkers released via hydropyrolysis with their solvent-extractable counterparts for a suite of Kimmeridge clays. Organic Geochemistry 29, 1487-1505.

Mycke, B., Narjes, F., Michaelis, W., 1987. Bacteriohopanetetrol from chemical degradation of an oil shale kerogen. Nature 326, 179-181.

Najm, I., Trussel, R.R., 2001. NDMA formation in water and wastewater. Journal of American Water Works Association 93, 92-99.

Namour, P., Müller, M.C., 1998. Fractionation of organic matter from wastewater treatment plants before and after a 21-day biodegradability test: a physical-chemical method for measurement of the refractory part of effluents. Water Research 32, 2224-2231.

Nanny, M.A., Minear, R.A. and Leenheer, J.A., (Eds.), 1997. Nuclear Magnetic Resonance Spectroscopy in Environmental Chemistry, Oxford University Press Inc., New York.

NHMRC and NRMMC (Eds.), 2004. Australian Drinking Water Guidelines 6 2004. National Health and Medical Research Council and National Resource Management Ministerial Council.

Nierop, K.G.J., 1998. Origin of aliphatic compounds in a forest soil. Organic Geochemistry 29, 1009-1016.

Nierop, K.A., Filley, T.R., 2007. Assessment of lignin and (poly-)phenol transformations in oak (Quercus robur) dominated soils by ^{13}C-TMAH thermochemolysis. Organic Geochemistry 31, 551-565.

Nimmagadda, R.D., McRae, C.R., 2006. A novel reduction of polycarboxylic acids into their corresponding alkanes using *n*-butylsilane or diethylsilane as the reducing agent. Tetrahedron Letters 47, 3505-3508.

Nimmagadda, R.D., McRae, C.M., 2007a. Characterisation of the backbone structures of several fulvic acids using a novel and selective chemical reduction method. Organic Geochemistry 38, 1061-1072.

Nimmagadda, R.D., McRae, C.R., 2007b. Characterisation of Antarctic fulvic acids by a novel and selective chemical reduction – implications for the identification of precursors of humic substances. Proceedings of the 23rd International Meeting of Organic Geochemistry (IMOG), Torquay, UK, September 2007, pp 219-220.

Ohta, K., Venkatesan, M.I., 1992. Experimental simulation of lignin diagenesis: pyrolysis of wood specimen with and without minerals. Energy and Fuels 6, 271-277.

Opsahl, S., Benner, R., 1997. Distribution and cycling of terrigenous dissolved organic matter in the ocean. Nature 386, 480-482.

Ourisson, G., Albrecht, P., Rohmer, M., 1982. Predictive microbial biochemistry - from molecular fossils to prokaryotic membranes. Trends in Biochemical Science 7, 236-239.

Page, D.W., van Leeuwen, J.A., Spark, K.M., Mulcahy, D.E., 2002. Pyrolysis characterisation of plant, humus and soil extracts from Australian catchments. Journal of Analytical and Applied Pyrolysis 65, 269-285.

Page, D.W., van Leeuwen, J.A., Spark, K.M., Mulcahy, D.E., 2003. Application of pyrolysis-gas chromatography/mass spectrometry for characterisation of dissolved organic matter before and after alum treatment. Journal of Analytical and Applied Pyrolysis 67, 247-262.

Paine, J.B., Pithawalla, Y.B., Naworal, J.D., 2008. Carbohydrate pyrolysis mechanisms from isotopic labelling Part 4. The pyrolysis of D-glucose: The formation of furans. Journal of Analytical and Applied Pyrolysis, *In press*.

Pancost, R.D., Boot, C.S., 2004. The palaeoclimatic utility of terrestrial biomarkers in marine sediments. Marine Chemistry 92, 239-261.

Park, N., Kwon, B., Kim, S-D., Cho, J., 2006. Characterizations of the colloidal and microbial organic matters with respect to membrane foulants. Journal of Membrane Science 275, 29-36.

Parsons, J.W., 1989. Hydrolytic degradations of humic substances. In: Humic Substances II - In Search of Structure, Hayes, M.H.B., MacCarthy, P., Malcolm, R.L., Swift, R.S. (Eds.), Wiley, Chichester, pp. 99-120.

Pastorova, I., Botto, R.E., Arisz, P.W., Boon, J.J., 1994. Cellulose char structure: a combined analytical Py-GC-MS, FTIR and NMR study. Carbohydrate Research 262, 27-47.

Patience, R.L., Baxby, M., Bartle, K.D., Perry, D.L., Rees, A.G.W., Rowland, S.J., 1992. The functionality of organic nitrogen in some recent sediments from the Peru upwelling region. Organic Geochemistry 18, 161-169.

Payne, D.F., Ortoleva, P.J., 2001. A model for lignin alteration – part I: a kinetic reaction-network model. Organic Geochemistry 32, 1073-1085.

Pearson, M.J., Obaje, N.G., 1999. Onocerane and other triterpenoids in Late Cretaceous sediments from the Upper Benue Trough, Nigeria: tectonic and palaeoenvironmental implications. Organic Geochemistry 30, 583-592.

Pedentchouk, N., Freeman, K.H., Harris, N.B., Clifford, D.J., Grice, K., 2004. Sources of alkylbenzenes in Lower Cretaceous lacustrine source rocks, West African rift basins. Organic Geochemistry 35, 33-45.

Peters, K.E., Moldowan, J.M., (Eds.), 1993. The Biomarker Guide, Interpreting Molecular Fossils in Petroleum and Ancient Sediments. Prentice Hall, Englewood Cliffs, New Jersey, 363pp.

Peters, K.E., Walters, C.C., Moldowan, J.M., (Eds.), 2005. The Biomarker Guide, Volume 2. Biomarkers and Isotopes in Petroleum Exploration and Earth History. Cambridge University Press, 700pp.

Petrovic, M., Eljarrat, E., López de Alda, M.J., Barceló, D., 2002. Recent advances in the mass spectrometric analysis related to endocrine disrupting compounds in aquatic environmental samples. Journal of Chromatography A 974, 23-51.

Peulvé, S., de Leeuw, J.W., Sicre, M-A., Baas, M., Saliot, A., 1996. Characterisation of macromolecular organic matter in sediment traps from the northwestern Mediterranean Sea. Geochimica et Cosmochimica Acta 60, 1239-1259.

Philp, R.P., 1985. Fossil fuel biomarkers. Methods in Geochemistry and Geophysics Volume 23. Elsevier, New York, 294 pp.

Philp, R.P., Gilbert, 1987. A review of biomarkers in kerogens as determined by pyrolysis-gas chromatography and pyrolysis-gas chromatography-mass spectrometry. Journal of Analytical and Applied Pyrolysis 11, 93-108.

Poinar, H.N., Stankiewicz, B.A., 1999. Protein preservation and DNA retrieval from ancient tissues. Proceedings of the National Academy of Sciences of the United States of America 96, 8426-8431.

Poirier, N., Derenne, S., Balesdent, J., Rouzaudd, J-N., Mariotti, A., Largeau, C., 2002. Abundance and composition of the refractory organic fraction of an ancient, tropical soil (Pointe Noire, Congo). Organic Geochemistry 33, 383-391.

Poirier, N., Derenne, S., Rouzad, J.N., Largeau, C., Mariotti, A., Balesdent, J., Maquet, J., 2000. Chemical structure and sources of the macromolecular, resistant, organic fraction isolated from a forest soil (Lacadé, south-west France). Organic Geochemistry 31, 813-827.

Pojana, G., Bonfa, A., Busetti, F., Collarin, A., Marcomini, A., 2004. Determination of natural and synthetic estrogenic compounds in coastal lagoon waters by HPLC-electro spray-mass spectrometry. International Journal of Environmental Analytical Chemistry 84, 717-727.

Prosser, I.P., Roseby, S.J., 1995. A chronosequence of rapid leaching of mixed podzol soil materials following sand mining. Geoderma 64, 297-280.

Pouwels, A.D., Eijkel, G.B., Boon, J.J., 1989. Curie-point pyrolysis-capillary gas chromatography-high-resolution mass spectrometry of microcrystalline cellulose. Journal of Analytical and Applied Pyrolysis 14, 237-279.

Pouwels, A.D., Tom, A., Eijkel, G.B., Boon, J.J., 1987. Characterisation of beech wood and its holocellulose and xylan fractions by pyrolysis-gas chromatography-mass spectrometry. Journal of Analytical and Applied Pyrolysis 11, 417-436.

Putschew, A., Schaeffer-Reiss, C., Schaeffer, P., Koopmans, M.P., de Leeuw, J.W., Lewan, M.D., Sinninghe Damsté, J.S., Maxwell, J.R., 1998. Release of sulfur- and oxygen-bound components from a sulfur-rich kerogen during simulated maturation by hydrous pyrolysis. Organic Geochemistry 29, 1875-1890.

Püttman, W., Villar, H., 1987. Occurrence and geochemical significance of 1,2,5,6-tetramethylnaphthalene. Geochimica et Cosmochimica Acta 51, 3023-3029.

Quénéa, K., Derenne, S., Largeau, C., Rumpel, C., Mariotti, A., 2005a. Spectroscopic and pyrolytic features and abundance of the macromolecular refractory fraction in a sandy acid forest soil (Landes de Gascogne, France). Organic Geochemistry 36, 349-362.

Quénéa, K., Derenne, S., González-Vila, F.J., Mariotti, A., Rouzaud, J.N., Largeau, C., 2005b. Study of the composition of the macromolecular refractory fraction from an acidic sandy forest soil (Landes de Gascogne, France) using chemical degradation and electron microscopy. Organic Geochemistry 36, 1151-1162.

Quénéa, K., Derenne, S., González-Vila, F.J., González-Pérez, J.A., Mariotti, A., Largeau, C., 2006. Double-shot pyrolysis of the non-hydrolysable organic fraction isolated from a sandy forest soil (Landes de Gascogne, South-West France). Comparison with classical Curie point pyrolysis. Journal of Analytical and Applied Pyrolysis 76, 271-279.

Radke, M., 1987. Organic geochemistry of aromatic hydrocarbons. In: Advances in Petroleum Geochemistry Vol. 2, Brooks, J., Welte, D.H., (Eds.), Academic Press, pp. 141-207.

Reckhow, D.A., Singer, P.C., Malcolm, R.L., 1990. Chlorination of humic materials: byproducts formation and chemical interpretations. Environmental Science and Technology 24, 1655-1664.

Reeves, J.B., Francis, B.A., 1997. Pyrolysis-gas-chromatography-mass-spectrometry for the analysis of forages and by-products. Journal of Analytical and Applied Pyrolysis 40-41, 243-265.

Richnow, H.H., Jenisch, A., Michaelis, W., 1992. Structural investigations of sulphur-rich macromolecular oil fractions and a kerogen by sequential chemical degradation. Organic Geochemistry 19, 351-370.

Rohmer, M., Brisseret, P., Neunlist, S., 1992. The hopanoids, prokaryotic triterpenoids and precursors of ubiquitous molecular fossils. In: Biological Markers in Sediments and Petroleum, Moldowan, J.M., Albrecht, P., Philp, R.P., (Eds.), Prentice-Hall, Englewood Cliffs, NJ, pp. 1-17.

Rohmer, M., Bouvier-Nave, P., Ourisson, G., 1984. Distribution of hopanoid triterpenes in prokaryotes. Journal of General Microbiology 130, 1137-1150.

Romero, J., Ventura, F., Caixach, J., Rivera, J., Godé, L.X., Ninerola, J.M., 1998. Identification of 1,3-dioxanes and 1,3-dioxolanes as malodorous compounds at trace levels in river water, groundwater, and tap water. Environmental Science and Technology 32, 206-216.

Rook, J., 1974. Formation of haloforms during chlorination of natural waters. Water Treatment Examination 23, 234-243.

Rook, J., 1976. Haloforms in drinking water. Journal of the American Water Works Association 68, 168-172.

Rook, J., 1977. Chlorination reactions of fulvic acids in natural waters. Environmental Science and Technology 11, 478-482.

Rostad, C.E., Leenheer, J.A., Daniel, S.R., 1997. Organic carbon and nitrogen content associated with colloids and suspended particulates from the Mississippi River and some of its tributaries. Environmental Science and Technology 31, 3218-3225.

Rowland, S.J., Maxwell, J.R., 1984. Reworked triterpenoid and steroid hydrocarbons in a recent sediment. Geochimica et Cosmochimica Acta 48, 617-624.

Ruble, T.E., Greenwood, P.G., Lisk, M., Ahmed, M., 2000a. Reconstructing biodegraded oils via asphaltene pyrolysis: Application of novel geochemical techniques in the Carnarvon Basin, Australia. Proceedings of the Australian Organic Geochemistry Conference, Townsville, Queensland, July 12-14th, 2000.

Ruble, T.E. Greenwood, P.G. Lisk, M., Ahmed, M. 2000b. Use of asphaltene pyrolysates to reconstruct biodegraded oils from the Carnarvon Basin, Australia. Proceedings of the 14th International Symposium on Analytical and Applied Pyrolysis, Seville, Spain, April 2-6th, p53.

Russell, C.A., Snape, C.E., Meredith, W., Love, G.D., Clarke, E., Moffatt, B., 2004. The potential of bound biomarker profiles released via catalytic hydropyrolysis to reconstruct basin charging history for oils. Organic Geochemistry 35, 1441-1459.

Saiz-Jimenez, C., 1993. Modern concepts on the origin and structure of terrestrial humic substances: the alkylaromatic network approach. In: Humic Substances in the Global Environment and Implications on Human Health, Senesi, N., Tiano, T.M. (Eds.), Elsevier, Amsterdam.

Saiz-Jimenez, C., 1994. Analytical pyrolysis of humic substances: pitfalls, limitations, and possible solutions. Environmental Science and Technology 28, 1773-1780.

Saiz-Jimenez, C., 1995. Reactivity of the aliphatic humic moiety in analytical pyrolysis. Organic Geochemistry 23, 955-961.

Saiz-Jimenez, C., de Leeuw, J.W. 1984a. Pyrolysis-gas chromatography-mass spectrometry of soil polysaccharides, soil fulvic acids and polymaleic acid. Organic Geochemistry 6, 287-293.

Saiz-Jimenez, C., de Leeuw, J.W. 1984b. Pyrolysis-gas chromatography-mass spectrometry of isolated, synthetic and degraded lignins. Organic Geochemistry 6, 417-422.

Saiz-Jimenez, C., de Leeuw, J.W., 1986a. Lignin pyrolysis products: their structures and their significance as biomarkers. Organic Geochemistry 10, 869-876.

Saiz-Jimenez, C., de Leeuw, J.W, 1986b. Chemical characterisation of soil organic matter fractions by analytical pyrolysis-gas chromatography-mass spectrometry. Journal of Analytical and Applied Pyrolysis 9, 99-119.

Sandison, C., Edwards, D., 2003. Users guide for NOSID database, Geoscience Australia - Internal report, Canberra, Australia.

Schenk, H.J., Horsfield, B., 1993. Kinetics of petroleum generation by programmed-temperature closed- versus open-system pyrolysis. Geochimica et Cosmochimica Acta 57, 623-630

Schlautman, M.A., Morgan, J.J., 1993. Effects of aqueous chemistry on the binding of polycyclic aromatic hydrocarbons by dissolved humic materials. Environmental Science and Technology 27, 961-969.

Schmid, J.C., Connan, J., Albrecht, P., 1987. Occurrence and geochemical significance of long-chain dialkthiacyclopentanes. Nature 329, 54-56.

Schmidt, H.-L., Kexel, H., Butzenlechner, M., Schwarz, S., Gleixner, G., Thimet, S., Werner, R.A., Gensler, M., 1995. Nonstatistical isotope distribution in natural compounds: mirror of their biosynthesis and key for origin assignment. In: Stable Isotopes in the Biosphere, Wada, E., Yoneyama, T., Minagawa, M., Fry, B., (Eds.). Kyoto University Press, Kyoto, pp. 17-35.

Schulten, H-R., 1993. Analytical pyrolysis of humic substances and soils: geochemical, agricultural and ecological consequences. Journal of Analytical and Applied Pyrolysis 25, 97-122.

Schulten, H-R., 1996a. A new approach to the structural analysis of humic substances in water and soils: humic acids oligomers. In: Humic and Fulvic Acids: Isolation, Structure and Environmental Role, Gaffney, J.S., Marley, N.A., Clark, S.B. (Eds.), American Chemical Society Symposium Series, Washington, DC, pp. 42-56.

Schulten, H-R., 1996b. Three-dimensional, molecular structures of humic acids and their interactions with water and dissolved contaminants. International Journal of Environmental Analytical Chemistry 61, 1-16.

Schulten, H-R., 1999. Analytical pyrolysis and computational chemistry of aquatic humic substances and dissolved organic matter. Journal of Analytical and Applied Pyrolysis 49, 385-415.

Schulten, H-R., Abbt-Braun, G., Frimmel, F., 1987. Time-resolved pyrolysis-field ionisation mass spectrometry of humic material isolated from freshwater. Environmental Science and Technology 21, 349-357.

Schulten, H-R., Gleixner, G., 1999. Analytical pyrolysis of dissolved organic matter in aquatic systems: Structure and origin. Water Research 33, 2489-2498.

Schulten, H-R., Leinweber, P., 1996. Characterisation of humic and soil particles by analytical pyrolysis and computer modelling. Journal of Analytical and Applied Pyrolysis 38, 1-53.

Schulten, H-R., Plage, B., Schnitzer, M., 1991. A chemical structure for humic substances. Naturwissenschaften 78, 311-312.

Schulten, H-R., Schnitzer, M., 1998. The chemistry of soil organic nitrogen: A review. Biology and Fertility of Soils 26, 1-15.

Schulten, H-R., Sorge-Lewin, C., Schnitzer, M., 1997. Structure of ‘unknown’ soil nitrogen investigated by analytical pyrolysis. Biology and Fertility of Soils 24, 249-254.

Senesi, N., 1990. Molecular and quantitative aspects of the chemistry of fulvic acid and its interactions with metal ions and organic chemicals: Part II. The fluorescence spectroscopy approach. Analytica Chimica Acta 232, 77-106.

Sephton, M.A., Meredith, W., Sun, C-G., Snape, C.E., 2005. Hydropyrolysis of steroids: a preparative step for compound-specific carbon isotope ratio analysis. Rapid Communications in Mass Spectrometry 19, 3339-3342.

SEQWater and Brisbane Water, 2006. Drought Water Quality Risk Assessment. Report by SEQWater and Brisbane Water.

Shang, C., Gong, W.L., Blatchley, E.R., 2000. Breakpoint chemistry and volatile by-product formation resulting from chlorination of model organic-N-compounds. Environmental Science and Technology 34, 1721-1728.

Sharma, R.K., Chan, W.G., Hajaligol, M.R., 2005. Product compositions from pyrolysis of some aliphatic α-amino acids. Journal of Analytical and Applied Pyrolysis 75, 69-81.

Sicre, M.A., Marty, J.C., Saliot, A., Aparicio, X., Grimalt, J., Albaiges, J., 1987. Aliphatic and aromatic hydrocarbons in different sized aerosols over the Mediterranean Sea: Occurrence and origin. Atmospheric Environment 21, 2247-2259.

Sigleo, A.C., Hoering, T.C., Helz, G.R., 1982. Composition of estuarine colloidal material: Organic components. Geochimica et Cosmochimica Acta 46, 1619-1626.

Silverstein, R.M., Webster, F.X., 1997. Spectrometric Identification of Organic Compounds. John Wiley and Sons, New York.

Simoneit, B.R.T., 1985. Cyclic terpenoids in the geosphere. In: Biological Markers in the Sedimentary Record, Johns, R.B. (Ed.), Elsevier, Amsterdam, pp. 43-49.

Simoneit, B.R., Grimalt, J.O., Wang, T.G., Cox, R.E., Hatcher, P.G., Nissenbaum, A., 1986. Cyclic terpenoids of contemporary resinous plant detritus and of fossil woods, ambers and coals. Organic Geochemistry 10, 877-889.

Simoneit, B.R.T., Rushdi, A.I., Bin Abas, M.R., Didyk, B.M., 2003. Alkyl amides and nitriles as novel tracers for biomass burning. Environmental Science and Technology 37, 16-21.

Simpson, M.J., Chefetz, B., Deshmukh, A.P., Hatcher, P.G., 2005. Comparison of polycyclic aromatic hydrocarbon distributions and sedimentary organic

matter characteristics in contaminated, coastal sediments from Pensacola Bay, Florida. Marine Environmental Research 59, 139-163.

Sinninghe-Damsté, J.S., de las Heras, F.X.C., de Leeuw, J.W., 1992b. Molecular analysis of sulphur rich brown coals by flash pyrolysis-gas chromatography-mass spectrometry. Journal of Chromatography 607, 361-376.

Sinninghe Damsté, J.S., de Las Heras, F.X.C., van Bergen, P.F., de Leeuw, J.W., 1993. Characterization of Tertiary Catalan lacustrine oil shales: Discovery of extremely organic sulphur-rich Type I kerogens. Geochimica et Cosmochimica Acta 57, 389-415.

Sinninghe-Damste, J.S., Eglington, T.I., De Leeuw, J.W., 1992a. Alkylpyrroles in a kerogen pyrolysate: Evidence for abundant tetra-pyrrole pigments. Geochimica et Cosmochimica Acta 56, 1743-1751.

Sinninghe Damsté, J.S., Kock-van Dalen, A.C., Albrecht, P.A., de Leeuw, J.W., 1991. Identification of long-chain 1,2-di-*n*-alkylbenzenes in Amposta crude oil from the Tarragona Basin, Spanish Mediterranean: Implications for the origin and fate of alkylbenzenes. Geochimica et Cosmochimica Acta 55, 3667-3683.

Smernik, R.J., Oades, J.M., 2000a. The use of spin counting for determining quantitation in solid state ^{13}C NMR spectra of natural organic matter. 1. Model systems and the effect of paramagnetic impurities. Geoderma 96, 101-129.

Smernik, R.J., Oades, J.M., 2000b. The use of spin counting for determining quantitation in solid state ^{13}C NMR spectra of natural organic matter. 2. HF-treated soil fractions. Geoderma 96, 159-171.

Smith, J.W., George, S.C., Batts, B.D., 1995. The geosynthesis of alkyl aromatics. Organic Geochemistry 23, 71-80.

Snape, C.E., Bolton C., Dosch, R.G., Stephens, H.P., 1989. High liquid yields from bituminous coal via hydropyrolysis with dispersed catalysts. Energy and Fuels 3, 421-425.

Snape, C.E., Lafferty, C.J., Eglington, G., Robinson, N., Collier, R., 1994. The potential for hydropyrolysis as a route for coal liquefaction. International Journal of Energy Research 18, 233-242.

Speth, T.F., Summers, R.S., Gusses, A.M., 1998. Nanofiltration foulants from a treated surface water. Environmental Science and Technology 32, 3612-3617.

Stankiewicz, B.A., van Bergen, P.F., Duncan, I.J., Carter, J.F., Briggs, D.E.G., Evershed, R.P., 1996. Recognition of chitin and proteins in invertebrate cuticles using analytical pyrolysis/gas chromatography and pyrolysis/gas chromatography/mass spectrometry. Rapid Communications in Mass Spectrometry 10, 1747-1757.

Steelink, C., 1985. Implications of elemental characteristics of humic substances. In: Humic Substances in Soil, Sediment, and Water, Aiken, G.R., McKnight, D.M., Wershaw, R.L., MacCarthy, P., (Eds.), John Wiley & Sons, New York, pp 457 - 476.

Stein, W.H., Moore, S., 1949. Amino acid composition of β-lactoglobulin and bovine serum albumin. The Journal of Biological Chemistry 178, 79-91.

Steinbrecht, R.A., Stankiewicz, B.A., 1999. Molecular composition of the wall of insect olfactory sensilla – the chitin question. Journal of Insect Physiology 45, 785-790.

Stephens D.W., Gillespie D.M., 1976. Phytoplankton production in the Great Salt Lake Utah, and a laboratory study of algal response to enrichment. Limnology and Oceanography 21, 74-87.

Stevenson, F.J., 1982. Humus Chemistry: Genesis, Composition, Reactions. John Wiley and Sons, New York.

Strachan, M.G., Alexander, R., Kagi, R.I., 1988. Trimethylnaphthalenes in crude oils and sediments: Effects of source and maturity. Geochimica et Cosmochimica Acta 52, 1255-1264.

Stout, S.A., Boon, J.J., Spackman, W., 1988. Molecular aspects of the peatification and early coalification of angiosperm and gymnosperm woods. Geochimica et Cosmochimica Acta 52, 405-414.

Sugden, M.A., Abbott, G.D., 2002. The stereochemistry of bound and extractable pentacyclic triterpenoids during closed system pyrolysis. Organic Geochemistry 33, 1515-1521.

Sugden, M.A., Talbot, H., M ., Farrimond, P., 2005. Flash pyrolysis – a rapid method for screening bacterial species for the presence of bacteriohopanepolyols. Organic Geochemistry 36, 975-979.

Takada, H., Ishiwatari, R., 1987. Linear alkylbenzenes in urban riverine environments in Tokyo: distribution, source and behaviour. Environmental Science and Technology 21, 875-883.

Takada, H., Ishiwatari, R., 1990. Biodegradation experiments of linear alkylbenzenes (LABs): Isomeric composition of C_{12} LABs as an indicator of the degree of LAB degradation in the aquatic environment. Environmental Science and Technology 24, 86-91.

Talbot, H.M., Farrimond, P., 2007. Bacterial populations recorded in diverse sedimentary biohopanoid distributions. Organic Geochemistry 38, 1212-1225.

Talbot, H.M., Squire, A.H., Keely, B.J., Farrimond, P., 2003b. Atmospheric pressure chemical ionisation reversed-phase liquid chromatography/ion trap mass spectrometry of intact bacteriohopanepolyols. Rapid Communications in Mass Spectrometry 17, 728-737.

Talbot, H.M., Summons, R.E., Jahnke, L.L., Cockell, C.S., Rohmer, M., Farrimond, P., 2008. Cyanobacterial bacteriohopanepolyol signatures from cultures and natural environmental settings. Organic Geochemistry 39, 232-263.

Talbot, H.M., Summons, R., Jahnke, L., Farrimond, P., 2003a. Characteristic fragmentation of bacteriohopanepolyols during atmospheric pressure chemical ionisation liquid chromatography/ion trap mass spectrometry. Rapid Communications in Mass Spectrometry 17, 2788-2796.

Talbot, H.M., Watson, D.F., Murrell, J.C., Carter, J.F., Farrimond, P., 2001. Analysis of intact bacteriohopanepolyols from methanotrophic bacteria by reversed phase high performance liquid chromatography – atmospheric pressure chemical ionisation mass spectrometry. Journal of Chromatography A 921, 175-185.

Tegelaar, E.W., de Leeuw, J.W., Saiz-Jimenez, C., 1989a. Possible origin of aliphatic moieties in humic substances. The Science of Total Environment 81/82, 1-17.

Tegelaar, E.W., Matthezing, R.M., Jansen, J.B.H., Horsfield, B., de Leeuw, J.W. 1989b. Possible origins of normal alkanes in high wax crude oils. Nature 342, 529-531.

Tehrani, K.A., Kersiene, M., Adams, A., Nenskutonis, R., de Kimpe, N., 2002. Thermal degradation studies of glucose/glycine melanoidins. Journal of Agricultural and Food Chemistry 50, 4062-4068.

Templier, J., Derenne, S., Croué, J-P., Largeau, C., 2005a. Comparative study of two fractions of riverine dissolved organic matter using various analytical pyrolytic methods and a ^{13}C CP/MAS NMR approach. Organic Geochemistry 36, 1418-1442.

Templier, J., Derenne, S., Mercier, F., Barre, N., Miserque, F., Largeau, C., 2005b. Nitrogen functionality in various fractions of riverine dissolved organic matter. Proceedings of the 22nd International Meeting of Organic Geochemistry, Seville, Spain, September 2005.

Thurman, E.M., Malcolm, R.L., 1981. Preparative isolation of aquatic humic substances. Environmental Science and Technology 15, 463-466.

Thurman, E.M., 1985. Organic Geochemistry of Natural Waters. Nijhoff, M., Junk, W., (Publishers), Dordrecht, Netherlands.

Tsuge, S., Matsubara, H., 1985. High-resolution pyrolysis-gas chromatography of proteins and related materials. Journal of Analytical and Applied Pyrolysis 8, 49-64.

United States Environmental Protection Agency, 2001. Stage 1 disinfectants and disinfection byproducts rule: A quick reference guide. United States Environmental Protection Agency.

van Aarssen, B.G., Alexander, R., Kagi, R.I., 2000. Higher plant biomarkers reflect palaeovegetation changes during Jurassic times. Geochimica et Cosmochimica Acta 64, 1417-1424.

van Aarssen, B.G.K., Cox, H.C., Hoogendoorn, P., de Leeuw, J.W., 1990. A cadinane biopolymer in fossil and extant dammar resins as a source for cadinanes and bicadinanes in crude oils from Southeast Asia. Geochimica et Cosmochimica Acta 54, 3021-3031.

van Aarssen, B.G.K., de Leeuw, J.W., Horsfield, B., 1991. A comparative study of three different pyrolysis methods used to characterise a biopolymer isolated from fossil and extant dammar resins. Journal of Analytical and Applied Pyrolysis 20, 125-139.

van Aarssen, B.G.K., de Leeuw, J.W., Collinson, M., Boon, J.J., Goth, K., 1994. Occurrence of polycadinene in fossil and recent resins. Geochimica et Cosmochimica Acta 58, 223-229.

van Aarssen, B.G.K., Hessels, J.K.C., Abbink, O.A., de Leeuw, J.W., 1992. The occurrence of polycyclic sesqui-, tri-, and oligoterpenoids derived from a resinous polymeric cadinane in crude oils from Southeast Asia. Geochimica et Cosmochimica Acta 56, 1231-1246.

van Heemst, J.D.H., Megens, L., Hatcher, P.G., de Leeuw, J.W., 2000. Nature, origin and average age of estuarine ultrafiltered dissolved organic matter as determined by molecular and carbon isotope characterisation. Organic Geochemistry 31, 847-857.

van Heemst, J.D.H., van Bergen, P.F., Stankiewicz, B.A., de Leeuw, J.W., 1999. Multiple sources of alkylphenols produced upon pyrolysis of DOM, POM and recent sediments. Journal of Analytical and Applied Pyrolysis 52, 239-256.

van Heemst, J.D.H., Peulvé, S., de Leeuw, J.W., 1996. Novel algal polyphenolic biomacromolecules as significant contributors to resistant fractions of marine dissolved and particulate organic matter. Organic Geochemistry 24, 629-640.

Vane, C.H., Abbott, G.D., 1999. Proxies for land plant biomass: Closed system pyrolysis of some methoxyphenols. Organic Geochemistry 30, 1535-1541.

Volk, C., Bell, K., Ibrahim, E., Verges, D., Amy, G., Lechevallier, M., 2000. Impact of enhanced and optimized coagulation on removal of organic matter and its biodegradable fraction in drinking water. Water Research 34, 3247-3257.

Voorhees, K.J., Zhang, W., Hendricker, A.D., Murugaverl, B., 1994. An investigation of the pyrolysis of oligopeptides by Curie-point pyrolysis-tandem mass spectrometry. Journal of Analytical and Applied Pyrolysis 30, 1-16.

Wakeham, S.G., Schaffner, C., Giger, W., 1980. Polycyclic aromatic hydrocarbons in recent lake sediments – II. Compounds derived from biogenic precursors during early diagenesis. Geochimica et Cosmochimica Acta 44, 415-429.

Wang, Z., Pant, B.C., Langford, C.H., 1990. Spectroscopic and structural characterization of a Laurentian fulvic acid: notes on the origin of the colour. Analytica Chimica Acta 232, 43-49.

Wang, S., Liu, B., Su, Q., 2004. Pyrolysis-gas chromatography/mass spectrometry as a useful technique to evaluate the pyrolysis pathways of phenylalanine. Journal of Analytical and Applied Pyrolysis 71, 393-403.

Watson, J.S., Sephton, M.A., Looy, C.V., Gilmour, I., 2005. Oxygen-containing aromatic compounds in a Late Permian sediment. Organic Geochemistry 36, 371-384.

Weishaar, J.L., Aiken, G.R., Bergamaschi, B.A., Fram, M.S., Fujii, R., Mopper, K., 2003. Evaluation of specific ultraviolet absorbance as an indicator of the chemical composition and reactivity of dissolved organic carbon. Environmental Science and Technology 37, 4702-4708.

Wershaw, R.L., 2004. Evaluation of conceptual models of natural organic matter (humus) from a consideration of the chemical and biochemical processes of humification. U.S. Geological Survey Scientific Investigations Report 5121.

Westerhoff, P., Mash, M., 2002. Dissolved organic nitrogen in drinking water supplies: A review. Journal of Water Supply: Research and Technology-AQUA 51, 415-448.

White, D.M., Garland, D.S., Narr, J., Woolard, C.R., 2003. Natural organic matter and DBP formation potential in Alaskan water supplies. Water Research 37, 939-947.

Wilson, M.A., 1987. NMR techniques and applications in geochemistry and soil chemistry. Pergamon Press, Oxford, England.

Wilson, M.A., Hatcher, P.G., 1988. Detection of tannins in modern and fossil barks and in plant residues by high-resolution solid-state ^{13}C nuclear magnetic resonance. Organic Geochemistry 6, 539-546.

Wise, S.A., Benner, B.A., Byrd, G.D., Chesler, S.N., Rebbert, R.E., Schantz, M.M., 1988. Determination of polycyclic aromatic hydrocarbons in a coal tar standard reference material. Analytical Chemistry 60, 83-99.

Xia, K., Weesner, F., Bleam, W.F., Bloom, P.R., Skyllberg, U.L., Helmke, P.A., 1998. Division S-2 – soil chemistry: XANES studies of oxidation states of sulfur in aquatic and soil humic substances. Soil Science Society of America Journal 62, 1240-1246.

Yamamoto, S., Ishiwatari, R., 1992. A study of the formation mechanism of sedimentary humic substances.III. Evidence for the protein-based melanoidin model. The Science of the Total Environment 117/118, 279-292.

Zang, X., Brown, J.C, van Heemst, J.D.H., Palumbo, A., Hatcher, P.G., 2001. Characterisation of amino acids and proteinaceous materials using online tetramethylammonium hydroxide (TMAH) thermochemolysis and gas chromatography-mass spectrometry. Journal of Analytical and Applied Pyrolysis 61, 181-193.

Zang, X., van Heemst, J.D.H., Dria, K.J., Hatcher, P.G., 2000. Encapsulation of protein in humic acid from a histosol as an explanation for the occurrence of organic nitrogen in soil and sediment. Organic Geochemistry 31, 679-695.

Zech, W., Senesi, N., Guggenberger, G., Kaiser, K., Lehmann, J., Miano, T.M., Miltner, A., Schroth, G., 1997. Factors controlling humification and mineralization of soil organic matter in the tropics. Geoderma 79, 117-161.

Zeng, L., Jingyu, S., Yongli, Z., Xiong, F., Tangsheng, P., Ye, Z., Yanhui, M., Yingzhou, C., Xiaohua, X., Yaohua, Z., Guiyangsheng, W., 1999. Search for new compounds and biologically active substances from Chinese marine organisms. Pure and Applied Chemistry 71, 1147-1151.

Zhiguang, S., Batts, B.D., Smith, J.W., 1998. Hydrous pyrolysis reactions of sulphur in three Australian brown coals. Organic Geochemistry 29, 1469-1485.

Appendix 1

TICs from three separate 300˚C/72hr MSSV pyrolysis GC-MS analyses (***I***) of Suwannee River fulvic acid. Relative abundances of a-c are indicated in italics. The relative proportions of the major product groups, averaged from the three analyses, are shown together with standard deviations. Peak areas were calculated by integrating up to 200 of the most abundant peaks ≥ 0.5% of the base peak. Individual peak areas and product groups were expressed as percentages of the total integrated pyrolysate area. A = aliphatics, CA = cylco-aliphatics, AK = aliphatic ketones, CK = cyclic ketones, B = alkyl benzenes, F = alkyl furans and benzofurans, P = alkyl phenols, MA = methoxy aromatics, NA = naphthalenes and other PAH products, HA = Hydroaromatics, S = sulfur products, N = nitrogen products, O = other unspecified products.

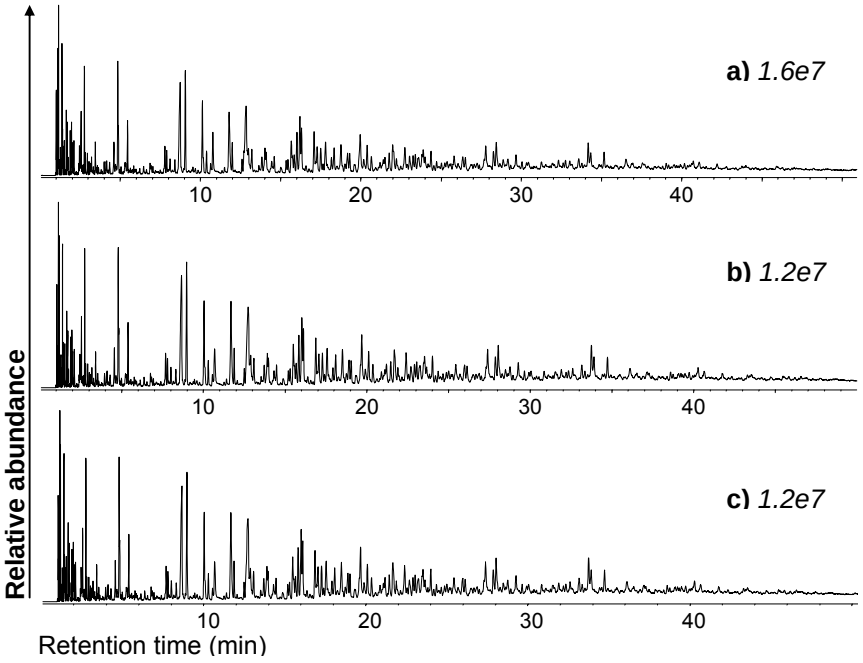

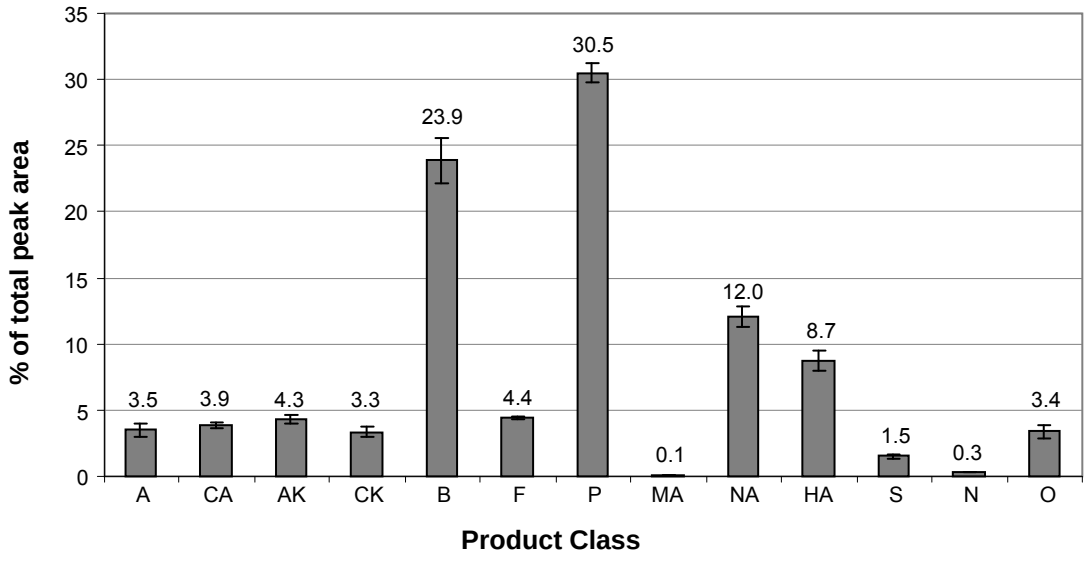

Appendix 2

TICs from 300˚C/72hr MSSV pyrolysis GC-MS analysis of **a)** Suwannee River Fulvic acid, **b)** St. Julien colloids and **c)** Naintré colloids. Relative abundances of a-c are indicated in italics. ● = alkyl benzenes, ○ = alkyl phenols, ▲ = alkyl naphthalenes, * = *n*-alkanes.

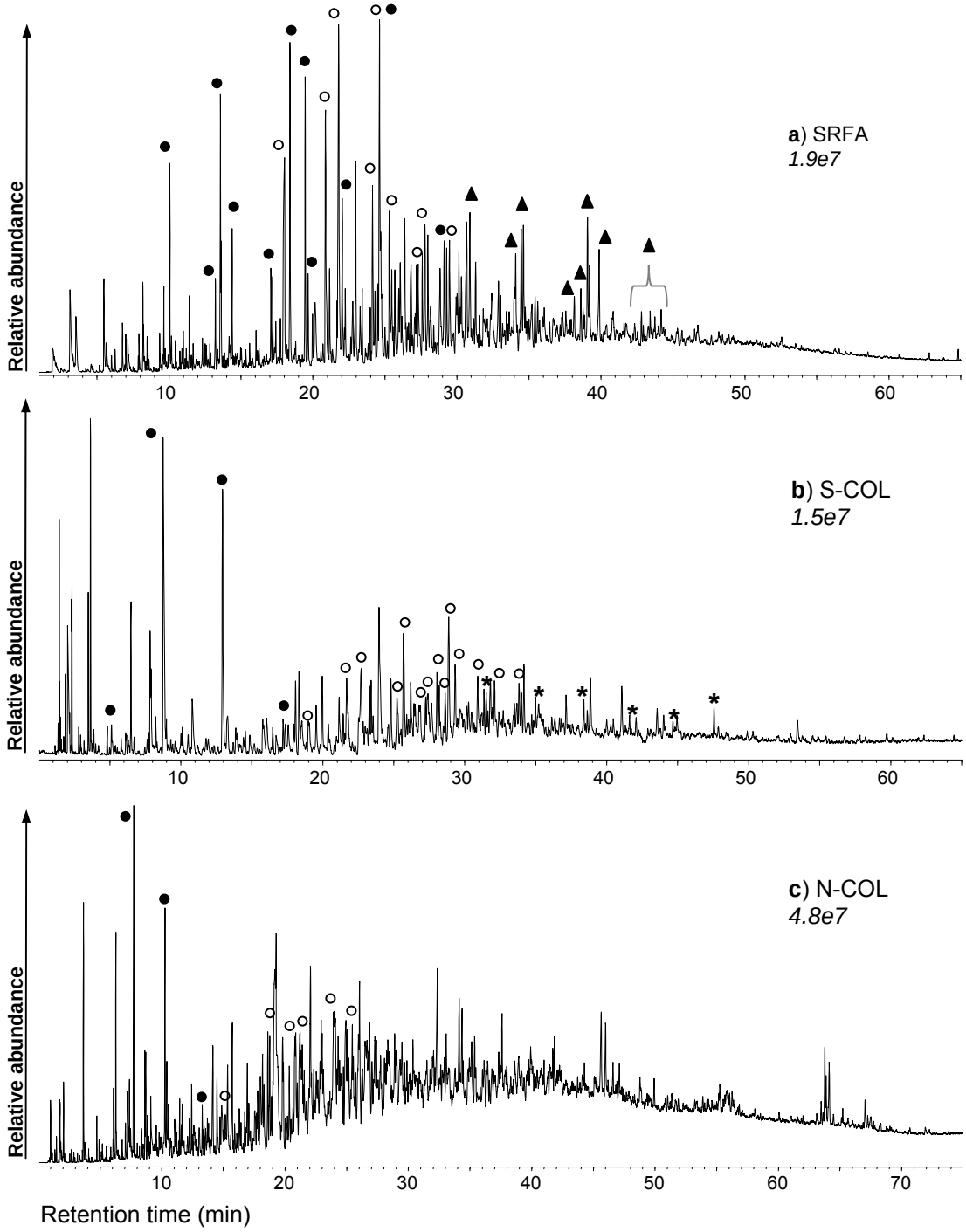

Appendix 3

Summed *m/z* 91+105+106+119+120+133+ 134+148 chromatograms showing the alkyl (C_1-C_5) benzene distributions from the 300˚C/72hr MSSV pyrolysis GC-MS analysis of **a)** *Pinus radiata* wood, **b)** *Wandoo eucalyptus* wood, **c)** syringic acid **d)** phenylalanine and **e)** chitin. Peak assignments correspond to the products listed in Table 3.1. Relative abundances of a-e are indicated in italics.

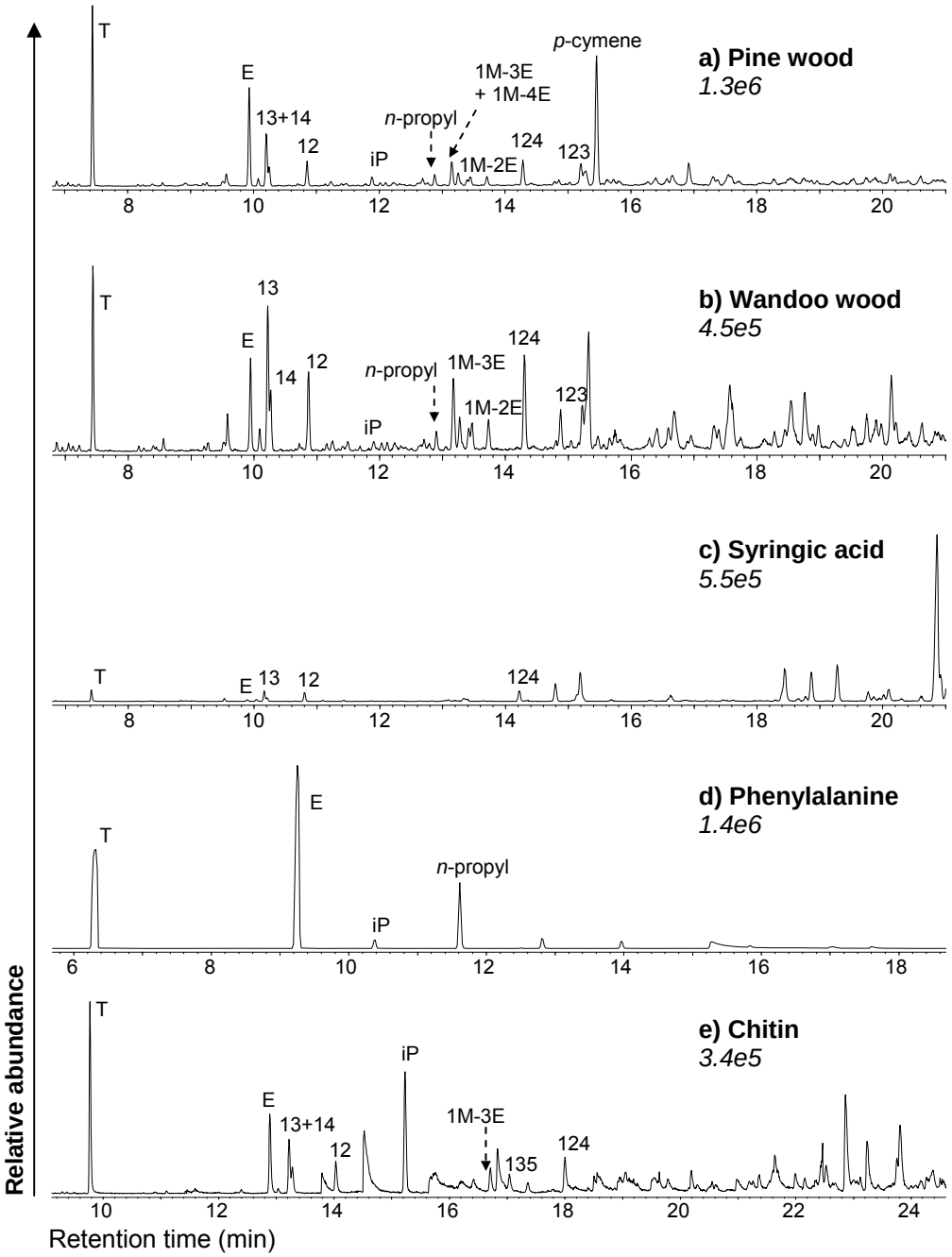

Appendix 4

Summed *m/z* 91+105+106+119+120+133+134+148 **(a)** and *m/z* 142+156+170+184+198 **(b)** chromatograms showing the alkyl (C_1-C_5) benzene and naphthalene distributions from the **(i)** 300˚C/72hr and **(ii)** 340˚C/72hr MSSV pyrolysis GC-MS analysis of lignin. Peak assignments correspond to the products listed in Table 3.1. Relative abundances are indicated in italics.

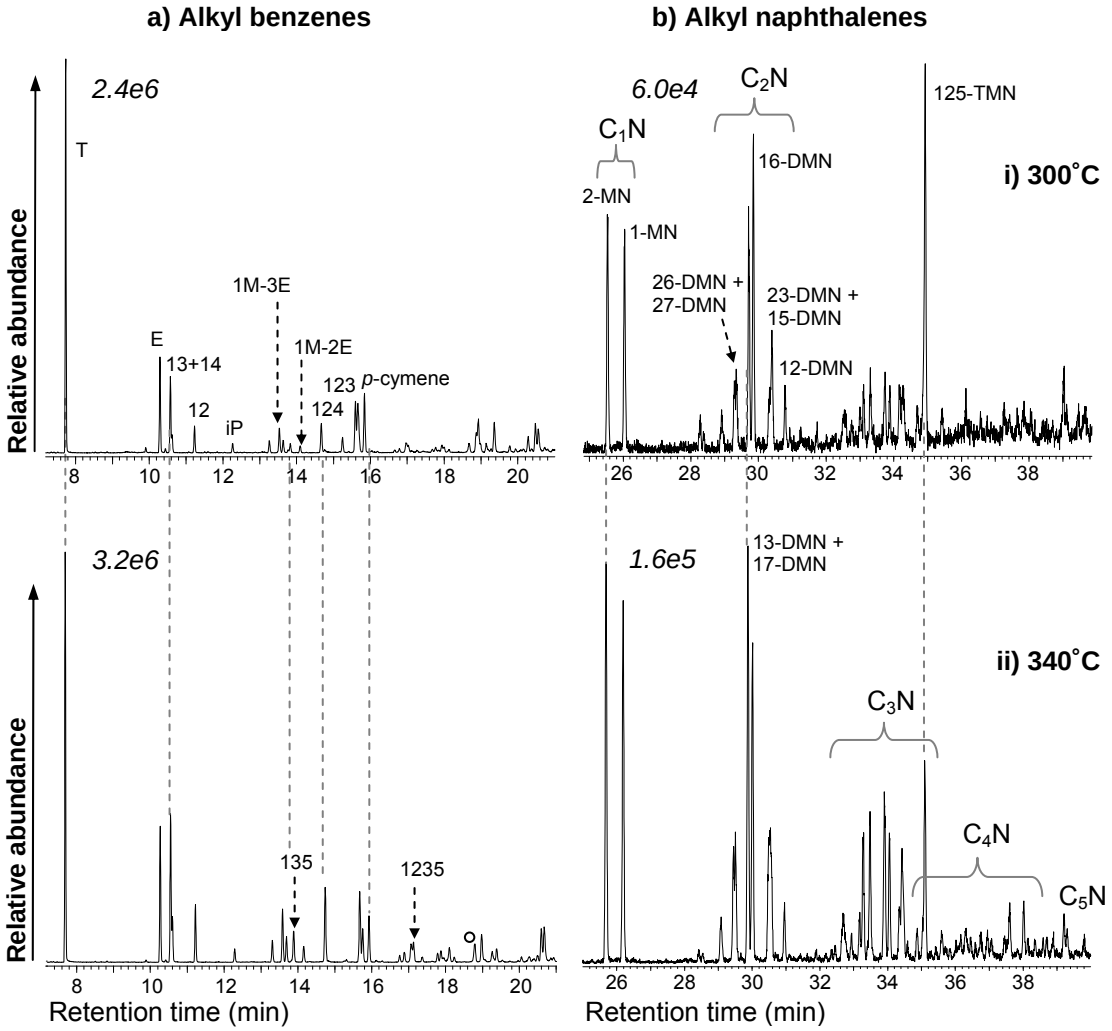

Appendix 5

Partial TICs of the major O-products detected by 300˚C/72hr MSSV pyrolysis GC-MS of **a)** D-glucose and **b)** N-acetyl-D-glucosamine. Peak assignments correspond to products listed in Table 4.1.

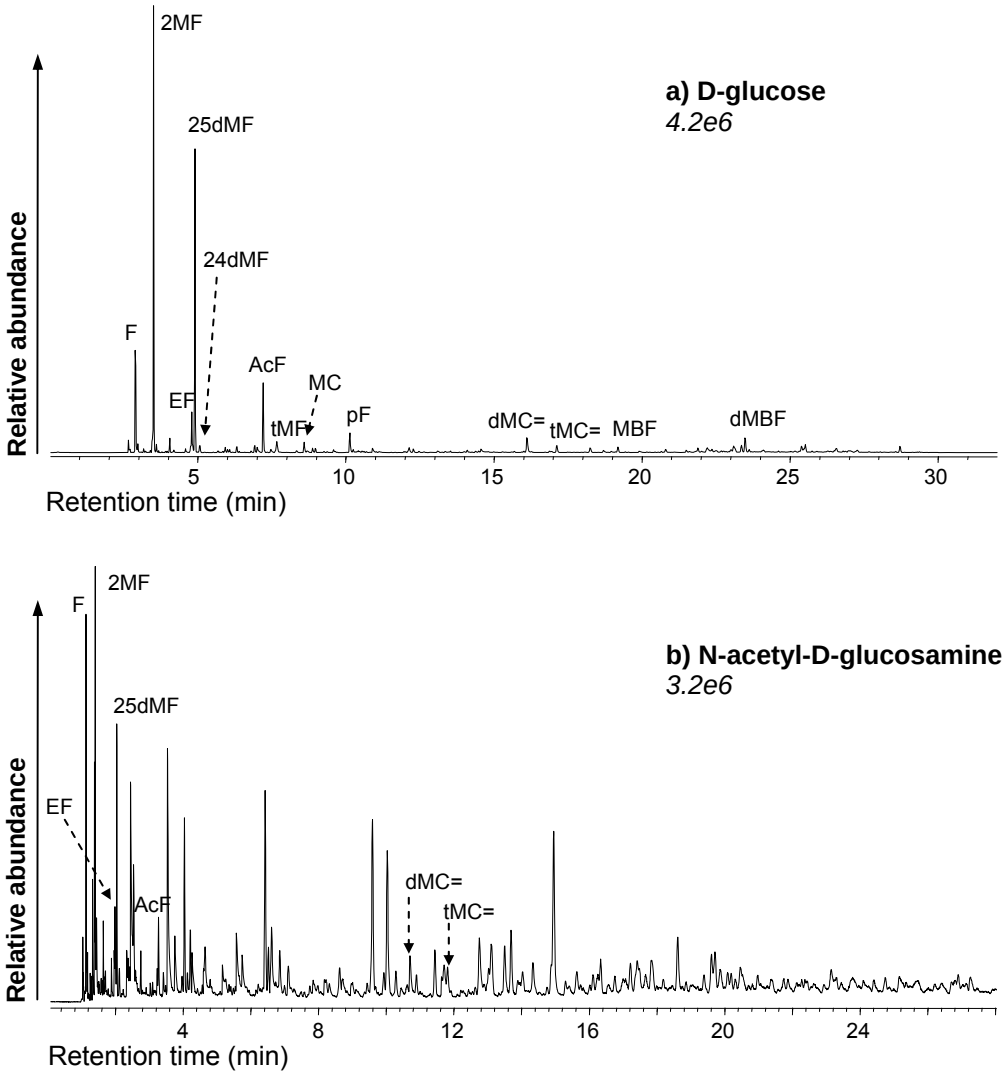

Appendix 6

Summed *m/z* 79+80+93+94+106+107+108+109+120+121+122+123 chromatograms showing the distribution of low MW N-heterocyclic products detected by 300˚C/72hr MSSV pyrolysis GC-MS analysis of Uruguay TPI. Peak assignments correspond to products listed in Table 5.1. Relative abundance is indicated in italics.

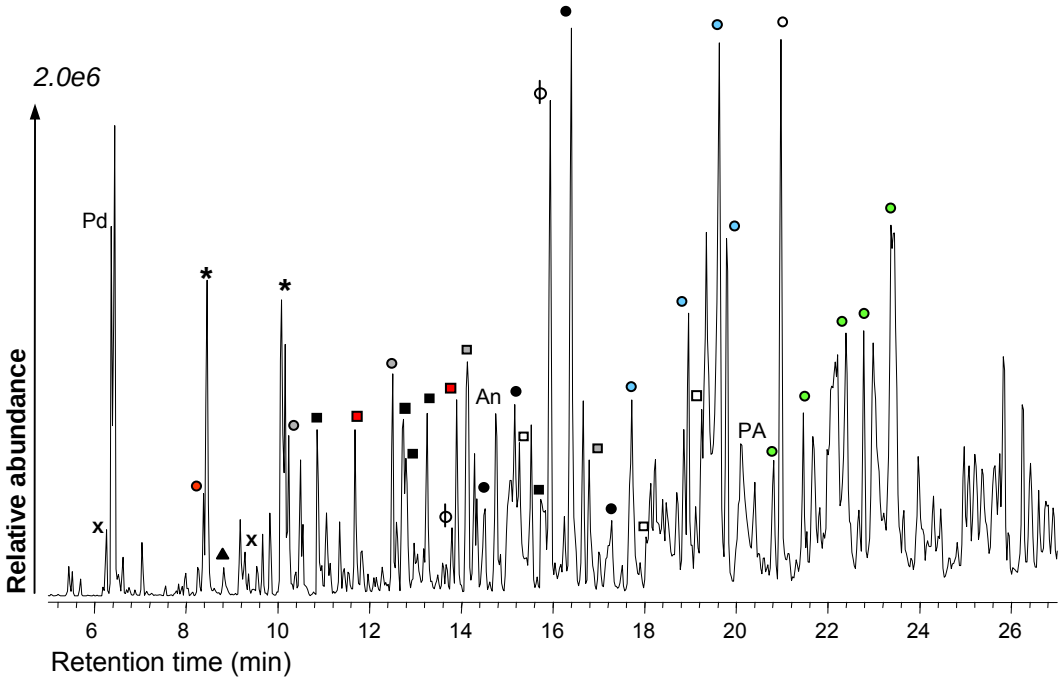

Appendix 7

TIC from the 300˚C/72 hr MSSV pyrolysis GC-MS analysis of L-proline. Peak assignments correspond to products listed in Table 5.1. Relative abundance is indicated in italics.

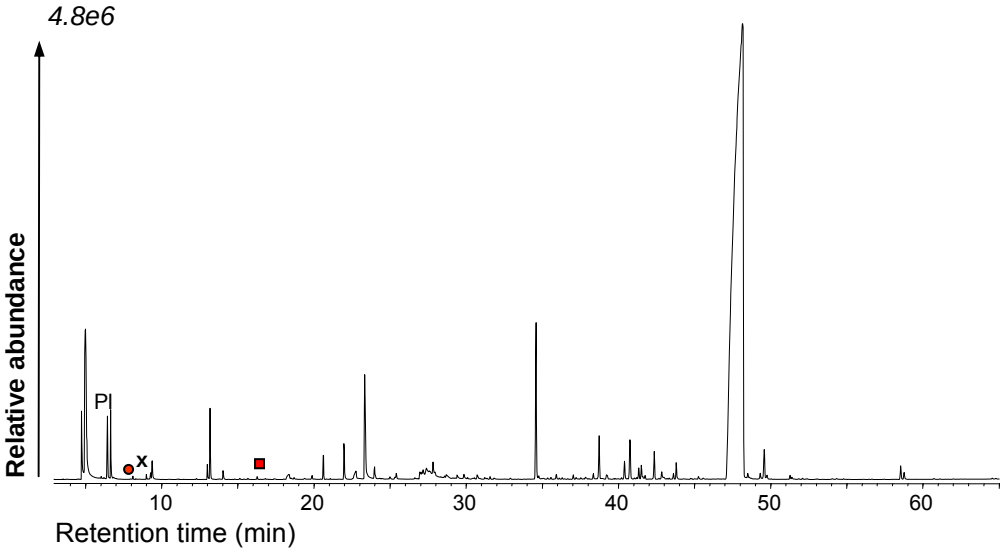

Appendix 8

Total ion chromatogram from the 550˚C/20s flash pyrolysis analysis of 2,3,7,8, 12,13, 17,18-octaethyl-21*H*,23*H*-porphine. Peak assignments correspond to products listed in Table 5.1. A = alkyl anilines. Relative abundance is indicated in italics.

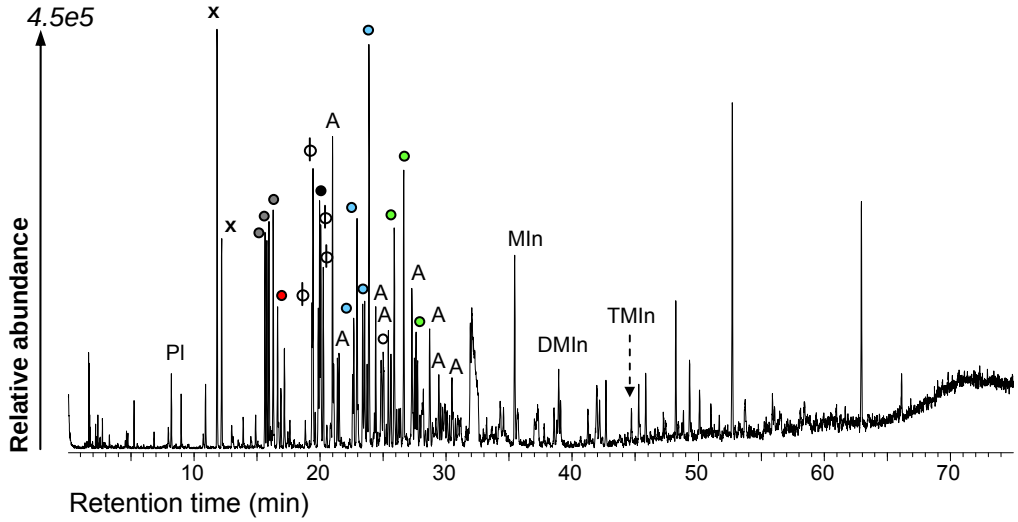

Appendix 9

Summed *m/z* 143+157 chromatograms showing the detection of naphthalenamine (NA) and methyl naphthalenamine (MNA) from the 300˚C/72hr MSSV pyrolysis GC-MS analysis of **a)** Naintré colloids and **b)** St. Julien colloids. Relative abundance is indicated in italics.